Coupled Modelling of Gas Migration in Host Rock and Application to a Potential Deep Geological Repository for Nuclear Wastes in Ontario

Submitted by

Xue Wei

Under the supervision of

Dr. Mamadou Fall

Thesis submitted to the Faculty of Engineering in partial fulfillment of the requirements for the Doctor of Philosophy in Civil Engineering

Department of Civil Engineering

Falcuty of Engineering

University of Ottawa

Abstract

With the widening and increasing use of nuclear energy, it is very important to design and build long-term deep geological repositories (DGRs) to manage radioactive waste. The disposal of nuclear waste in deep rock formations is currently being investigated in several countries (e.g., Canada, China, France, Germany, India, Japan and Switzerland). In Canada, a repository for low and intermediate level radioactive waste is being proposed in Ontario's sedimentary rock formations. During the post-closure phase of a repository, significant quantities of gas will be generated from several processes, such as corrosion of metal containers or microbial degradation of organic waste. The gas pressure could influence the engineered barrier system and host rock and might disturb the pressure-head gradients and groundwater flows near the repository. An increasing gas pressure could also cause damage to the host rock by inducing the development of micro-/macro-cracks. This will further cause perturbation to the hydrogeological properties of the host rock such as desiccation of the porous media, change in degree of saturation and hydraulic conductivity. In this regard, gas generation and migration may affect the stability or integrity of the integrate barriers and threaten the biosphere through the transmitting gaseous radionuclides as long-term contaminants. Thus, from the safety perspective of DGRs, gas generation and migration should be considered in their design and construction. The understanding and modelling of gas migration within the host rock (natural barrier) and the associated potential impacts on the integrity of the natural barrier are important for the safety assessment of a DGR. Therefore, the key objectives of this Ph.D. study include (i) the development of a simulator for coupled modelling of gas migration in the host rock of a DGR for nuclear waste; and (ii) the numerical investigation of gas migration in the host rock of a DGR for nuclear waste in Ontario by using the developed simulator. Firstly, a new thermo-hydro-mechanical-chemical (THMC) simulator (TOUGHREACT-COMSOL) has been developed to address these objectives. This simulator results from the coupling of the well-established numerical codes, TOUGHREACT and COMSOL. A series of mathematical models, which include an elastoplastic-damage model have been developed and then implemented into the simulator. Then, the predictive ability of the simulator is validated against laboratory and

field tests on gas migration in host rocks. The validation results have shown that the developed simulator can predict well the gas migration in host rocks. This agreement between the predicted results and the experimental data indicates that the developed simulator can reasonably predict gas migration in DGR systems. The new simulator is used to predict gas migration and its effects in a potential DGR site in Ontario. Valuable results regarding gas migration in a potential DGR located in Ontario have been obtained. The research conducted in this Ph.D. study will provide a useful tool and information for the understanding and prediction of gas migration and its effect in a DGR, particularly in Ontario.

Acknowledgements

First and foremost, I would like to express my immense gratitude and respect to my supervisor, Dr. Mamadou Fall, for his enduring support, patient guidance, and warm encouragement throughout the duration of my Ph.D. study. Without the trust and encouragement from my supervisor, I wouldn't have made it to the end. During these years of study at the University of Ottawa, his passion and dedication to research and his careful, hard-working, and self-motivated attitude towards work inspired me to become a rigorous and precise researcher. His support and inspiration will continue to give me motivation and courage in my future studies and life.

I would like to sincerely acknowledge Dr. Alireza Ghirian, Dr. Ousmane Seidou, and Dr. Liang Cui for their invaluable feedback and advice towards my research. I am truly grateful to all of you.

My sincere appreciation is extended to Dr. Zhenze Li for his insightful advices and encouragement on my research work. I would also like to thank my colleagues, Dr. Guanlong Guo, Dr. Kun Fang, and Jianxiong Yang, for their generous and kind help throughout the process of conducting this Ph.D. research.

Last but not least, I deeply appreciate my parents; their love provided me with inspiration and was my driving force. I wish to deeply thank my husband, Sheng Liu for his unconditional support for me to pursue my study, and my daughter Lucia, whose love allowed me to finish this journey. Without their support, encouragement, trust and love, I could not imagine how hard it would have been to complete the study.

Contents

List of Figures

List of Tables

List of Equations

CHAPTER 1 General Introduction

1.1 Introduction

With the rapid development and wide use of nuclear energy, more and more radioactive waste is being produced, which poses a threat to the safety of humans and the environment. Therefore, many countries, including Canada, China, France, Germany, India and Switzerland etc., have considered deep geological repositories (DGRs) as the most preferred option for the long-term management of radioactive waste (Alzamel and Fall, 2019; Fall et al. 2018). The safe long-term disposal of radioactive wastes in a repository and their isolation from the biosphere are provided by a multi-barrier system consisting of natural barriers (host rocks) and an engineered barrier system (EBS) (Shehata et al. 2020). There are several types of rock formations, including igneous (e.g., granite, basalt) and sedimentary rocks (e.g., limestone, sandstone), which have been considered suitable as host rocks for DGR systems.

Several processes such as the biological degradation of low-and intermediate-level wastes, and the corrosion of metal containers, have been reported as generating significant quantities of gas-including carbon dioxide, methane and hydrogen (Fall, 2009). In the post closure stage, the gas pressure is expected to build up to a significant level that would approach or even surpass the formation stress, in which case the host rock may be fractured by the accumulated gas, with the formation and propagation of micro/macrocracks. Gas accumulation could further cause perturbation to the hydrogeological properties of the host rock, i.e., desiccation of the porous media, change in saturation and hydraulic conductivity, and impact on the effective stress by poroelastic responses. In this regard, the gas generation and migration may not only affect the stability or integrity of the barriers, but also threaten the biosphere with gaseous radionuclides in the long-term (Fall, 2009; Wei and Fall 2019).

For gas migration, four potential gas transport paths have been identified, which include the engineered barrier system, the excavation-damaged zone (EDZ) around the excavated shaft, the host rocks and overlying rocks, and the preferential flow path via structural discontinuities such as faults (Alkan and Müller, 2008). The mechanisms of gas transport are closely related to individual gas paths (Nagra, 2008). The thermo-hydro-mechanical-

chemical (THMC) coupled processes that occur in a DGR, with consideration of damage, could influence the gas pathways in certain manners. For instance, the geochemical reactions (C) in porous media, i.e. dissolution and precipitation, take place in contact with groundwater (H) and directly modify the media's porosity and permeability. The temperature (T) can change the rate of dissolution and precipitation and induce mechanical stress and rock deformation (M). Porosity and permeability are key material properties that connect the entire THMC processes and mechanical damage as well as the gas transport (Nasir and Fall, 2014).

1.2 Problem statement

For the long-term stability of a DGR, the multiphysics processes, such as coupled HM and THMC processes, can strongly affect gas migration and thus influence the safety assessment (SA). The temperature, stress, negative pore water pressure (suction) and material properties will relatively change with time under the interaction effect during the multiphysics processes. Furthermore, due to the increasing gas pressure, the development of micro-/ macro-cracks (mechanical damage) will affect the strength, stiffness and hydraulic properties of the host rock. From the perspective of modelling, nine main elements should be considered for the THMC evaluation (Nasir, 2013). Figure 1.1 shows the main elements. In the post closure stage of the DGR, through the effect of THMC processes, these nine elements are fully or partially coupled with each other. For the long term safety and stability of the DGRs, any elements might influence other elements during the long-life span of a DGR system. Therefore, to predict the gas migration accurately, the damage coupled with HM or THMC processes with the evaluation of the nine elements changes should be fully considered and explained with the mathematical models.

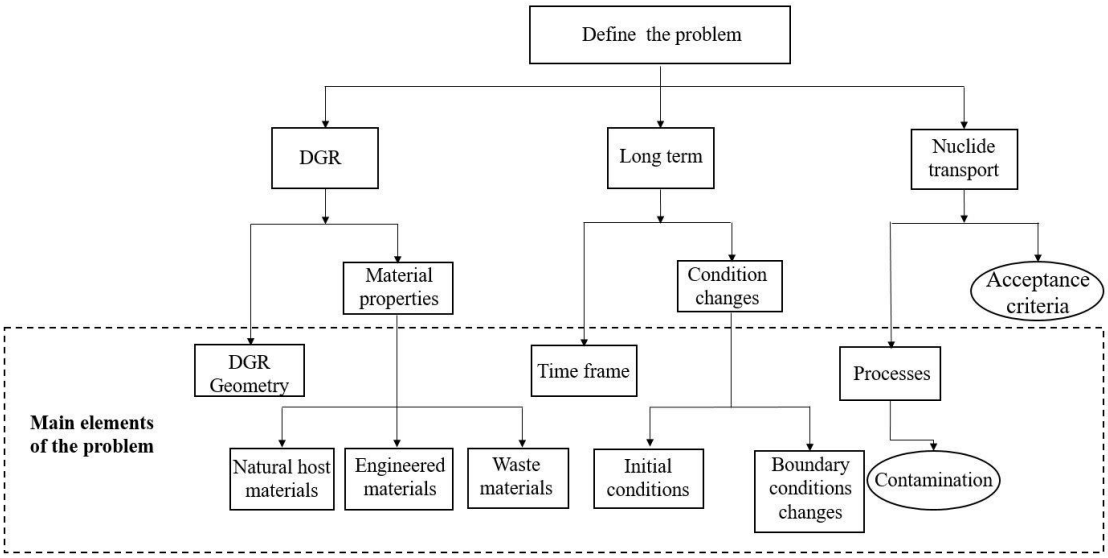

Figure 1.1 The definition of problem and the elements of study (Nasir, 2013)

1.3 Research rational and need

In recent years, several researches have focused on the prediction of the behavior of gas generation and migration in DGR systems. These researches emphasized the importance of considering multiphysics coupled processes in the assessment and prediction of gas migration in DGR. Since numerical methods are the best practical ways to analyze and quantify the coupling of the THMC processes (Nasir, 2013), to predict gas migration accurately, in the past few decades, the development of coupled numerical tools has gained significant interest.

In the beginning, single codes were used to deal with the related coupled processes in porous media with different levels of coupling. Most of them (e.g., Zheng and Wang, 1998; Cheng and Yeh, 1998; Parkhurst and Appelo, 1999; Mayer, 2000; Xu et al., 2006) only handle the partially coupled THMC processes (e.g. THC, THM, etc.). Fall et al. (2014) proposed a coupled hydro-mechanical (HM) model with damage. This model simulated gas migration in sedimentary host rocks for the deep geological repositories. This model verified the importance of induced mechanical damage by high gas pressure and described the formation of micro-cracks. Although the reliability and accuracy of this new simulator

were improved to a certain degree, it still has limitations, considering the elasto-plastic mechanical behavior of the host rock and the impacts produced by geochemical reactions. Some used specialized simplified approaches to deal with the coupled THMC processes by single computer code (Tao et al., 2019). Some used the two computer codes to deal with coupled THM processes without the consideration of the geochemical reactions, which will influence the reliability of the simulation (Rutqvist et al., 2002). Nasir (2013) developed a coupled THMC model by using coupled codes (COMSOL-PHREEQC). It described the THMC processes of gas migration under the impact of glaciation. However, in his research, the geomechanical process was simplified. The plastic deformation and the induced rock damage due to high gas pressure have not been taken into the consideration as part of the method. Although the sequential coupling of two codes or programs is less efficient than using a single program, the greatest advantage is that the programs that are coupled and often well-established, have been extensively validated or verified, widely used, and thus approved by many regulatory agencies. Moreover, most of the available numerical simulators and commercial software cannot simultaneously solve and analyze all of the coupled THMC processes that are relevant for gas migration in DGRs, as described in Table 1-1. Therefore, there is a need to develop a simulator, based on the coupling of well-established codes, which can integrate and solve all THMC processes that are relevant for assessing and predicting gas migration in a host rock of DGR.

Table 1-1 Examples of codes and software for modeling of the coupled processes

Name of the code	**Reference**	**Mechanical processes**	**Flow**	**Heat transfer**	**Solute transport**	**Chemical reaction**	**Mainly applied area /comments**
ROCMAS	Woorishad and Tsang (1984)	√	√	√			Nuclear waste storage
GEOCRACK	Swenson et al. (1994)	√	√	√			Dry and hot rock
FRACTure	Kohl et al.(1995)	√	√	√	√		Dry and hot rock
THAMES	Ohnishi and Kobagashi (1996)	√	√	√	√		Nuclear waste storage
FRACON	Nguyen (1996)	√	√	√			Nuclear waste storage
FEHM	Bower and Zyvoloski (1997)	√	√	√			Dry and hot rock
3DHYDROGEOCHEM	Cheng and Yeh (1998)		√	√	√	√	Focus on inorganic chemical transport
MOTIF	Guvanasen and Chan (1999)	√	√	√	√		Nuclear waste storage
PHREEQC	Parkhurst and Appelo (1999)		√		√	√	Aqueous geochemical calculations
MIN3P	Mayer(2000)		√		√	√	Coupled flow and mass transfer and reactive mine wastes

OpenGeoSys	UFZ (2001)	√	√	√	√	√	Porous and fractured media
TOUGH-FLAC	Rutquist et al. (2002)	√	√	√			Nuclear waste storage
HP1(HYDRUS1D-PHREEQC)	Jacqus and Šimůnek (2005)		√		√	√	Water, heat, solute movement and geochemical reactions in porous media
TOUGHREACT	Xu et.al (2006)		√	√	√	√	Chemically reactive non-isothermal flow of multiphase fluids in porous and fractured media
FRT-THM	Liu et al. (2009)	√	√	√			Nuclear waste storage
MT3DMS	Taron et.al (2009)		√		√	√	Changes in concentration of miscible contaminant in groundwater and basic chemical reactions
FLAC3D-TOUGHREACT	Taron et.al (2009)	√	√	√	√	√	Undrained loading behavior of a fractured rock mass; no mechanical damage
CODE-ASTER	Rohmer and Seyedi (2010)	√	√	√			CO2 storage
COMSOL-IPHREEQC	Wissmerier and Barry (2011)		√		√	√	Extends the capability of COMSOL and PHREEQC
COMSOL-PHREEQC	Nasir and Fall (2014)	√	√	√	√	√	Nuclear waste storage; 1D and no mechanical damage
Proposed work TOUGHREACT-COMSOL		√	√	√	√	√	Nuclear waste storage

1.4 Objectives

The main objectives of this study are summarized as follows:

(i) To develop a fully coupled THMC-damage model for predicting the gas migration in initially unfractured sedimentary host rock

(ii) To develop a simulator for coupled modeling of gas migration in host rock of DGR for nuclear wastes

(iii) To numerically investigate the gas migration in a potential host rock of DGR for nuclear wastes in Ontario by using the developed simulator

(iv) To gain a better understanding of gas migration in sedimentary host rocks of DGR and its impact on DGR safety.

1.5 Research approach and methods

The research approach and methods used in this study are schematically described in Figure 1.2. Based on a comprehensive literature review, the problem definition and research objectives are defined. Then, a new THMC simulator has been developed by coupling two well-established and validated numerical codes, COMSOL Multiphysics and TOUGHREACT in which a series of new mathematical models were implemented. The series of developed mathematical models include: (1) An elastoplastic-damage model, and (2) a fully coupled THMC model. The elastoplastic damage model describes the mechanical behavior of the host rock. The effective stress principle for unsaturated porous media is adopted. An isotropic damage is assumed and the continuum damage mechanics is proposed. Based on the Drucker-Prager yield function, a plastic-damage model is adopted to describe the plastic strain. The non-associated plastic flow rule is employed in this study. The mechanical parameters, such as cohesion, internal friction of angle and stiffness, are expressed as a function of the degree of damage. To explain the volumetric deformation of the host rock, a new code is programed in MATLAB to calculate the

variation in pore space. The pore space change is related to the solid skeleton of the host rock and is equal to the total volume change of the pore water and pore air. The new code calculates the volumetric changes by stress, thermal expansion and contraction, chemical reaction and damage. It updates the porosity and permeability dependent on time. This new MATLAB code enables the coupling of the elastoplastic damage model (M, mechanical processes) implemented in COMSOL with the THC model that exists in TOUGHREACT to develop a THMC model. The coupled THMC model enables to describe or capture the impact of the THMC processes on gas migration in the host rocks. To describe the coupled THMC processes, a set of conservation and constitutive equations are considered. Four balance equations (water and air mass, momentum (mechanical equilibrium) and energy conservation equations) are considered. The coupled THMC model includes the full coupling of thermal, hydraulic, chemical and mechanical processes and considers the changes in the rock properties, such as the porosity permeability and the strength. The developed THMC simulator is then validated through laboratory and field tests on host rocks of DGR. Subsequently, the developed simulator is used to assess gas migration in the host rock of a potential Ontario's DGR.

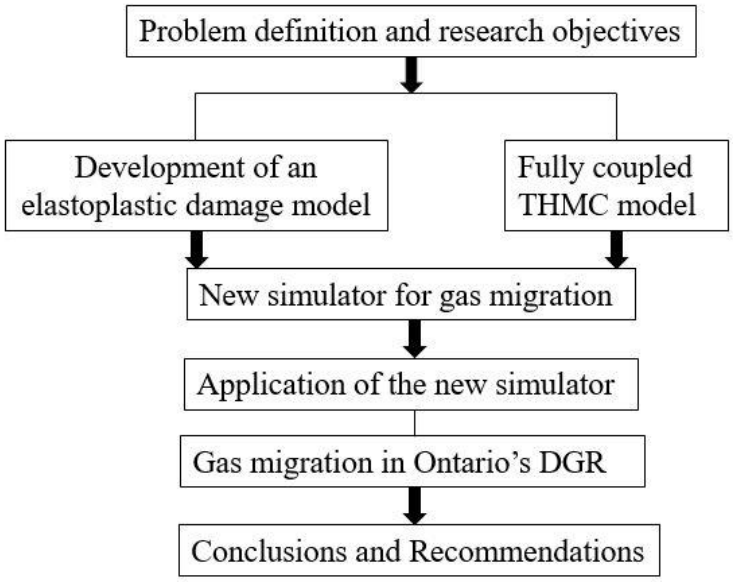

Figure 1.2 Research approach

1.6 Tasks and organization of the thesis

To achieve the tasks and objectives of this thesis, the manuscript is divided into seven chapters. Figure 1.3 shows the structure of the main tasks that have been carried out to achieve the specific objectives.

- **Chapter 1** is about the general introduction. It consists of the problem statement, objectives, and research approach and methods adopted in the research.
- **Chapter 2** includes a comprehensive literature review and/or background information about the deep geological repositories and nuclear wastes, THMC coupled processes in the porous media and also about the numerical codes COMSOL Multiphysics and TOUGHREACT.
- **Chapter 3** presents a literature review on previous studies on gas migration in host rock of DGR, which focus on the partial coupled processes (i.e., HM or THM) or fully coupled THMC and single code or coupled codes for the simulation.
- **Chapter 4** describes the geotechnical and geological characteristics of the study area. It is sub-divided into six sub-chapters. Section 4.1 introduces the geology of the repository; Sections 4.2, 4.3, 4.4 and 4.5 present the geomechanical, geochemical, hydrogeological, and geothermal characteristics of the DGR, respectively.
- **Chapter 5** focuses on the development of the fundamental multiphysics model and the fully coupled THMC model of gas migration in host rock of DGR for nuclear wastes, and proposes an innovative approach of coupling the two codes, COMSOL and TOUGHREACT, to develop a new simulator, COMSOL-TOUGHREACT.
- **Chapter 6** focuses on the modeling of gas migration in a DGR in Ontario's sedimentary rocks.
- **Chapter 7** analyzes the results from the study with emphasis on the results of the long-term safety of the DGRs and presents the conclusions and recommendations.

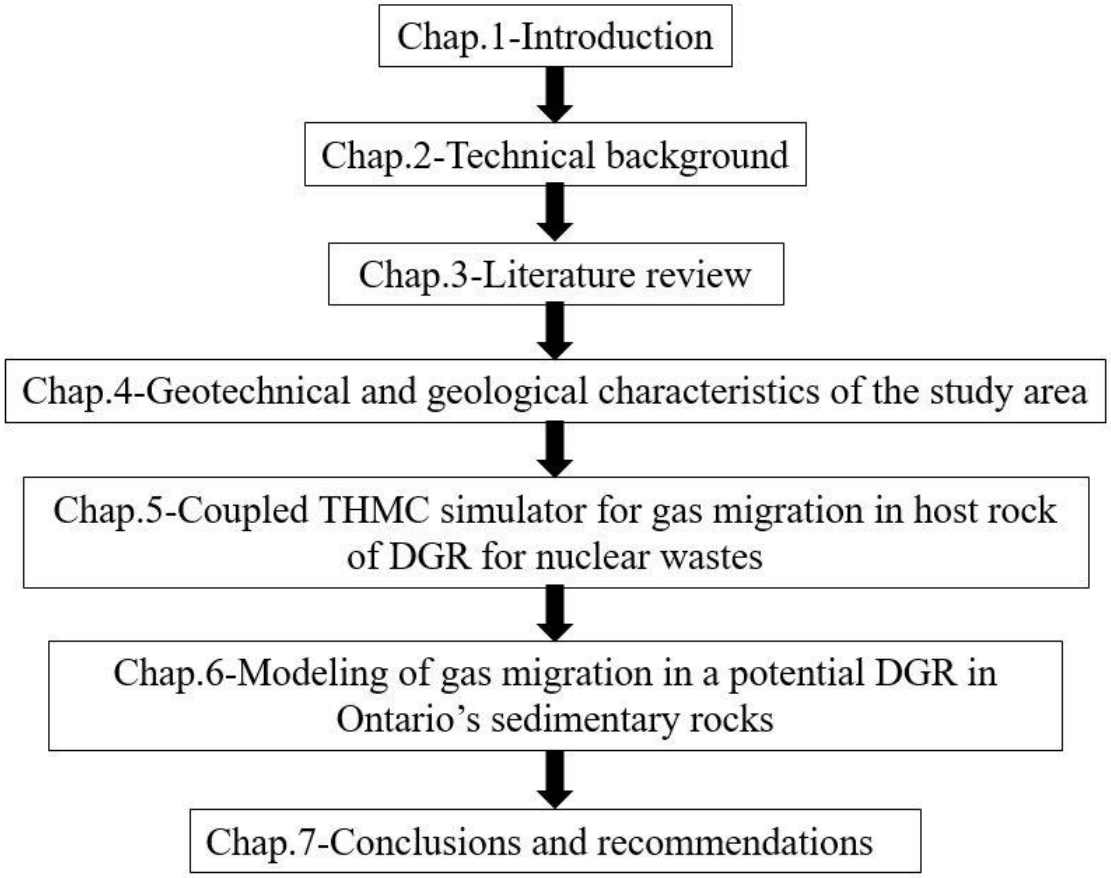

Figure 1.3 Tasks and organization of the thesis

1.7 Novel Research Contributions

Compared to other previous related research on gas migration in host rocks of deep geological repositories, thekey specific achievements and contributions of this study are summarized as follows:

1. An elastoplastic-damage model has been developed in this research that characterizes the mechanical behaviors of sedimentary host rock for DGR. This model takes into account the elastoplastic strain under the influence of mechanical damage. It is worth mentioning that this is the first time an elastoplastic-damage model has been built to describe the mechanical process of gas migration in the coupled THMC model. It is more accurate for the modeling of gas migration.

2. A novel Multiphysics-damage model (THMC-D) was developed to assess and predict the multiphysics processes of gas migration. For the mechanical processes, the elastoplastic damage model can describe the elastic degradation by damage. The coupled fluid flow and mechanical stresses influence the rock deformation and permeability, the pore water pressure, the diffusion coefficient and the variation of porosity. The variation of porosity was due to the rock deformation and/or the mechanical damage.

3. A novel numerical simulator (coupled COMSOL and TOUGHREACT) was developed for the simulation of gas migration in deep areas of the host rock. This research, which is applied with interdisciplinary programming, established the connecting and coupling of the two softwares by using an external tool, MATLAB, as a bridge. The whole program can perform data exchange, analysis and visualization. The numerical simulator is continuously optimized and improved based on the operating speed. This new simulator, with comprehensive functions from COMSOL and TOUGHREACT, can simulate gas migration with greater flexibility and efficiency.

4. New and useful insights for understanding of gas migration in the potential host sedimentary rocks of a DGR for the LILWs in southern Ontario have been obtained. It was found that both permeability and porosity of the host rocks will increase with a rise in the pore gas pressure. The porosity gradually decreased with an increase in the distance from the top of the repository. Rock permeability changes result from changes in porosity. Under high gas injection pressure, gas migration can reach the shallow rock formation, which means that the gas generation (worst case scenario) and migration could influence the safety assessment (SA) to a degree, and such should be taken into consideration for the SA of the deep geological repository.

CHAPTER 2 Technical Background

2.1 Introduction

To provide a better understanding of the methods used in this thesis and the results presented, a review of the fundamental theoretical and technical background information on DGR, nuclear wastes and THMC coupled processes in porous media is provided in this chapter. Moreover, background information on the two numerical codes or software used in this thesis is given.

2.2 Deep geological repositories

Usually, a nuclear waste repository is excavated deeply within a stable geologic environment. This concept of deep geological repository has been proposed since the 1950s.

As a preferred option for nuclear waste disposal, the DGRs should isolate the long-lived radioactive wastes from humans and the environment for a very longtime from tens of thousands to a million years. DGR can reduce releases of the contained radioactivity into the environment (Feiveson, et al., 2011). Generally, a DGR facility includes surface and underground facilities, access and ventilation shafts, radioactive waste, containers enclosing the waste, other engineered barriers or seals around the containers, the tunnels housing the containers, and the geologic makeup of the surrounding area. The concept of a DRG facility is shown in Figure 2.1. The safe long-term disposal of the radioactive wastes in a repository and their isolation from the biosphere are guaranteed by a multi-barrier system consisting of natural barriers (host rocks) and an Engineered Barrier System (EBS). When considering the performance expectations of the DRGs, they should satisfy a range of geological and hydrogeological features of the proposed storage site (NWMO, 2011A), including but not limited to: site predictability, multiple natural barriers (low permeability), low natural resource potential, diffusion dominated contaminant transport (i.e., no evidence of glacial perturbation or cross- formational flow), and others.

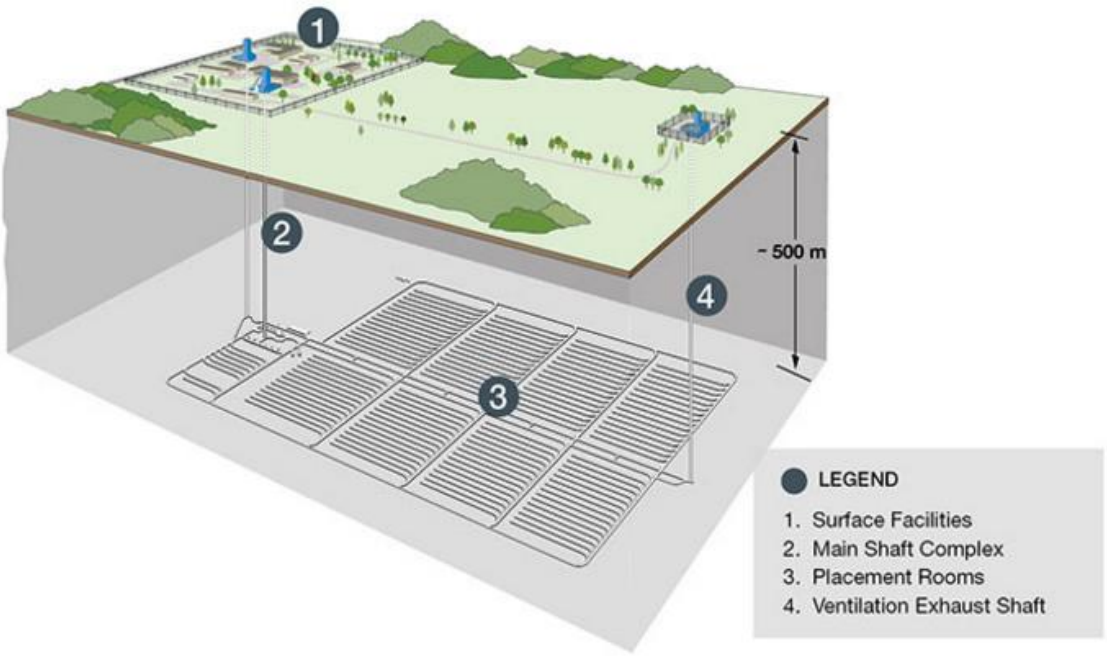

Figure 2.1 Concept of a DGR facility (Noronha, 2016)

2.3 Nuclear wastes and gas generation in repositories

Generally, the major sources of radioactive wastes are produced by electricity generation and military activities (Miller et al., 2000). In addition, numerous applications in the fields of medicine, industry and scientific research generate a small amount of radioactive waste (NAGRA, 2016). For the purpose of disposal, International Atomic Energy Agency (IAEA) classifies the radioactive wastes into the following categories (IAEA, 2009):

- Exempt waste (EW): the waste is qualified in the criteria of clearance exemption or can be excluded from regulatory control.
- Very Short-Lived Waste (VSLW): the waste can decay in a limited period of up to a few years.
- Very Low-level Waste (VLLW): the waste does not need to meet the criteria of EW, but needs to be isolated in a high-level containment.

- Low-Level Waste (LLW): the waste is above the clearance level but with limited amounts of long-lived radionuclides. This kind of waste needs robust containment for isolation for periods of up to hundreds of years.
- Intermediate-Level Waste (ILW): the waste requires a greater degree of containment for the isolation because of the content of long lived radionuclides. Moreover, it needs repositories to be located tens of meters to hundreds of meters below the ground surface. However, the ILW does not need to consider the heat dissipation during its storage and disposal.
- High-Level Waste (HLW): the waste contains enough high-level activity concentration that can generate significant quantities of heat during the radioactive decay process. Alternatively, the waste contains large quantities of long-lived radionuclides. It needs to be stored in deep disposal repositories several hundreds of meters below the surface.

For the disposal or management of radioactive waste, two main aspects of the radionuclides should be considered: the amount of activity and the half-life period. From the consideration of these two major aspects, and to protect humans and the environment from radiation risk, there are seven options for the radioactive waste disposal as below (Miller et al. 2000):

- storage until activity levels decay to below exemption limits
- disposal into space
- disposal in polar icecaps
- disposal on or beneath the seabed
- nuclear transmutation
- shallow land burial
- deep geological disposal

A variety of processes can contribute to gas generation in repositories. The primary mechanisms for gas generation are corrosion of metals, radiolysis of water and other

organic matter, and microbial degradation. Because LLW and ILW repositories contain larger amounts of metals and organics than HLW repositories, gas generation rates are likely to be higher in the former repositories (Fall et al. 2014).

2.4 THMC coupled processes in porous media

2.4.1 Introduction

THMC processes are one of the most important phenomena in geotechnical and environmental engineering. In this section, a brief explanation of the governing interactions of the THMC processes in porous media will be provided. THMC processes play an increasingly important role in the field of rock and soil mechanics and engineering, such as deep nuclear waste repositories, oil/gas production and storage, landslide, and slope stability (Tsang, 1987).

2.4.2 Coupled THMC processes

Coupled THMC processes are complex in that one process can affect the initiation and process of the others (Jing and Feng, 2003). It implies that, for the evolution of the whole processes, it may result in misunderstanding of the study if considering the processes individually and independently. For the study of the THMC models in a clear way, it is necessary to adopt the method of two-way interactions among thermal, hydraulic, mechanical and chemical components. For each process, there is a 'direction' that the 'origin' can impact the 'object' (Jing and Feng, 2003). For example, in the MH coupled processes, "M" is an origin and may affect "H" by the effects of stress-deformation-damage on matrix porosity and permeability. While in the HM coupled processes, the hydro factor (H) may affect the mechanical factor (M) in different process rates or strength (e.g., capillary and swelling pressure-relative saturation) (Jing and Feng, 2003). It means that $MH \neq HM$.

The coupled THMC processes considered here are illustrated by Figure 2.2. Because it is impractical to include all existing processes in the model for the simulation due to the site size and complexity of the computational problems, only strong coupling processes, which

are relevant for the long-term stability, are considered in this study, and the weak coupling is ignored (Hudson et al., 2005). Some of the important processes in the porous media are: thermal (T, e.g., temperature, heat generation, heat transfer), hydraulic (H, e.g., water flow, gas flow, pore fluid pressure, phase change), mechanical (M, e.g., stress, deformation, damage) and chemical (C, e.g., dissolution, precipitation) processes.

In Figure 2.2, M-mechanical process include stress (σ), strain (ε), strength (S_t) and damage (D) of the rock matrix. H-hydraulic process include fluid pressure (p), velocity (V), saturation or relative saturation (S), density (ρ) and viscosity (ν), matrix porosity (φ), permeability (K). T-thermal processes comprise primary variable of temperature (T), dissipated energy (W) and C-chemical processes include property (T_p), transport path (P_t) and reaction rate R. Δx means change in variable or property x. Because of the insignificant influence from the chemical reactions toward the temperature for the current research, this coupling of the $C \rightarrow T$ process is not further elaborated.

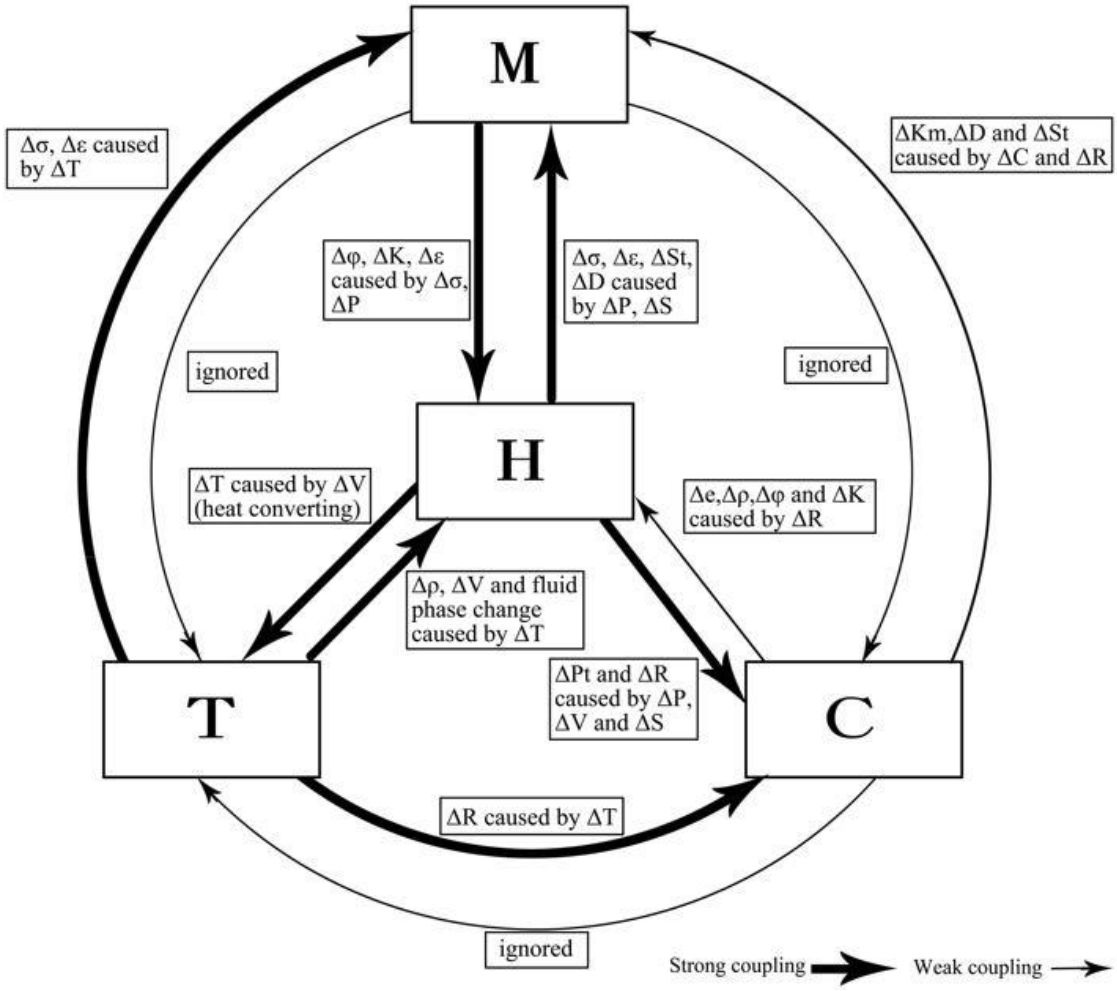

Figure 2.2 Fundamental mechanisms of THMC coupling processes considered in the developed numerical simulator (Jing and Feng, 2003)

2.5 Simulation Tools

The new simulator developed in the study is based on the coupling of COMSOL and TOUGHREACT. Both pieces of software are extensively verified and widely used in their relevant fields. The softwares are briefly described below.

2.5.1 COMSOL

COMSOL Multiphysics is an interactive environment for modeling and solving many kinds of scientific and engineering problems, from one type of physics into multiphysics

models. It can solve coupled physics phenomena simultaneously (COMSOL Multiphysics User's Guide, 2012). It can be used for modeling and simulating the physics-based system. By using COMSOL Desktop graphical user interface (GUI) and a set of predefined user interfaces of associated modeling tools, COMSOL Multiphysics can be used to build models of comprehensive applications. With a suite of add-on products, this simulation platform is expanded to model specific application areas and interfacing with the third-party software and their abilities. The software enables the straightforward implementation of user-defined constitutive models, such as variable material properties and stress-strain relations. Detailed technical information and data on COMSOL Multiphysics is available in COMSOL (2012). There is no existing model in COMSOL Multiphysics for THMC simulating gas migration in DGR under the influence of the THMC processes that occur in DGR.

COMSOL has built-in physics interfaces and advanced properties for building models. Applying the variables of the relevant physical quantities like material properties, loads, sources and fluxes, even the underlying equations to the solid and fluid domains, boundaries, edges, and points of the computational mesh. COMSOL Multiphysics is complied with a set of corresponding equations for the entire model (COMSOL Multiphysics User's Guide, 2012).

By using the physics interfaces, it can simulate the types of studies as follows (COMSOL Multiphysics User's Guide, 2012):

- Stationary and time-dependent (transient) studies
- Linear and nonlinear studies
- Eigen frequency, modal, and frequency response studies

The THMC coupled model of gas migration is time-dependent. In every time step, COMSOL and TOUGHREACT will transfer and exchange the updated data by MATLAB by using the function of APIs (Application Programming Interfaces). By using Java to program, APIs can drive the software by complying object oriented code. LiveLink for MATLAB can make the connection between COMSOL Multiphysics and other software.

COMSOL has the function of exporting results and generating reports in text files. By using this function, the data transmission and exchange can be realized between COMSOL and TOUGHREACT.

2.5.2 TOUGHREACT

Based on the existing multi-phase fluid and heat flow code TOUGH2 (Pruess, 1991), Xu and Pruess (1998) released the first version of TOUGHREACT with the introduction of reactive geochemistry. Compared with TOUGH2, TOUGHREACT was improved in the following aspect (TOUGHREACT User's Guide, 2006):

- Disposal of mineral-water-gas reactive-transport under the conditions of boiling
- An enhanced HKF (Helgeson-Kirkham-Flowers) activity model for aqueous
- The calculation of gas species diffusion coefficients will be a function of pressure, temperature, and molecular properties
- The formulations for mineral reactive surface area of fractured and porous media
- The changes of porosity, permeability and capillary pressure by mineral precipitation/dissolution (Sonnenthal et al., 1998, 2000, 2001; Spycher et al., 2003a)

TOUGHREACT includes all the previous extensions to TOUGH V2 (Pruess, 1991) and TOUGH 2. TOUGHREACT is a comprehensive non-isothermal multi-component reactive fluid flow and geochemical transport simulator. It can model the coupled subsurface multiphase fluid and heat flow, solute transport, and chemical reactions. The coupling function can be used on many geologic systems and environmental problems (e.g., geothermal systems, nuclear waste disposal in deep area, groundwater quality and etc.). Under the complex thermo-hydrological and geochemical underground situations of pressure, temperature, water saturation and ionic strength, the thermo-hydro-chemical (THC) processes can be simulated in TOUGHREACT (TOUGHREACT User's Guide). One of the powerful capabilities of TOUGHREACT is that it can simulate a variety of chemical reactions (e.g., aqueous complexation, gas dissolution/exsolution, and cation exchange). In unsaturated systems, the coupling of mineral dissolution/precipitation and the changes of porosity, permeability, and capillary pressure can occur in local equilibrium

or kinetic controls. TOUGHREACT has been tested and verified in a variety of different areas by several researchers, such as Dobson et al., (2004), Singleton et al., (2003), Xu et al., (2003a), and Xu et al., (2003b and 2004). TOUGHREACT is a 'self-documenting' program. It provides 'EOS' (Equation-Of-State) modules as the sample problem. With a range of input data files and the benchmarks for the code installation, TOUGHREACT provides a self-teaching method for coupling processes.

CHAPTER 3 Literature review on gas transport mechanisms and previous studies on gas migration in host rock of DRG

3.1 Introduction

During recent decades, theoretical research, numerous experimental and modeling studies have been conducted to assess and understand gas migration in host rock for DGR (Grupa and Schröder, 2009; Haijtink and Rodwell, 1998; Manai, 1997; Noriis, 2015; Ortiz et al., 1997; Rodwell, 1998; Rodwell et al., 2003;) (Justinavicius, 2016). There were a series of reports or technical documents about gas migration: e.g., Bate et al., 2006; Goodfield and Rodwell, 2001; Goodfield et al., 2000; Hoch, 2005; Hoch et al., 2003; Hoch et al., 2002; Hoch et al., 2001; McCarthy et al., 2001; Mott and Rodwell, 1998; Nash and Rodwell, 2000; Nash et al., 2000; Nirex, 2006d; Nirex, 2006g; Nirex, 2000; Rodwell and Goodfield, 2000; Rodwell and Nash, 1992; Stenhouse and Grogan, 1991. In order to estimate the rock permeability, some laboratory experiments with a view to gas transport behaviour have been carried out on argillaceous rock specimen over the last decades (e.g., Boisson et al., 2001; Zhang & Rothfuchs, 2004; Marschall et al., 2005; Davy et al., 2007; Popp et al., 2007 and Yang et al., 2010). Shao & Schuster (2009) performed *in-situ* borehole gas migration experiments to study the hydraulic properties of the Opalinus Clay at different gas pressures. There were only few large-scale gas injection tests that were carried out to investigate the gas migration processes during the closure phase of the nuclear waste disposal repository (Xu, 2013). For example, the HG-A test was performed in the Mont Terri Rock Laboratory (Marschall et al., 2006 ans Tsang et al., 2012). A Gas Migration Test (GMT) (at the Grimsel site in Switzerland) was carried out to study the gas migration through the engineered barrier system.

Jockwer (2000) summarized the experimental studies on gas migration in granitic and argillaceous rocks. Volckaert et al. (1995) overviewed the modelling and experiments on gas migration in repository host rocks. The project studied the phenomena of chemical reaction, diffusion, two-phase flow and the creation of preferential pathway. Zhang (2015) investigated gas migration in damaged and resealed claystone. As a potential escape route for gases, the Excavation Damaged Zone (EDZ) of gas-flow behavior in his research was characterized, understood and predicted. Fall and Nasir (2012) carried out a comprehensive study on numerical modelling of gas migration from a DGR in Ontario's sedimentary rocks, to evaluate the disturbances of the host rock impacted by gas generation and to perform

scoping calculations for gas migration. Neretnieks (1984), Kreis (1991), Askarieh et al. (2000), Ekeroth et al. (2006) and Smart et al. (2006) build appropriate conceptual models to predict the gas migration in argillaceous materials of the geological disposal system (Cuss et al., 2014).

Mont Terri rock laboratory (Canton of Jura, Switzerland) has been devoted to the study of the evolution of a repository and investigates processes related to the safety functions of a repository hosted in a clay rock in the last 20 years (Bossart et al., 2017) and published 20 papers about this special issue (Hostettler et al., 2017; Nussbaum et al., 2017; Jaeggi et al., 2017; Yu et al., 2017; Clauer et al., 2017; Mazurek and de Haller, 2017; Amann et al., 2017; Marschall et al., 2017; Ziefle et al., 2017; Schuster et al., 2017; Abednego et al., 2017; Wieczorek et al., 2017; Gens et al., 2017; Müller et al., 2017; Maeder et al., 2017; Necib et al., 2017; Leupin et al., 2017a; Bleyen et al., 2017; Vinsot et al., 2017;Leupin et al., 2017b). Croisé et al. (2006) and Marschall et al. (2003) carried out the gas threshold pressure tests in the Mont Terri Rock Laboratory.

There were also some other organizations that carried out research to describe and model the gas evolution and migration in the deep geological repository. The Fate of Repository GasEs (FORGE) project (2009) was committed to solve the gas generation and migration issues of the repository by linking the international organizations of radioactive waste management, the regulators and the academia. By carrying out a series of laboratory experiments and field-scale tests, this project would lower the uncertainty factors during the process of quantitative gas treatment. A large-scale gas injection test (Lasgit) was conducted to study the influence of gas accumulation and migration through the engineered barrier system (Sellin, 2014; Shaw, 2015b). By carrying out a series of laboratory experiments and field-scale tests on gas transport processes through host rocks and engineered barriers, it was found that above a certain level of gas pressures, the preferential pathways caused by pressure and the clay dilation would be generated with the gas flow (Harrington and Horseman, 1999; Horseman et al., 1999, 2003; Graham et al., 2012; Harrington et al., 2012, 2017; Cuss et al., 2014; Sellin, 2014; Bennett et al., 2015 Dagher et al., 2018). In order to fully understand gas migration of the repository in clay formation, the international multiphase flow simulation benchmark Couplex-Gaz (Talandier, 2007a;

Talandier, 2007b) was published in 2007. The Couplex-Gaz increased the confidence into the numerical tools for the two-phase flow modelling and evaluated some critical parameters like the maximum gas pressure in the repository, the saturation around the containers and water flux induced by gas. According to the observation of the experiments, the GAMBIT Club programme was aimed to build a computational model to simulate the gas migration through compacted bentonite (Nash et al., 1998). Fall et al. (2014) established a coupled hydro-mechanical-damage model to simulate the gas migration in host sedimentary rock for the nuclear wastes repository under the high pressure condition. The coupled model can predict the gas migration and its influences on the host sedimentary rock. The limitation of this model was that it did not consider the plastic mechanical behavior of the rock. Nguyen and Le (2015) established a numerical model to simulate the gas migration in Opalinus clay with the consideration of the elastoplastic behavior. This model can predict the gas migration against the laboratory experiments and *in-situ* gas injection tests. While there was also some space to improve the model reliability for the last phase of gas flow controlled by macroscopic fractures (Dagher et al., 2018).

In order to predict and analyse the REP experiment carried by ANDRA (2000) and Ozanam et al. (2000) investigated the hydro-mechanical response of the argillite to shaft sinking, the European research project MODEX-REP was started in October 2000. In the framework of the MODEX-REP project, a series of laboratory experiments were carried out in Meuse/Haute-Marne Underground Research Laboratory (MHM-URL) in Eastern France. These laboratory experiments provided basic data for the modelling the hydro-mechanical response of the argillite to shaft sinking, and proved the suitability of Callovo-Oxfordian argilaceous formation for the disposal of high-level and long lived radioactive nuclear wastes. A laboratory test programme in the framework of the project was performed by the Gesellschaft für Anlagen-Und Reaktorsicherheit (GRS) for the sake of determination of the material parameters of different constitutive models which could be used in numerical simulations of the international project participants (MODEX-REP Mid-Term Report, 2002). In the laboratory programme, the short-term mechanical behavior of the argillite was deterimined by the uniaxial and traixial compression tests and the long-term behavior was examined by the uniaxial creep and relaxation tests (Zhang and

Rothfuch (2004)). In following chapter, a literature review of gas transport paths and mechanisms, as well as of the main previous modeling studies is provided.

3.2 Gas transport paths and mechanisms

Due to groundwater chemistry and the disposal repository system hydrodynamics, the gas generated within the repository could dissolve in the groundwater (Rodwell et al., 2003), which will result in the dissipating pressure rising and the ensuing consequences. Except the hydraulic and mechanical properties of the rock mass (intrinsic permeability, porosity and rock strength), gas transport is also controlled by the gas pressure at the generation locus and the rock hydromechanical state (i.e. water saturation, porewater pressure, stress state) (Marschall et al, 2005). Hence, it is necessary to study the potential gas transport paths in a repository system. According to gas pressure level and the relationship with external stress applied, gas migration processes can be divided into four phases (Marschall et al., 2005; NAGRA, 2008; Dymitrowska et al., 2009; Yu and Weetjens, 2009; Guo and Fall 2018, 2019) (Figure 3.1).

1. Advective-diffusive transport of gas dissolved,
2. Visco-capillary two-phase flow,
3. Dilatancy-controlled gas flow
4. Gas transport along macroscopic tensile fractures (hydro-and gas-fracturing).

For any of the mechanisms mentioned above, although small-scale heterogeneities may have a distinct influence on the gas transport on a large-scale (NAGRA 2008), it is impossible to resolve heterogeneities in sufficient detail, since it requires an accurate numerical simulation. Therefore, simplification of the models of the flow processes is necessary for sufficient consideration of heterogeneities (Dagan 1989, Gelhar 1993, NAGRA 2008).

- **Advective-diffusive transport of gas dissolved**

With the continued increase in gas production rate during the repository post-closure phase, the generated gas would initially be transported by advection/diffusion in a dissolved state.

Under the influence of pressure and gravitational forces, gas advection and diffusion dissolved in pore water is governed by Darcy's law. Because of the concentration gradients, Fick's law can describe the diffusion of dissolved gas and the solubility of gas in pore water. It is noted that if the host rocks are clay, mud rock, or salt, advection is not obvious to the dissolved gas transport (Fall and Nasir, 2012).

- **Visco-capillary two-phase flow**

Once the rate of gas production is higher than the solubility limit, a free gas phase forms; the gas attempts to displace water through the largest pore in the rocks (Fall et al. 2014). This gas transport mechanism is governed by two-phase flow controlled by the visco-capillary system (Marschall et al, 2005). Worgan (1990) proposed scoping calculations on hydrogen gas dissolution and diffusion. In this method, it is indicated that the interaction of a free gas phase with pore-water is usually examined in two-phase system models. Usually the two-phase system is composed of miscible fluids and immiscible fluids (Volckaert et al., 1995). For miscible fluids, one fluid dissolves and is transported by the other. For the immiscible liquid, each fluid flow is under the impacts of pressure, gravity, viscous and inertial forces. To describe the gas and liquid flow, the equations of mass and momentum balance are modelled with the supplemented equations of fluids state, capillary pressures and relative permeability (Volckaert, et al., 1995). It is assumed in this research that the gas phase is an ideal gas and water is incompressible (Preuss, 1987; Bixler, 1985; Hadley, 1985).

- **Dilatancy-controlled gas flow ("pathway dilatation")**

With high gas transport capacity, dilatancy-controlled gas transport is a coupled hydro-mechanical transport mechanism. Because the speed of two-phase flow transportation is not quick enough, microscopic gas pathways may form by the reason of poroelastic variations under the condition of increasing gas pressure (Alkan and Muller 2008). There are two factors that can determine the critical level of pressure: the strength of the host rock and local stress conditions around the emplacement caverns (NAGRA, 2008, Fall and Nasir, 2012).

- **Gas transport along macroscopic tensile fractures (hydro-and gas-fracturing)**

Usually when gas pressure is higher than the sum of the minimum principal stress and the tensile strength of the medium, a macroscopic tensile fracture will be formed. Gas flow occurs as a single-phase flow in the macroscopic tensile fracture. In the excavation disturbance zone (EDZ) around underground repository excavations, the extensile fractures are dilated, which can lead to the gas permeability being enhanced. Apart from the hydro-mechanical coupled process, the hydro-chemical interactions may greatly influence gas permeability. The coupled hydro-chemical interactions that will impact the gas permeability are presented as follows (Fall and Nasir, 2012):

- The reaction of pore water with clay
- The reaction of clay pore water with cement
- The interaction of waste with cement pore water
- Chemical reactions in the unsaturated rock zone during construction period

The mechanisms of the gas transport are impacted by several aspects: the gas pressure, the minimum principle stress (σ_3) and the formation of the related hydro-mechanical properties (e.g. P_{ae} - gas entry pressure, T_{rock}-tensile trength of the rock) (Nagra 2004). Figure 3.1 shows the subdivision of the basic transport mechanism and the analysis of gas transport processes in Opalinus Clay (Nagra, 2002a, Marschall et al, 2005). For the gas migration in a geological repository, there are four periods to describe the whole sequence of the processes in Figure 3.2 summarized by Mallants and Jacques (2004) and Mallants et al. (2007).

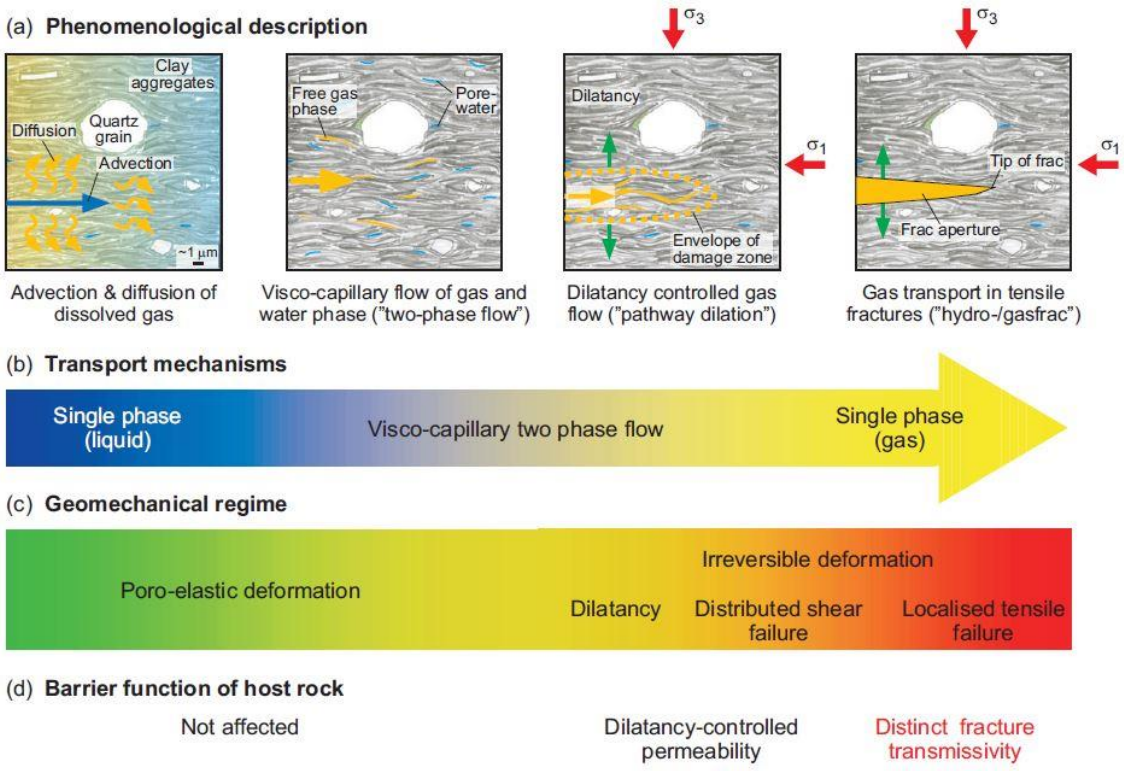

Figure 3.1 a) Phenomenological description of gas migration processes based on the microstructural model concept (Nagra, 202a); b) Gas transport mechanisms; c) Geomechanical regime; and d) Gas transport effect on the barrier function of the host rock (Marschall et al, 2005).

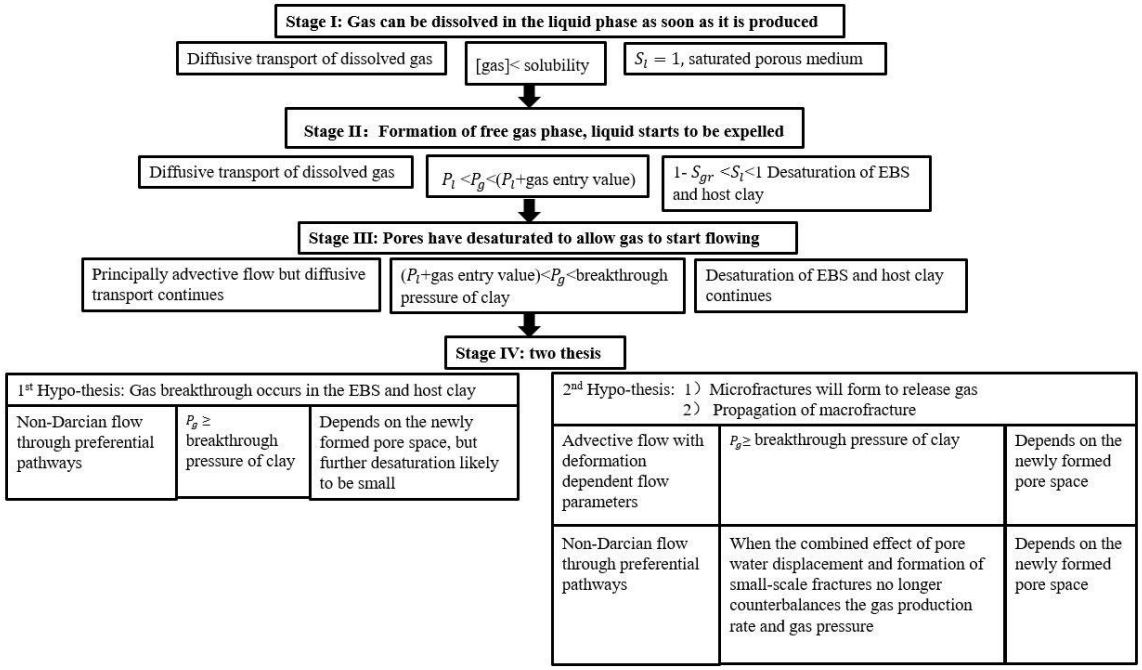

Figure 3.2 Summary of different period of gas migration (FORGE, 2010)

There is no definite conclusion which can accurately predict the changes in rock properties when the gas pressure keeps increasing in the host rock. Since the generated gas cannot be evacuated by advective gas flow synchronously because of the low rock permeability, Mallants and Jacques (2004) proposed when the increasingly gas pressure surpasses the minimum principal tensor, a preferential pathway perpendicular to this tensor will be created. The gas pressure will then reduce rapidly since the open, highly conducting preferential pathways have formed. The cracks trend to be closed due to the self-sealing capacity after the gas pressure fell off. After the decreasing gas pressure reaches the level of the gas breakthrough threshold, it will increase again. The cyclic processes of the preferential flow paths opening and closing will continue until all the generated gas can be dissolved in the pore water and evacuated by the pore medium. Another probability is proposed by NAGRA (2008). When the accumulated generated gas pressure is higher than the minimum principal stress, the microcrackes will form in the host rock. It will lead to the intrinsic permeability and the retention curve change by the increased porosity. The macrocrackes will be produced when the micro-cracks cannot counterbalance the generated gas anymore. However, the gas flow still suit for the continuous two-phase flow model

since there are no discontinuous pore network created. This kind of two-phase flow is deformation and time dependent.

3.3 Models for gas migration

In recent decades, the development of modelling approaches has gained significant relevance for the prediction and simulation of gas migration in the host rock of repository systems, especially in clay formation (Fall, 2009). Several models and approaches have been developed or adopted for the multicomponent gas phase transport in the subsurface systems, especially for predicting gas migration in repository systems. Darcy's law gives the key formulation for the transport of gases, either dissolved in the liquid phase or in free phase with the liquid phase. But the limitations of Darcy's formulation for modeling fluid flow in clay rock formations are noted (Alkan and Müeller (2008). In this sub-chapter, the main approaches for gas transport in DGR systems or porous media are briefly discussed. Previous modelling studies on gas migration in engineered barrier materials or natural barriers (host rocks) of DGR are comprehensively described in Guo and Fall (2021a,b,c) and Yang and Fall (2021a,b,c).

3.3.1.1 Continuum modeling

Usually, the continuum models are used in areas such as oil and gas recovery and storage, geothermal systems, and industrial processing.

Advective-Diffusive Model (ADM) (Ho and Webb, 2006)

For the ADM model, by using the phenomenological flux laws, the contributions of advective and diffusive are evaluated separately. The following equation of a multiphase version of Darcy's law shows the advective gas flux.

$$\mathbf{F}_g = \rho_g \mathbf{u}_g = -k \frac{k_{rg}\rho_g}{\mu_g} (\nabla \mathbf{p}_g - \rho_g \mathbf{g}) \tag{3.1}$$

where: $\mathbf{F}_g$: advective gas flux

$\mathbf{u}_g$: volume flux

k: liquids absolute permeability

ρ_g: gas density

k_{rg}: relative gas permeability

μ_g: gas-phase viscosity

$\nabla \mathbf{p}_g$: gas-phase pressure gradient

As a material constant, it will depend on the gas pressure as the following equation described (Klinkenberg, 1941):

$$k = k\infty(1 + \frac{b}{P_g}) \tag{3.2}$$

where: b: Klinkenberg coefficient and P_g: gas-phase pressure.

Diffusive transport is modeled as Fickian diffusion in the gas phase in the ADM. In the TOUGH2 code, the diffusive flux is written as

$$\mathbf{j}_g^k = -\phi\tau_0\tau_g\rho_g D_g^\kappa \nabla X_g^\kappa \tag{3.3}$$

where: ϕ: porosity

$\tau_0\tau_g$: tortuosity, τ_0 a porous medium dependent factor

$\mathbf{j}_g^\kappa$: diffusive flux of component κ

D_g^κ: diffusion coefficient of component κ

X_g^κ: mass fraction of component κ in the gas.

$\tau_g = \tau_g(S_g)$, S_g gas phase saturation,

Dusty gas model

The Dusty gas model describes the porous medium as a collection of giant spherical molecules, which is held by external force. The kinetic theory defines the gas molecules between dust particles. ŠolcovÁ and Schneider (2006) gave more details about the dusty gas model.

3.3.1.2 Approaches related to Darcy's law

The models built based on the Darcy's law or the precursors like Navier-Stokes equations are discussed in this section.

Capillary bundle model

Ortiz et al. (1996) proposed a capillary bundle model to simulate a two phase (gas and water) flow through a clay host. In addition, he verified that the simulation results obtained from this model were nearly consistent to the experimental data. Figure 3.3 describes the principle of the model. A Navier-Stokes equation as follows shows the gas-water interface *R (r,t)* (Alkan and Mueller, 2008):

$$R^2(r,t) = \tau^2 L^2 - \frac{t}{4\mu_w}\left(r^2\left(p_g - p_w\right) - r\sqrt{2\gamma}\right)$$
$$0 \le R(r,t) \le \tau L \qquad (3.4)$$

where: $R(r,t)$: gas-water intherface equation, τ: tortuosity; τL: length of each capillary, t: time, μ_w: water-phase viscosity, P_g: gas pressure, P_w:water pressure, r: radius and γ: capillary pressure.

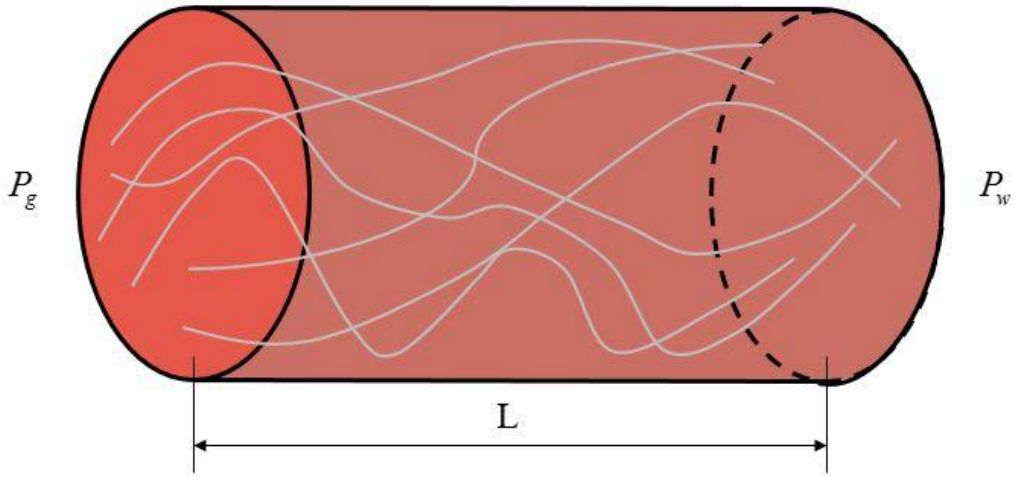

Figure 3.3 Schematic of the capillary bundle model (Oritiz et al., 1996)

In this model, it is supposed that the porous medium is made of a series of intersecting capillaries. The uniform γ and tortuosity (τ) are the characteristics of this model. The number of capillaries per unit cross sectional area of core is expressed by $N(r)dr.r$ is during the range of $[r, r + dr]$. τL is the length of each capillary (Fall and Nasir, 2012).

Only if the gas pressure is higher than the combined water and capillary pressure, will the capillary begin to desaturate. The smallest capillary pressure (r_s) can be calculated by the equation of (3.5)which based on the capillary pressure concept.

$$r_s = \frac{\gamma\sqrt{2}}{(p_g - p_w)} \tag{3.5}$$

Brush model

Brush model was proposed by Lege and Shao (1996), and it focused on considering matrix diffusion of clay formations. This model is executed by the computer code Rockflow. Figure 3.4 shows the principle of the model. The porous media in this model is assumed as a fractured medium geometrically (Fall and Nasir, 2012).

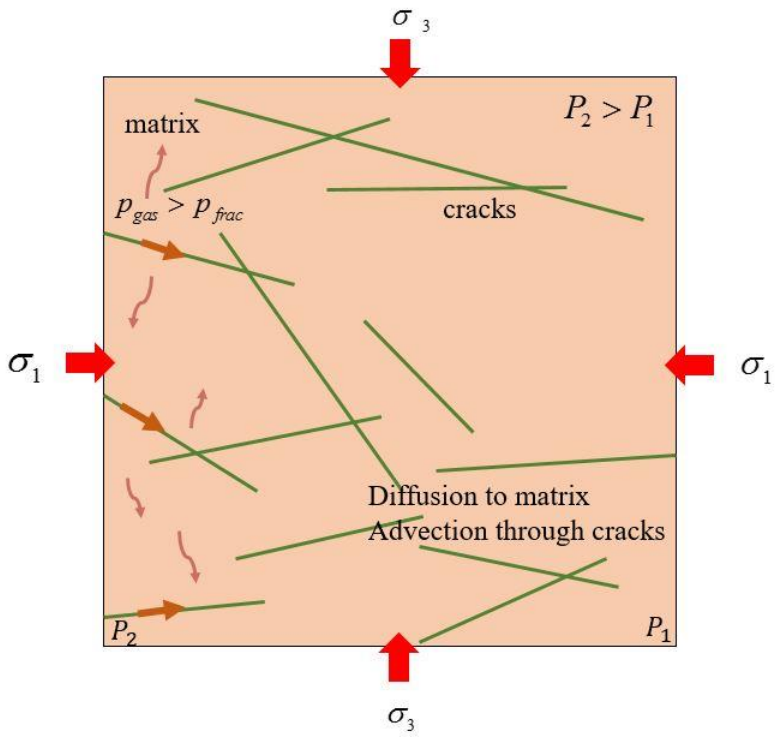

Figure 3.4 The mechanisms of transport in fractures geological media (Alkan and Müeller, 2008)

It is assumed that there is no retardation of the advective-dispersive. The transport is modeled using the 2-D advective-dispersive equation (Alkan and Mueller, 2008):

$$\frac{\partial c}{\partial t} = D_L \frac{\partial^2 c}{\partial x^2} + D_T \frac{\partial^2 c}{\partial y^2} - \frac{v_D}{\phi_c}\frac{\partial c}{\partial x} \tag{3.6}$$

where c is the solute concentration (mg/l). The tracer velocity (v_D/ϕ_c) is enough high as the D_m (molecular diffusivity) and it does not have the obvious contribution to D_L (longitudinal dispersion coeffieicents) and D_T (transversal dispersion coefficients) (Alkan and Müeller, 2008). Alkan and Mrüeller (2008) applied the model for water-tracer transport.

3.3.1.3 Modified Darcy approaches

Due to the limitations of the Darcy's law (e.g., not suitable for non-linear flow), some efforts have been made for coupling non-linearities based on modifying Darcy's law. Alkan

and Müeller (2008) pointed out that the geomechanical influences have the leading function for controlling the shape of the pathway. For example, when the gas pressure exceeds the local effective stress, the micro-fracture will be enlarged.

Planar pathway model

Horseman and Harrington (1997) proposed the planar model (Figure 3.5) to determine the flow rate by using the cubic law that derived from the Poiseuille equation. Alkan and Müeller (2008) assumed the pore of the pathway is a function of the applied stress (σ) and pore pressure (p_g):

$$b = f(\sigma - p_g) \tag{3.7}$$

The flow pathway is closured ($b=0$) by the result of the critical value ($\sigma - p_g$), which is verified by the sealing criterion.

$$q = 0 \ \ for \ \ (\sigma - p_g) > (\sigma - p_g)_{crit} \tag{3.8}$$

The sealing criterion will not be satisfied when the fluid pressure is progressively increased.

where: q: gas discharge, σ: overburden (confining stress).

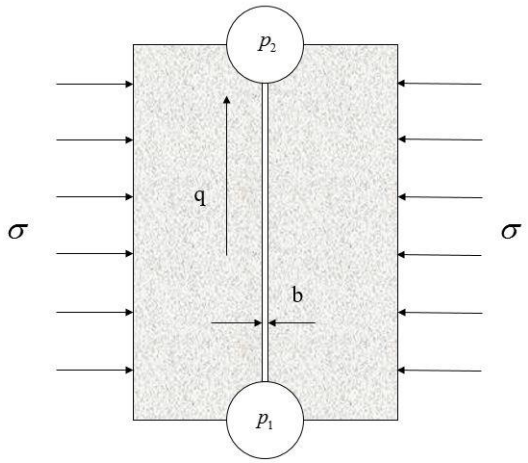

Figure 3.5 Simple schematic model of pathway flow in clay formation (Horseman and Harrington, 1997)

Multiple front propagation model

Brown (1999) presented a MFPM (multiple propagation model) with simpler dynamics on cylindrical clay cores. It emulates the micro-structural heterogeneity of the medium by using random independent gas pathways. This model predicts gas pressure, gas and water fluxes.

The MFPM is composed of two parts: outer part (handling changed experimental pressures), inner part (managing gas migration through the sample core) (Brown 1999). Based on the mass conservation and Poiseuille flow equations, the model can simulate wetting and non-wetting fluids (Alkan and Mueller, 2008).

The model is implemented within QuantiSci's uncertainty shell (QUEST) on a PC. As the model contains time stepping, it can be implemented to vary the experimental pressure stress by using a piecewise constant manner. The parameter values can be defined or uncertain in QUEST shell or can be set as a function of other parameters (Brown, 1999).

3.3.1.4 Models for gas flow through EDZ

Duppendecker et al. (1997) proposed a model for gas-oil migration in shales with the dilation behavior of gas pathways. The theoretical basis of this model is based on linear elastic fracture mechanics (Alkon and Müeller, 2008). Johnson et al. (2005) represented a simplified model for corrosion gases evolution and migration, which was used for an underground nuclear waste disposal system in Finland. This model realized the simulations of gas generation, pressure build-up, draining of pore water, gas dissolution and diffusion in the pore media, capillary leakage within fractures, the development of gas pathways, and the enhanced transmissivity by gas breakthrough (Fall and Nasir, 2012). Figure 3.6 shows the schematic of different gas transport routes. When the corrosion gas pressure develops more than the sum of pore pressure and gas entry pressure, the gas leakage will initiate to happen within the fracture network in the host rock and the EDZ (Autio et al., 2006).

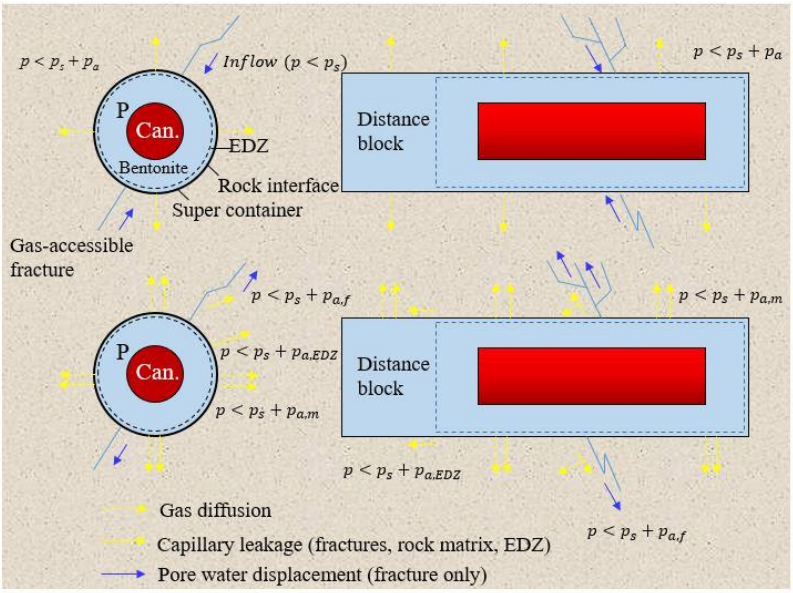

Figure 3.6 Different gas transport routes and repository domains (Autio et al., 2006)

3.4 Conclusions

Gas migration is strongly governed by coupled hydro-mechanical (HM) or thermo-hydro-mechanical-chemical THMC) processes, which means that the assessment and prediction of gas migration must consider and incorporate the coupled HM or THMC processes that take place in the DGR system during gas transport. From the literature review of this chapter, some conclusions are drawn as following:

There are still some limitations in of the past experiments and models. The effects of the chemical reactions are typically simplified in most of the models, which resulted in discrepancy between the simulated and experimental results. Moreover, the existing mechanical constitutive models of gas migration reproduce conventional elastic behavior with damage or elastoplastic behavior. There is rarely full consideration of elastoplastic-damage for the model. Moreover, the existing coupled models are usually partially coupled as HM or THM. These oversimplifications will impact the accuracy of the assessment to a certain extent. Besides these issues from a modelling perspective, the limitation of the experimental data has also hindered the development of more advanced models. Most of

the investigation of gas migration relating to the safety of underground repositories of nuclear waste only begun in the last 15-20 years, so the published field data and studies in the area are limited. The next steps of the study will make more attempts on the whole coupling of THMC as well as the influences from the damage caused by the mechanical processes.

CHAPTER 4 Geotechnical and geological characteristics of the study area

4.1 Introduction

This chapter will provide a description of the geochemical, mechanical, hydraulic and thermal characteristics of sedimentary rock formations in the study area. These information and data are important for simulation of gas migration in potential DGR for nuclear wastes in Ontario.

4.2 Geographical Location and Geology

Figure 4.1 shows the location of the study area (Bruce site) which has been proposed for deep geological repository for low and intermediate wastes in Ontario Canada. The proposed DGR will be located 680m below the ground as suggested by Ontario power generation. It will be built within low permeability limestone which is underlain by 200m of low-permeability shale. Although the site was subjected to many geologic events over the past 450 million years, these rock formations are intact and do not have any major faults and fractures, which in turn can provide stability, predictability and excellent isolating capabilities (NWMO, 2011A). The bedrock types located at Bruce site are layers of sedimentary rocks formed in the depression of the Michigan basin. Sedimentary rock types in the Michigan basin typically include carbonates, shale, evaporite, limestone, and sandstone. Figure 4.2 shows the geologic setting for the DGR.

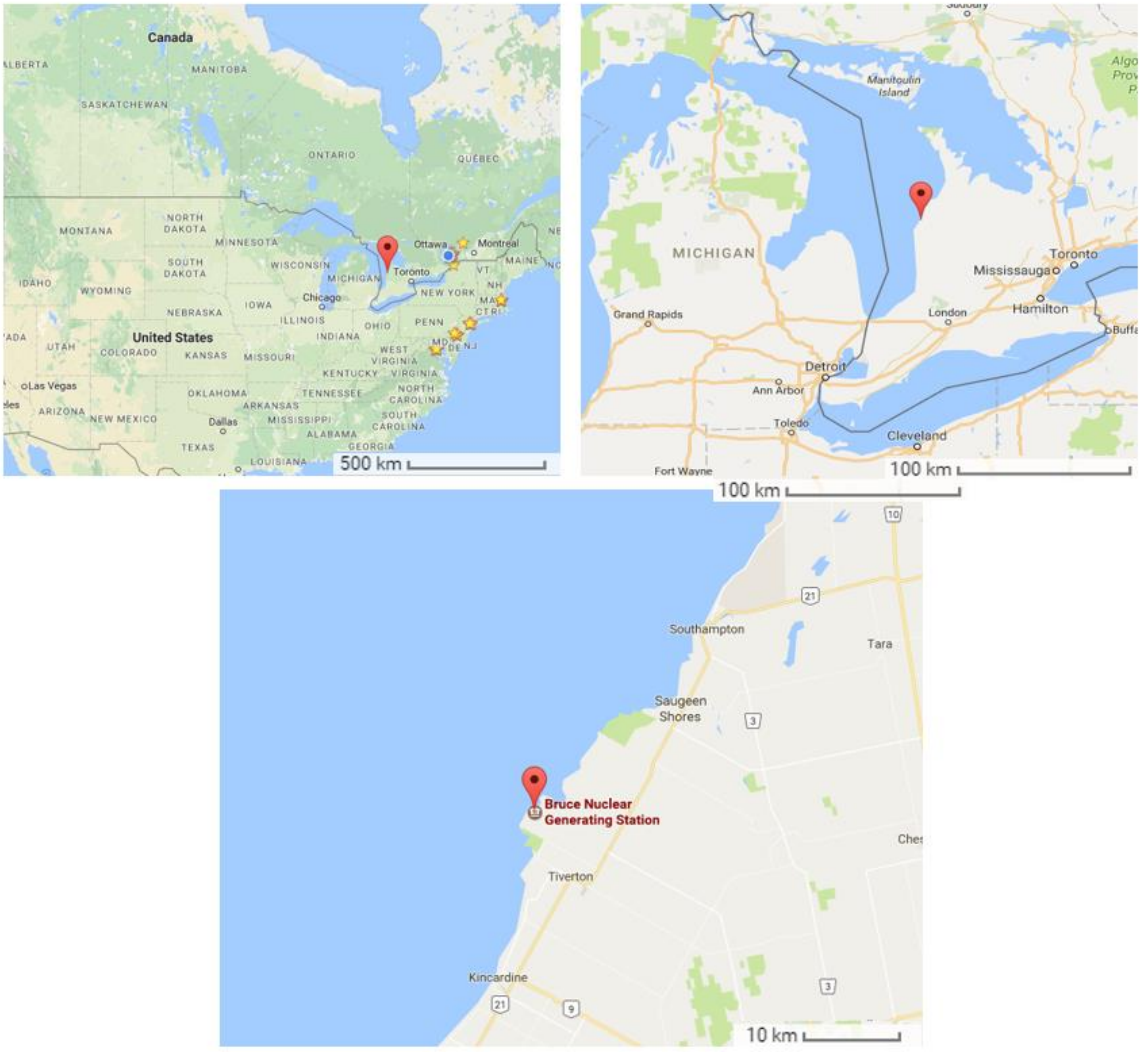

Figure 4.1 Proposed DGR location by OPG (source: Google Maps)

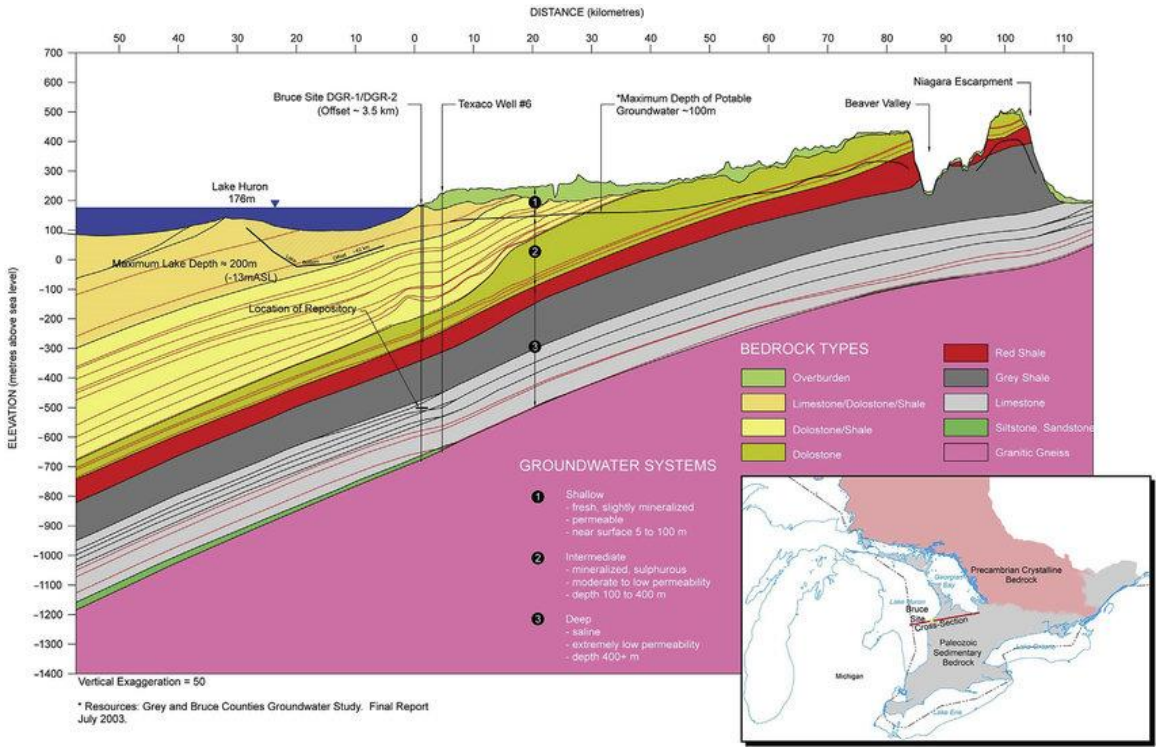

Figure 4.2 Geologic setting for the deep geologic repository (OPG website)

4.3 Geomechanical characteristics

The geomechanical characteristics described here provide an overview on the rock properties and behaviors in the proposed location of the DGR of Bruce nuclear site. The data can be divided into two categories: rock stress properties and rock mass properties. These primary sources of data are mainly from the NWMO (2011A).

4.3.1 Rock strength and other properties

The host rock of the proposed DGR is argillaceous limestone of the Cobourg Formation. Based on the uniaxial compression strength (UCS) tests on 67 samples, the UCS values range from 58 to 175 MPa. The mean value of elastic modulus is 39 GPa. The results show that the limestone with high strength and average modulus ratio has a high stability degree for the excavation of DGR (NWMO 2011A).

Two other important parameters that describe the rock strength are crack initiation (CI) and crack damage (CD). Andersson et al. (2007) presented that CI could be used to estimate the spalling strength of the lower bound of *in-situ* rock mass. Damjanac and Fairhurst (2010) suggested that CI can be used to estimate long-term strength of the unconfined rock. From the USC test results, CI and CD of Cobourg limestone range from 24 to 75 MPa with a mean value of 47 MPa, and from 45 to 162 MPa with a mean value of 97 MPa, respectively. Figure 4.3 shows the distribution of the CI and CD.

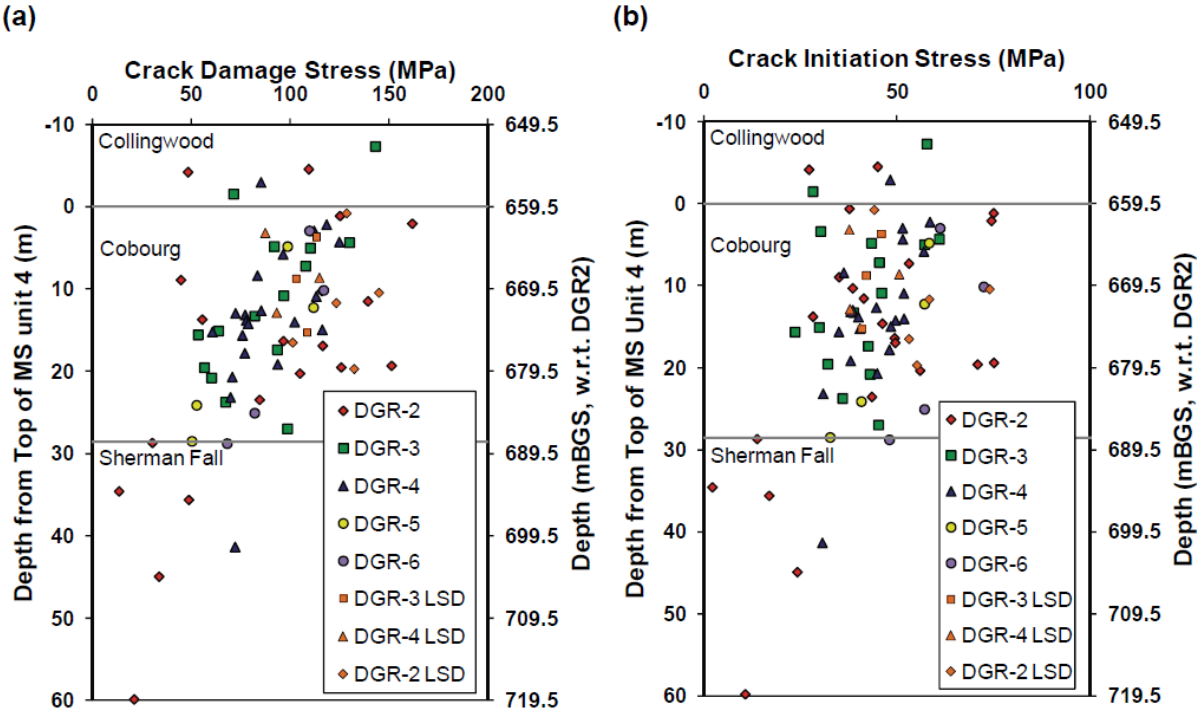

Notes: LSD = Long-term Strength Degradation. Results determined from intact DGR core.

Figure 4.3 Distribution of CD (a) stresses and CI (b) stress (NWMO, 2011)

Another very important parameter of the host rock is the tensile strength, which can be used for the evaluation of the development of potential overstressing room roof with the horizontally bedded direction. Figure 4.4 shows the Brazilian tensile strength test for the Cobourg Formation (INTERA, 2011). The other properties of the sedimentary rocks formations of the proposed location are shown in Table 4-1.

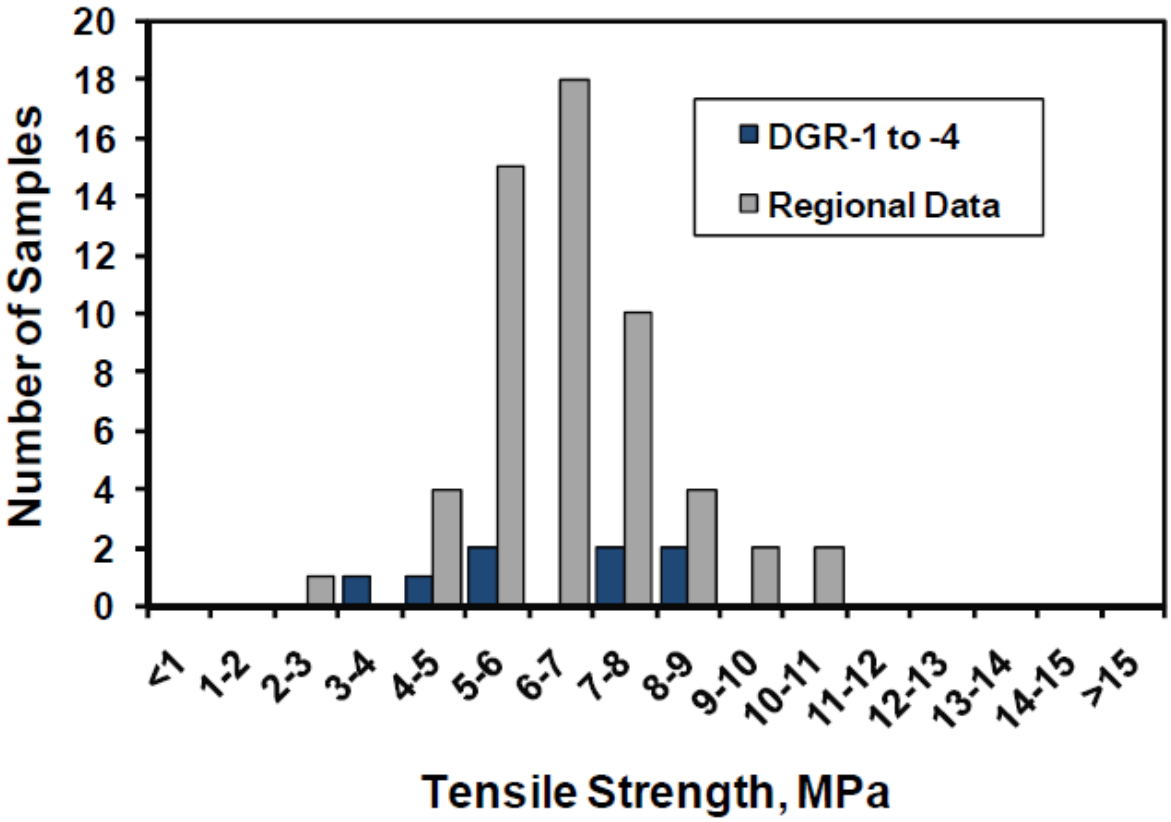

Figure 4.4 Brazilian tensile strength of the Cobourg Formation (NWMO, 2011)

Table 4-1 Mechanical properties of the sedimentary rocks in the proposed area of the DGR (NWMO, 2011B)

Subdomain number	**Rock formation**	**Depth (m)**	**Poison's ratio**	**Young's modulus(GPa)**
1	Overburden Aquifer	0-20	0.2	10
2	Dolostone Aquifer	20-169.3	0.2	40
3	Silurian Aquifer	169.3-178.6	0.2	18
4	Silurian Aquifer	178.6-325.5	0.2	6
5	Silurian Aquifer	325.5-328.5	0.2	38
6	Silurian Aquifer	328.5-374.5	0.2	38
7	Silurian Aquifer	374.5-378.6	0.2	38
8	Silurian Aquifer	378.6-411	0.2	38
9	Silurian Aquifer	411-447.7	0.2	16
10	Ordovician Shale	447.7-659.5	0.2	16
11	Ordovician Limestone	659.5-688.1	0.2	39

12	Ordovician Limestone	688.1-762.0	0.2	24
13	Ordovician Limestone	762.0-838.6	0.2	24
14	Cambrian	838.6-860.7	0.2	24
15	Precambrian	>860.7	0.2	60

4.4 Geochemical characteristics

Based on the existing data, the geochemical characteristics can be described from two aspects: mineralogy and geochemistry of the rocks for the proposed DGR and the ground water geochemistry. Figure 4.5 shows the mineralogical composition of the rock formation in the study area. It can be observed that the mineralogy of the Cobourg Formation at the depth of 660 to 680 m namely (i.e., the proposed host rock) is predominately calcite.

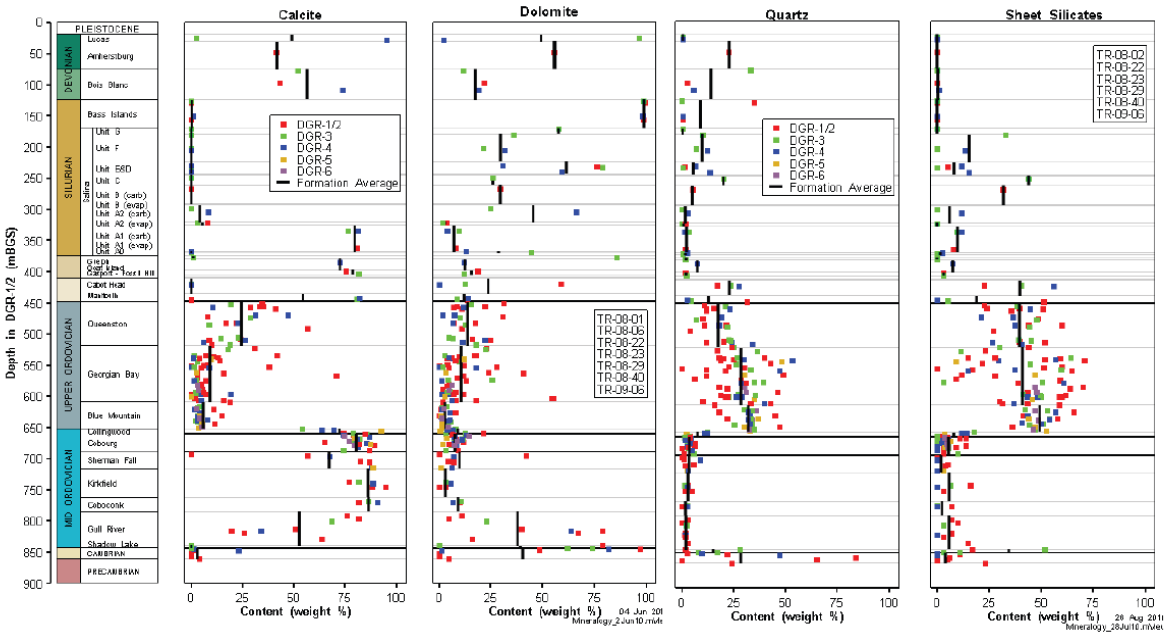

Figure 4.5 Rock formation mineralogy (NWMO, 2011B)

McNutt et al. (1987) presented that strontium isotope can be used as a geochronological tool to indicate the changes in water chemistry. Table 4-2 describes the strontium isotope composition of the rocks from the proposed area. For the ground water geochemistry, Table 4-3 shows the different types of water samples collected by NWMO (2011E).

Table 4-2 Strontium isotopic composition of some rocks (McNutt et al., 1987)

Stratigraphic unit	**87Sr/86Sr**
Cambrian Rock	0.73302
Trenton Rock	0.70858

Table 4-3 Some types of water samples summarized by NWMO (2011E)

Age	**Formation**	**Rock Type**	**Depth/Range (m)**	**Water Type**	**TDS (mg/L)**
Devonian	Berea	Sandstone	720-760	Na-Ca-Cl	176,000 to 380,000
	Kettle Point	Shale	40-50	Na-Cl-HCO3	640 to 15,500
	Hamilton	Shale	40-50	Na-Cl	7500 to 19,100
	Antrim	Shale	Not Known	Na-Cl	123,000 to 241,000
	Dundee	Carbonate Carbonate	100-140 1130	Na-Mg-Ca-Cl Na-Ca-Cl	3300 to 25,200 292,000
	Detroit River	Carbonate	100-120	Na-Ca-Mg-Cl	13,150 to 48,700
	Richfield	Carbonate	1445	Ca-Na-Cl	282,000
Silurian	Salina F	Salt	150	Na-Cl	305,000 to 322,000
	Salina A2	Salt	250	Ca-Na-Mg-Cl	340,000
	Salina A1	Carbonate	650	Ca-Na-Cl	284,000 to 306,000
	Guelph	Carbonate	355-770	Ca-Na-Cl	159,000 to 335,000
	Guelph /Lock port/Goat Island	Carbonate	5-65	Ca-Mg-SO4	480 to 15,100
	Niagara	Carbonate	715-1305	Ca-Na-Cl	310,000 to 397,000

	Grimsby/Thorhold	Sandstone	290-570	Na-Ca-Cl	181,000 to 326,000
	Thorold	Sandstone	55-75	Na-Ca-Cl	12,600 to 15,200
	Whirlpool	Sandstone	360-460	Ca-Na-Cl	205,000 to 268,000
Ordovician	Blue Mountain	Carbonate	173	Ca-Na-Cl	186,000
	Trenton: Lindsay	Carbonate	50 200	Na-Ca-Cl Ca-Na-Cl	44,100 to 137,000
	Trenton: Verulum	Carbonate	85	Na-Ca-Cl	102,000
	Trenton: Bobcaygeon	Carbonate	30-325	Ca-Na-Cl	251,000 to 298,000
	Black River: Gull River	Carbonate	190 to 350	Ca-Na-Cl	97,000 to 304,000
	Black-River: Shadow Lake	Sandstone	370	Ca-Na-Cl	154,000
	Trenton-Black River	Carbonate	310 to 1300	Na-Ca-Cl	141,000 to 346,000
	Prairie du Chien	Sandstone	3234 to 3425	Ca-Cl	325,000 to 392,000
Cambrian	undifferentiated	Sandstone	890-1265	Ca-Na-Cl	174,000 to 338,000

4.5 Hydrogeological characteristics

To describe the hydrogeological characteristics, the collected data are divided into two aspects: the hydrogeological system and the hydraulic properties of the rock formations. McIntosh and Walter (2006) summarized the hydrogeological characteristics of the Great Lakes region in Figure 4.6. This area consists of three different ground-water aquifer systems, while the proposed area has two of the aquifer systems including the Sil-Dev and the Cambrian-Ordovician aquifer systems. The hydraulic properties are summarized by the

NWMO (2011B). Table 4-4 presents the hydraulic conductivities, while Figure 4.7 shows the porosity values for each formation.

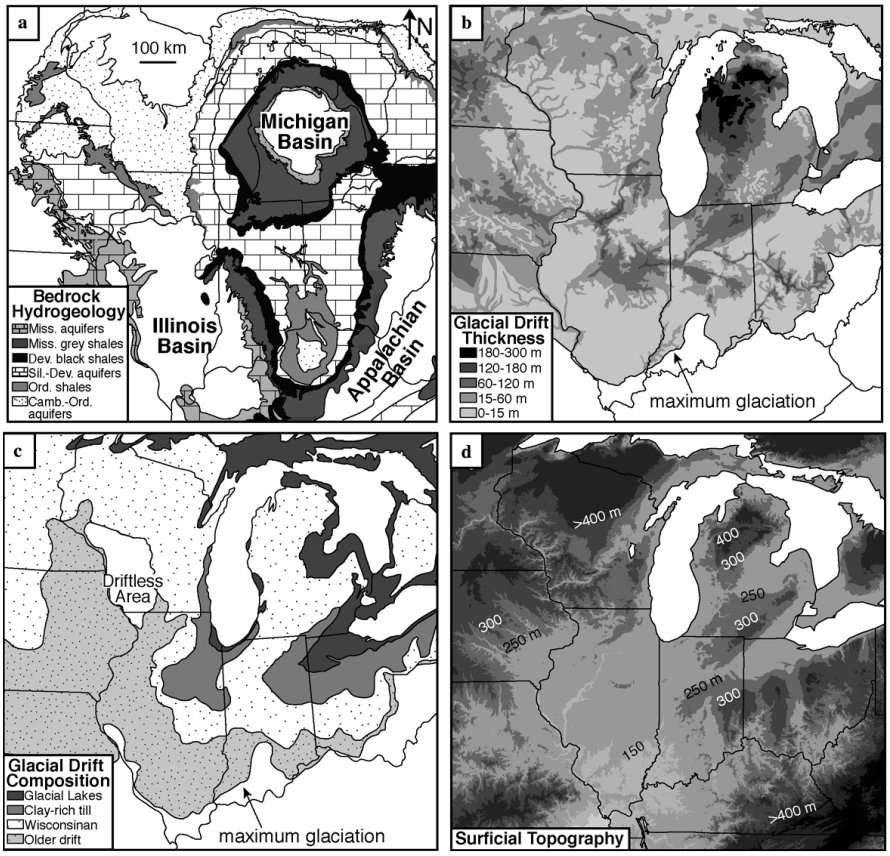

Figure 4.6 Hydrogeologic framework of the study area (McIntosh and Walter, 2006)

Table 4-4 Hydraulic conductivities for sedimentary rocks of southern Ontario (NWMO, 2011B)

Subdomain number	**Rock Formation**	**Depth**	**Hydraulic Conductivity K_h (m/s)**	K_h/K_v	**Diffusion m^2/s**
1	Overburden Aquifer	0-20	8.0E-10	2:1	6.0E-10
2	Dolostone Aquifer	20-169.3	1.0E-5	10:1	8.0E-12
3	Silurian Aquifer	169.3-178.6	5.0E-12	10:1	1.0E-12
4		178.6-325.5	5.0E-12	10:1	1.0E-12
5	Silurian Aquifer	325.5-328.5	2.0E-7	1:1	7.0E-12

6		328.5-374.5	5.0E-12	10:1	1.0E-12
7	Silurian Aquifer	374.5-378.6	3.0E-8	1:1	3.0E-11
8		378.6-411	5.0E-12	10:1	1.0E-12
9		411-447.7	5.0E-12	10:1	1.0E-12
10	Ordovician shale	447.7-659.5	2.0E-14	10:1	1.0E-13
11	Ordovician limestone	659.5-688.1	1.0E-15	10:1	3.0E-13
12		688.1-762.0	1.0E-15	10:1	3.0E-13
13	Ordovician limestone	762.0-838.6	6.0E-12	100:1	3.0E-13
14	Cambrian	838.6-860.7	1.0E-7	1:1	1.0E-11
15	Precambrian	>860.7	1.0E-11	1:1	3.0E-13

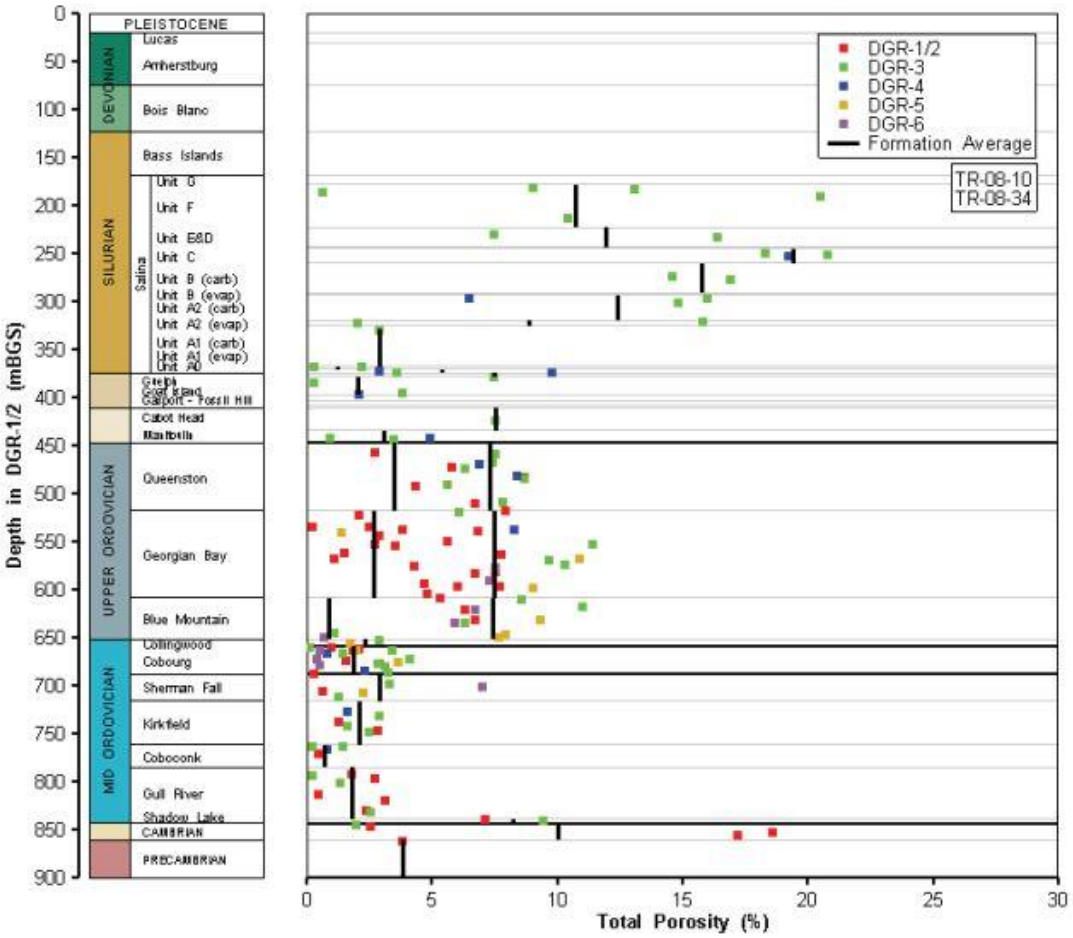

Figure 4.7 Porosity values with the depth in the study area (NWMO, 2011)

4.6 Geothermal characteristics

There are two aspects to describe the geothermal properties: geothermal gradient ($T(℃) = 14.5 + 0.0192 \times depth(m)$) which is shown by Figure 4.8 and thermal properties of the rock layers. The thermal properties of the rock formation in the study area as shown in Table 4-5.

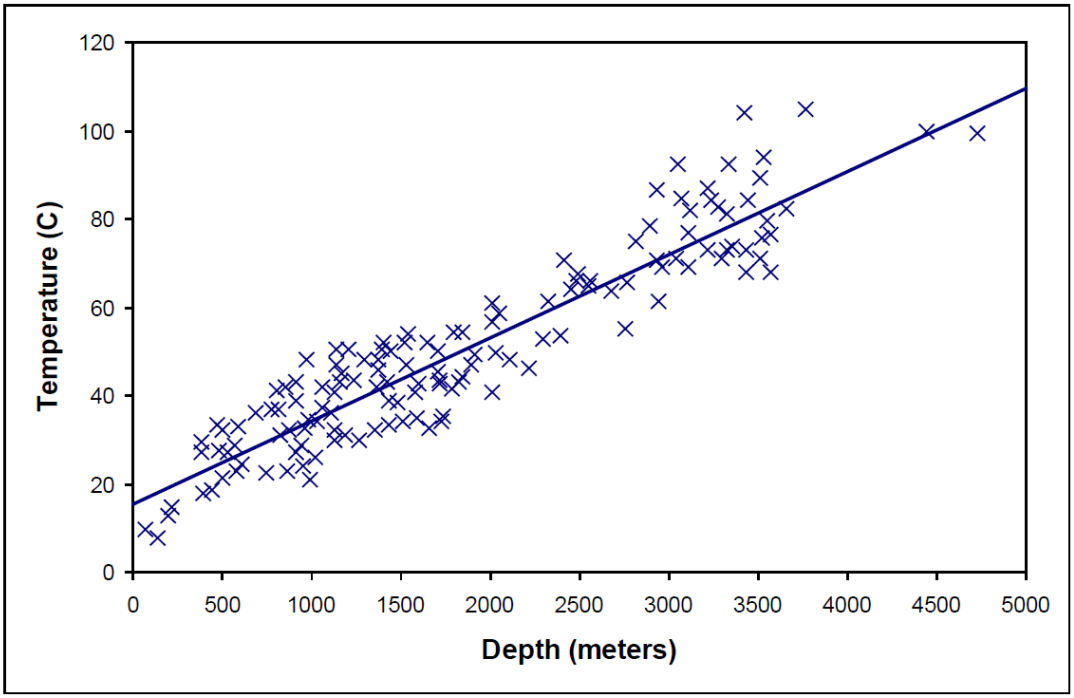

Figure 4.8 Temperature distribution with depth in Michigan basin (Vugrinovich, 1989)

Table 4-5 Thermal properties of the sedimentary rocks in the study area (Everham, 2004; Clauser and Huenger, 1995; Cermak and Rybach, 1982)

Subdomain number	**Rock formation**	**Depth**	**Thermal conductivity W/(m.K)**	**Specific heat capacity J/(kg.K)**	**Density Kg/m3**
1	Overburden Aquifer	0-20	2	700	2500
2	Dolostone Aquifer	20-169.3	2	700	2500

3	Silurian Aquifer	169.3-178.6	2	700	2500
4		178.6-325.5	2	700	2500
5	Silurian Aquifer	325.5-328.5	2	700	2500
6		328.5-374.5	2	700	2500
7	Silurian Aquifer	374.5-378.6	2	700	2500
8		378.6-411	2	700	2500
9		411-447.7	2	700	2500
10	Ordovician shale	447.7-659.5	2	700	2500
11	Ordovician limestone	659.5-688.1	2	700	2500
12		388.1-762.0	2	700	2500
13	Ordovician limestone	762.0-838.6	2	700	2500
14	Cambrian	838.6-860.7	2	700	2500
15	Precambrian	>860.7	1.375	700	2500

4.7 Conclusions

This chapter described the geological, hydrogeological and geomchanical conditions of the Bruce nuclear site, which are relevant for the modeling of the gas migration in a potential Ontario's DGR for nuclear wastes as well as functions or the safety assessment. As located in a tectonically stable region, the Bruce site had the superiority to be the selected location for the DGR.The collection of geochemical, mechanical, hydraulic and thermal data on sedimentary rock formation in Ontario could help to study the mechanism of gas generation and migration. The geological and hydrogeological features of the repository are crucial to guarantee the safe isolation of the radioactive waste from the biosphere for a period of more than one million years. After the study of the gas transport mechanism and under the investigation of the geotechnical and geological features, the sedimentary rock is an appropriate potential host rock for the underground repository.

CHAPTER 5 A simulator for coupled modeling of gas migration in host rock of DGR for nuclear wastes

5.1 Introduction

This chapter presents a new simulation tool (simulator) in which two computer codes, TOUGHREACT and COMSOL, are coupled to model the coupled heat transfer, multiphase fluid flow, deformation, damage, and chemical precipitation/dissolution that occur in the host rocks of repository for nuclear wastes during gas migration. TOUGHREACT is a high-precision coupling analysis software, which can express the thermo-hydro-chemical (THC) phenomena in saturated or partially saturated porous media, while COMSOL is used to solve the mechanical processes. First, an elastoplastic damage model is developed and then implemented into COMSOL Multiphsics finite element code. Then, the two numerical codes (THOUGHREACT, COMSOL Multiphysics) are coupled via MATLAB. A special external module programmed by MATLAB has been developed to couple the two codes. Based on the changes in effective stress, TOUGHREACT calculates the pore pressure and liquid satuation, which will be transferred to COMSOL by the external module. COMSOL dictates the mechanical part, which is based on an elastoplastic model coupled with isotropic damage to calculate the displacements and stress. These data will be inputted into the external module for updating the variations of porosity and permeability during the rock deformation process. The developed numerical tool has been verified and tested against laboratory and field gas injection tests on sedimentary host rocks (e.g., Opalinus Clay) for nuclear wastes as well other types of gas (e.g., CO_2) injection tests. The validation results have shown that there is a good agreement between the predicted and the experimental values of the gas flow rates. In the next sections, the following topics with respect to the development of the simulator and the assumptions made are presented and discussed.

(i) The key THMC processes considered in the development of the simulator and the assumptions made;

(ii) The structure of the simulator and the coupling procedure adopted;

(iii) The theoretical formulations of the mathematical models developed and the governing equations in TOUGHREACT;

(iv) The validation of the simulator and simulation results.

5.2 Overview of THMC processes and assumptions

Migration of pore fluid in low-permeability rock of geological repository systems is governed by the coupled thermal (T, e.g., heat conduction and convection), hydraulic (H, e.g., flow of water, gas flow, pore fluid pressure, phase change), mechanical (M, e.g., stress, deformation, damage) and chemical (C, e.g., dissolution, precipitation) processes. However, only a few modeling studies (e.g., Lege and Shao, 1996; Ortiz et al., 1996; Alonso et al., Du et al., 2006; Gerard et al., 2008; Yang and Fall, 2020) developed mathematical and / or numerical models that have specifically addressed solving the coupled processes associated with gas migration in sedimentary rocks and predicting the gas transportation and its impacts on the host rock (Fall et al., 2014). In the present study, we mainly focus on the processes of THMC taking into account the mechanical damage that can impact on the gas migration behaviors. In the terms of the coupled processes, one factor can affect the initiation and evolution of others. Hence, when predicting the situation under the perturbation of natural or man-made factor, it should avoid considering each process independently (Jing and Feng 2013).

To develop the THMC coupled model, the main assumptions adopted are as follows:

(I) The porous medium consists of three phases components: solid, water and gas. These three constituents are independent of each other as the overlapping continua (Fall et al., 2014). The pores of the rock skeleton are filled with multiphase fluid, which is partially liquid and partially gas.

(II) In the present study, the gas is generated by Low-level waste (LLW) and intermediate-level waste (ILW). The variation of the temperature induced by LLW and ILW is commonly low (Fall and Nasir, 2010), so only the temperature gradient caused by depth variations is considered. However, the temperature changes induced by glaciations may significantly affect the temperature of the subsurface rocks. So the changes of stress and strain induced by small variations of temperature will not be considered.

(III) In the area and depth where the DGR in Ontario will be constructed, the sedimentary rock formations do not have joints or faults. This is one of the reasons why this area and depth were chosen. Therefore, joints and faults have not been included in the modeling. However, the sedimentary formations have bedding planes. Modeling of bedding would require to consider the

anisotropic behavior of the rock, which was out of the scope of my Ph.D. research, were not considered in the modelings of the current study.

(IV) Darcy's law is adopted in the modeling study. Darcy's law describes a linear relationship between specific discharge and hydraulic gradient. This relationship is applicable for most all groundwater conditions. However, if the hydraulic gradient is every high, flow may not be linear, thus, Darcy's law is not appropriate to represent the groundwater flow.

5.3 Simulator structures and coupling procedure

In the developed numerical tool (Figure 5.1), five coupled processes are solved: thermal process (T), mechanical process (M), hydraulic flow (H), solute transport and chemical reactions (C). In the M to THC process, the deformation (volumetric strain and thermal expansion/constriction) of each finite element is sampled from the simulation results of COMSOL, and is used to update the porosity and permeability for TOUGHREACT, using modules (Coupling Module, Figure 5.1) that are developed using MATLAB. The THC to M process takes multiphase pressure, saturation degree and temperature from TOUGHREACT and updates the temperature, pore pressure in COMSOL, and extracts the porosity and permeability for the next step in MATLAB (Figure 5.1).

Because TOUGHREACT mesh uses one grid point within each element, while COMSOL nodes are located in element corners, the data from TOUGHREACT has to be interpolated from mid-element (TOUGHREACT) to corner locations (COMSOL) by using the external module (MATLAB). Then, input the multiphase pore pressure to calculate the effective stress for COMSOL. Identically, the data from COMSOL also need to be interpolated for TOUGHREACT.

The developed simulator has four main sub-routines: (1) COMSOL generates the geometric model and mesh, initializes and applies boundary conditions; (2) The external module (MATLAB) reads and extracts the data of mesh, translate these data into the format for TOUGHREACT; (3) Using the program in MATLAB to generate the three input files (flow.inp, solute.inp, and chemical.inp) for TOUGHREACT. (4) After every time step of computation by COMSOL, the external module extracts volume strain and thermal expansion/contraction to update the porosity and permeability which will be used for the next time step and runs TOUGHREACT. Then, we use the three-

dimensional Lagrange interpolation method to convert and input the pore pressure for COMSOL. This is the whole procedure of the data synchronization.

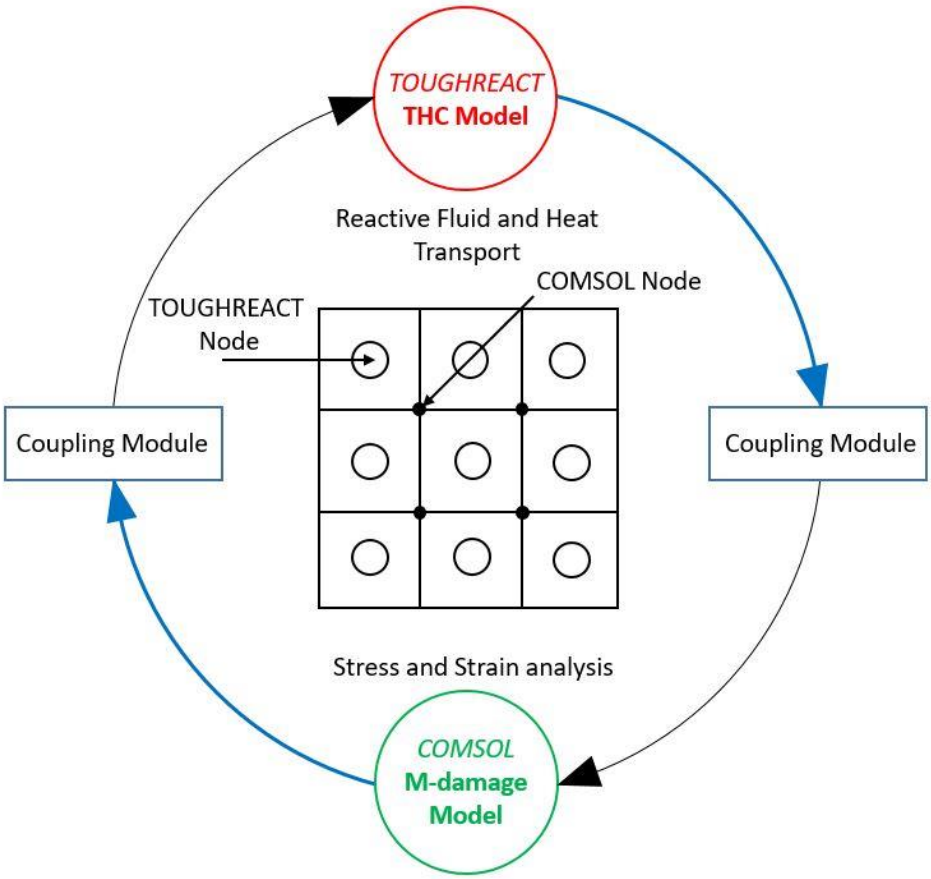

Figure 5.1 The linked TOUGHREACT and COMSOL simulator

5.4 Theoretical formulation

5.4.1 Basis of the mathematical formulation

The representative elementary volume (REV) contains three phases (solid, s; liquid, l and gas, g) in a deformable unsaturated porous medium which is governed by both volume and mass conservations (Fall et al., 2014):

$$V = V_s + V_l + V_g \tag{5.1}$$

$$M = M_s + M_l + M_g \tag{5.2}$$

where V presents the total volume; V_s is the solid volume, V_l and V_g refer to the liquid volume and gas volume; M, M_s, M_l and M_g are the total mass of medium, solid mass, liquid mass and gas mass, respectively.

The conservation involves momentum, energy and mass. The macroscopic balance equation of any thermodynamic in a continuum can be expressed in the general form (Fall et al., 2014)

$$\frac{\partial}{\partial t} M^{\alpha} + \nabla \cdot (\mathbf{j}^{\alpha}) - \mathrm{f}^{\alpha} = 0 \tag{5.3}$$

Where M^{α} refers to the mass or energy per unit volume of the unsaturated medium. α the mass components (solid, liquid or gas). $\mathbf{j}_{\pi}^{k}$ is the total flux of a fixed reference system, and f^{α} is the rate of the production/removal of the component α unit volume.

Let the volume fraction of phase α as $n^{\alpha} = V_{\alpha}/V$ and the partial mass density as

$$\rho^{\alpha} = M_{\alpha}/V \tag{5.4}$$

and it must satisfy the constraint condition as below:

$$\begin{gathered} n^s + n^l + n^g = 1 \\ n^s S^s \rho^s + n^l S^l \rho^l + n^g S^g \rho^g = \rho \end{gathered} \tag{5.5}$$

where $\rho = M/V$ is the mixture mass density, ρ^s the density of the solid, ρ^l the density of the liquid (water), and ρ^g the density of gas. S^s, S^l and S^g are the degrees of saturation for solid, water and gas.

The degree of saturation S and the porosity can be expressed as

$$\mathrm{S} = V_l/V_v\,,\ S^l + S^g = 1 \tag{5.6}$$

$$\phi = \frac{V_v}{V} = n^l + n^g \tag{5.7}$$

Through the equations above, the volume fractions are given by

$$n^s = 1 - n, n^l = nS, n^g = n(1 - S) \tag{5.8}$$

5.4.2 Mechanical model

An elastoplastic damage model is adopted to describe the mechanical response of the host rock assuming isotropy of the host rock, which although may simplify the orientation dependent damage induced by micro-cracks, ensures soundness in physics and mathematics. The effective stress principle for saturated porous media and suction-induced enhancement for unsaturated porous media is adopted here as it is superior in expressing deformation in terms of single "effective" stress variable to the double stress variable concept usually adopted in unsaturated soil mechanics (Fall et al. 2014). Treating the tensile stresses and pore water pressure as positive, and following Biot's approach (Biot, 1941), the effective stress is then expressed as:

$$\sigma_{ij} = \sigma'_{ij} - \alpha\bar{p}\delta_{ij} \tag{5.9}$$

where σ'_{ij} effective stress, σ_{ij} total stress, δ_{ij} Kronecker's delta defined as 1 for $i = j$ and 0 for $i \neq j$. $\bar{p}$ the average pore pressure, α Biot's coefficient. Bear and Bachmat (1991), Zienkiewicz et al. (1977) has defined average pore pressure $\bar{p}$ as

$$\bar{p} = S_l p_l + S_g p_g = S_l p_l + (1 - S_l) p_g \tag{5.10}$$

In the above formula, S_l and S_g are the liquid saturation degree and the gas saturation degree, respectively. S_l and S_g sum to one. p_l the pore water pressure, p_g the pore gas pressure, so the suction s (capillary pressure, p_c) can be expressed as

$$\mathrm{s}(p_c) = p_g - p_l \tag{5.11}$$

$\alpha(\leq 1)$ is the Biot's coefficient which is defined in (Fall and Nasir, 2012) as:

$$\alpha = 1 - \frac{K_D}{K_s} \leq 1 \tag{5.12}$$

where K_D is the bulk modulus of the porous medium and K_S is the bulk modulus of solid matrix.

By assuming small strain and displacement, the total incremental strain can be divided into elastic, plastic and thermal strains that are shown as:

$$d\varepsilon = d\varepsilon_M^e + d_M^p + d\varepsilon^T \tag{5.13}$$

where ε is the total strain, ε_M^e and ε_M^p are the elastic strain and plastic strain respectively, and ε^T is

the thermal strain. Each of these types of strain is described in the following subsections.

The continuum damage mechanics for geomaterials was first proposed by Kachanov (1958), and then improved subsequently by several authors (e.g. Lemaitre (1971), Lemaitre and Chaboche (1990)). An isotropic damage is assumed here and represented by the scalar D. Kachanov (1958) considered the damage in a cross section to be measurable by a relative area of voids. The damage-relevant 'effective stress' in the case of isotropic damage can be written as Tang et al., (2002) as:

$$\sigma_{ij}^{*} = \frac{\sigma_{ij}'}{1 - D} \tag{5.14}$$

where σ_{ij}^{*} is the modified "effective stress" in the damage-susceptible geomaterials, σ_{ij}' is the effective stress, D is the damage variable. The effective stress in Eq. (5.14) should be introduced into Eq. (5.9) and the subsequent equations which contain σ_{ij}'.

5.4.2.1 Elastic strain

According to the generalized Hooke's law and taking the thermal expansion effect into consideration, the elastic stress-strain relation reads:

$$\mathrm{d}\sigma_{ij}' = 2G\varepsilon_{ij} + \lambda\varepsilon_{kk}\delta_{ij} - I\beta_T dT \cdot \delta_{ij} \tag{5.15}$$

where: σ_{ij}' is the effective stress, ε_{ij} is the elastic strain, ε_{kk} is the normal strain, λ Lamé constants as $\lambda = \frac{Ev}{(1+v)(1-2v)}$, G shear modulus as $G = \frac{E}{2(1+v)}$, E is elastic modulus, v is Posson ratio, δ_{ij} is Kronecker delta tensor defined as 1 for $i = j$ and 0 for $i \neq j$. β_T is volume thermal expansion coefficient, I is identity tensor and T is temperature (Rutquvist, 2013).

Inserting Eq. (5.9) into the above equation results in an incremental form of the total stress

$$\mathrm{d}\sigma_{ij} = 2G\varepsilon_{ij} + \lambda\varepsilon_{kk}\delta_{ij} - \alpha d\bar{p}\delta_{ij} - I\beta_T dT \cdot \delta_{ij} \tag{5.16}$$

For isotropic damage, the mechanical properties, i.e. the elastic stiffness reduces with the propagation of damage-induced micro-cracks and are independent of their orientation and depend on a scalar variable D. The degradation in the mechanical properties of geomaterials, e.g. elastic modulus, can be defined as (Alnajim, 2004)

$$E = E^d = E_0(1 - D) \tag{5.17}$$

where: E^d is damaged elastic modulus, E_0 is the original elastic modulus of rock material without damage.

5.4.2.2 Plastic strain

To describe the plastic strain, a suitable yield function, plastic flow rule and plastic potential should be defined. This manuscript adopts a plastic-damage model based on Drucker-Prager yield function, which was proposed by Salari et al. (2004). In this model, the authors assumed that the plasticity and damage have different loading function and damage enters the plasticity yield function in terms of effective stress.

Yield function

The Helmholtz free energy function for Salari et al. (2004)'s model is:

$$\psi = \psi^e(\boldsymbol{\varepsilon}^e, D) + \psi^p(\bar{e}^p, D) \tag{5.18}$$

where: ψ is Helmholtz free energy, ψ^e is elastic component of Helmholtz free energy, ψ^p is plastic component of Helmholtz free energy, $\boldsymbol{\varepsilon}^e$ denotes the elastic strain tensor, $\bar{e}^p$ is the scalar-valued internal variables of plasticity and D is damage.

The Clausius-Duhem inequality takes the following form

$$\left(\boldsymbol{\sigma} - \frac{\partial \psi^e}{\partial \varepsilon^e}\right) d\varepsilon + \frac{\partial \psi^e}{\partial \boldsymbol{\sigma}^e} d\varepsilon^p - \frac{\partial \psi^p}{\partial \kappa} d\kappa - \frac{\partial \psi}{\partial D} dD \gg 0 \tag{5.19}$$

The plastic loading function of Drucker-Prager model needs to be modified to include the mechanical damage effect which can be expressed as:

$$f^p(\boldsymbol{\sigma}, \bar{e}^p, D) = \alpha I_1 + \sqrt{J_2} - (1 - D)k \tag{5.20}$$

where f^p is plastic loading function, $\bar{e}^p$ is the effective deviatoric plastic strain, α is Drucker-Prager internal friction parameter, $I_1 = \sigma_{kk}$ is the first invariant of the nominal stress tensor σ, $J_2 = 1/2\, s_{ij} s_{ij}$ is the second invariant of the deviatoric stress tensor σ, s_{ij} is the deviatoric strain tensor; D is the damage, α and k are Drucker-Prager friction and cohesion parameter, respectively, which can be written in terms of uniaxial tensile and compressive strength values as (Salari et al. 2004)

$$\alpha = \frac{1}{\sqrt{3}}\frac{f_c - f_t}{f_c + f_t} \; and \; k = \frac{2}{\sqrt{3}}\frac{f_c f_t}{f_c + f_t} \tag{5.21}$$

It should be emphasized that if equation (5.14) is divided by (1-D), the stress becomes "effective" stress. f_c, f_t are the uniaxial compressive and tensile strengths, respectively. It is assumed that the plastic hardening depends only on the equivalent deviatoric plastic strain $\bar{e}^p$ not the total plastic strain (Salari et al. 2004). Then, the friction parameter α and cohesion parameter k are expressed in the following forms by Shao et al. (1998).

$$\alpha = \alpha_m - (\alpha_m - \alpha_0)e^{-b_1\bar{e}^p} \tag{5.22}$$

$$k = k_m - (k_m - k_0)e^{-b_2\bar{e}^p} \tag{5.23}$$

where: α_0, α_m, k_0 and k_m represent the initial and maximum values of the frictional and cohesive parameters α and k, respectively. b_1 and b_2 are the material parameters of plasticity. Generally, the equivalent deviatoric plastic strain $\bar{e}^p$ can be defined by using the Odquist parameter. The Odquist parameter is commonly used in J_2 plasticity to express plastic dissipation (Salari et al. 2004) as follows:

$$\bar{e}^p = \int_0^{\bar{e}^p} d\bar{e}^p \tag{5.24}$$

$$d\bar{e}^p = \sqrt{\frac{2}{3}d\boldsymbol{e}^p : d\boldsymbol{e}^p} \tag{5.25}$$

where: $d\boldsymbol{e}^p$ the rate of deviatoric plastic strain, $\bar{e}^p$ the equivalent deviatoric plastic strain. This model assumes that the volumetric part of the plastic strain does not affect the hardening. It only enters the damage formulation and therefore governs the softening behaviour.

Plastic potential and flow rule

The modified Drucker-Pager loading function can be used as plastic potential:

$$g^p(\sigma, \bar{e}^p) = \beta I_1 + \sqrt{J_2} \tag{5.26}$$

The dilatation parameter β is adopted to control inelastic volume expansion.

where: I_1 first invariant of the deviatoric stress, J_2 second invariant of the deviatoric stress tensor,

and g^p is plastic potential function.

The plastic flow rule is expressed as follows (Jia, 2007):

$$d\boldsymbol{\varepsilon}^p = d\lambda \frac{\partial g^p}{\partial \boldsymbol{\sigma}} \tag{5.27}$$

The non-associated plastic flow rule is employed in this study. The deviatoric strain $\boldsymbol{e}^p$ and the rate change of mean plastic strain ε_m^p can be expressed as (Salari et al. (2004)):

$$d\boldsymbol{e}^p = d\lambda \frac{\boldsymbol{s}}{2\sqrt{J_2}} \tag{5.28}$$

$$d\varepsilon_m^p = d\lambda\beta \tag{5.29}$$

where $\boldsymbol{s}$ is deviatoric strain tensor.

Prager's plastic consistency condition ensures that the stress state maintains on the yield surface during persistent plastic loading and it is expressed (Salari et al., 2004) as:

$$\mathrm{d}f^p = \frac{\partial f^p}{\partial \boldsymbol{\sigma}} : d\boldsymbol{\sigma} + \frac{\partial f^p}{\partial \bar{e}^p} d\bar{e}^p + \frac{\partial f^p}{\partial D} dD = 0 \tag{5.30}$$

and $d\sigma$ is expressed as:

$$d\boldsymbol{\sigma} = \boldsymbol{E}^d : \boldsymbol{\varepsilon}^e + d\boldsymbol{E}^d : \boldsymbol{\varepsilon}^e \tag{5.31}$$

where $\boldsymbol{E}^d$ denotes the secant tensor of damaged elastic modulus (as described previously) and $\boldsymbol{\varepsilon}^e$ is the elastic strain tensor, and f^p is plastic loading function.

Differentiating and plugging the Eq. (5.17) and Eq. (5.27) into Eq. (5.31), we can obtain:

$$d\boldsymbol{\sigma} = \boldsymbol{E}^d : \left(d\boldsymbol{\varepsilon} - d\lambda \frac{\partial g^p}{\partial \boldsymbol{\sigma}} \right) - dD\boldsymbol{E}^0 : \boldsymbol{\varepsilon}^e \tag{5.32}$$

Introducing Eq. (5.24) into Eq. (5.25), the equivalent deviatoric plastic strain rate $d\bar{e}^p$ can be simplified into:

$$d\bar{e}^p = \frac{d\lambda}{\sqrt{3}} \tag{5.33}$$

Therefore, using the unknown plastic and damage multipliers and the prescribed strain rate, the plastic consistency condition can be expressed as (Salari et al., 2004):

$$\left(\frac{\partial f^p}{\partial \boldsymbol{\sigma}}:\boldsymbol{E}^d:\frac{\partial g^p}{\partial \boldsymbol{\sigma}}-\frac{\partial f^p}{\partial \bar{e}^p}\frac{1}{\sqrt{3}}\right)d\lambda+\left(\frac{\partial f^p}{\partial \boldsymbol{\sigma}}:\boldsymbol{E}^0:\boldsymbol{\varepsilon}^e-\frac{\partial f^p}{\partial D}\right)dD=\frac{\partial f^p}{\partial \boldsymbol{\sigma}}:\boldsymbol{E}^d:d\boldsymbol{\varepsilon} \tag{5.34}$$

5.4.2.3 Damage formulation

The damage induced by thermodynamic damage force is written as (Salari et al., 2004):

$$Y_V=\frac{1}{2}K^0\langle\varepsilon_V^e\rangle^2+c\int_0^{\varepsilon_V^p}|\sigma_m|\langle d\varepsilon_V^p\rangle \tag{5.35}$$

where $c=c_c$ for $\varepsilon_V^e<0$

$c=c_t$ for $\varepsilon_V^e>0$

K^0 is the undamaged bulk modulus, σ_m is mean nominal stress, and ε_V^e and ε_V^p are the volumetric elastic strain and volumetric plastic strain, respectively. The dilatant volumetric plastic energy dissipation contributes to the thermodynamic damage force, which is controlled by the plastic damage parameter *c*. The bracket $\langle x\rangle$ denotes the MacAuley discontinuity function ($\langle x\rangle=x$ when $x>0$ and $\langle x\rangle=0$ otherwise). c_c, c_t are the plastic participation factors in damage force, the values of them are different by the volumetric elastic strain.

The loading function of the damage initiation is defined by the energy-based damage function (Salari et al. (2004)):

$$f^d(Y_V,D)=Y_v-r(D) \tag{5.36}$$

where $r(D)=r_0(1-D)^{p-1}$ (Carol et al. (2001)) is the energy resistance function, Y_v is volumetric thermodynamic conjugate force for damage, r_0 denotes the modulus of resilience. In Figure 5.2, it describes the volumetric strain energy in uniaxial tension, r_0 is the peak value, p is the ratio between the modulus of resilience and the modulus of toughness:

$$p=\frac{r_0}{g_f} \tag{5.37}$$

Figure 5.2 describes the uniaxial tension test, and the physical meaning of $r_0=\frac{1}{2}\sigma_m^0\varepsilon_v^0$ and $g_f=\int_0^\infty\sigma_m(\varepsilon_v)d\varepsilon_v$.

where: ε_v is volumetric strain, σ_m is mean nominal stress.

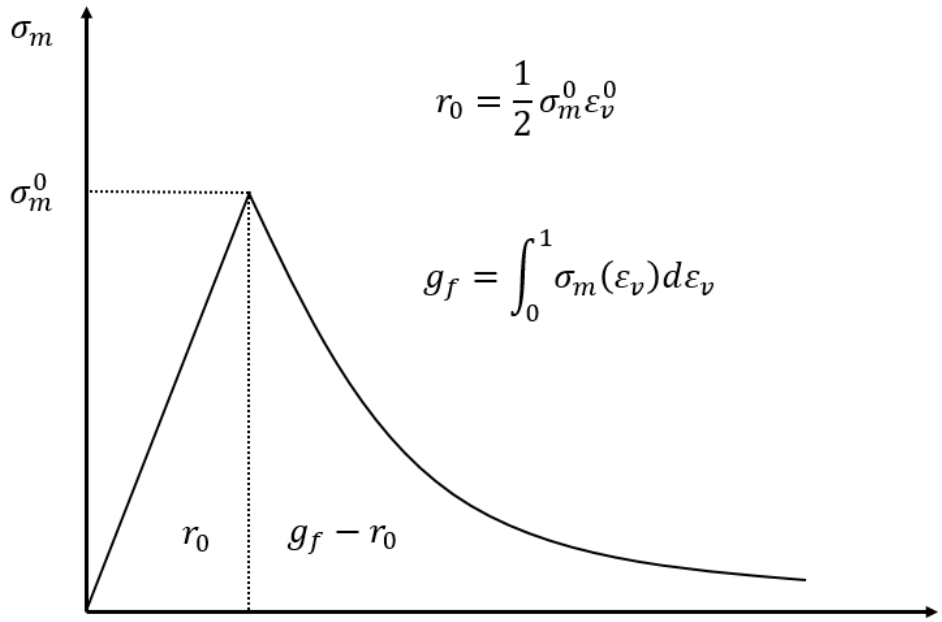

Figure 5.2 Uniaxial stress-strain curve (Salari et al., (2003)

The damage consistency function that can make sure the stress state satisfies the damage function under persistent damage is (Salari et al., 2004)

$$df^d = \frac{\partial f^d}{\partial Y_V} dY_v + \frac{\partial f^d}{\partial D} dD = 0 \tag{5.38}$$

The partial derivatives function of Eq. (5.27) can be expressed as:

$$dY_V = K^0 \langle \varepsilon_V^e \rangle d\varepsilon_V^e + c|\sigma_m| \langle d\varepsilon_V^p \rangle \tag{5.39}$$

Decomposing dY_V into elastic and plastic portions and taking the volumetric plastic strain rate into Eq. (5.39) gets:

$$dY_V = K^0 \langle \varepsilon_V^e \rangle \mathbf{I} : d\varepsilon - 3d\lambda \left(K^0 \langle \varepsilon_V^e \rangle \frac{\partial g^p}{\partial I_1} - c|\sigma_m| \langle \frac{\partial g^p}{\partial I_1} \rangle \right) \tag{5.40}$$

where: $f^d$is damage function, Y_v is volumetric thermodynamic conjugate force for damage, D is damage, K^0 undamaged bulk modulus, σ_m is mean nomimal stress, ε_V^e and ε_V^p are the volumetric elastic strain and volumetric plastic strain, $\mathbf{I}$ is second order identity tensor, I_1 is first invariant of the nominal stress tensor, g^p is plastic potential function, and $d\varepsilon$ is the strain tensor rate.

Then substituting Eq. (5.40) into Eq. (5.38), we can get the second consistency condition analogous to Eq. (5.34):

$$-3R_d\left(K^0\langle\varepsilon_V^e\rangle\frac{\partial g^p}{\partial I_1}-c|\sigma_m|\langle\frac{\partial g^p}{\partial I_1}\rangle\right)d\lambda+dD-R_dK^0\langle\varepsilon_V^e\rangle\mathbf{I}:d\varepsilon=0 \tag{5.41}$$

where $R_d=\frac{\partial f^d}{\partial Y_V}/\frac{\partial f^d}{\partial D}$ with $R_d<0$,and the plastic multiplier $d\lambda$ can be expressed as:

$$d\lambda=\frac{\frac{\partial f^p}{\partial\boldsymbol{\sigma}}:\boldsymbol{E}^d:d\varepsilon+R_d\left(\frac{\partial f^p}{\partial\boldsymbol{\sigma}}:\boldsymbol{E}^0:\varepsilon^e-\frac{\partial f^p}{\partial D}\right)K^0\langle\varepsilon_V^e\rangle\boldsymbol{I}:d\varepsilon}{\frac{\partial f^p}{\partial\boldsymbol{\sigma}}:\boldsymbol{E}^d:\frac{\partial g^p}{\partial\boldsymbol{\sigma}}-\frac{\partial f^p}{\partial\bar{e}^p}\frac{1}{\sqrt{3}}+3R_d(\frac{\partial f^p}{\partial\boldsymbol{\sigma}}:\boldsymbol{E}^0:\varepsilon^e-\frac{\partial f^p}{\partial D})(K^0\langle\varepsilon_V^e\rangle\frac{\partial g^p}{\partial I_1}-c|\sigma_m|\langle\frac{\partial g^p}{\partial I_1}\rangle)} \tag{5.42}$$

where: f^d is damage function.

The rate change of the damage variable can be expressed as:

$$dD=-R_dK^0\langle\varepsilon_V^e\rangle\mathbf{I}:d\varepsilon+3R_d\left(K^0\langle\varepsilon_V^e\rangle\frac{\partial g^p}{\partial I_1}-c|\sigma_m|\langle\frac{\partial g^p}{\partial I_1}\rangle\right)d\lambda \tag{5.43}$$

On the right-hand side, the first term is the traditional damage evolution controlling by strain, the second term is the coupling of the damage and the plastic dissipation process (Salari, et al. (2004))

5.4.2.4 Elastoplastic damage tangent operator

This part is proposed by Salari, et al. (2004). Substituting the Eqs. (5.41) and (5.42) into Eq. (5.32), the elastoplastic damage tangent operator can be obtained:

$$d\boldsymbol{\sigma}=\boldsymbol{E}^{epd}:d\boldsymbol{\varepsilon} \tag{5.44}$$

where E^{edp} is the tangential elastoplastic damage operator.

$$\begin{aligned}&\mathbf{E}^{epd}\\&=\mathbf{E}^d+R_dK^0\langle\varepsilon_V^e\rangle\mathbf{I}\\&\otimes(\mathbf{E}^0:\boldsymbol{\varepsilon}^e)\ \frac{\mathbf{E}^d:\frac{\partial f^p}{\partial\boldsymbol{\sigma}}+R_d(\frac{\partial f^p}{\partial\boldsymbol{\sigma}}:\mathbf{E}^0:\boldsymbol{\varepsilon}^e-\frac{\partial f^p}{\partial D})K^0\langle\varepsilon_V^e\rangle\mathbf{I}\otimes(\mathbf{E}^d:\frac{\partial g^p}{\partial\boldsymbol{\sigma}}+3R_d\left(K^0\langle\varepsilon_V^e\rangle\frac{\partial g^p}{\partial I_1}\right)-c|\sigma_m|\langle\frac{\partial g^p}{\partial I_1}\rangle\mathbf{E}^0:\boldsymbol{\varepsilon}^e)}{\frac{\partial f^p}{\partial\boldsymbol{\sigma}}:\mathbf{E}^d:\frac{\partial g^p}{\partial\boldsymbol{\sigma}}-\frac{\partial f^p}{\partial\bar{e}^p}\frac{1}{\sqrt{3}}+3R_d(\frac{\partial f^p}{\partial\boldsymbol{\sigma}}:\mathbf{E}^0:\boldsymbol{\varepsilon}^e-\frac{\partial f^p}{\partial D})(K^0\langle\varepsilon_V^e\rangle\frac{\partial g^p}{\partial I_1}-c|\sigma_m|\langle\frac{\partial g^p}{\partial I_1}\rangle)}\end{aligned} \tag{5.45}$$

If there is no damage induced, Eq. (5.45) can be simplified to the traditional elastoplastic tangent operator:

$$\mathbf{E}^{ep}=\mathbf{E}^0-\frac{(\mathbf{E}^0:\frac{\partial f^p}{\partial\boldsymbol{\sigma}})\otimes(\mathbf{E}^0:\frac{\partial g^p}{\partial\boldsymbol{\sigma}})}{\frac{\partial f^p}{\partial\boldsymbol{\sigma}}:\mathbf{E}^0:\frac{\partial g^p}{\partial\boldsymbol{\sigma}}-\frac{\partial f^p}{\partial\bar{e}^p}\frac{1}{\sqrt{3}}} \tag{5.46}$$

The elastic damage tangent operator simplified by Eq. (5.46) as:

$$\mathbf{E}^{ed} = \mathbf{E}^{d} + R_d K^0 \langle \varepsilon_V^e \rangle \mathbf{I} \otimes (\mathbf{E}^0 : \varepsilon^e) \tag{5.47}$$

5.4.3 The evolution of porosity (inserted in the Coupling Module, MATLAB)

In the host rock, the variation of its porosity ϕ from its initial value ϕ_0 can be induced by mechanical (elastic and plastic deformation, mechanical damage), chemical (mineral precipitation and dissolution) and thermal processes (expansion or contraction) (Fusseis et al., 2009; Kuhl et al., 2004). This porosity evolution can be expressed as follows (neglecting the thermal strain due to the limited temperature variation of LILWs)

$$\phi - \phi_0 = \phi_m^{de} + \phi_m^{dp} + \phi_c \tag{5.48}$$

where: ϕ_0 is the initial porosity value, ϕ_m^{de} and ϕ_m^{dp} are the elastic partitions and plastic partitions of the porosity variation due to mechanical deformation with damage, ϕ_c is the porosity evolution due to mineral dissolution and precipitation. Chemically and mechanically induced damage is mainly coupled by the porosity (Kuhl et al. 2004). It should be emphasized that the apparent porosity influences only the transport, stiffness and strength of the rock, but not the mass balance. This assumption is supported by the fact that the opening of cracks does not result in mass loss (Kuhl et al. 2004). The various constituents of porosity i.e. ϕ_m^{de}, ϕ_m^{dp} and ϕ_c are described in the followings. For the elastic part, ϕ_m^{de} can be expressed as (Yu et al., 2013)

$$\phi_m^{de} = \left(\phi_0 - \phi_\gamma\right) \exp(-5 \times 10^{-8} \sigma_m'^d) + \phi_\gamma \tag{5.49}$$

where; ϕ_0 is initial porosity, ϕ_r is the residual porosity, $\sigma_m'^d$ is mean effective stress under the damage influence. The elastic volumetric strain can also be applied directly to compute the elastic porosity change.

The plasticity-induced porosity ϕ_m^{de} can be expressed (Poulet et al., 2012) as;

$$\phi_m^{dp} = (\phi_{max} - \phi_0) D^{\frac{3}{2}} \tag{5.50}$$

where: ϕ_{max} is the maximum porosity of the host rock, ϕ_0 is the initial porosity of the host rock and D is the scalar damage factor ($0 \leq D \leq 1$). The dissolution/precipitation of mineral phases by chemical reaction induces the change in porosity as well, which will be described in the next section.

5.4.4 Governing equations in TOUGHREACT

5.4.4.1 Conservation equation

Because of the nature of both mass and energy conservations, they can be written in a similar form consisting of the flow and transport equations. These equations have been discussed by Pruess (1987 and 1991). Xu (2004) summarized these equations as followings:

For water:

$$M_w = \phi(S_l\rho_l X_{wl} + S_g\rho_g X_{wg}) \tag{5.51}$$

$$F_w = X_{wl}\rho_l\vec{u}_l + X_{wg}\rho_g\vec{u}_g \tag{5.52}$$

$$q_w = q_{wl} + q_{wg} \tag{5.53}$$

For air:

$$M_c = \phi(S_l\rho_l X_{cl} + S_g\rho_g X_{cg}) \tag{5.54}$$

$$F_c = X_{cl}\rho_l\vec{u}_l + X_{cg}\rho_g\vec{u}_g \tag{5.55}$$

$$q_c = q_{cl} + q_{cg} + q_{cr} \tag{5.56}$$

For heat:

$$M_h = \phi\left(S_L\rho_L U_l + S_g\rho_g U_g\right) + (1-\phi)\rho_s U_s \tag{5.57}$$

$$F_h = \sum_{\beta=l,g} h_\beta\rho_\beta\vec{u}_\beta - \lambda\nabla T \tag{5.58}$$

$$q_h \tag{5.59}$$

where

$$\vec{u}_\beta = -k\frac{k_{r\beta}}{\mu_\beta}(\nabla P_\beta - \rho_\beta - \rho_\beta\vec{g}) \tag{5.60}$$

$$\beta = l, g \tag{5.61}$$

Millington and Quirk (1961) gave the equation for chemical components in the liquid phase ($j = 1,2,\ldots.,N_l$):

$$M_j = \phi S_l C_j \tag{5.62}$$

$$F_j = \vec{u}_l C_{jl} - (\tau \phi S_l D_l) \nabla C_{jl} \tag{5.63}$$

$$q_j = q_{jl} + q_{js} + q_{jg} \tag{5.64}$$

$$\tau_\beta = \phi^{1/3} S_\beta^{7/3} \tag{5.65}$$

where, M is mass accumulation (kg/m^3), ϕ is porosity, S is degree of saturation, ρ is density (kg/m^3), X is mass fraction, F is mass flux ($kg/m^2 s$), $\vec{u}$ is Darcy velocity, q is source/sink, U is internal energy (J/kg), λ is heat conductivity ($W/m \cdot K$), T is temperature (℃), k is permeability (m^2), k_r is relative permeability, $\vec{g}$ is gravitational acceleration (m/s^2), C is the component concentration (*mol/L*), D is diffusion coefficient (m^2/s), p is pressure (*Pa*), μ is viscosity ($kg/m \cdot s$), N is number of chemical components. And the subscripts: c is air, g is gas phase, h is heat, j is aqueous chemical component, l is liquid phase, r is reaction, S is solid phase, w is water, κ is governing equation index, β is phase index, τ medium tortuosity.

Xu et al., (2004), also wrote the gas species diffusion coefficients as:

$$D = \frac{RT}{3\sqrt{2} P N_A d_m^2} \sqrt{\frac{8RT}{\pi M}} \tag{5.66}$$

where: D is diffusion coefficient (m/s^2), R is molar gas constant ($8.31451 m^2 kg/s^2 \cdot mol \cdot K$), T is temperature in Kelvin units, P is pressure (*Pa*), N_A is Avogadro's number ($6.0221367 \times 10^{23} molecules/mol$), d_m is molecular diameter (m), M is molecular weight (kg/mol).

5.4.4.2 Mathematical formulation of chemical reactions

To analyze the effect of the chemical reactions, mathematical formulation is necessary, Xu (2004) gave all the secondary species, which can be represented as a linear combination of the set of chemical species:

$$S_i = \sum_{j=1}^{N_c} v_{ij} S_j \qquad\qquad i = 1,2, \ldots . N_R \tag{5.67}$$

where: N_c is a subset of aqueous species as basis species (or component or primary species), S is the chemical species, *i, j*, respectively are the secondary species index and the basis species index, N_R is the number of reactions, and v_{ij} is the stoichiometric coefficient of *j-th* basis species in the

i-th reaction.

5.4.4.3 Porosity and permeability change

The following expression shows the porosity evaluation of the process by chemical precipitation/dissolution TOUGHREACT User's Guide Xu (2004):

$$\phi_c = 1 - \sum_{m=1}^{nm} f_{rm} - f_{ru} \tag{5.68}$$

where *nm* is the number of number of minerals, fr_m is the volume fraction, *m* in the rock ($V_{mineral}/V_{medium}$, including porosity), and fr_u is the volume fraction of nonreactive rock

Permeability is one of the most critical parameters in the coupling analysis in this manuscript. The permeability can be presented as follows (TOUGHREACT, Xu 2004):

$$k = k_0(\frac{\phi}{\phi_0})^3 \tag{5.69}$$

where k_0 is the initial (zero stress) intrinsic permeability, ϕ_0 is the initial porosity.

5.4.4.4 Water retention curve and relative permeability, capillary pressure

In the present study, the well-established van Genuchten model is used to express the relationship between liquid saturation degree S_l and capillary pressure ($p_c = p_g - p_l$) (van Genuchten, 1980; Xu,2004):

$$P_c = -P_0([S^*])^{-1/m} - 1)^{1-m} \tag{5.70}$$

Subject to the restriction $-P_{max} \leq P_c \leq 0$, where $S^* = (S_l - S_{lr})/(S_{ls} - S_{lr})$, $1/P_0 = \alpha/\rho_w g$ where: *m* and α the van Genuchten's parameters. S_{lr} is the residual saturation, S_{ls} is the maximal saturation.

5.4.4.5 Solute transport

Most of the chemical species are only subject to transport in the liquid phase (Xu, 2004). Therefore, in the present research, we only derive the numerical formulation of the reactive transport in the liquid phase. The multi-component chemical transport equation in the liquid phase can be expressed as (Xu, 2004):

$$\frac{\Delta t}{V_n}\sum_m A_{nm}[u_{nm}^{k+1}C_{nm}^{(j),k+1,s+1/2} + D_{nm}\frac{C_m^{(j),k+1.s+1/2} - C_n^{(j),k+1,s+1/2}}{d_{nm}}] \tag{5.71}$$
$$= \Delta M_n^{(j),k+1} - q_n^{(j),k+1}\Delta t - R_n^{(j),k+1,s}\Delta t \qquad j = 1,2,\ldots\ldots,N_c$$

where: n is the label of the grid block, m is the label of the adjacent grid blocks connected to n, j is the label of the chemical component, l is the label liquid phase while it is neglected for simplicity, k is the label of the number of the time step, s is the label of the number of the transport-chemistry iteration, Δt is time step size, V_n is an arbitrary domain, A_{nm} is a discrete sum of averages over surface segments, u_{mn} is the liquid volumetric flux or the Darcy velocity (m/s), C_{nm} is the concentrations in the advective and diffusive flux terms, D_{mn} is the effective diffusion coefficient which includes effects of porosity, phase saturation, tortuosity and weighting factors between the two grid blocks, d_{mn} is the nodal distance, $R_n^{(j)k+1}$ are the total chemical reaction source/sink terms, ΔM_n is mass accumulation, q_n is average value of source/sink term per unit volume and unit time, N_c is the total number of chemical components.

In the Eq. (5.48), the concentrations in the advective and diffusive flux terms can be calculated by

$$C_{nm}^{(j),k+1,s+1/2} = \theta\left[\varepsilon_{nm}C_n^{(j),k+1.s+1/2} + (1-\varepsilon_{nm})C_m^{(j),k+1,s+1/2}\right](1$$
$$-\theta)\left[\varepsilon_{nm}C_n^{(j),k} + (1-\varepsilon_{nm})C_m^{(j),k}\right] \tag{5.72}$$
$$C_n^{(j),k+1,s+1/2} = \theta C_n^{(j),k+1,s+1/2} + (1-\theta)C_n^{(j),k}$$
$$C_m^{(j),k+1,s+1/2} = \theta C_m^{(j),k+1,s+1/2} + (1-\theta)C_m^{(j),k}$$

where θ is the time weighting factor, the values of θ is from 0 to 1; $\theta = 1$ means a fully implicit calculation, and

$$\varepsilon_{nm} = \begin{cases} 0 & if \quad u_{nm} \geq 0 \quad inflow \\ 1 & if \quad u_{nm} < 0 \quad outflow \end{cases} \tag{5.73}$$

The mass accumulation terms can be calculated as:

$$\Delta M_n^{(j),k+1} = S_{l,n}^{k+1}\phi_n^{k+1}C_n^{(j),k+1,s+1/2} - S_{l,n}^{k}\phi_n^{k}C_n^{(j),k} \tag{5.74}$$

The chemical reaction source/sink term $R^{(j),k+1,s}$ represents the mass transfer of component j between aqueous and solid phases. It can be expressed as:

$$R_n^{(j),k+1,s}\Delta t = -\Delta P_n^{(j),k+1,s} \tag{5.75}$$

where $\Delta P_n^{(j),k+1,s}$ represents the mass transfer of component j from the liquid phase to the solid phase at iteration s, grid block n and time step k+1.

5.5 Model validation and application to laboratory and field scale experiments

The developed simulator, as described above, will be validated against data from the laboratory and field experiments on gas migration in host rocks of DGR for nuclear waste. It should be underlined that there are no lab or field experiments on gas migration in host rocks that consider or include all THMC processes that can take place in a host rock. Up to now, all laboratory or field experiments consider only the H or HM processes. Consequently, only the coupled HM components of the simulator will be validated in the following sections.

5.5.1 Simulation of laboratory experiments

5.5.1.1 Description of laboratory tests

To verify the capabilities of the developed simulator to accurately predict the gas migration within a rock at laboratory scale, experimental results from laboratory scale gas injection tests on Opalinus Clay were used (Popp et al., 2008). These rock specimens were taken from the Mont Terri rock laboratory. The cylindrical specimens with length of 150.45 *mm* and diameter of 73.59 *mm* were subject to monotonic triaxial tests, under a certain confining pressure and axial loading with incrementally increasing gas injection pressure. There were two holes drilled at symmetric axis of the cylindrical specimen from the top and bottom. In Figure 5.3, the apparatus of the test is illustrated in detail.

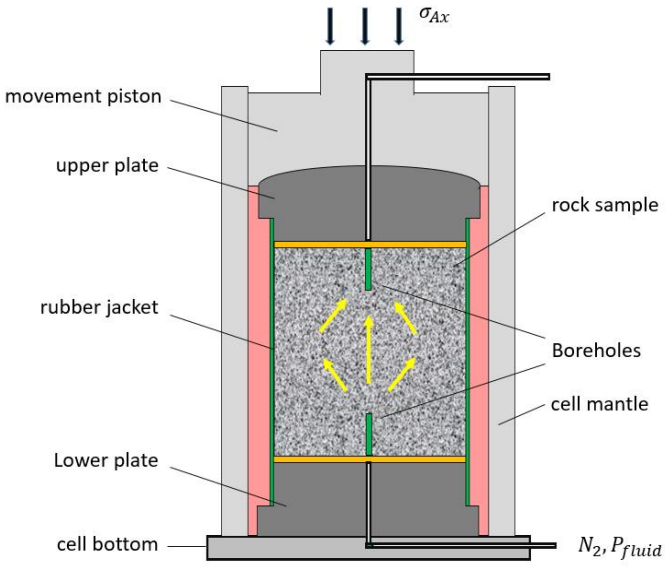

Figure 5.3 The sketch of the laboratory experiment for the gas injection (Popp et al., 2008)

Nitrogen was used as the test gas and injected at controlled pressure in the hole at the central borehole of the bottom (Figure 5.3). The gas flow rate was monitored at the upper outflow borehole. The experiments included two gas injection tests. In the first test, the specimen was subjected to a constant confinement pressure ($P_{c0} = 3MPa$) (Figure 5.4), while the gas pressure was increased sequentially. The second test was conducted with increased confinement pressure and sequential increase of the gas pressure (Figure 5.5). More details about the experimental set up and the tests are provided by Popp et al., (2008) and Xu et al., (2011).

Table 5-1 shows the values of the main parameters used for simulating the gas injection. Figure 5.7 and Figure 5.8 present the validation results, respectively. Figure 5.7 shows the comparion between measured gas flow rate and the predicted gas flow rate with and without the influence of mechanical damage for the first test of a constant confinement pressure. Figure 5.8 shows the comparison between measured and simulated gas flow rate for the second test of an increased confinement pressure.

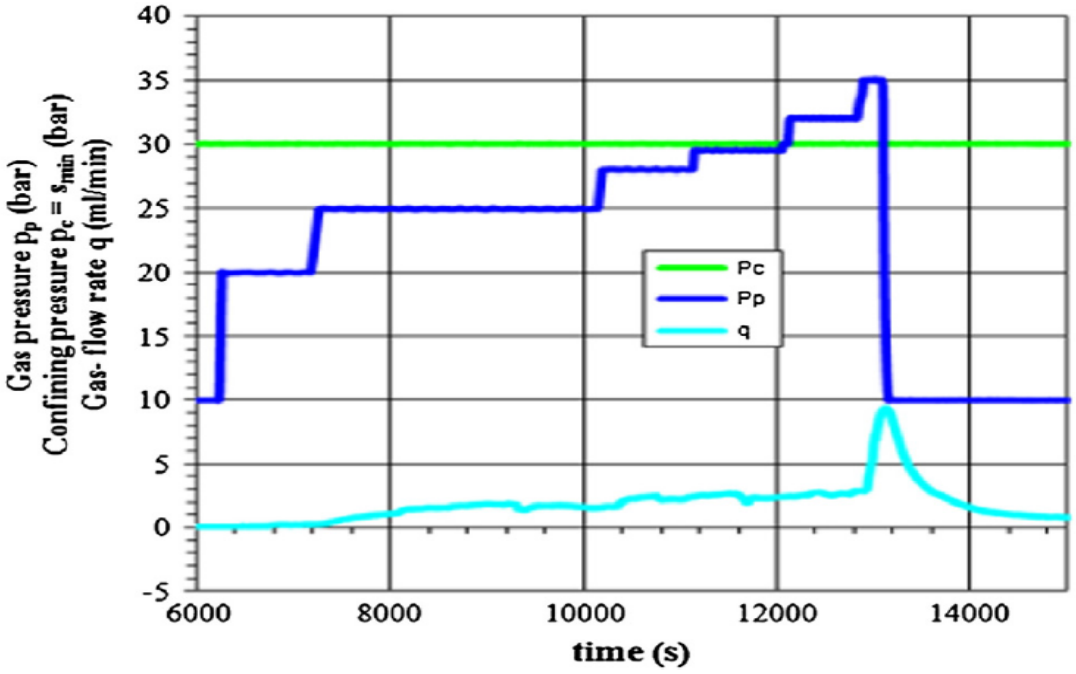

Figure 5.4 Gas injection pressure versus time (Pp) and constant confinement pressure (Pc) vs out-flow rate variation (ɳ) (Popp et al., 2008)

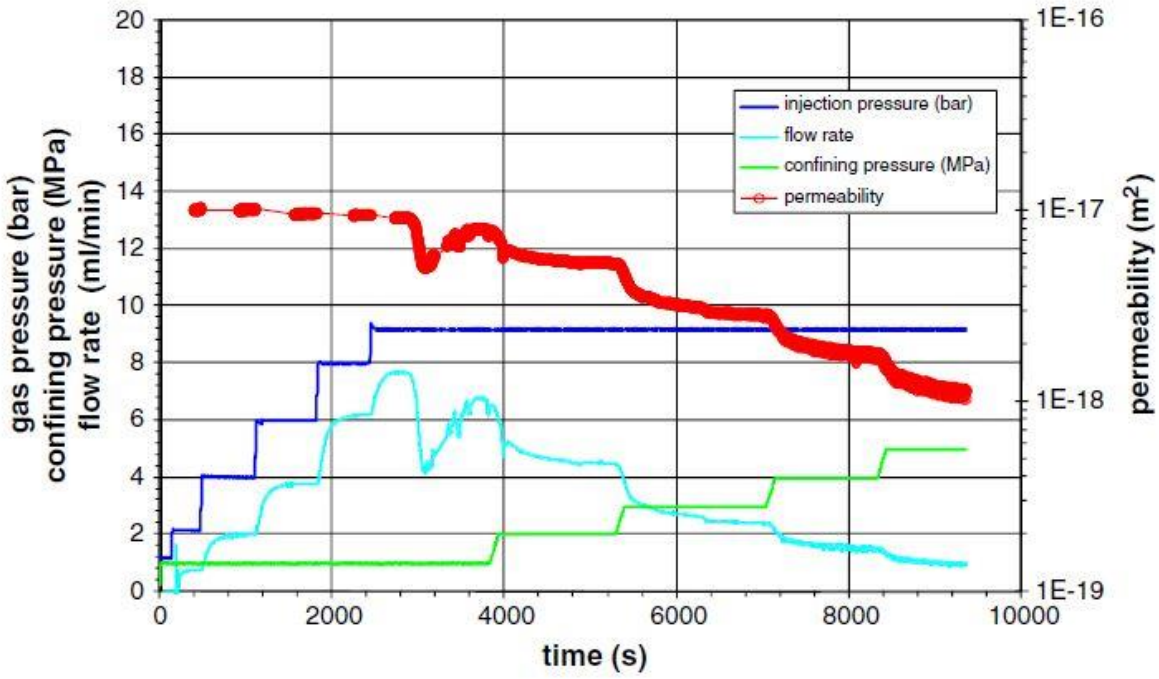

Figure 5.5 Gas injection versus time (p_p) and evolutive confining pressure (p_c) vs out-flow rate (q) (Popp, 2006)

Figure 5.6 shows the finite element mesh and the boundary conditions for the 2-D axisymmetric numerical model. The confining pressure as the constant load is applied on the circumferential boundary and the top boundary, while the bottom boundary is fixed in deformation. The borehole is set as a roller boundary. For the gas and liquid boundary conditions, the pressure of bottom borehole boundary is equal to the gas injection pressure, while the pressure of the top borehole boundary is equal to the atmospheric pressure. The rest of the boundaries are all treated as impermeable. The main HM parameters for the specimens are shown in Table 5-1 which are after Popp et al. (2008).

Table 5-1 Material properties for the validation model

Parameters	**Unit**	**Value**
Bulk density ρ	[kg/m^3]	2400
Initial permeability k	[m^2]	9.5×10^{-16}
Biot coefficient α		1.0
Gas entry pressure p_0	[Pa]	9×10^4
Water viscosity η^w	[Pa.s]	0.001
Gas viscosity η^g	[Pa.s]	1.6×10^{-5}
Water residual saturation $S_{w,r}$		0.5
Gas residual saturation $S_{g,r}$		0
Initial porosity n_0	[-]	0.16
Initial saturation S_0	[%]	90
Residual saturation S_{lrm}	[%]	0
Modulus of elasticity E	[GPa]	10
Poisson ratio v	[-]	0.27
Van Genuchten's parameter		
M		0.5
α	[m^{-1}]	0.1
Damage equation parameters		
Strain ε_{to}		7.2×10^{-4}
Friction angle θ	[˚]	24
Dilation angle φ	[˚]	0
Cohesion c	[MPa]	4.5
f_c is the uniaxial compressive strength	[MPa]	120
f_{cr} is the residual compressive strength	[MPa]	3.0
Permeability vs porosity fitting constant (A)	[-]	200

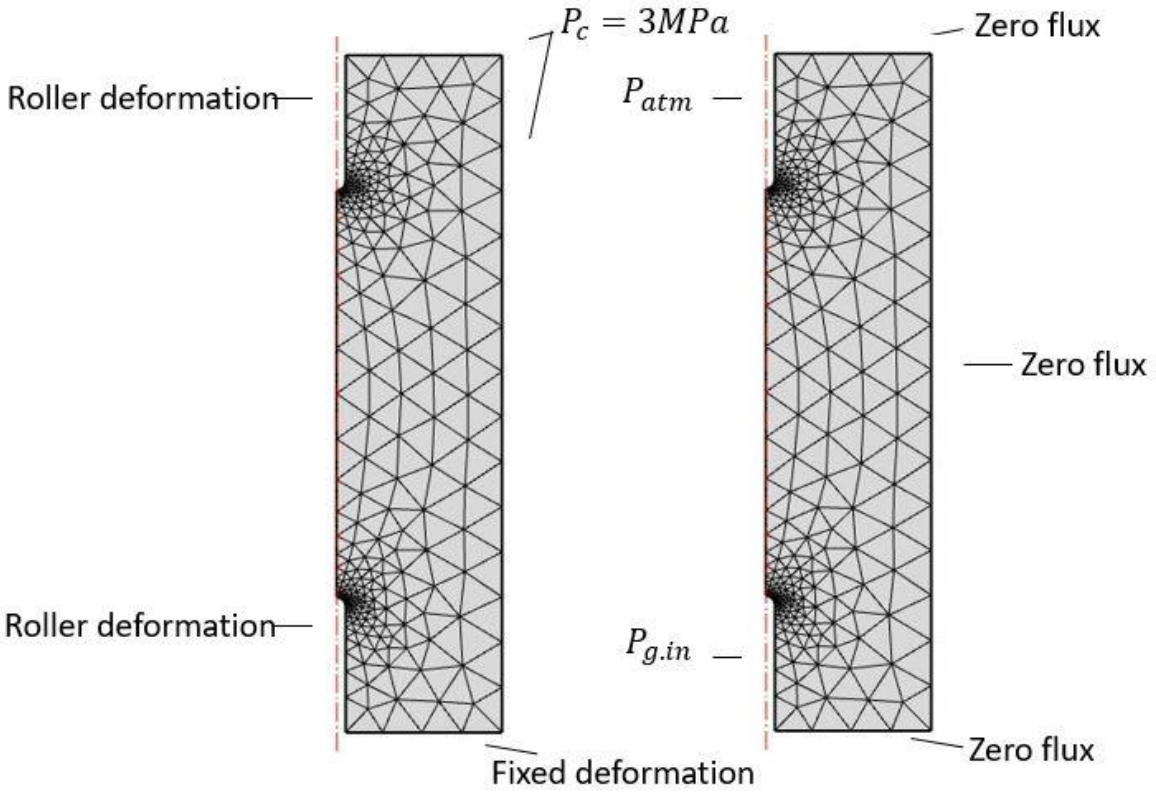

Figure 5.6 The meshing of the FE model and the hydraulic-mechanical boundary conditions

5.5.1.2 Numerical results

5.5.1.2.1 The gas flow rates comparion of the laboratory measurements to modelling results

Figure 5.7 shows the simulation results and the comparison with test data regarding the gas flow rate with elapsing permeation time. To highlight the important influence of the mechanical damage caused by high gas pressure on gas migration in host rock, we compared two scenarios of modelling with and without mechanical damage, as shown in Figure 5.7. It clearly demonstrated that the model with damage can adequately predict the peak gas flow rate and the following rapid reduction within the Opalinus Clay, while without damage, under high gas injection pressure (>30 bar), the predicted peak value in gas flow rate matches the measured gas flow rate less. Thus, it is necessary to take into account the mechanical damage in the THMC coupled modelling for assessment of gas migration in the sedimentary rock.

From Figure 5.4 and Figure 5.7, it can be seen that until gas injection pressure of approximately 2.8 MPa (t<10,500*s*), the models with damage or without damage have the same trend to predict the gas flow rates. Both models can reproduce the early evolution of the gas flow rate very well. However, there seems to exist a distinct flow regime between calculated gas flow rate and measured flow rate (from 6,200 to 12,800 *s*). The model with damage overestimates the gas flow when the gas pressure starts to surpass the confinement pressure. This overestimation can be explained by the permeability enhancement that is expressed as a function of the damage-induced porosity in Eq. (5.49) and (5.50). It is assumed in the elastoplastic damage model that the formed cracks are connected and this contributes directly to the permeability growth. This may neglect the fact that the nucleation and propagation of the micro-cracks, which could induce significant modification of the permeability, are usually time-dependent and take place gradually under loading conditions beyond the crack initiation threshold. The results of simulations indicate that the developed simulator model can adequately predict the gas migration within the laboratory sample and satisfactorily describe the THMC coupled processes in the porous media.

Permeability shift in rock is found to relate strongly with the volumetric strain. Popp et al. (2007) measured the gas permeability of Opalinus Clay during the triaxial compression test, and observed clear switching of permeability from decreasing to increasing trend near the Crack Damage (CD) threshold where dilatancy in volume strain happens. The CD threshold for Opalinus Clay is reporded to be 80-90% under deviatoric loading. The gas injection test as analyzed in this study revealed a similar threshold value of CD=80% for Opalinus Clay, instead, under the hydrostatic loading conditions. As shown in Figure 5.4 at t=7200 s, the gas pressure was elevated to 25 MPa, which simultaneously resulted in an obviously enhanced permeability increase as shown in Figure 5.7. While maintaining a constant pore pressure p=25 MPa from t=7,200 to 10,000 s, the measured flow rate is increasing continuously and steadily, suggesting a cumulative damage effect of fracturing on the tested sample. Therefore, the threshold value of CD=80% for the rock sample under the hydrostatic pressure of 30 MPa indicates the onset of crack damage and volumetric dilatancy. This value corresponds very well with the experimentally measured CD value under deviatoric stress conditions (Popp and Salzer, 2007), implying that the CD value is likely an intrinsic material property and independent of the loading conditions. The modelling with elastoplastic damage model briefly catches the onset of cracking and well reproduces the peak permeability and the following quick sealing of cracks by reducing the injection gas pressure.

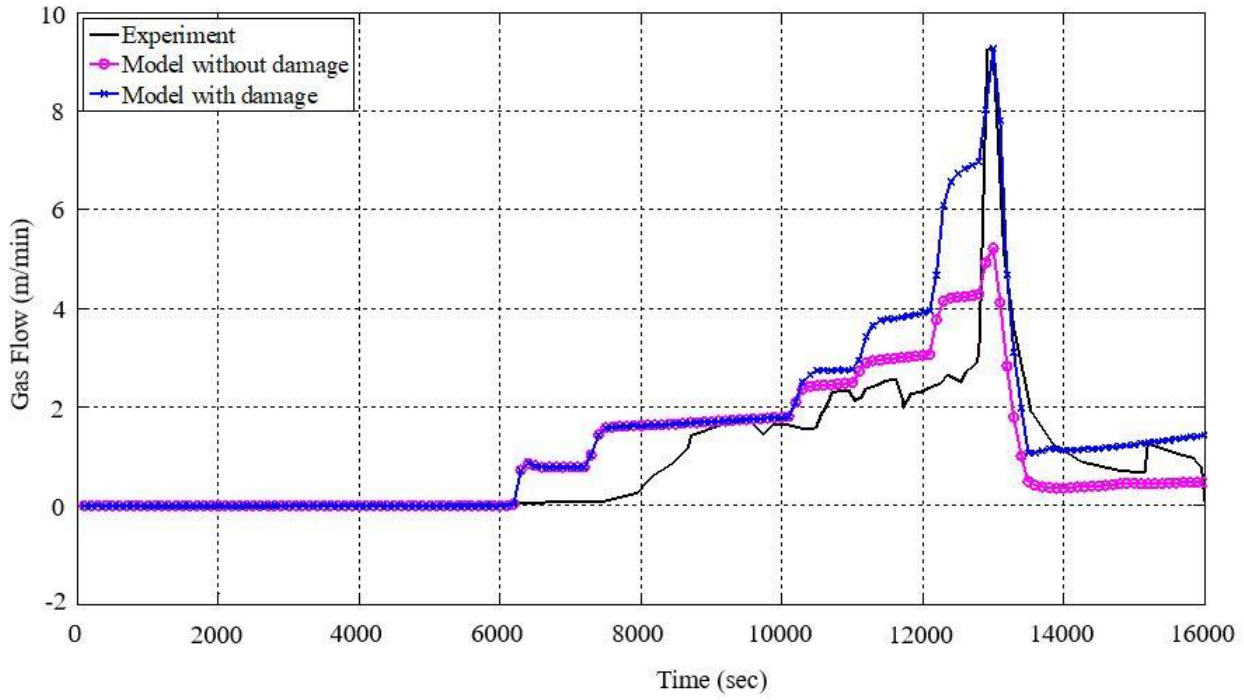

Figure 5.7 Comparison between laboratory measurement and numerical results

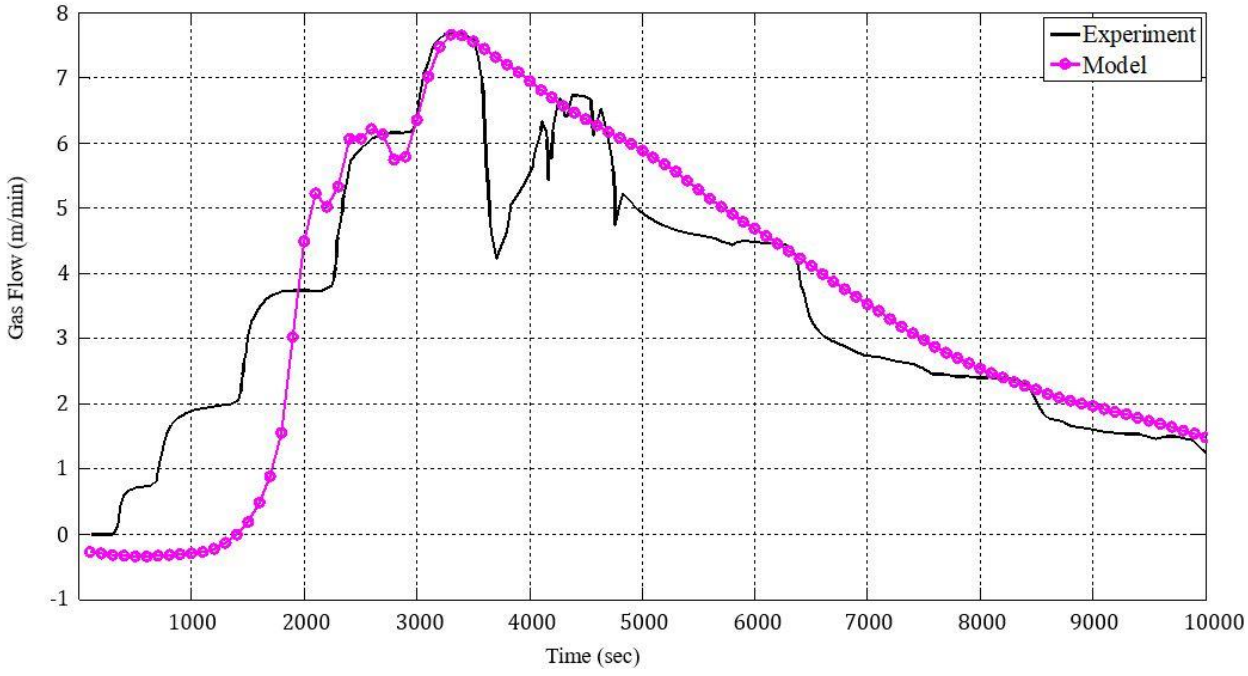

Figure 5.8 Comparison between the measured and predicted gas flow rate with the increased confinement pressure

5.5.1.2.2 Other results of the numerical simulation of the gas injection tests

Other results from the numerical simulation of the gas injection tests on the laboratory samples of Oplinus Clay are described and discussed in this section. The mechanism of gas flow through the Oplinus Clay will be more clearly illustrated by these results. Figure 5.9 and Figure 5.11 show that evolutions of the spatial distributions of the gas pressure and rock permeability separately. From Figure 5.9 and Figure 5.11, it can be seen that, the maximum gas pressure is nearly 3.5 MPa at the time of 13,000s. At the same time, the rock damage is developed in a certain degree. It is clearly and graphically demonstrated that the high gas pressure can induce the mechanical damage in the sedimentary rock. The generation and propagation of the damage result in the sudden increase in gas flow rate and a quick decrease of the gas pressure after the peak at the time of 13,000s. Figure 5.10 shows the spatial distribution of the rock permeability. At the time of 10,000s, although the induced damage of the sample is negligible, there is still an obvious increase of the permeability. It means that other factors can influence the change of the rock permeability, in addition to the mechanical damage. While at the time 13,000s, it is obvious that the damage has a contribution in the significant increase of rock permeability. These results illustrate again the importance of the consideration of the mechanical damage in the whole simulation.

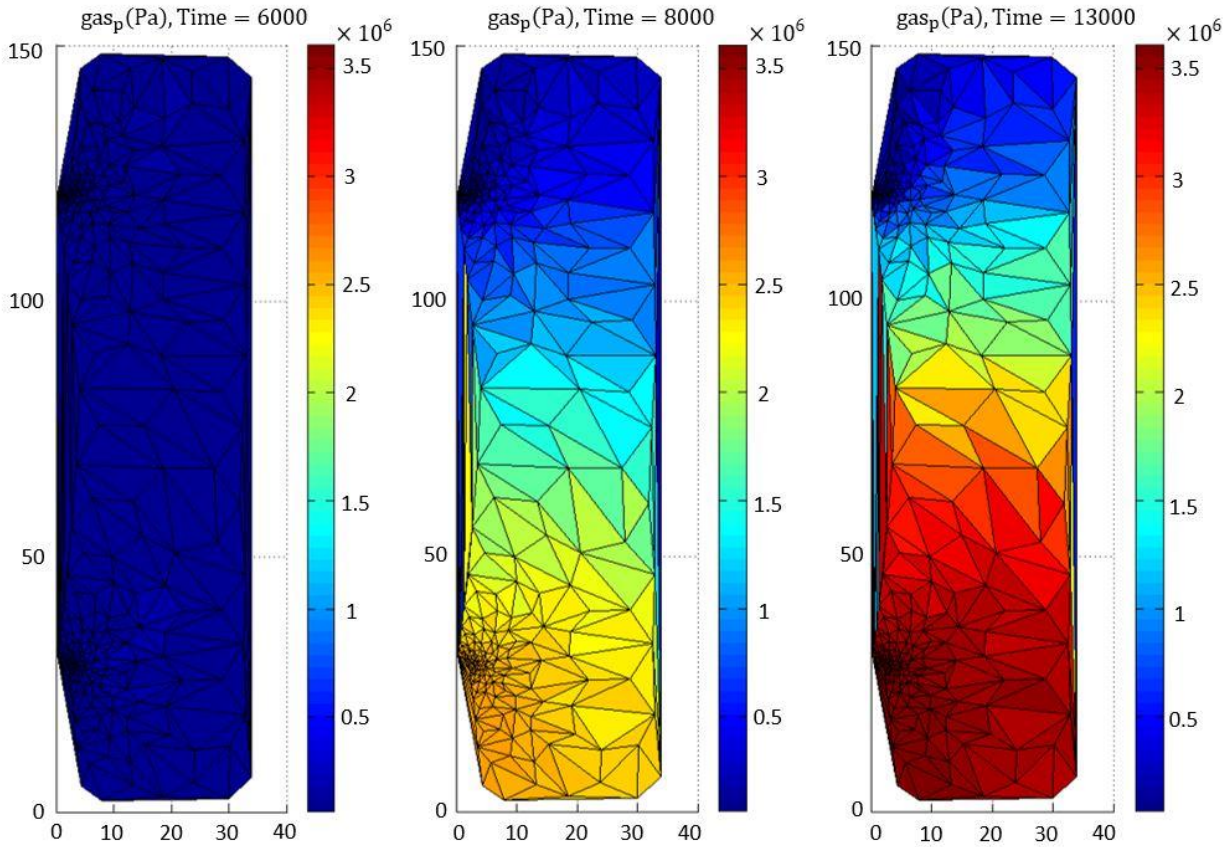

Figure 5.9 Simulated evolution of the spatial distribution of the gas pressure from TOUGHREACT

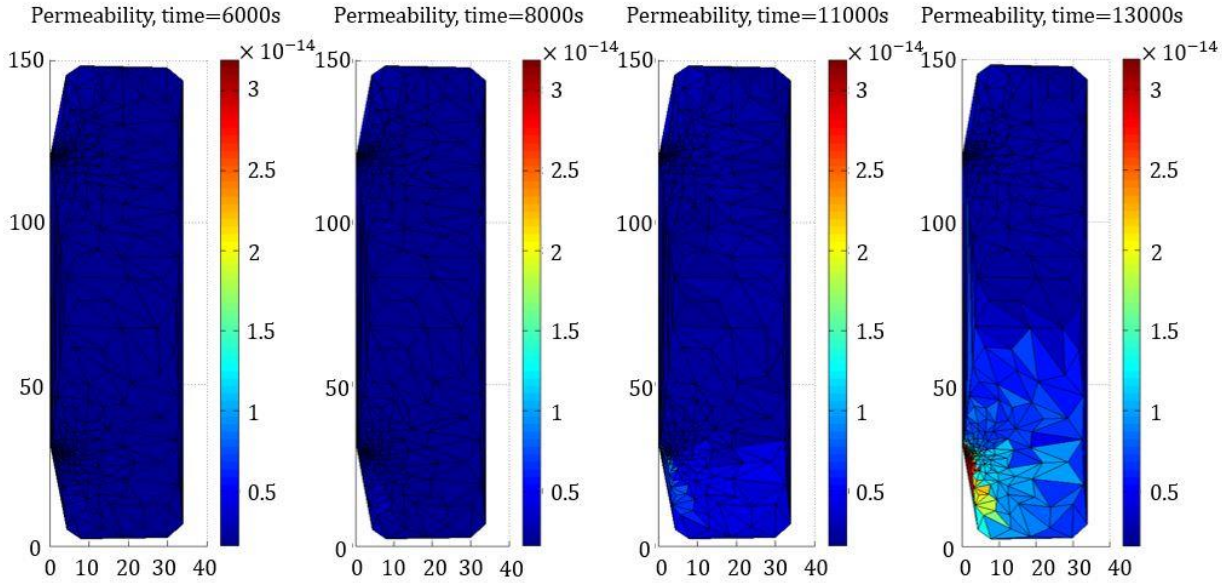

Figure 5.10 Computed evolution of the spatial distribution of the rock permeability from TOUGHREACT

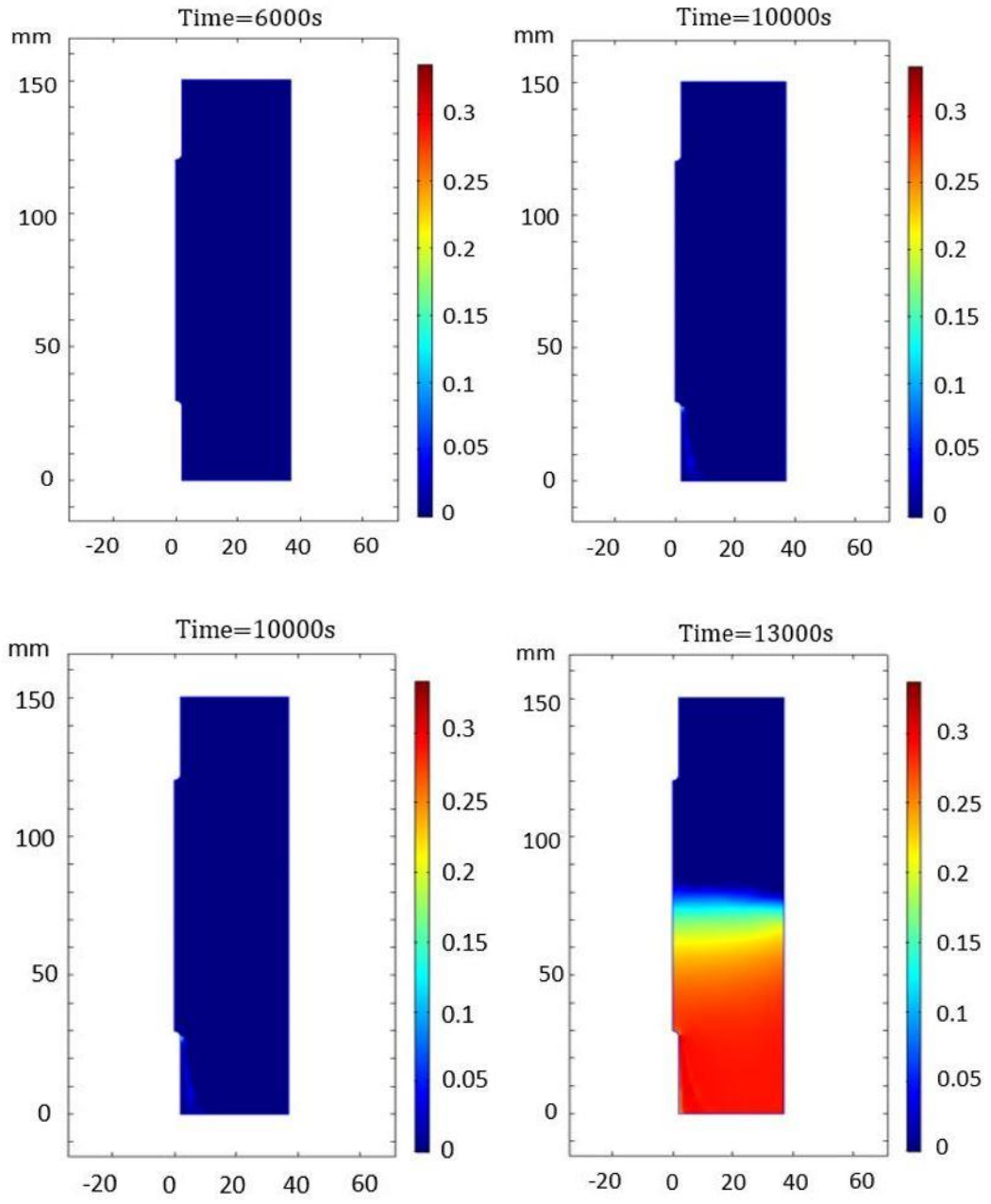

Figure 5.11 Computed evolution of the spatial distribution of the rock damage induced by gas pressure from COMSOL

5.5.2 Simulation of the *in-situ* tests

5.5.2.1 Description of *in-situ* tests

The Mont Terri Project is an international project for the characterization of the clay-shale formation (OPC) in the aspects of hydrogeology, geochemistry, and geotechnique to ensure the potential suitability of the geological formation for the disposal of radioactive wastes (Nguyen and Le, 2014). A series of *in-situ* gas injection tests were conducted to further understand gas flow processes in sedimentary rock under different injection pressure at the Mont Terri Underground Laboratory (Figure 5.12). The laboratory is located in the Jura Mountains of northwestern Switzerland. As shown in Figure 5.12, Mont Terri is an asymmetrical anticline folded mountain formed during the Late Miocene to Pliocene period. The HG-B experiment at Mont Terri Rock Laboratory was carried out to further research the gas migration under different injection pressures at different locations (Shao and Schuster, 2009). The gas injection tests of the HG-B experiment are conducted at the location of EZ-A niche (Figure 5.13). It is situated in the shaly faces of the Opalinus Clay and was excavated in the fall of 2003. There are four boreholes drilled in parallel with a same diameter of 86 mm (Figure 5.13), which were for hydraulic testing (gas and water) and seismic monitoring. The boreholes are perpendicular to the bedding plane and 45°oriented upwards. (e.g. 45°angle between the bedding plane and the tunnel) (Shao and Schuster, 2009). The central borehole BHG-B9 used for the pneumatic and hydraulic testing with a single packer system at 10m length is situated at the same distance with the boreholes BHG-B6 to BHG-B8 (Fall and Nasir, 2012).

A measurement of gas permeability was carried out to determine the gas permeability of the undisturbed rock mass after the drilling of each borehole. Nitrogen gas was injected into the last one-metre section of the boreholes during the test. The gas injection pressure was 0.2 MPa. During the beginning of the test, a very low pressure decay rate was monitored due to the low rock permeability (Xu, et al., 2013)

As showing in Figure 5.14, after the permeability measurement, the following pulse tests with a stepwise increase of gas injection pressure were carried out in the test section of BHG-B9. It was sealed with a 0.6 *m* long packer at the end of the 1 *m*. There were three series of the gas injection tests and two series of formation water injection tests, as shown in Figure 5.15. Each series consisted of several tests with a stepwise instantaneous increased of gas injection pressure.

Nitrogen was used as the test gas. The maximum injection pressure of the gas was 2.5 MPa. The details of the gas injection tests are presented in Shao and Schuster (2009).

The ultrasonic measurements were carried out stepwise in each borehole to monitor crack generation, opening or closing and the changes of the near field properties induced by gas injection. In addition, the progressive failure of the rock could be characterized from the temporal change of ultrasonic velocity. The ultrasonic borehole probe and the whole measurement procedures are described in detail by Schuster et al. (2001).

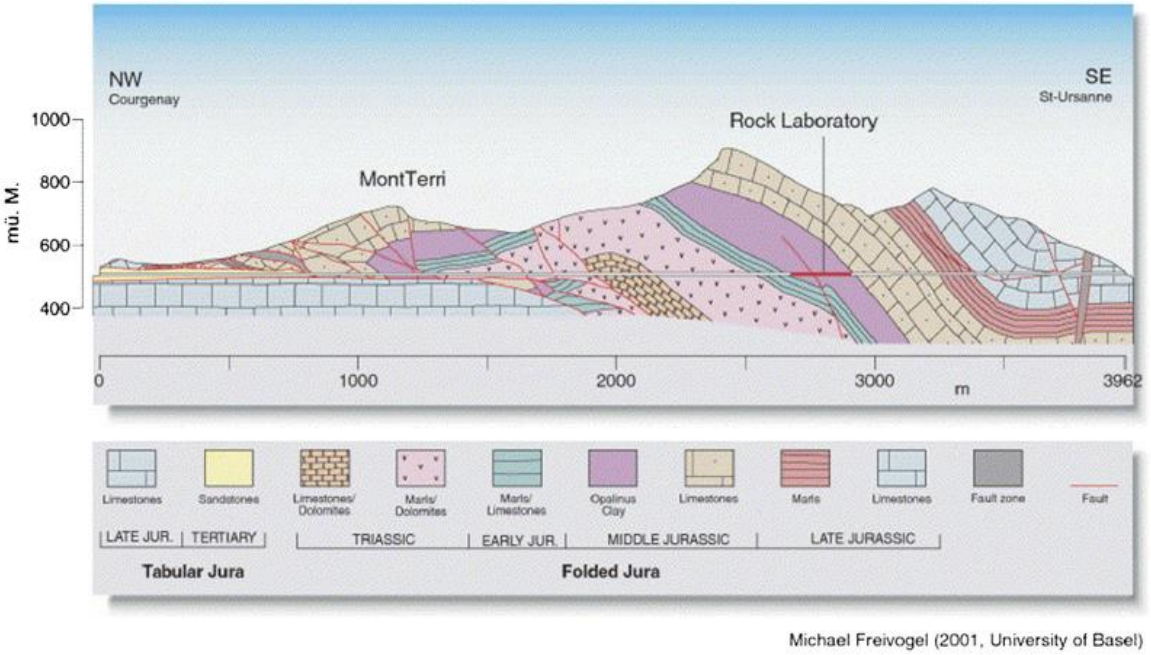

Figure 5.12 Geological section showing the location of the Mont Terri Underground Rock Laboratory (Freivogel, 2001)

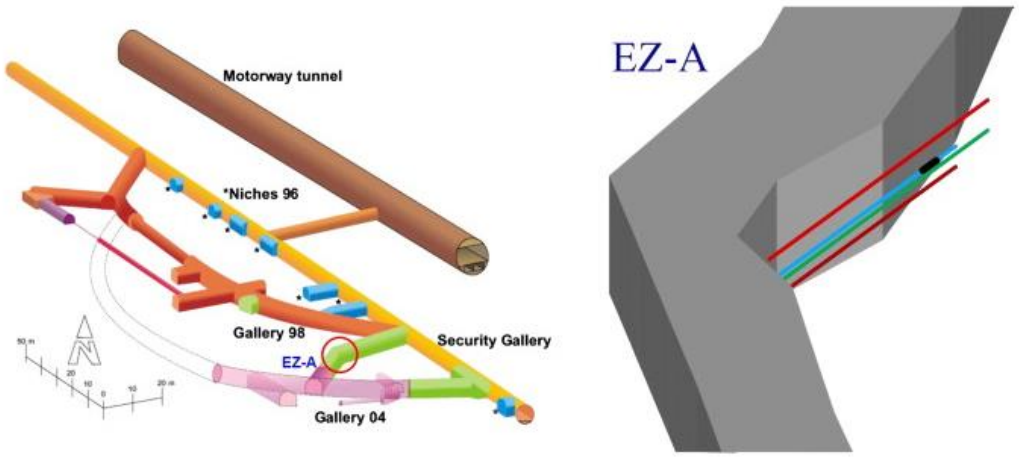

Figure 5.13 Details of Mont Terri Underground Rock Laboratory (left) and location of the boreholes for the *in-situ* experiment (right) (Shao and Schuster, 2009)

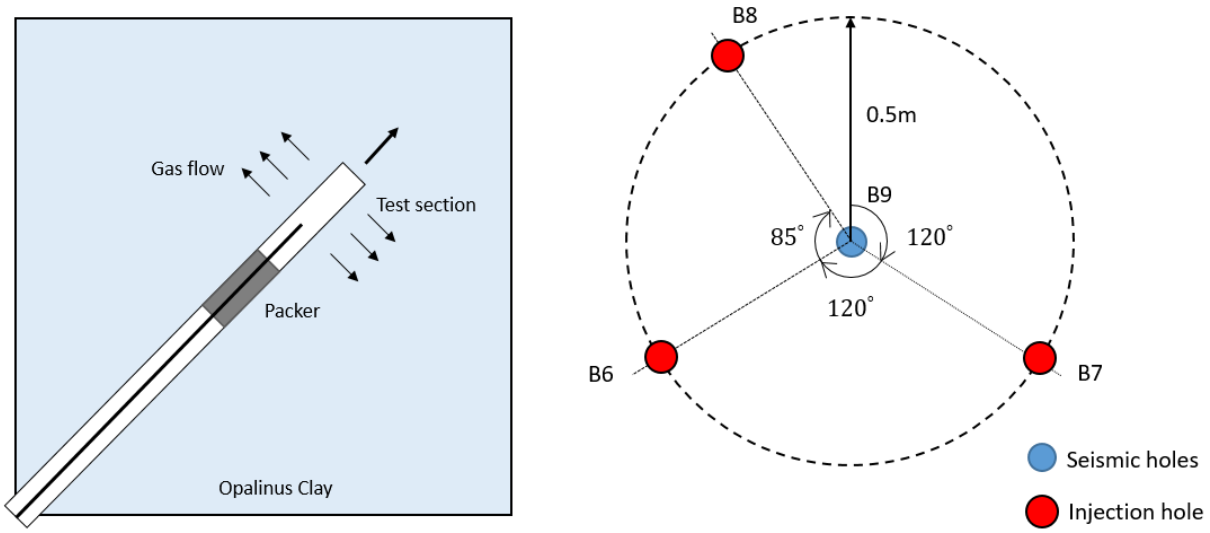

Figure 5.14 Schematic presentation of field gas injection test and the layout of the boreholes in the underground laboratory Mont Terri (Shao and Schuster, 2009)

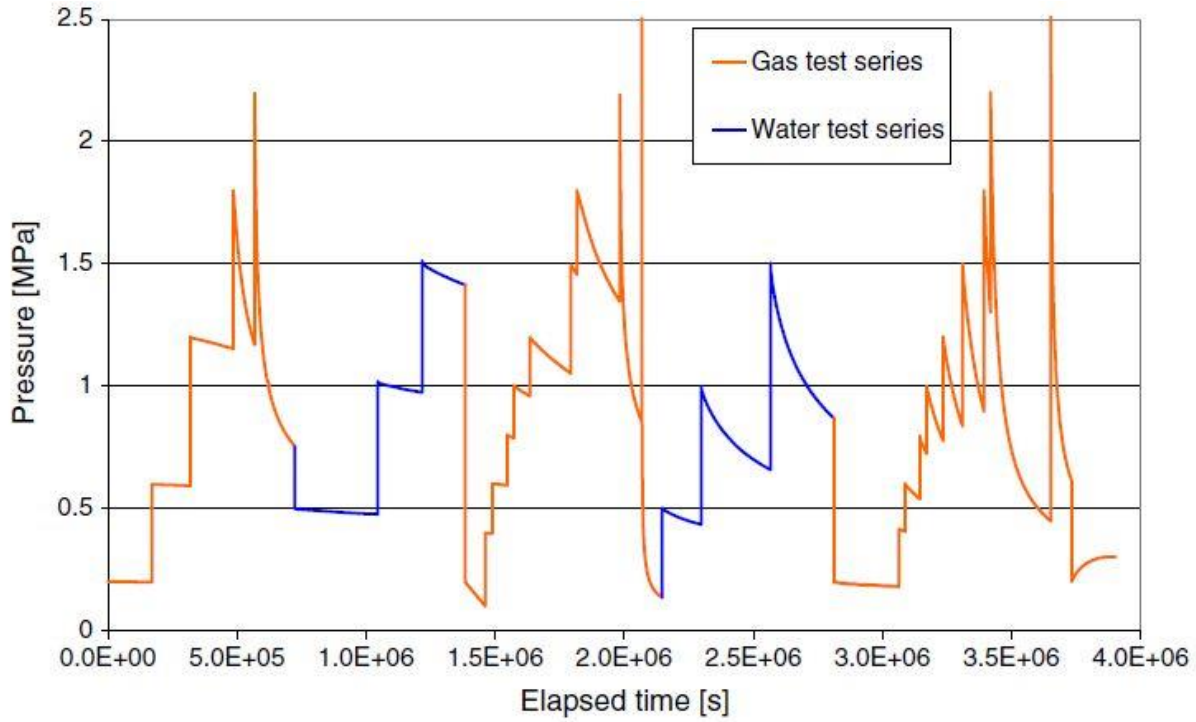

Figure 5.15 *In-situ* tests of the gas and water injection series (Shao and Schuster, 2009)

In this study, a 2-D FEM model was developed to numerically simulate the HM coupled processes during the gas injection test. Figure 5.16 shows the graphical description of the conceptual model as well as the mechanical and hydraulic boundary conditions. The geomechanical characteristics and hydraulic properties of the rock mass are shown in Table 5-2. Three series of gas injection and two of water injection were carried out (Shao and Schuster, 2009). In this study, we focus on the first series of the pneumatic experiment. It included five test phases with the peak values of 0.2, 0.6, 1.2, 1.8, and 2.2 MPa (Figure 5.15). A pulse of pressure was first applied to the borehole in a transient mode and was then shut off to the pressure source in order to allow the pressure to decrease when gas migrated outwards into the host rock. The numerical simulation employs the same boundary condition, i.e. elevating the pressure in the borehole temporarily and releasing the pressure boundary in the next time step to mimic the pulse decay process. The evolution of gas pressure at the boundary of rock/borehole interface was monitored for verification.

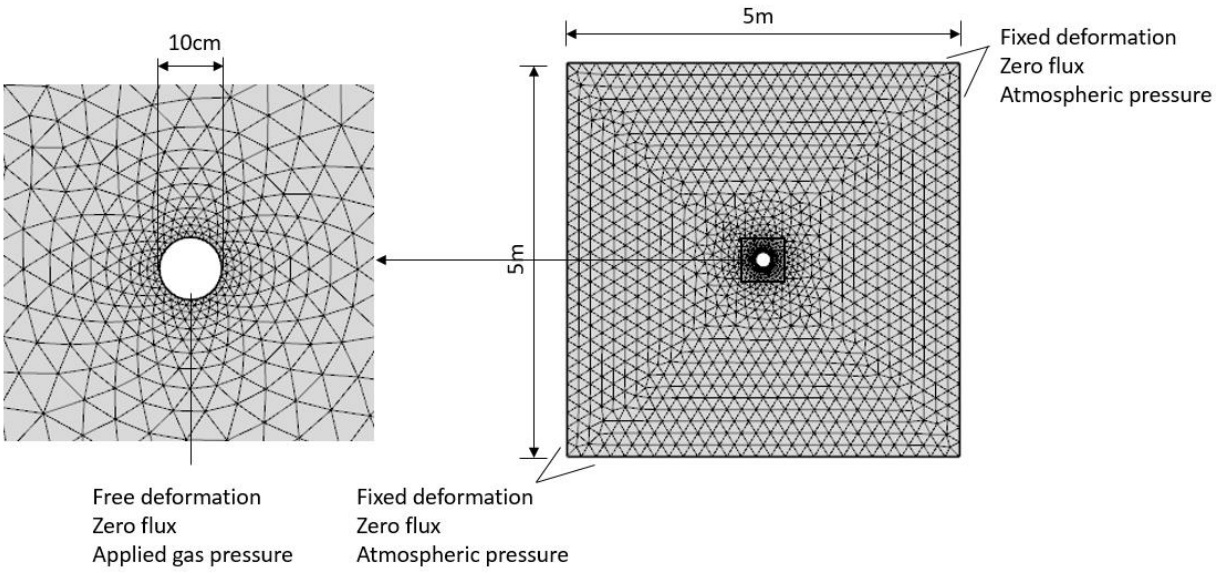

Figure 5.16 The grids of the two-dimensional model with the mechanical-hydraulic boundary conditions

Table 5-2 Material properties for the validation model

Parameters	**Unit**	**Value**
Initial gas pressure p_g	[Pa]	1.5×10^{5}
Gas entry pressure p_0	[Pa]	1×10^{6}
Permeability	[m^2]	1e-20
Water viscosity η^w	[Pa.s]	0.001
Gas viscosity η^g	[Pa.s]	1.6×10^{-5}
Porosity	[-]	0.12
Initial saturation	[%]	100
Residual water saturation	[-]	0
Residual gas saturation	[-]	0
Poisson ratio	[-]	0.27
Biot coefficient α		1
Young's modulus	[GPa]	11.4
Friction angle	[°]	24.5
Dilation angle φ	[°]	0
Cohesion	[MPa]	8.6
Tensile strength σ^t	[MPa]	2.5
Residual tensile strength	[MPa]	0.8
Van Genuchten's parameter		
M	[-]	0.5

a	m^{-1}	0.1
Strain ε_{to}	[-]	0.9×10^{-4}
f_c is the uniaxial compressive strength	[MPa]	12
f_a is the residual compressive strength	[MPa]	3.0
Strain ε_{co}		7.2×10^{-4}
Permeability vs porosity fitting constant (A)	[-]	200

5.5.2.2 Numerical results

Figure 5.17 shows the comparison between the calculated and measured gas pressure during the simulation period of the first injection series. In order to study the impact of the mechanical damage induced by high gas pressure during the gas injection tests, two models were simulated. In the first case, only the THMC (excluding mechanical damage) coupling behavior was modeled. In the second case, the mechanical damage coupled with the the THMC processes was simulated. In Figure 5.17, two scenarios of modelling results with and without mechanical damage compared with the measured gas pressure are presented.

It can be observed that there is a similar trend between results predicted by the simulator using the THMC-Damage model and the values of gas pressure measured in the field. For the first two injection steps (0.2 and 0.6 MPa), the modelling with the consideration of damage or not resembles the experimental observation very well, which might be attributed to the low injection pressure under the critical pressure level (1.2 MPa). During the following test phases, there is a discrepancy between the predicted results and the experimental results, when the mechanical damage was ignored in the model. The reason is likely due to the high gas pressure beyond the minimum principal stress (σ_1 is 6-7MPa, σ_2 is 4-5MPa and σ_3 is 0.6-2MPa), which causes not only the rock deformation but also the mechanical damages (connections of cracks and pores enlargement) and leads to the increase of the permeability. It means that the mechanical damage has significant impact on the gas migration or model response and needs to be considered to simulate the gas migration processes reliably especially under the high pressure situation. Conclusionly, the THMC model with damage can be better than the model without damage to reproduce the processes of the gas injection experiment. From the Figure 5.17, it can be noticed that during the third phase (gas injection pressure of 0.8 MPa), the THMC model with damage predict the gas pressure a little lower than the model without damage. This overestimate can be explained that at the beginning of

the rock deformation or damage formation, most of the enlarged rock pores or the micro-cracks are not connected to induce the consequential increase of the permeability. At the stage of 2.2 MPa gas injection pressure, it existed a very little difference between the simulated gas pressure calculated under the model with damage and the measured gas pressure. The main reason for this acceptable difference was that the connected micro-cracks enlarged to the cracks under the high gas pressure. The actual gas migration rate therefore faster than the expected results at the same time.

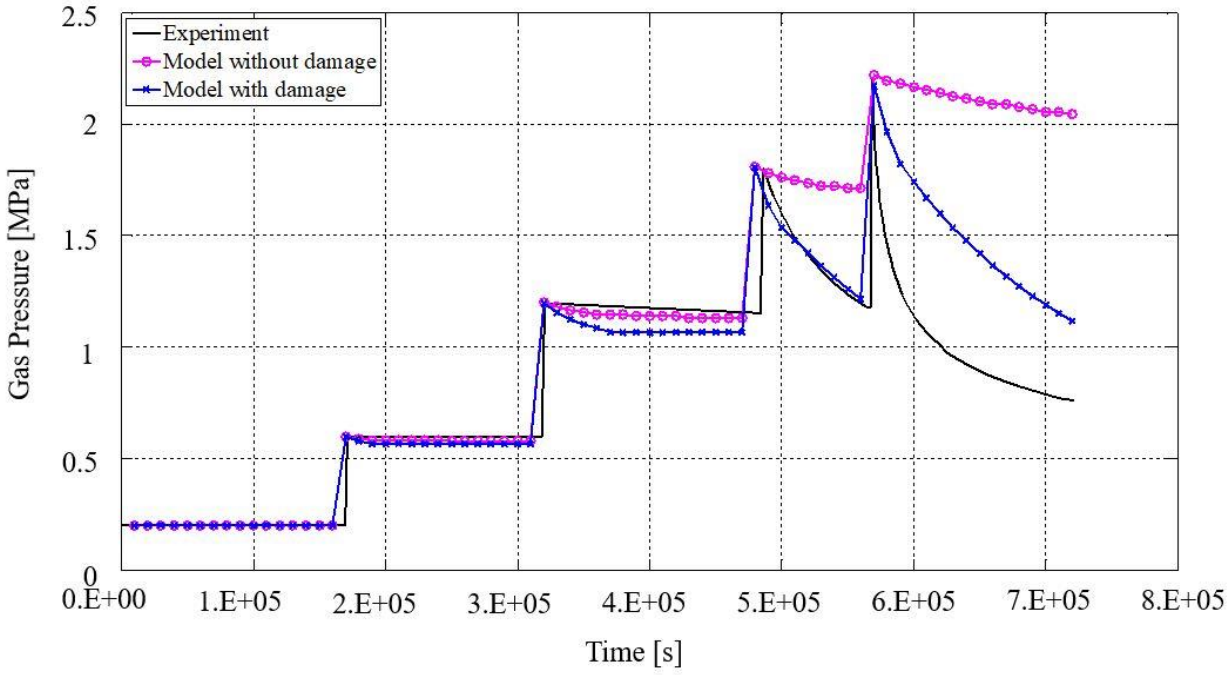

Figure 5.17 Comparison between the measured and simulation results of gas pressure of the *in-situ* experiment

5.5.2.3 Other results of the numerical simulation of the *in-situ* gas injection tests

Some other representative simulation results from the numerical calculation to show the variation of gas pressure, rock permeability and rock damage at different times during the *in-situ* tests will be presented in this section. Figure 5.18 shows the evolution of the spatial distribution of the gas pressure within the rock mass at the stage of 0.2, 0.6, 1.2, 1.8 and 2.2 MPa gas injection pressure. From Figure 5.18, the maximal gas pressure is at the injection zone and decreases gradually along with the horizontal distance. Additionally, after the gas breakthrough, the gas pressure decreases. Figure 5.19 illustrates the temporal evolution of the rock permeability. The simulation of the

permeability was based on the fully coupled THMC-D aspects. Therefore, the development of the permeability was dependent on the volumetric strain due to mechanical deformation with damage and the chemical reactions. The permeability increased significantly when the damage zone was developed and the volume strain was accumulated. The permeability was simulated by about 1000 times higher ($1 \times 10^{-17} m^2$) than the initial intrinsic permeability ($1 \times 10^{-20} m^2$) in the damage zone. Figure 5.20 presents the spatial and temporal evolution of the mechanical damage. It can be seen that the maximum damage at every instant is concentrated on the region surrounding the gas injection area, which corresponds to the highest gas pressure zone. It also can be noticed that, at the low gas injection pressure (under 1.2 MPa), there is no mechanical damage. The micro-cracks are generated from at the gas injection pressure of 1.2 MPa to 1.8 MPa around the gas injection zone. The main reason of this phenomenon is that the gas pressure increases with the effective stress decreases in the pore space of the rock (Eq.(5.9)). When the increased gas pressure is equal or higher than the minimal principal stress component, the mechanical damage is induced by the high gas injection pressure.

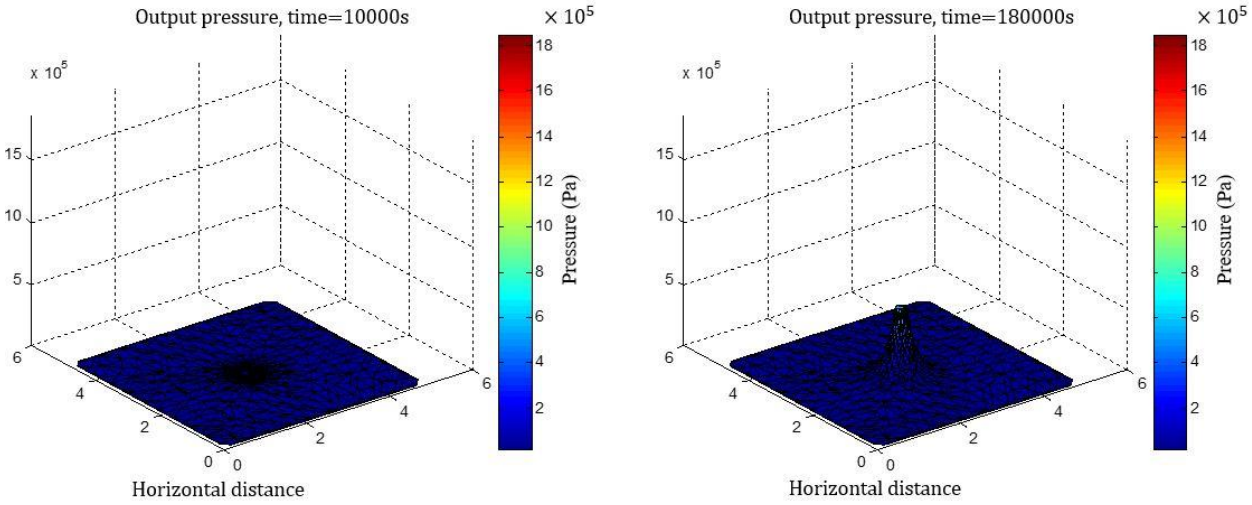

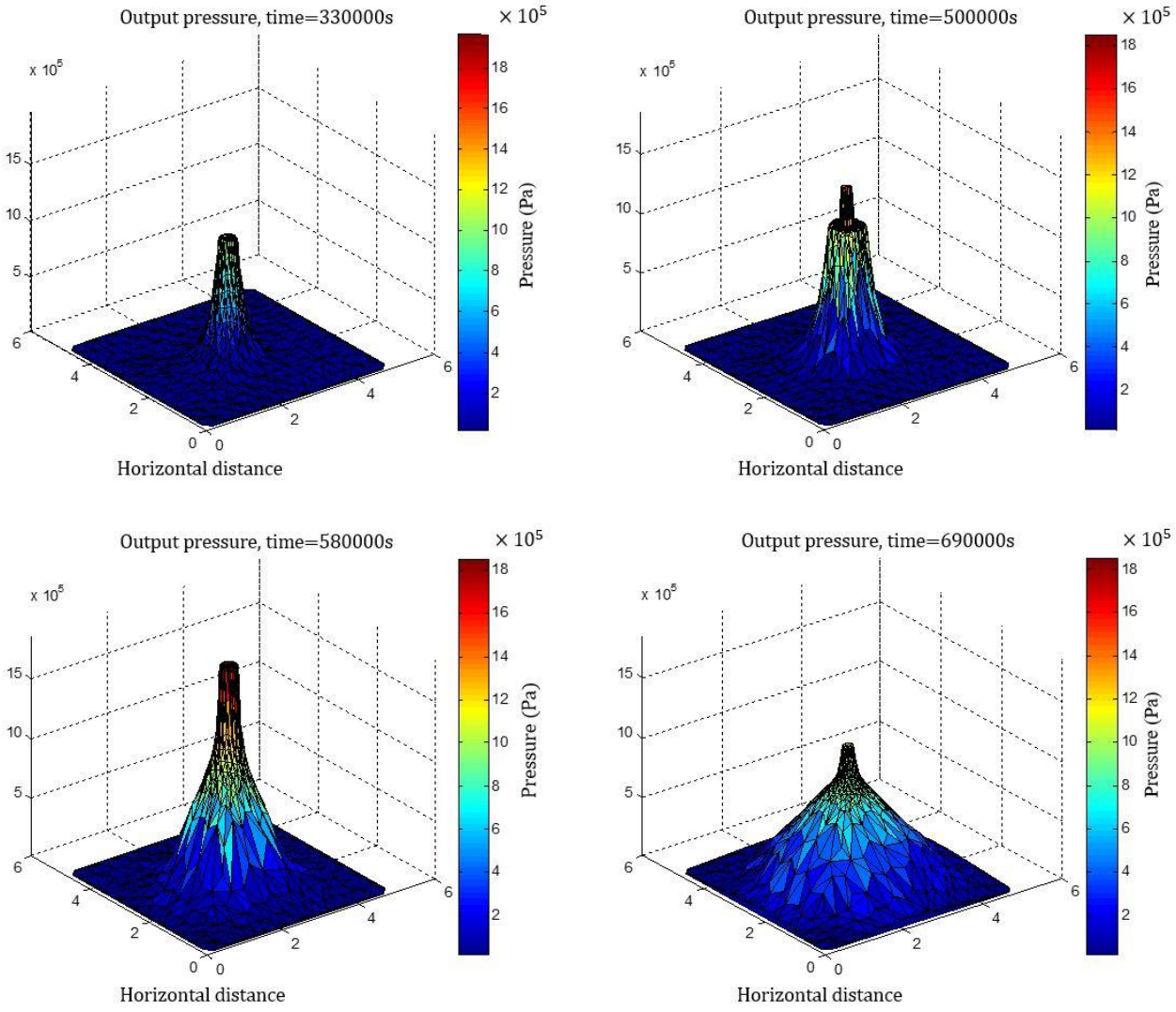

Figure 5.18 Computed evolution of the gas pressure distribution within the rockmass

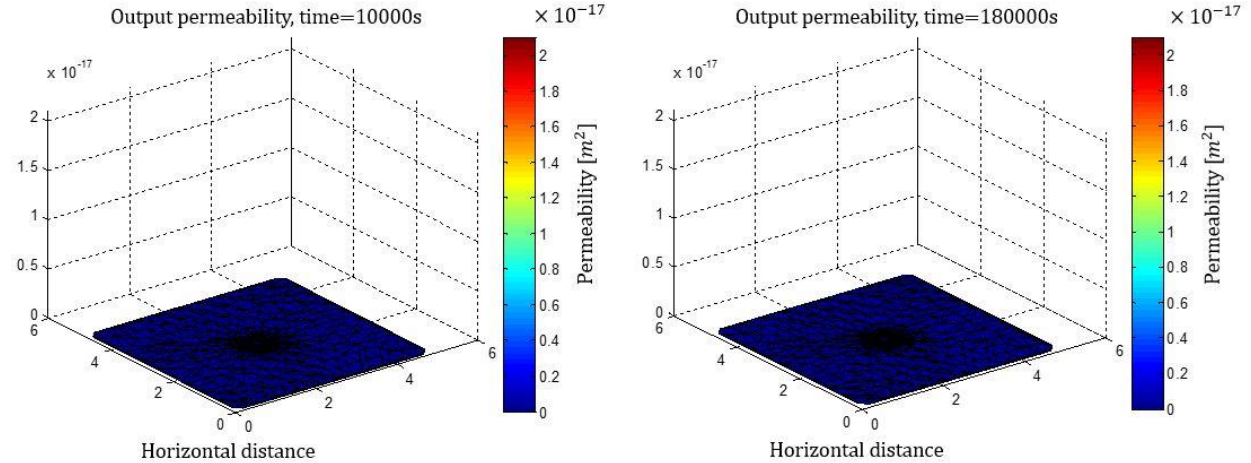

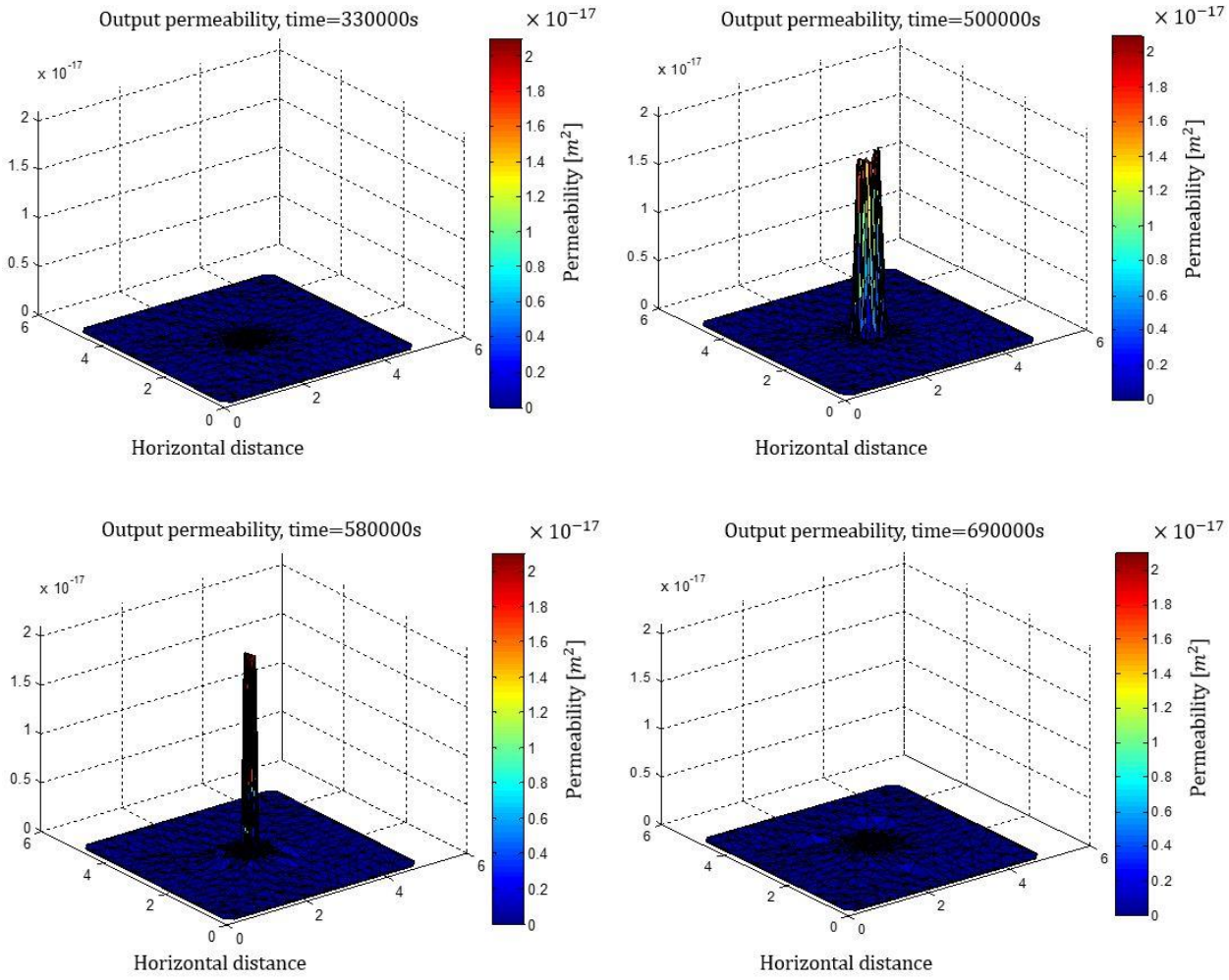

Figure 5.19 Calculated evolution of the permeability distribution of the rockmass

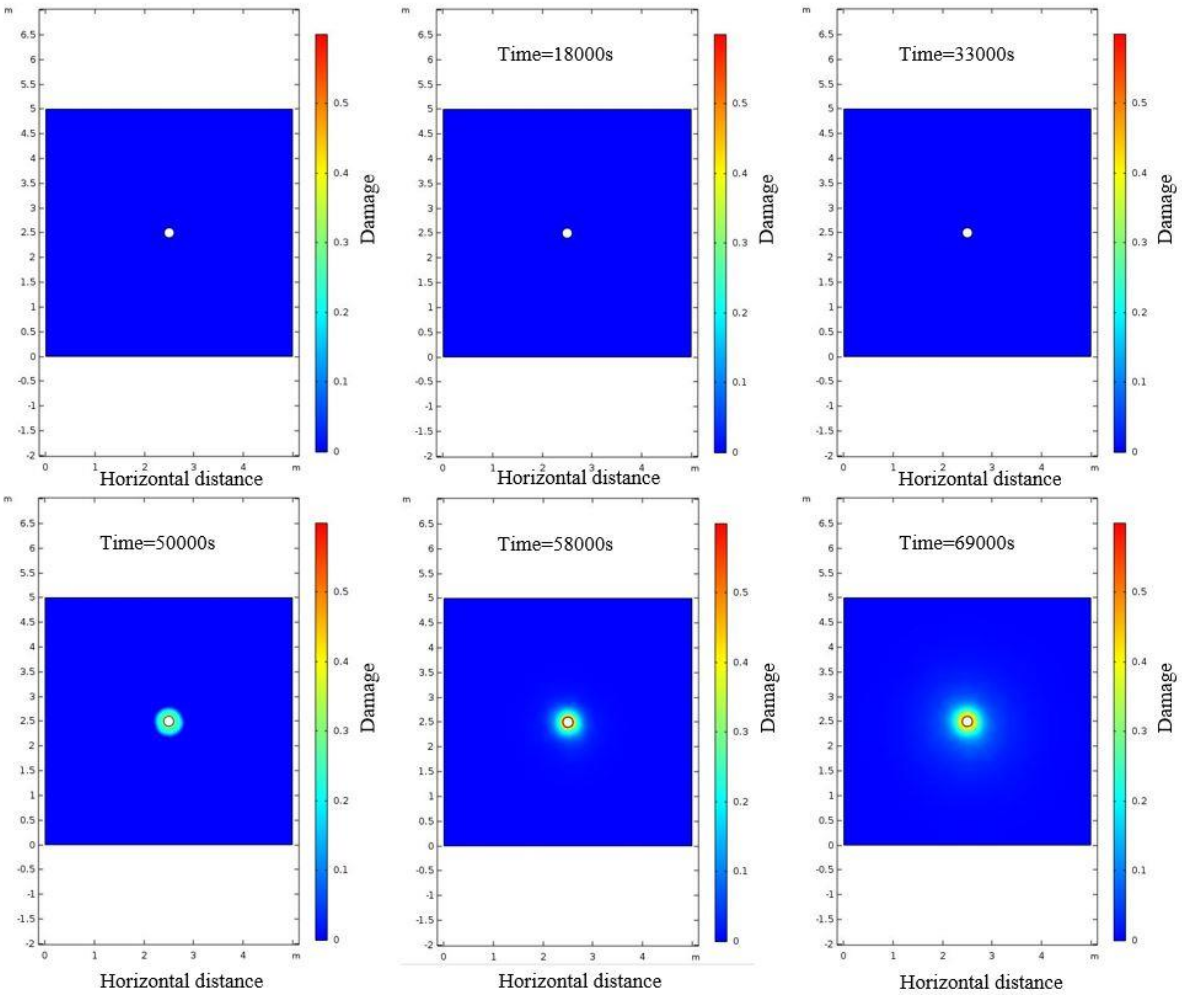

Figure 5.20 Evolution of the rock damage spatial distribution

5.6 Summary and conclusions

Production of gas and its migration in the host rock is a critical to evaluate the long-term safety of the EDZ and DGR for radioactive wastes. This study was aimed at developing numerical tools and constitutive models for the THMC coupled modelling of gas migration in host rocks. Therefore, a simulator consisting of integrative running of COMSOL and TOUGHREACT and a THMC-D coupled numerical model have been developed, and verified successfully by using laboratory and field experiments on gas migration in host rocks. The following conclusions can be drawn.

1. A coupled thermal-hydro-mechanical-chemical with damage (THMC-D) model for evaluating

and analyzing gas migration in sedimentary rock has been developed. For the mechanical processes, the elastoplastic damage model can describe the elastic degradation by damage. The coupled fluid flow and mechanical stresses influence the rock deformation and permeability, the pore water pressure, the diffusion coefficient and the variation of porosity. The variation of porosity was due to the rock deformation and/or the mechanical damage.

2. Laboratory experiment and *in-situ* tests at the Mont Terri Underground Research Laboratory were well modelled and the test data showed a good agreement with the modelling predictions. This provides confidence in the presented numerical tool (COMSOL-TOUGHREACT) to model the gas transport process in sedimentary rocks.

3. The numerical results indicate that high gas pressure can induce mechanical damage (via the formation of micro-cracks). When the gas injection pressure is higher than the crack damage threshold and more obviously the yielding stress, the permeability of the host rock increases significantly due to mechanical damage and irrecoverable deformations (e.g., plastic strain). Hence, the damage-controlled gas migration mechanism can lead to the increase of gas flow rates. It means that when large gas pressure is expected, it is necessary to consider the fully coupling effects of THMC-D processes of the gas transport in the host rock.

4. The new numerical tool is proven to be reliable for the modelling of gas migration in sedimentary host rocks of deep repositories for nuclear wastes disposal. While the three different pieces of software (COMSOL, TOUGHREACT, MATLAB) have been integrated by intensive programming to run successfully in iterative manner at the same time including data processing and manipulation, there is still space for the computation efficiency to improve. Optimization of code modules and computation procedures will be continued in further works. Moreover, despite the developed coupled models have considered the thermal factor, the validations in this study only involve experiments with constant temperatures. Hence the temperature module should be verified in future studies.

CHAPTER 6 Modeling of Gas Migration from a DGR in Ontario's Sedimentary Rocks

6.1 Introduction

Gas generation in deep geological repositories (DGR) for nuclear wastes could impair the long term performance of the host rocks and the safety of DGRs to a great extent. Since the middle of the last century, radioactive waste disposal has received considerable attention as nuclear energy was gradually and widely used in various fields (Hatch, 1953). Over those decades, different methods and techniques were proposed to manage the radioactive waste disposal, such as disposal into space, disposal in polar icecaps, and disposal on or beneath the seabed etc. (Miller et al., 2000).

To dispose of the radioactive wastes, the deep geologic repositories (DGRs) perform the functions of long-term isolation and containment of waste from the biosphere and human environment, also preventing the release of radionuclide attenuation to the subsurface (Bossart et al., 2017). For the repository evolution, the time considered for the high-level waste repository is usually 1 million years, including the first transient phase (10,000 years) and the followed equilibrium phase (Bossart et al., 2017). It means that the long-term stability of both the geosphere and engineered components of the geological disposal system is a key factor for the nuclear wastes (Vidstrand et al., 2008). For the aspect of the geosphere, site selection is the first and significant step to guarantee the safety and stability of the repositories. In many European countries (e.g. Belgium, France, Italy, Sweden, Switzerland, and the UK), they choose argillaceous rocks as the potential host rock for the disposal of radioactive waste repositories: Opalinus clay in Switzerland, Boom clay in Belgium and Callovo-Oxfordian clay in France (Fall and Nasir, 2012). Also, some other kinds of rocks are considered the host rocks for the nuclear waste repositories. The Grimsel Test Site (Switzerland) conducted the "Full-Scale Engineered Barriers Experiment (FEBEX)" in granite; Äspö Hard Rock Laboratory (Sweden) conducted the "Two Phase Flow Experiment in fractured Rock" (Jockwer, 2003). In Canada, France and Switzerland etc., they currently propose the sedimentary rock as the host rock.

As the most preferred option for the long-term management of radioactive wastes, Ontario Power Generation (OPG) proposed a Deep Geologic Repository (DGR) location at the Bruce nuclear site, Municipality of Kincardine, Ontario. This DGR is for the long-term management of Low and Intermediate Level Waste (L&ILW). The host rock of the repository is a sedimentary rock, located at 680m depth (Jensen et al., 2009). In this chapter, the developed THMC simulator will be used

to investigate gas migration in the sedimentary horst rock formations of the aforementioned potential Ontario's DGR.

For the organization of this chapter, after the introduction, the characteristics of the study area DGR site and DGR, including the geological setting and the geometry of the DGR system, are described. In the third section, the adopted numerical modeling approach is presented. The fourth section presents the selected significant results under the influence of gas migration on the main processes. Finally, the conclusions and recommendations are presented.

6.2 Characteristics of the DGR site and DGR

Ontario Power Generation (OPG) has considered a DGR system for the disposal of low and intermediate level radioactive wastes (LILWs). Figure 6.1 shows the location of the DGR. In southern Ontario, the study area is in a limestone formation overlain by multiple low permeability formations. This section will present the detailed geological setting information and the investigated site-specific data and parameters that have the relationship by analyzing the gas generation/migration in such a repository.

6.2.1 Geological setting

The DGR is situated on the Western margin of the Michigan Basin at the Bruce nuclear site within the limestone host rock at a depth of about 680 m below the existing ground surface. The Michigan Basin started to form during the Paleozoic era, more than 450 million years ago (Nasir, 2013). This area consists of Paleozoic sedimentary formations typically characterized by carbonates, shale, limestone, evaporite and sandstone. From a hydrogeological perspective, there are three horizons: a shallow zone (from the Devonian and extended to the Bass Islands Formation), an intermediate zone (Salina and Niagaran Group and extended from the base of the Bass Islands Formation to the Manitoulin Formation), and a deep groundwater zone (from the base of the Manitoulin Formation to the Precambrian) with a high total solids concentration of up to 300g/L (Sykes et al., 2008). In Figure 6.2, it seems that the stratigraphy is continuous and predictable in the study area. This area is simple and has no active faults (Gartner Lee Limited, 2008). The maximum depth is approximately 4,800 m of the Paleozoic rocks at the center of the Michigan Basin and decreases towards nearly 850 m in the study area (Figure 6.2). The proposed DGR is located within the

limestone Cobourg formation of low permeability, overlain by 200 m of upper Ordovician shale formations. According to the field measurements, these two formations have very low horizontal hydraulic conductivities (6.0E-12 to 1.0E-15 m/s). Figure 6.3 shows the Paleozoic sedimentary formations (host rock and shaft seals) of the DGR. MS Unit 4 is the argillaceous limestone host rock for the proposed DGR. By performing site-specific field and laboratory testing techniques on core samples from the DGR series of boreholes, OPG established the geomechanical behavior of the rock mass in Figure 6.3 (NWMO, 2011A).

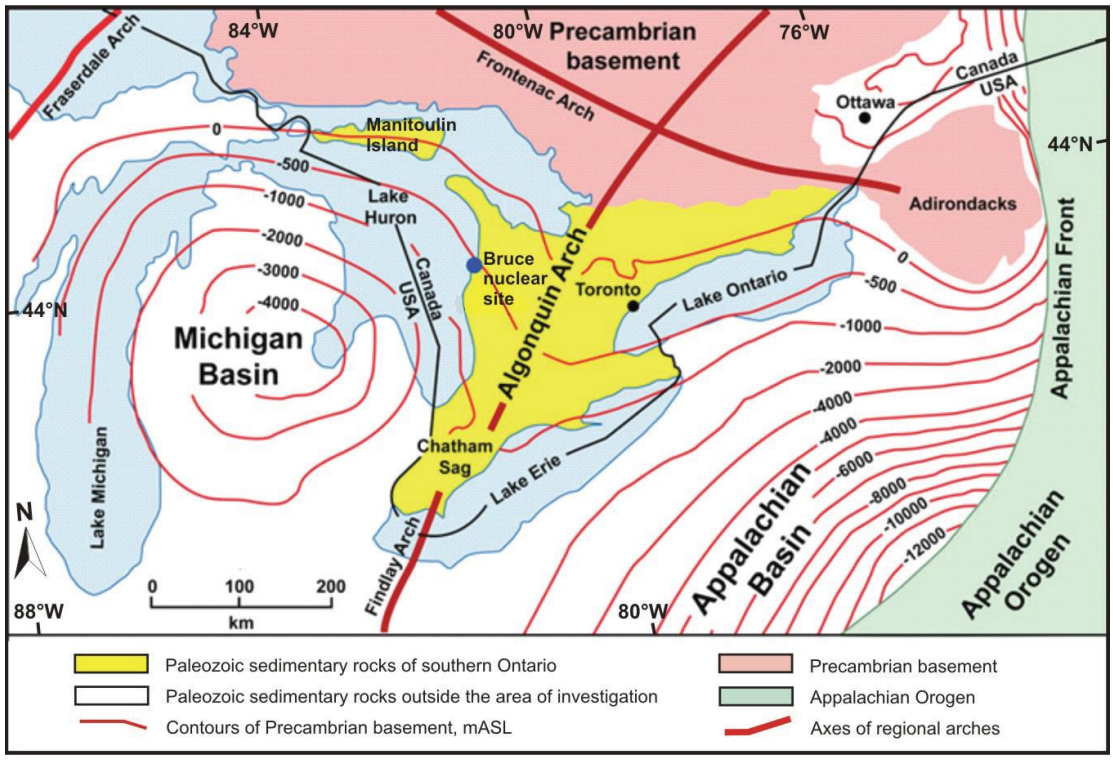

Figure 6.1 Geological features of the study area of Southern Ontario (this figure was published by NWMO (2011A) and modified from Johnson et al. (1992))

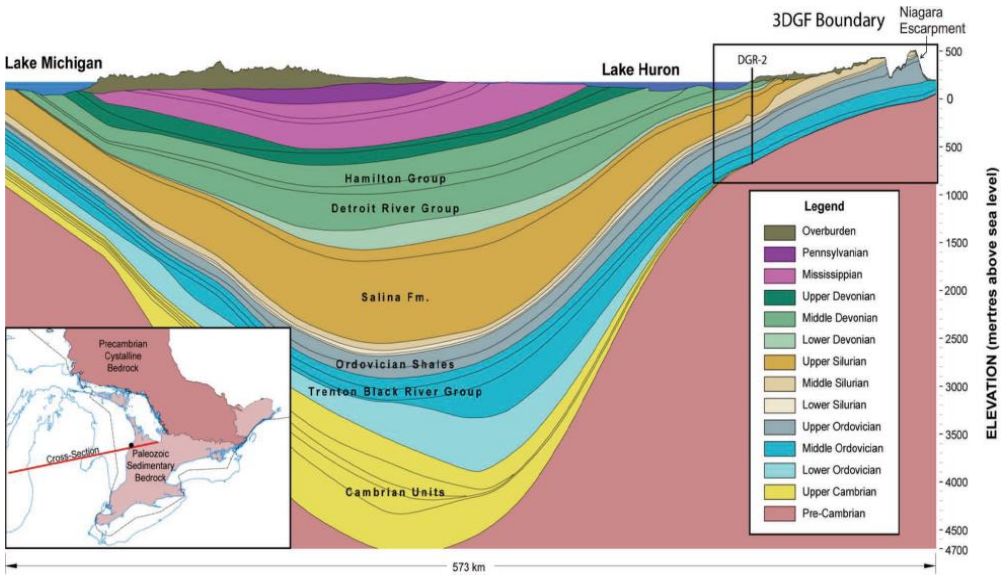

Figure 6.2 Geological cross-section of the Michigan Basin (NWMO 2011A)

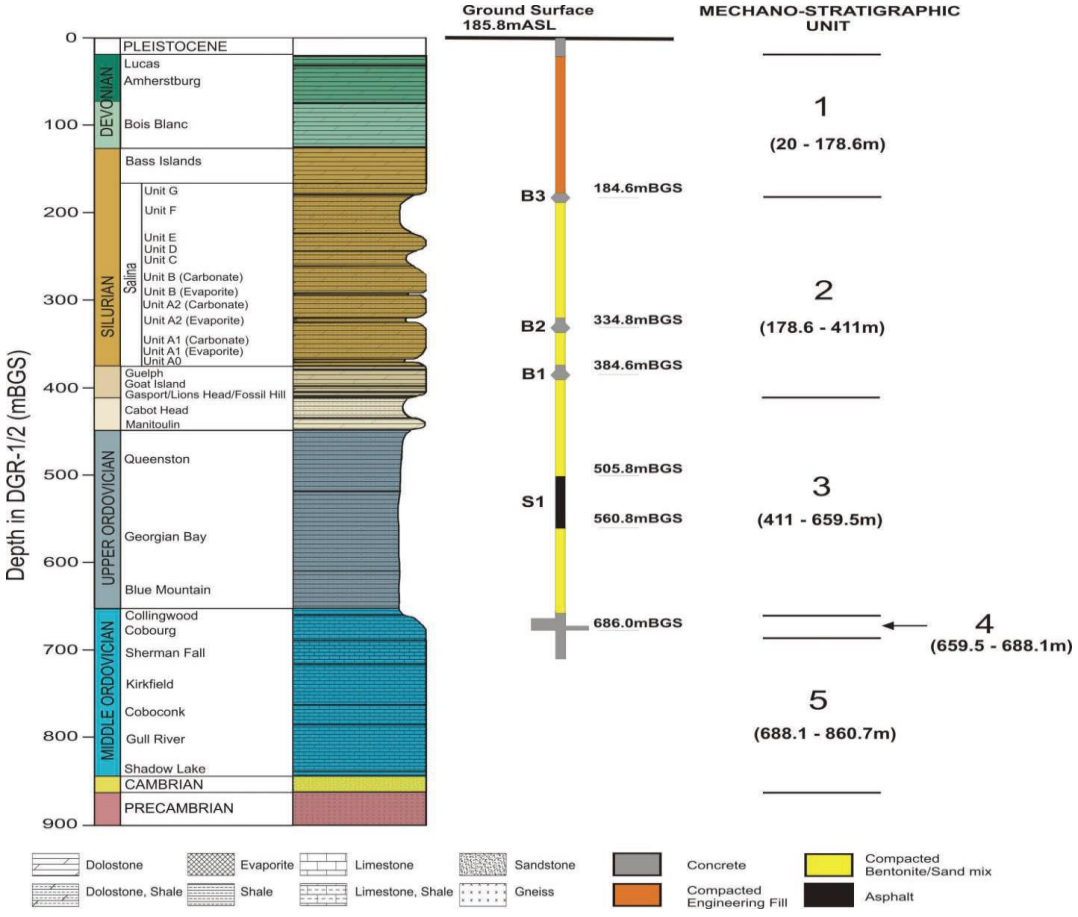

Figure 6.3 MS Units and shaft seal system at Bruce nuclear site (this figure was published by INTERA (2011) and modified by NWMO (2011A))

6.2.2 Geometry of DGR

The proposed DGR is located within the low permeability limestone and overlain by approximately 200 m of low permeability shales. The conceptual diagram of the DGR facility is shown in Figure 6.4. For the operation part of the DGR, the underground facilities consist of access-ways (shafts and tunnels), emplacement rooms and various underground service areas and installation. The ground facilities are comprised of two series of buildings: the main shaft area (main shaft headframe, waste package receiving building (WPRB), office, main control room and amenities building, the ventilation shaft area (ventilation shaft headframe and hoist house, and the Waste Rock Management Area (WRMA)). (NWMO, 2011B).

Figure 6.5 shows the detailed design of the underground services area of the repository. There are two panels of the emplacement rooms, with a width of 8.6 m and a height of 7 m, with the total volume at 420, 000 m^3. The emplacement rooms are separated by the pillars with 17.2 m width resistant to the roof loading. The main shaft has a radius of 6.5 m and the ventilation shaft with a radius of 5.0 m connected to the underground services and the ground facilities.

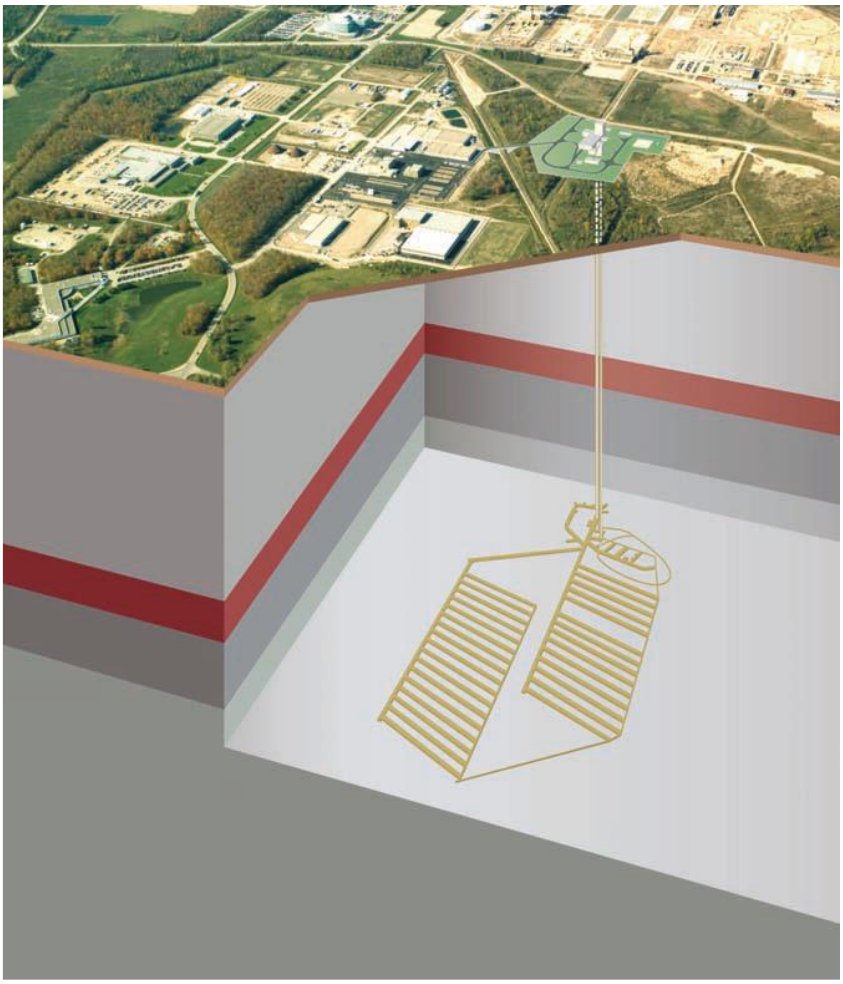

Figure 6.4 Proposed DGR conceptual layout (figure from NWMO (2011A))

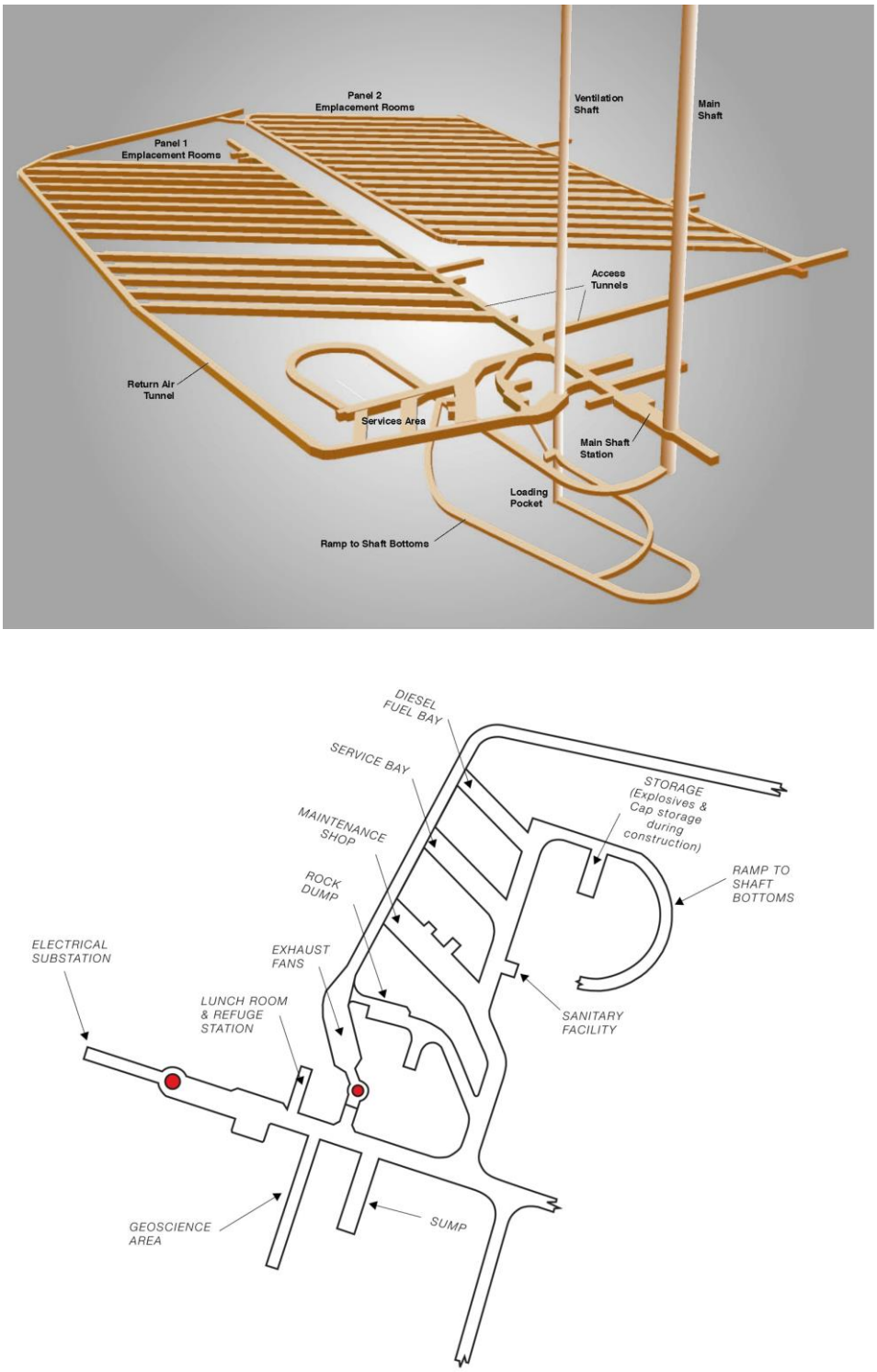

Figure 6.5 Isometric view of the underground facilities of the repository (top) and the design sketch of the underground services area (bottom) (OPG letter, 2012)

6.2.3 Material Properties

There is a large amount of geological data related to the study area, including published literature (e.g., Mazurek (2004) and Gartner Lee Limited (2008) etc.), government open file reports (e.g., Ontario Power Generation) and supporting technical reports produced by the related organization (e.g., Nuclear Waste Management Organization). The mechanical properties and hydraulic-thermal-chemical properties of the rock formations within the model are shown in Table 6-1 and Table 6-2 (NWMO 2011, Nasir 2013). The permeability and porosity of the rock formations at the DRG site used in the modeling work are shown in Figure 4.7 (NWMO, 2011) and Figure 6.6 (Li, 2017).

Table 6-1 Mechanical properties of sedimentary rocks in the study area (used in COMSOL)

Rock formation	**Depth (m)**	**Poisson's ratio**	**Young's modulus (GPa)**	**Density (kg/m^3)**
1: Overburden Aquifer	0-20	0.2	10	2590
2: Dolostone Aquifer	20-169.3	0.2	40	2590
3: Silurian Aquifer	169.3-178.6	0.2	18	2590
	178.6-325.5	0.2	6	2590
4A: Silurian Aquifer	325.5-328.5	0.2	38	2590
	328.5-374.5	0.2	38	2590
4B: Silurian Aquifer	374.5-378.6	0.2	38	2590
	378.6-411	0.2	38	2590
	411-447.7	0.2	16	2590
5: Ordovician shale	447.7-659.5	0.2	16	2660
6:Ordovician limestone	659.5-688.1	0.2	39	2660
	688.1-762.0	0.2	24	2660
7: Ordovician limestone	762.0-838.6	0.2	24	2660
8: Cambrian	838.6-860.7	0.2	24	2540
9: Precambrian	>860.7	0.2	60	2540

Table 6-2 hydraulic-thermal-chemical properties of sedimentary rock in the study area (used in TOUGHREACT)

Rock formation	**Depth (m)**	**Horizontal hydraulic conductivity Kh(m/s)**	**Kh/ Kv***	**Thermal conductivity W/(m.K)**	**Specific heat conductivity J/(kg.K)**	**Diffusion m^2/s**	**TDS (mg/L)**	**Type**
1:Overburden Aquifer	0-20	8.0E-10	2:1	2	700	6.0E-10	<500	*Ca,Na-* HCO_3
2:Dolostone Aquifer	20-169.3	1.0E-5	10:1	2	700	8.0E-12	500 to 5000	*Ca,Mg-* HCO_3 to *Ca-* SO_4
3:Silurian Aquifer	169.3-178.6	5.0E-12	10:1	2	700	1.0E-12	10,000 to 350,000	*Ca-* $SO_4$to *Na-Cl*
	178.6-325.5	5.0E-12	10:1	2	700	1.0E-12	30,000	*Na-Cl*
4A:Silurian Aquifer	325.5-328.5	2.0E-7	1:1	2	700	7.0E-12	370,000	*Na-Cl*
	328.5-374.5	5.0E-12	10:1	2	700	1.0E-12	370,000	*Na-Cl*
4B:Silurian Aquifer	374.5-378.6	3.0E-8	1:1	2	700	3.0E-11	370,000	*Na-Cl*
	378.6-411	5.0E-12	10:1	2	700	1.0E-12	10,000 to 350,000	*Ca-* SO_4 to *Na-Cl*
	411-447.7	5.0E-12	10:1	2	700	1.0E-12	10,000 to 350,000	*Ca-* $SO_4$to *Na-Cl*
5:Ordovician shale	447.7-659.5	2.0E-14	10:1	2	700	1.0E-13	300,000	*Na-Cl*
6:Ordovician limestone	659.5-688.1	1.0E-15	10:1	2	700	3.0E-13	285,000 to 230,000	*Na-Cl*
	688.1-762.0	1.0E-15	10:1	2	700	3.0E-13	285,000 to 230,000	*Na-Cl*

7:Ordovician limestone	762.0-838.6	6.0E-12	100:1	2	700	3.0E-13	230,000 to 200,000	*Na-Cl*
8:Cambrian	838.6-860.7	1.0E-7	1;1	2	700	1.0E-11	205,000 to 235,000	*Na,Ca-Cl*
9:Precambrian	>860.7	1.0E-11	1:1	1.375	700	3.0E-13	50,000 to 350,000	*Ca,Na-Cl*
* Kv: vertical hydraulic conductivity								

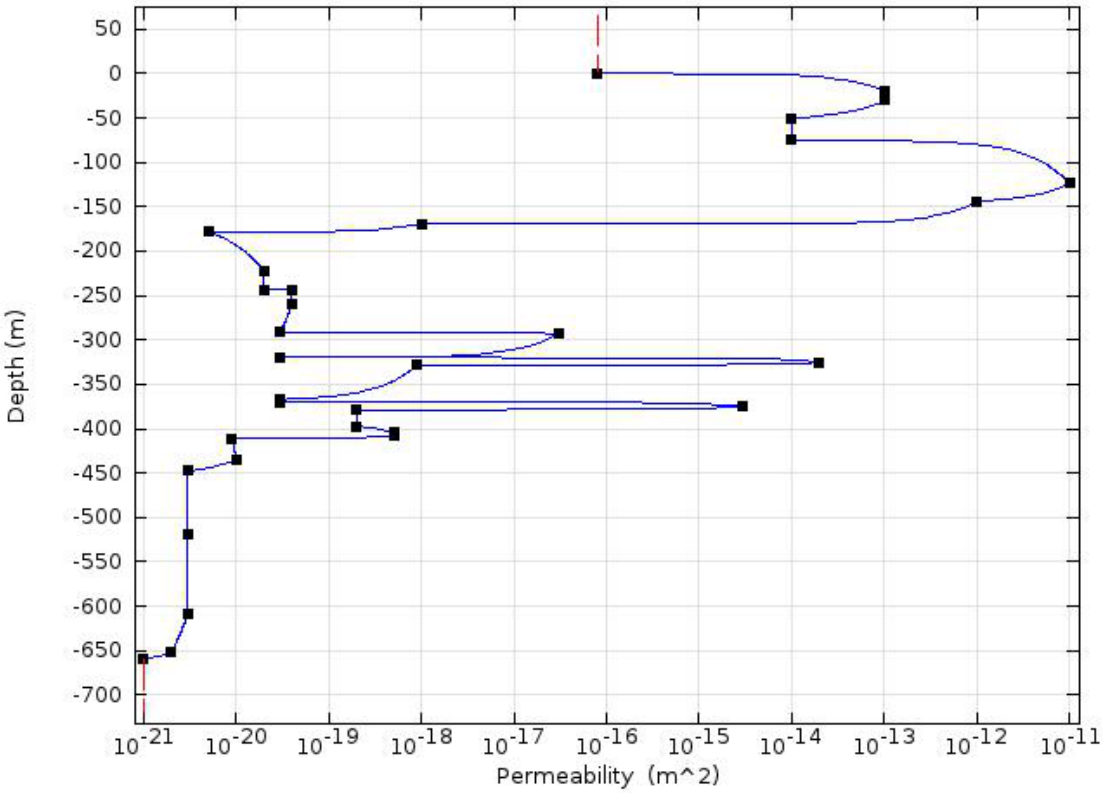

Figure 6.6 Permeability profile with depth of the study sedimenrary rocks (used in TOUGHREACT)

6.3 Modelling approach

6.3.1 Simulator structure and coupling procedure

There are five coupled processes solved in this study: thermal process, mechanical process, saturated gas and water flow, solute transport and chemical reactions. The numerical modeling

follows a circle solution concept. First, the M to THC process, by using the modules of MATLAB, the effective stress, volumetric strain and thermal expansion/contraction results from the COMSOL is used to update the porosity and pore pressure for TOUGHREACT. The second, THC to M porcess, the temperature, pore pressure, porosity and permeability will be updated in MATLAB by using the multiphase pressure, saturation, temperature and the rate of dissolution and precipitation from the TOUGHREACT simulator. It should be emphasized that, during the first circle, the data transfer is no need for interpolation in space, because the stress and strain are defined as averages of the elemental domains in both COMSOL and TOUGHREACT. While in the second process, the pore pressure has to be interpolated from mid-element (TOUGHREACT) to corner locations (COMSOL) in the external module (MATLAB,) because TOUGHREACT mesh uses one grid point within each element, while COMSOL nodes are located in element corners (Rutqvist and Wu, 2002).

6.3.2 Model conceptualization

The conceptual model of the proposed DRG is shown in Figure 6.7. There are four main underground components: main and ventilation shafts, underground services, access tunnels, and storage rooms. The numerical conceptual model, along with the boundary conditions, is described in Figure 6.8. The proposed DGR is located on the upper part of the Middle Ordovician limestone formation, which is under the Upper-Ordovician shale formation. Both of these two formations are approximately 200m thick. In order to overcome the difficulty of the large number of mesh elements, demand for the proposed geometry requires, based on the proposed DGR dimensions, a simplified equivalent geometry is generated (Quintessa Ltd. and Geofirma Engineering Ltd., 2011). The services area, access tunnels, and storage rooms are merged into an equivalent room, and the main and ventilation shafts are merged into an equivalent shaft (Nasir et al., 2013). Considering the effect of the excavation damage zone (EDZ), the shafts and the access tunnel are merged into an equivalent shaft area with a radius of 1R (R is the excavation radius). In this model, R is equal to 13m (ANDRA, 2005). For the 2D axial symmetry model of the proposed DGR, the axis of symmetry is along the equivalent shaft. In order to improve the calculation speed of the coupling process, the rock formations from -325.5m to -411m, -422m to -659.5m, and -688.1m to -860.7 are merged into three layers correspondingly and separately. This simplification can reduce the number of grids to some extent without compromising accuracy. The reason is that the merged

rock formations have the same mechanical properties in the calculation of COMSOL. Meanwhile the hydraulic-thermal-chemical properties in TOUGHREACT are applied based on the mesh coordinates instead of rock layering (Figure 6.9).

6.3.3 Initial and boundary conditions

The appropriate initial conditions and boundary conditions related to THMC processes used will be presented in the following section.

6.3.3.1 Initial conditions

In this model, the initial conditions present the conditions at the beginning of the post-closure period. The initial vertical mechanical stress is assumed to be the self-weight of the rock formations, and the initial horizontal stress is assumed to be 1.5 times of the vertical stress as usually found in North America (Nasir, et al., 2013).

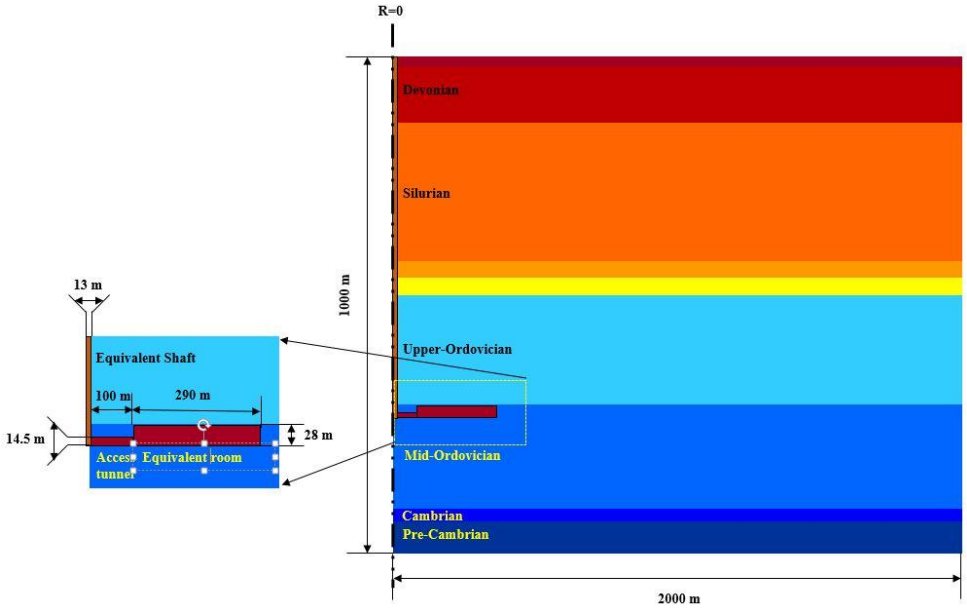

Figure 6.7 Conceptual numerical model

The initial hydraulic conditions are set as linear hydrostatic. For the thermal initial conditions in this study, it takes the linear geothermal gradient expressed by the equation as follows (Vugrinovich, 1989):

$$T = 14.5 + 0.0192 \times D \tag{6.1}$$

where T is the temperature, the unit is $^{\circ}C$, 14.5 ($^{\circ}C$) is the initial temperature profile near the surface, and D is the depth with the unit of m.

The initial solute in the host rock and the shaft is zero, and the existing total dissolved solids chemistry is as the initial chemical conditions. The chemical boundary conditions are adopted from the NWMO reports (NWMO, 2011). For the chemical initial conditions, Table 6-3 shows the filed measurements of the ground water density and the total dissolved solids (TDS) of the research area (NWMO, 2011).

Table 6-3 Field measurements of total dissolved solids of the research area

Formation	**Depth (mBGs)**	**TDS(mg/L)**	**Water type**
1:Overburden Aquitard	0-20	<500	*Ca, NA-*HCO_3
2: Dolostone Aquifer	20-169.3	500 to 5000	*Ca, Mg-* $HCO_3$to *Ca-* SO_4
3: Silurian Aquitards	169.3-447.7	10,000 to 350,000	*Ca-* SO_4 *to Na-Cl*
4A: Silurian Aquitards 4B: Silurian Aquifer	325.5-328.5 374.5-380.0	30,000 370,000	*Na-Cl* *Na-Cl*
5: Ordovician Shale Aquiclude	447.7-659.5	300,000	*Na-Cl*
6:Ordovician Carbonate Aquiclude	659.5-762.0	230,000 to 270,000	*Na-Cl*
7: Ordovician Carbonate Aquitard	762.0-838.6	200,000 to 230,000	*Na-Cl*
8:Cambrian Aquifer	838.6-860.7	225,000 to 235,000	*Na, Ca-Cl*
9: Precambrian Aquitard	>860.7	50,000 to 350,000	*Ca, Na-Cl*

6.3.3.2 Boundary conditions

By using the corresponding mechanical conditions, the mechanical boundary conditions (BCs, 1 to 4) of the model are shown in Figure 6.8. Hydraulic, chemical and thermal boundary conditions are set in TOUGHREACT code. Table 6-4 shows the values of the BCs in this model. Figure 6.9 shows the relationship of the computational mesh between COMSOL and TOUGHREACT. In this study, there are two cases with the regards of the gas pressure applied in the tunnel (Figure 6.10 and Figure 6.11).

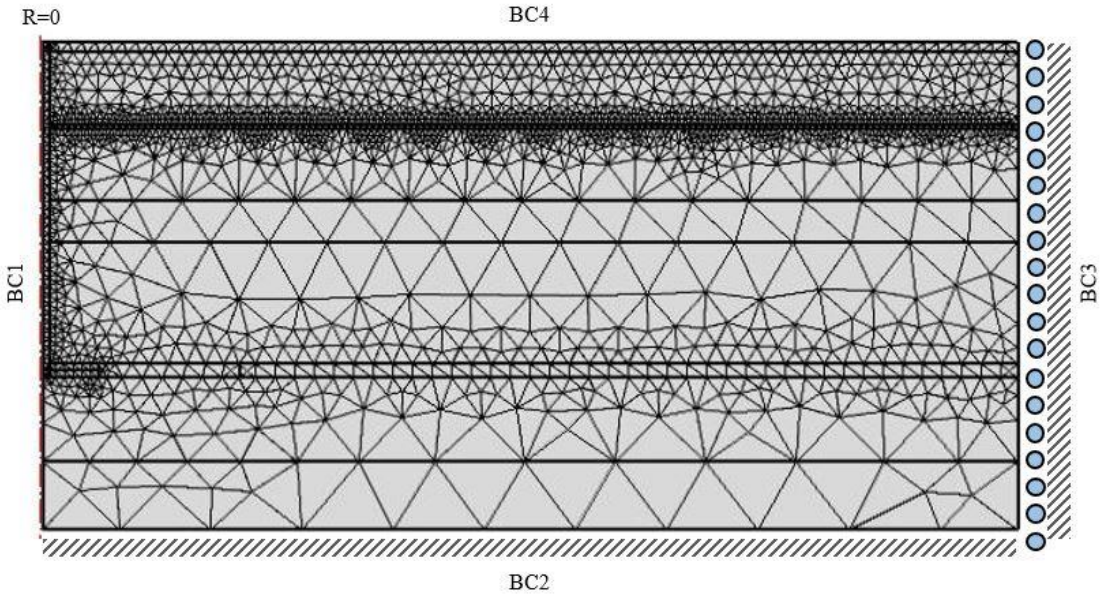

BC1 = Axi-symmetric axis BC2 = Fixed BC3 = Roller BC4 = Free deformation

Figure 6.8 Finite element method (FEM) mesh (By COMSOL mesh generation) and mechanical boundary conditions

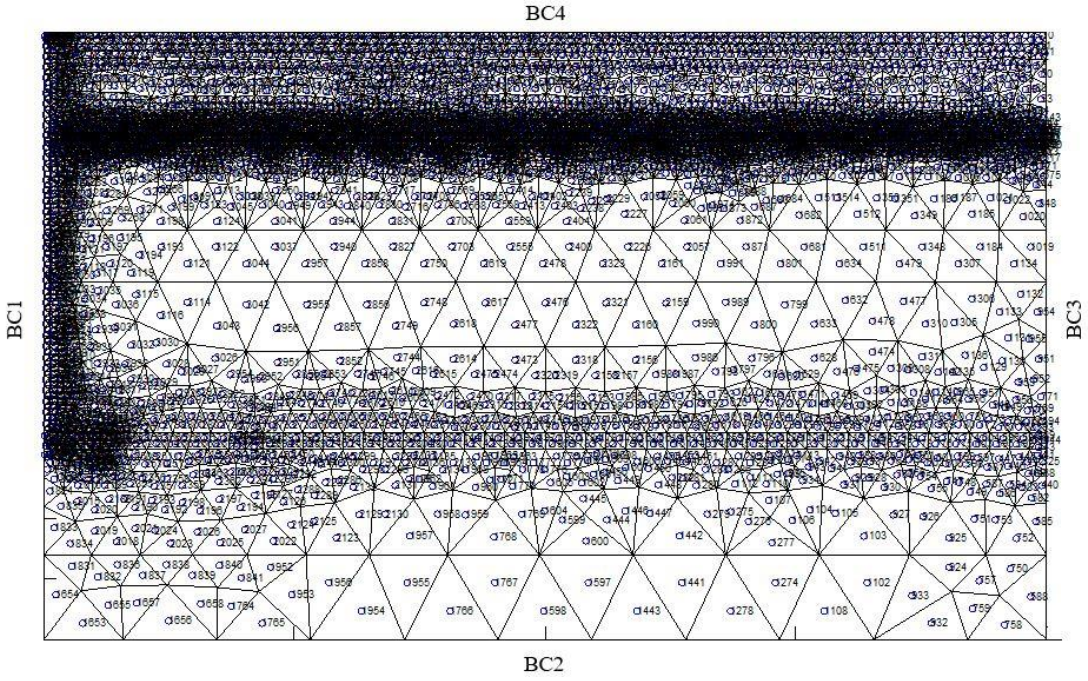

Figure 6.9 TOUGHREACT mesh generated corresponding to COMSOL mesh

Table 6-4 THC BCs in TOUGHREACT used for simulation

TOUGHREACT	**Hydraulic**	**Chemical**	**Thermal**
BC1 (Axi-symmetric)	No flow	Insulation	Insulation
BC2 (Bottom)	Zero liquid and gas flux	Insulation	33.7℃
BC3 (side)	Zero liquid and gas flux	Insulation	linear geothermal gradient
BC4 (top)	Free drainage	Zero concentration	14.5℃

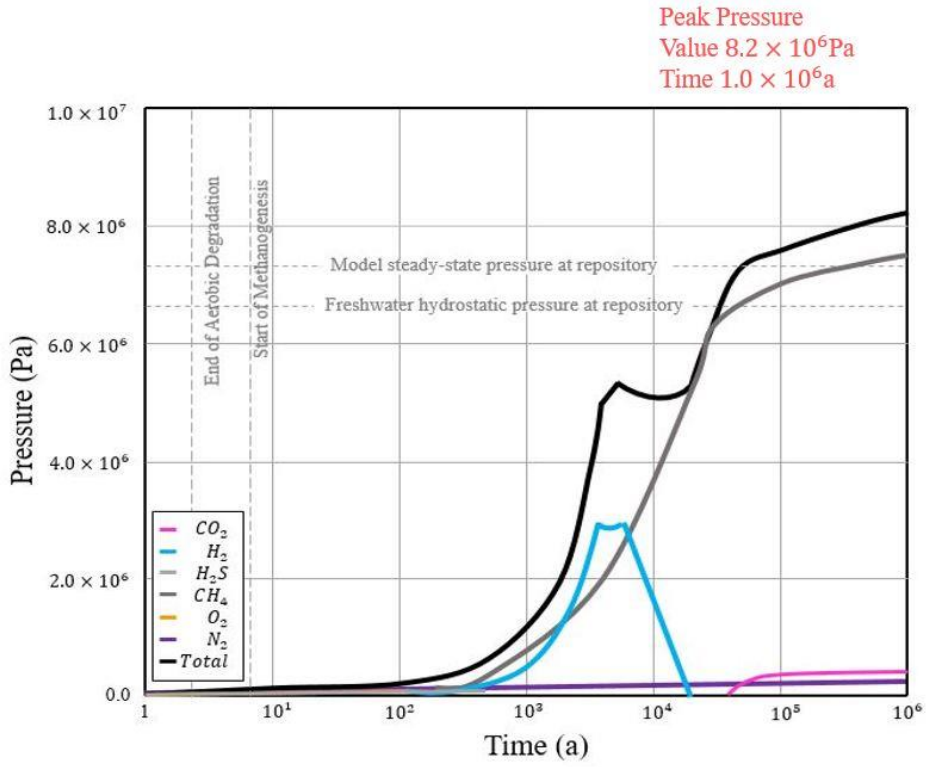

Figure 6.10 Total gas pressure in the repository (normal scenario) (NWMO 2011E)

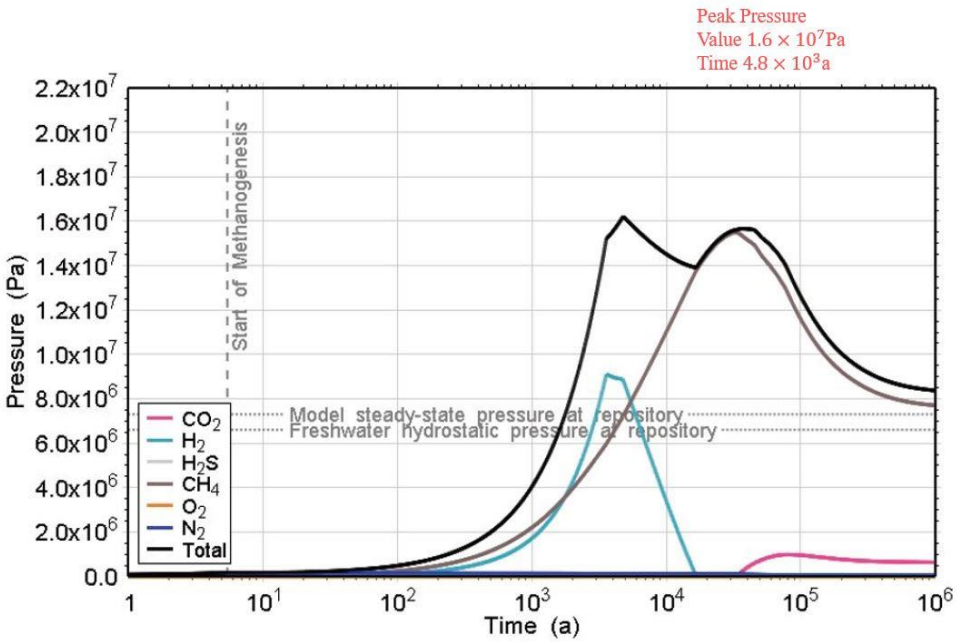

Figure 6.11 Total gas pressure in the repository (worst scenario) (NWMO 2011E)

The first case simulated in this study is that the peak repository gas pressure is in the range of 7 to 8 MPa. The second one is the worst situation; the peak repository gas pressure is 16 MPa. The initial hydraulic and mechanical properties of the failed shaft are shown in Table 6-5 (obtained from NWMO 2011E). For the sake of simplicity, the excavated spaces (repository rooms and access tunnels) are assumed to be filled with a mixture of material. The single equivalent material with a porosity of 0.5 and a permeability of 1.16E-13 from NWMO (2011E) is considered for the material filled the excavated part. In the present study, the normal shaft and the repository post-closure properties are assumed to be similar to the failed shaft properties. The permeability is $10^{-18}m^2$ of the normal design. The failed shaft is assumed to increase by four orders of magnitude compared with the normal design condition (Nasir, 2013).

Table 6-5 Main properties of the shaft (the worst case conditions for a failed shaft; data from NWMO 2011e)

Property	**Value**
Hydraulic conductivity (m/s)	10^{-7}

Permeability (m^2)	10^{-14}
Density (kg/m^3)	2500
Poisson ratio (-)	0.2
Modulus of elasticity (GPa)	20
Porosity	0.5
Biot coefficient	0.9

6.4 Simulation results

By using the developed simulator, different sets of results were obtained from TOUGHREACT and COMSOL separately. Only the results relevant to the gas migration of the DGRs are selected, presented and discussed in the following sections.

6.4.1 Simulation results for the normal scenario

Figure 6.12 (a) shows the selected points (point 2816, 2818, 2934 and 2933) in the grid map of TOUGHREACT which have the same original porosity and permeability within the same rock layer of Ordovician shale while different distances from the top of the repository. Figure 6.12 (b) and (c) show the horizontal profile of the developments of porosity and permeability separately within the host rock formation for four different points of the whole time with respect to the normal scenario. Figure 6.12 (b) demonstrates the porosity evolutions of these four points. The results show that a maximum porosity increase is 0.005 of point 2816. The porosity changes gradually decrease with the increase of the distances from the top of the repository. The rock permeability changes result from the changes in the porosity. Figure 6.12 (c) indicates the permeability evolutions of these four points. The results show that the maximum change in permeability is less than on the order of magnitude. Furthermore, it indicates that the further away from the repository, the less the permeability changes within the same rock layer. The porosity induced- changes in permeability can be explained by Eq. (5.69).

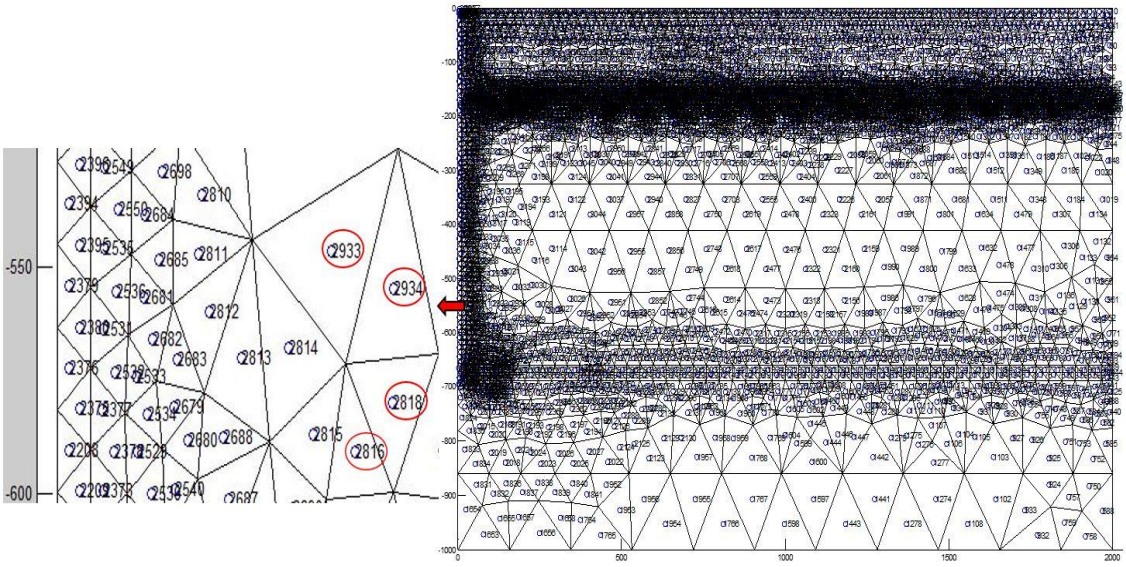
-550
-600
2933
2934
2818
2816
2815
2814
2813
2812
2811
2810
2698
2685
2684
2683
2682
2681
2680
2679
2688
0
500
1000
1500
2000

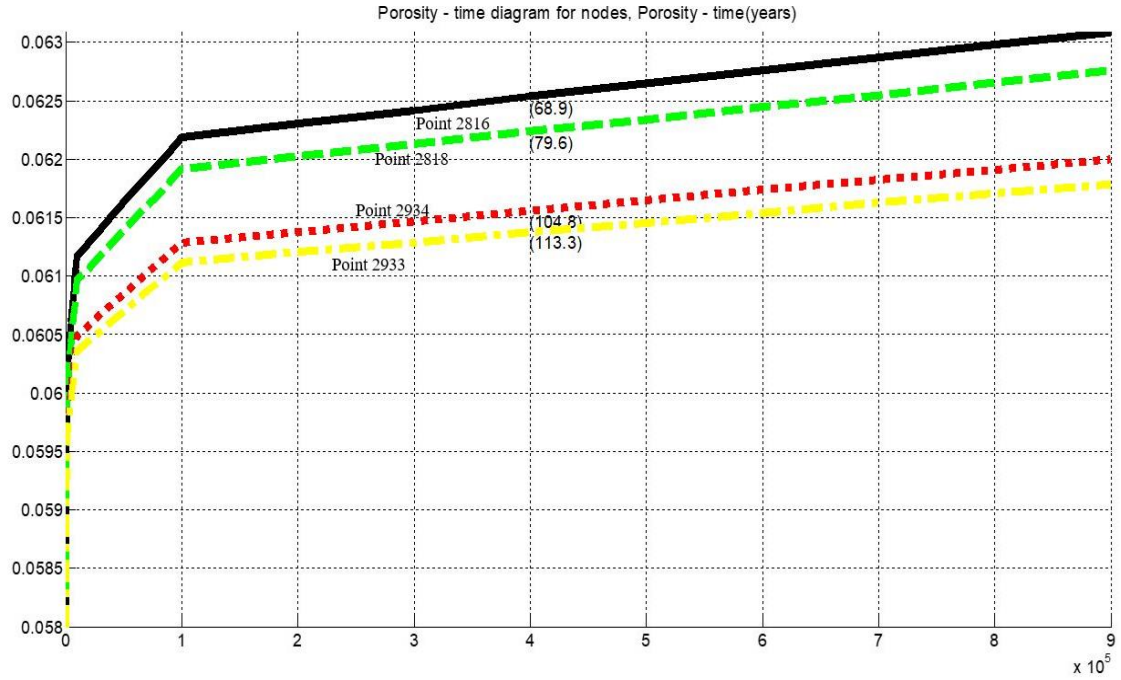
Porosity - time diagram for nodes, Porosity - time(years)
Point 2816
Point 2818
Point 2934
Point 2933
(68.9)
(79.6)
(104.8)
(113.3)
0.063
0.0625
0.062
0.0615
0.061
0.0605
0.06
0.0595
0.059
0.0585
0.058
0
1
2
3
4
5
6
7
8
9
x 10^5

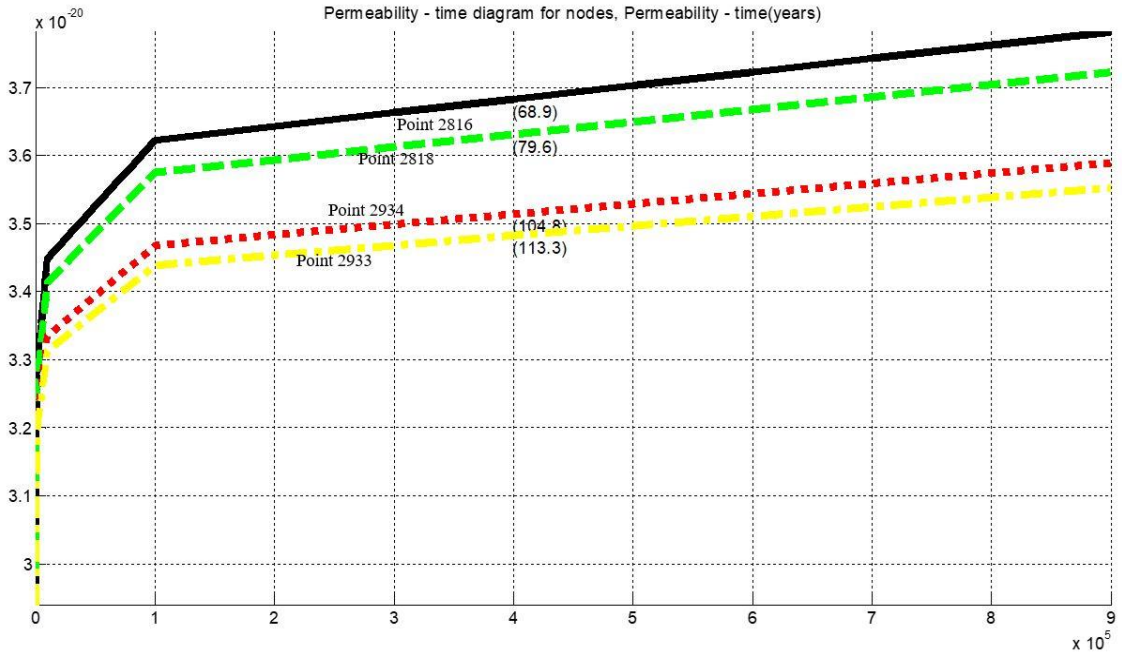

Figure 6.12 (a) The selected points in the grid map of TOUGHREACT within the host rock formation to demonstrate the porosity and permeability developments; (b) The porosity evolution of the four selected points over the whole time; (c) The permeability development of the four selected points over 100 million years

Figure 6.13 shows the distribution and temporal evolution of gas pressure in the DGR repository and host rock with regards to the normal case (Peak gas pressure around 8 MPa). It illustrates the gas pressure distributions of 10, 3,000, 5,000, 10,000, 20,000, 70,000, 500,000, 1,000,000 years, respectively. It clearly shows that the gas pressure increased with the increase of the total gas pressure in the repository. The peak value of the total gas pressure in the repository is approximately 8 MPa, which is equivalent to or slightly higher than the steady-state hydrostatic water pressure at the repository horizon of around 7.2 MPa, and much less than the lithostatic (i.e., overburden) pressure of around 17 MPa (NWMO, 2011). In Figure 6.13 (c)-(f), the pore gas pressure of the regions near the vertical shaft in the layers of the Silurian and Queenstonde increases more rapidly than the areas far away from the shaft. This phenomenon is because the higher permeability of the shaft has limited influence on the gas dissipation from the repository tunnel in these formations. Figure 6.13 (c) and (d) illustrate a slight drop of the gas pressure around the repository, which corresponds to the decrease of the total pressure in the repository. It reflects the high sensitivity and accuracy of the coupling simulator. After 1 million years, when the peak

total gas pressure in the repository is more than 8 MPa, the maximum value of the gas pressure is around 8 MPa in the tunnel and 6-7 MPa in the surrounding near-field, which is far below the lithostatic pressure (17 MPa). It indicates that the tensile fractures would not generate in the host rock, which is more confident for the safety of the DGR.

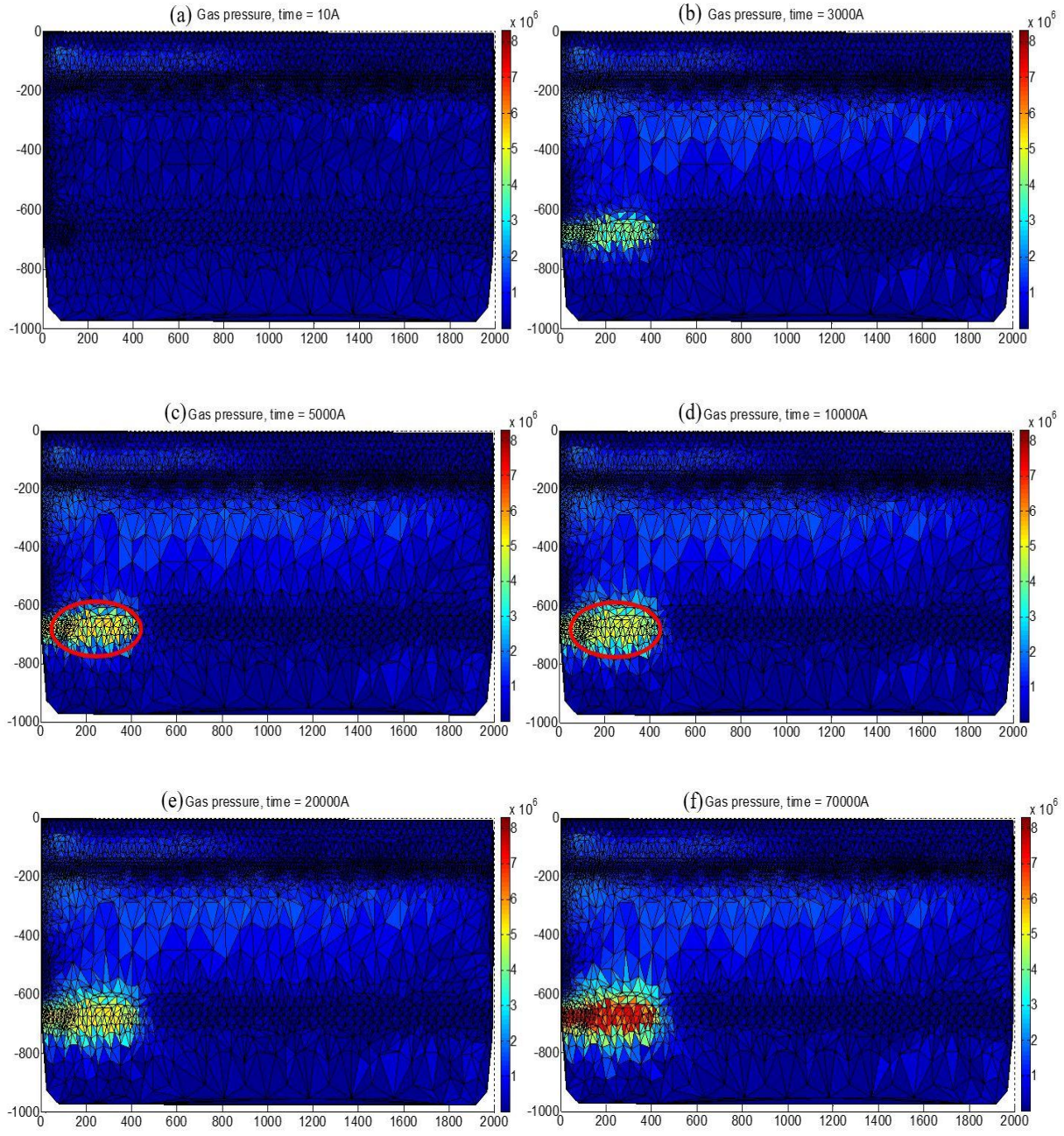

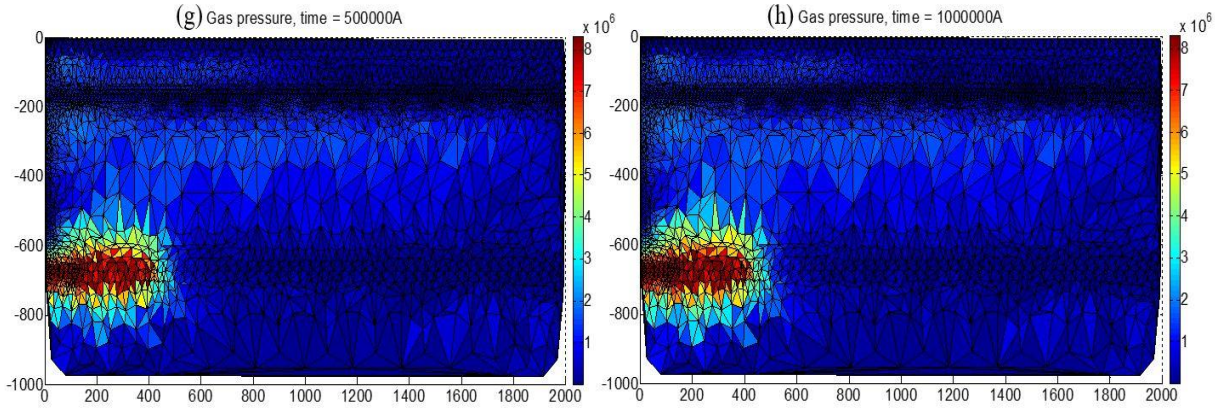

Figure 6.13 Temporal evolution of gas pressure (Pa) spatial distribution in the study area

6.4.2 Simulation results for the worst case

For the worst case of a failed shaft (peak gas pressure = 15 MPa), the main simulation results are presented in Figure 6.14. Figure 6.14 a to h shows the spatial distribution and temporal evolution of the gas pressure in the DGR repository and the host rock in the study area after 10, 3,000, 5,000, 8,000, 40,000, 70,000, 100,000,and 1,000,000 years, respectively. It can be noticed that the gas pressure in the host rock surrounding the repository is increased until 5,000 years with the maximum gas pressure of 15.8 MPa approximately. There is a fluctuation between 5,000 years and 40,000 years; the gas pressure goes down and then goes up. After 40, 000 years, the gas pressure maintains a steady descent. In order to demonstrate the evolution of the gas pressure clearly, the upper limit setup of the color picture legend is 5 MPa (the maximum gas pressure at this time is around 15.8 MPa) in Figure 6.15. Compared with the gas pressure distribution at 10 years (Figure 6.15 (a)), it is shown obviously in Figure 6.15 (b) that the gas migration can reach the shallower level of the Silurian (Salina) formation at 5,000 years when the gas pressure in the repository is nearly 16 MPa. It means that the impacts of gas migration in the host rock reaching the shallow rock formations should be considered for the safety assessment of the deep geological repository.

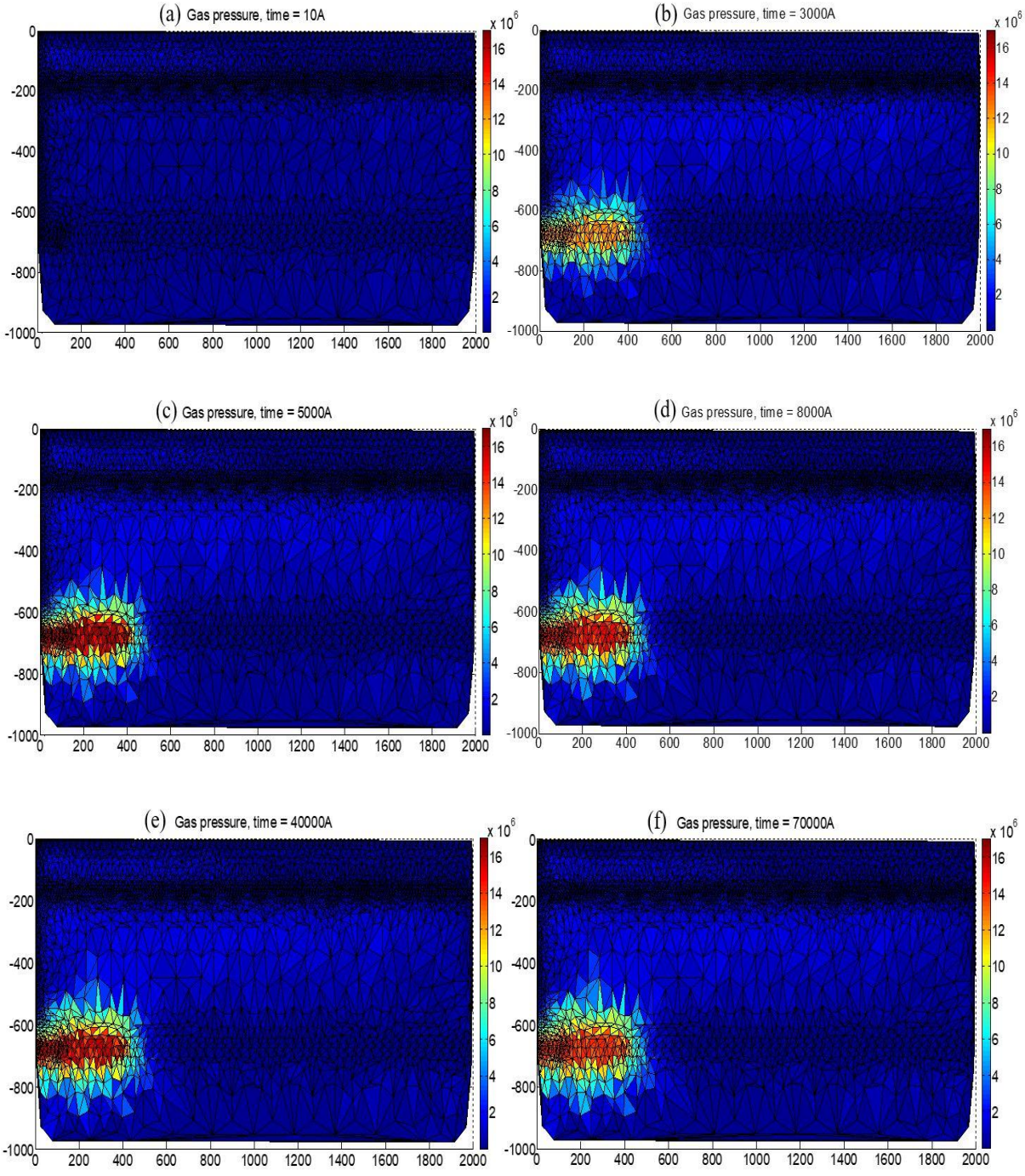
(a) Gas pressure, time = 10A
(b) Gas pressure, time = 3000A
(c) Gas pressure, time = 5000A
(d) Gas pressure, time = 8000A
(e) Gas pressure, time = 40000A
(f) Gas pressure, time = 70000A
x 10^6
0
-200
-400
-600
-800
-1000
0 200 400 600 800 1000 1200 1400 1600 1800 2000
2 4 6 8 10 12 14 16

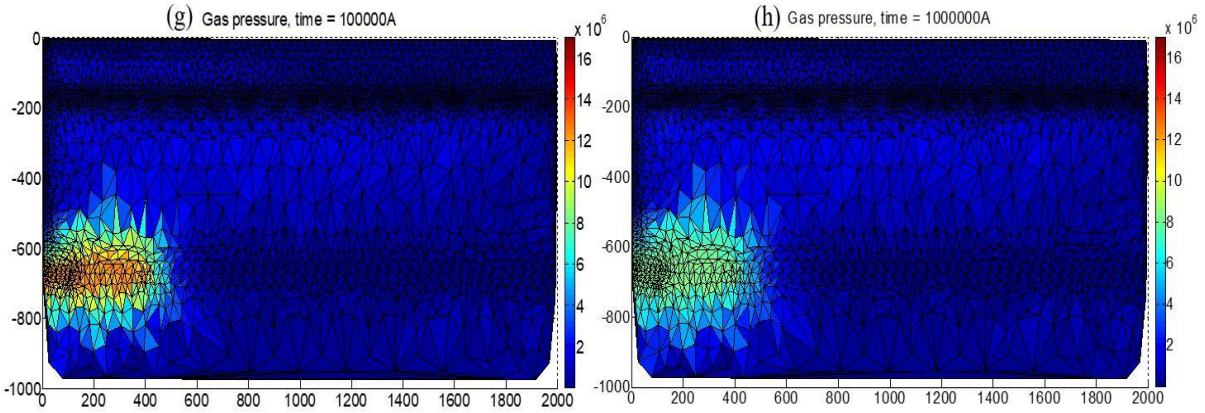

Figure 6.14 Gas pressure (Pa) evolution of spatial distribution with time change in the study area

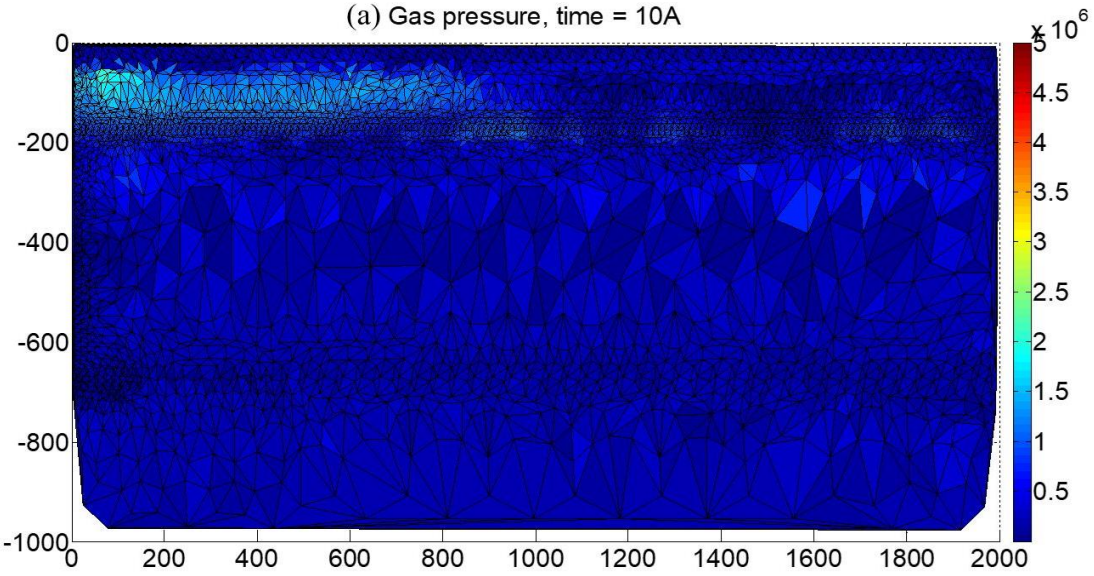

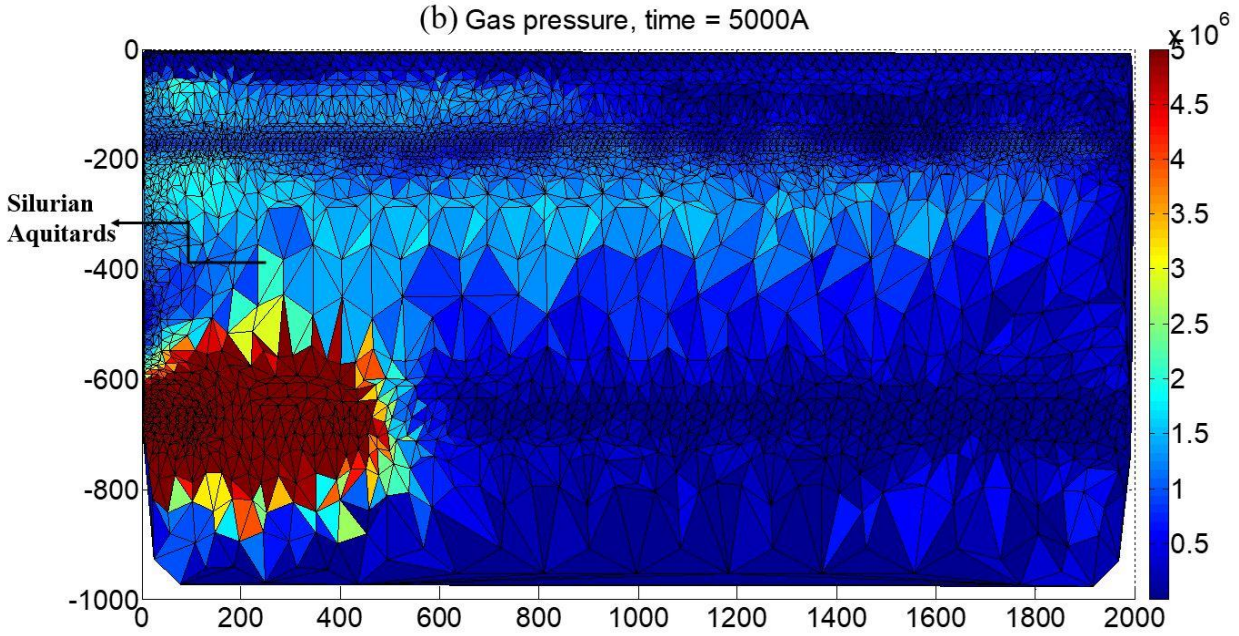

Figure 6.15 The gas pressure distributions at 10 years (a) and 5,000 years (b)

6.5 Conclusions

The developed THMC simulator has been used in this present work to evaluate the gas migration in the host sedimentary rocks of a DGR for the LILWs in southern Ontario. The simulator is also adopted to study the porosity and permeability evolutions considering the whole THMC processes impact in the normal scenario of the long-term closure period. The results show that both permeability and porosity will increase with the rise of the pore gas pressure. Although the permeability change is limited in one order of magnitude at the area near the repository, the results could still be used to re-estimate the permeability value for that range to calculate of the long-term safety assessments. To predict the gas migration in the host sedimentary rocks, until 1,000,000 years, the high gas pressure and gas migration still remain in the shale and limestone layers of the normal case. It means that the limestone and shale formations are very effective for protecting the safety of the repository with regard to gas migration after the closure. While for the worst case simulation, at around 5,000 years with the peak gas injection of 15.8 MPa, the gas migrates upward through the shale and limestone layers to the shallower level of the Silurian formation. This kind of situation should be considered for use in long-term safety assessments.

CHAPTER 7 General Conclusions and Recommendations

7.1 General conclusions

With wider and more extensive use of nuclear energy, the safe long-term disposal of nuclear wastes is critical and important for many countries. As the preferred option for long-term management of radioactive wastes, the deep geological repository (DGR) can isolate the radioactive wastes from the biosphere by the natural barriers (host rocks) and an engineered barrier system (EBS). However, significant quantities of gas could be produced in a DGR, jeopardizing its integrity and safety. So, understanding the mechanisms of gas migration in a DGR as well as predicting the migration is crucial for ensuring the long-term safety of a repository for nuclear waste. In the present thesis, new coupled HM models and THMC simulators have been developed to simulate the gas migration process in host rocks as well as the observed behaviors.

The whole coupling model can describe gas migration more accurately. The coupling model was verified by a novel and tested simulator (TOUGHREACT-COMSOL by MATLAB). The modelling predictions are consistent with the experimental observation and other research results. The following conclusions are drawn based on the obtained results.

1. Gas migration of the deep geological repository for nuclear waste in the sedimentary host rock is predominately controlled by the coupled multiphysics or THMC processes during the closure stage.
2. A comprehensive literature review has been carried out to study and compare the advantages and limitations of different experimental methods, numerical models and simulators.
3. An evolutive elastoplastic-damage model has been developed in this research that characterizes the mechanical behaviors of sedimentary host rock for DGR. This model takes into account the elastoplastic strain under the influence of mechanical damage. From the good agreement between the predicted and experimental values, the model can be used to predict the mechanical behaviors under the influence of high gas pressure, which can induce fractures of the rock formations.
4. A new THMC simulator, COMSOL-TOUGHREACT, has been developed. The good agreements between measured values in terms of both laboratory experiments and *in-situ* measurements and the simulation results suggest that the developed THMC simulator can be used to predict the behaviors of gas migration on sedimentary host rock formations in this

study. These three different pieces of software have been integrated by intensive programming. This new simulator can execute the entire THMC processes at the same time, including data processing and manipulation in an iterative manner. The flexibility and comprehensive output function can make this simulator be used for many applications (i.e., the influence of glaciation cycles, the deep geological repository for CO_2 gas, and the gas migration in geomaterical barrier system of a DGR).

5. Based on the principle of effective stress and porous media theory, a coupled THM (elastoplastic-damage)-C model has been developed to predict the impacts of THMC processes in gas migration on sedimentary host rock formations in Ontario. Based on the basic laws of force equilibrium, mass, energy conservation, and heat conservation, a set of governing equations are derived and developed to simulate the mechanical response, coupled solute, and fluid and heat transfer or transport in deformable porous media.
6. The numerical study was conducted for gas migration of THMC-Damage coupling processes in laboratory- scale gas injection tests on Opalinus Clay and *in-situ* tests at the Mont Terri Underground Research Laboratory. It was found that high gas pressure can induce mechanical damage, and it was also verified that the elastoplastic damage model could describe the elastic degradation by damage accurately. The damage-controlled gas migration mechanism can increase gas flow rates, which means that such is necessary to consider taking the mechanical damage into the THMC processes.
7. A numerical study for gas migration of long term THMC coupling processes in the host sedimentary rocks of a DGR for the LILWs in southern Ontario for normal and worst scenarios seperately was carried out. It was found that both permeability and porosity will increase with a rise in the pore gas pressure. The porosity changes gradually decreased with an increase in the distance from the top of the repository. Rock permeability changes result from changes in porosity. Under high gas injection pressure, gas migration can reach the shallow rock formation, which means that the gas generation (worst case scenario) and migration could influence the safety assessment (SA) to a degree, and such should be taken into consideration for the SA of the deep geological repository.

8. The results of this study have proved the importance of considering gas migration in the long-term closure stage of the DGR. It has also provided useful insights for understanding different

geological parameters on the influence of the long-term performance of the DGRs. Furthermore, the last part of the research results has enhanced confidence in the safety of the DGRs in Ontario sedimentary rocks for nuclear wastes.

7.2 Recommendation for future studies

The following recommendations are proposed for future studies.

1. In addition to the THMC processes for the gas migration of the host rock, there are still other factors that can influence the long-term performance of DGRs, such as glaciations, earthquakes, and geological defects. More investigations are required to be carried out and more factors and processes need to be considered in future research.
2. Since the model size of DGR in Ontario's sedimentary rocks is immense, and the total number of meshes (3882 meshes in total) in COMSOL and TOUGHREACT are large, these two factors have a serious impact on the simulating time by using the new simulator. So, for the further development of the simulator, the focus will be on improving the power and performance to enable complex situations, comprehensive factors, and boundary conditions.
3. The elastoplastic damage model in this study neglects the facts of nucleation and propagation of the micro-cracks. These will over-estimate the modification of the permeability and the gas pressure change at the beginning of the simulation. A more advanced damage model needs to be developed to simulate the development of the micro-cracks realistically.

References

Abednego, M., Blascheck, P., Schefer, S., Mosar, J., Nussbaum, C., Joswig, M., & Bossart, P., 2017. Seismotectonic analysis around the Mont Terri rock laboratory (Switzerland): a pilot study. Swiss Journal of Geosciences, 110.

Alkan, H., Müller, W., 2008. Approaches for modeling gas flow in clay formations as repository systems. In: J, Pys. Chem. Earch. 33, 2008, P. 5260-5268.

Alnajim, A., 2004. Modélisation et simulation du comportement du béton sous hautes températues par une approche thermo-hydro-mécanique couplée. Application à des situations accidentielles. (PhD thesis) University of Marne La Vallée (172 pp.).

Alonso, E.E., Olivella, S., Arnedo, D., 2006. Mechanisms of gas transport in clay barriers. J. Iber. Geol. 32 (2), 175-196.

Alzamel M., Fall M., 2019. Effect of pore water salinity on swelling behaviour, mineralogical and microstructural properties of bentonite-sand barrier materials. Proc. 3rd International Conference of Recent Trends in Environmental Science and Engineering (RTESE'19), June 11-12, Ottawa.

Amann, F., Wild, K. M., Loew, S., Yong, S., Thoeny, R., and Frank, E., 2017. Geomechanical behaviour of Opalinus Clay at multiple scales: results from Mont Terri rock laboratory (Switzerland). Swiss Journal of Geosciences, 110.

ANDRA 2005. Dossier 2005 Les recherches de l'Andra sur le stockage géologique des déchets radioactifs à haute activité et à vie longue. Collection les rapports.

ANDRA 2000. Experimental programme at the Meuse/Haute-Marne Underground Research Laboratory. A short view. June 2000, C RP ASRP 2000 – 2006.ANDRA (2001): Laboratoire de Recherche Souterrain Meuse / Haute-Marne, Lot 3 – Forages D'investigation Geologique Complementaire – Rapport de Synthese. DRP 0ANT 01-022.

Andersson, J., H. Ahokas, J.A. Hudson, L. Koskinen, A. Luukkonen, J. Löfman, V. Keto, P. Pitkänen, J. Mattila, A. Ikonen and M. Ylä-Mella. 2007. Olkiluoto Site Description 2006. POSIVA 2007-03. Posiva Oy, Finland.

Arnedo, D., Alonso, E.E., Olivella, S., Romero E., 2008. Gas injection tests on sand/bentonite mixtures in the laboratory. Experimental results and numerical modelling. Physics and Chemistry of the Earth, Parts A/B/C. Volume 33, Supplement 1, 2008, Pages S237-S247.

Askarieh, M. M., Chambers, A. V., Dabniel, F. B. D., Fitzgerald, P. L., Holtom, G. J., Pilkington, N. J. & Rees, J. H. 2000. The chemical and microbial degradation of cellulose in the near field of a repository for radioactive wastes. Waste Management, 20, 93–106.

Autio J., Gribi P., Johnson L., Marschall P., 2006. Effect of excavation damaged zone on gas migration in a KBS-3H type repository at Olkiluoto. Physics and Chemistry of the Earth, Parts A/B/C Volume 31, Issues 10-14, 2006, Pages 649-653.

Bate, F., Hoch, A.R. and Jackson, C.P. 2006. Gas migration calculations: report to Nirex. Serco Assurance Report, SA/ENV-0850.

Bear, J., Bachmat, Y., 1991. Introduction to modeling of transport phenomena in porous media Kluwer academic, Publisher, Netherlands (553 pp.).

Bennett, D.P., Cuss, R.J., Vardon, P.J., Harrington, J.F., Sedighi, M. and Thomas, H.R., 2015. Exploratory data analysis of the Large Scale Gas Injection Test (Lasgit) dataset, focusing on 'second-order' events around macro-scale gas flows. In: SHAW, R.P. (ed.) Gas Generation and Migration in Deep Geological Radioactive Waste Repositories. Geological Society, London, Special Publications, 415, 225–239, https://doi.org/10.1144/SP415.14.

Biot, M. A., 1941. A mechanical analyzer for the prediction of earthquake stress. Bull. Seism. Soc. Amer., Vol. 31, pp. 151-171.

Bixler, N.E., 1985. NORIA-A finite element computer program for analyzing water, vapour, air and energy transport in porous media. Sandia National Laboratories report SAND84-2057, Albuquerque, N.M.

Bleyen, N., Smets, S., Small, J., Moors, H., Leys, N, Albrecht, A., De Cannie`re, P., Schwyn, B., Wittebroodt, C., and Valcke, E., 2017. Impact of the electron donor on *in-situ* microbial nitrate reduction in Opalinus Clay: results from the Mont Terri rock laboratory (Switzerland). Swiss Journal of Geosciences, 110.

Boisson, JY., Bertrand, L., Heitz, JF., Golvan, Y., 2001. *In-situ* and laboratory investigations of fluid flow through an argillaceous formation at different scales of space and time, Tournemire tunnel, southern France. Hydrogeology Journal, 9(1), 108–123. doi:10.1007/s100400000119.

Bossart, P., Bernier, F., Birkholzer, J., Bruggeman, C., Connolly, P., Dewonck, S., Fukaya, M., Herfort, M., Jensen, M., Matray, J-M., Mayor, J., Moeri, A., Oyama, T., Schuster, K., Shigeta, N., Vietor, T., Wieczorek, K., 2017. Mont Terri rock laboratory, 20 years of research: introduction, site characteristics and overview of experiments. Open access at Springerlink.com.

Bossart, P., Jaeggi, D. and Nussbaum,C., 2017. Experiments on Thermo-hydro-mechanical Behaviour of Opalinus Clay at Mont Terri rock laboratory, Switzerland. In: Journal of Rock Mechanics and Geotechnical Engineering 9 (2017) 502-510.

Bower, K. M., Zyvoloski, G., 1997. A Numerical Model for Thermo-Hydro-Mechanical coupling in Fractured Rock [J]. International Journal of Rock Mechanics and Mining Sciences, 34: 1201-1211.

Brown, R.C., 1999. A multiple front propagation model for gas migration through clay, Engineering Geology 54, pp. 151–158.

Carol, I., Rizzi, E., Willam, K., 2001. On the formulation of anisotropic degradation I. Theory based a pseudo-logarithmic damage tensor, Int.J. Solids Struct. 38/4 491-518.

Carol, I., Rizzi, E., Willam, K., 2001. On the formulation of anisotropic degradation. II. Generalized pseudo-rankine model for tensile damage, Int. J. Solids Struct. 38/4 519–546.

Cermak V. and Rybach L. 1982. Thermal conductivity and specific heat of minerals and rocks.‖ Volume 1 of Landolt-Bornstein Numerical Data and Functional Relationships in Science and Technology, New Series, Group V, Geophysics and Space Research, chapter 4.1, pages 305-343. Springer, October 1982.

Cheng, H.P., Yeh, G.T., 1998. Development and demonstrative application of a 3-D numerical model of subsurface flow, heat transfer and reactive chemical transport: 3DHYDROGEOCHEM. J. Contam. Hydrol. 34 (1–2), 47–83. Comsol Multiphysics 3.5a, 2009.http://www.comsol.com2009.

Clauser C., Huenger E. 1995. Thermal conductivity of rocks and minerals. Washington, DC:

American Geophisical Union, pp. 105-126.

Clauer, N., Techer, I., Nussbaum, C., and Laurich, B., 2017. Geochemical signature of paleofluids in microstructures from Main Fault of the Opalinus Clay of the Mont Terri rock laboratory, Switzerland. Swiss Journal of Geosciences, 110.

COMSOL Multiphysics User's Guide, 2012. Version, COMSOL 4.3.

Croisé, J., Mayer, G., Marschall, P., Matray, JM., Tanaka, T., Vogel, P., 2006. Gas Threshold Pressure Test Performed at the Mont Terri Rock Laboratory (Switzerland): Experimental Data and Data Analysis, Oil & Gas Science and Technology - Rev. IFP, Vol. 61 (2006), No. 5, pp. 631-645. doi: 10.2516/ogst:2006003

Cuss, R., Harrington, J., Giot, R. and Auvray, C., 2014. Experimental observations of mechanical dilation at the onset of gas flow in Callovo-Oxfordian claystone. In: NORRIS, S., Bruno, J. ET AL. (eds) Clays in Natural and Engineered Barriers for Radioactive Waste Confinement. Geological Society, London, Special Publications 400, 507–519, https://doi.org/10.1144/SP400.26.

Cuss, R. J., Harrington, J. F. & Noy, D. J. 2012. Final report of FORGE WP4.1.1: The stress-path permeameter experiment Conducted on Callovo-Oxfordian Claystone. British Geological Survey on November 21, 2014 Claystone. British Geological Survey Commissioned Report CR/12/140.

Dagan, G., 1989. Flow and transport in porous formations. Springer Press, New York.

Dagher, E.E., Nguyen, T.S. and Infante sedano, J.A., 2018. Development of a mathematical model for gas migration (two-phase flow) in natural and engineered barriers for radioactive waste disposal. 2018 Canadian Nuclear Safety Commission. Geological Society, London, Special Publications, ISSN:0305-8719.

Davies, P., 1991. Evaluation of the role of threshold pressure in controlling flow of waste-generated gas into bedded salt at the Waste Isolation Pilot Plant. SANDIA report, SAN90-3246 UC-721.

Damjanac, B. and C. Fairhurst. 2010. Evidence for a long-term strength threshold in crystalline rock. Rock Mechanics and Rock Engineering 43(5), 513-531.

Davy, C.A., Skoczylas, F., Barnichon, J.-D., Lebon, P., 2007. Permeability of macro-cracked argillite under confinement: Gas and water testing, Physics and Chemistry of the Earth, Parts A/B/C, Volume 32, Issues 8-14, 2007, Pages 667-680.

DIT-UPC, 2000. CODE-BRIGHT. A 3-D program for thermo-hydro-mechanical analysis in geological media. User's guide. Centro Internacional de Métodos Numéricos en Ingeniería (CIMNE), Barcelona.

Dobson, P. F., Salah, S., Spycher, N., and Sonnenthal, E. L., 2004. Simulation of water-rock interaction in the Yellowstone geothermal system using TOUGHREACT, Geothermics, v. 33, p. 493-502.

Duppendecker, S.J., Dohmen, L., Welte, D.H., 1997. Numerical modelling of petroleum expulsion in two areas of the lower saxony basin, northern Germany. In: Petroleum Migration, Geol. Soc. of London, Special Publication 59, pp. 47–64.

Du, Y., Wang, W., Kolditz, O., 2006. Dual-continua model for unsaturated flow and application to Decovalex Task D. Geosys Preprint-10, Tubingen.

Dymitrowska, M., et al., 2009. Performance assessment methodologies in application to guide the development of the safety case (PAMINA): PA approach to gas migration DELIVERABLE, European Commission (Contract Number: FP6-036404).

Ekeroth, E., Roth, O. & Jonsson, M. 2006. The relative impact of radiolysis products in radiation-induced oxidative dissolution of UO2. Journal of Nuclear Materials, 355, 38–46.

Everham, W. D. 2004. Thermal history of the Michigan basin.‖ Ph.D thesis. Michigan Technological University.

Fall, M., 2009. Safety-related aspects of a radioactive waste repository in sedimentary rock formations-generation and migration of gas from the waste repository, a report submitted to the CNSC.

Fall, M., Nasir, O., 2012. Coordinated Assessment and Research Program on Safety-Related Aspects of a Radioactive Waste Repository in Sedimentary Rock Formations: Generation and Migration of Gas from the Waste Repository. Report for the Canadian Nuclear Safety Commission (CNSC).

Fall, M., Nasir O., 2012. Numerical Modelling of Gas Migration from a DGR in Ontario's Sedimentary Rocks, A report submitted to the CNSC (Contract No.: 87055-08-1075).

Fall, M., Nasir, O., Nguyen, S., 2014. A coupled hydro-mechanical model for simulation of gas migration in host sedimentary rocks for nuclear waste repositories. Engineering Geology 176:24-44.

Fall M., Li, Z, Guo G, Wei X. 2018. Simulation of gas migration in Canadian potential host rocks for radioactive waste disposal (Invited paper and talk). Proceedings of 47. Geomechanik-Kolloquium, 2018, Freiberg, Germany, Nov 16, 2018.

Feiveson, H., Mian, Z., Ramana, M.V., Von Hippel, F. (Eds.), 2011. Experience and Lessons from Around the World. International Panel on Fissile Materials, Princeton.

FORGE, 2010. EURATOM 7th Framework project. Summary of gas generation and migration current state-of-the-art, complied by: Simon Norri.

Freivogel, M. 2001. Diplomkartierung im Gebiet La Croix – Mont Terri (JU). Unpublished Diploma Thesis: Univ. of Basel.

Fusseis, F., Regenauer-Lieb, K., and Revets, S., 2009. A review of porosity-generating mechanisms in crustal shear zones. Multiscale Earth System Dynamics, The University of Western Australia, School of Earth & Environment, Perth, Australia. Geophysical Research Abstracts, Vol. 11, EGU2009-8871-1, 2009 EGU General Assembly 2009.

Gallé, C., 2000. Gas breakthrough pressure in compacted Fo–Ca clay and interfacial gas overpressure in waste disposal context. Appl. Clay Sci. 17, 85–97.

Gartner Lee Limited, 2008. Phase I Regional Geology, Southern Ontario. Supporting technical report. OPG 00216-REP-01300-00007-R00.

Gas generation and migration from a deep geological repository for radioactive waste, a review of Nirex/NDA's work, 2008.

Gelhar, L.W., 1993. Stochastic subsurface hydrology. Prentice Hall, 390pp.

Gens, A., Wieczorek, K., Gaus, I., Garitte, B., Mayor, J.C., Schuster, K., Armand, G., Garcı´a-Sin˜eriz, J-L., and Trick, T., 2017. Performance of the Opalinus Clay under thermal loading:

experimental results from Mont Terri rock laboratory (Switzerland). Swiss Journal of Geosciences, 110.

Gerard, P., Charlier, R., Barnichon, J.D., Su, K., 2008. Numerical modeling of coupled mechanics and gas transfer around radioactive waste in long. J. Theor. Appl. Mech. 38(1-2), 25-44.

Goodfield, M., Nash, P.J., Tate, M.J., Wikramaratna, R.S. and Rodwell, W.R. 2000. Gas migration through water-saturated fracture networks: modelling studies relevant to the potential localization of gas release as the surface and the potential inducing of groundwater flow. AEA Technology Report, AEAT-R-ENV-174.

Goodfield, M. and Rodwell, W.R. 2001. Microscopic and macroscopic approaches to understanding gas-water interactions in gas migration through fractured rock AEA Technology Report, AEAT-ERRA-0308.

Graham, C.C., Harrington, J.F., Cuss, R.J. and Sellin, P. 2012. Gas migration experiments in bentonite: implications for numerical modelling. Mineralogical Magazine, 76, 3279–3292.

Grupa, J., Schröder, T.J., 2009. PA approach to gas migration. Project PAMINA — Report D3.2.1.

Guvanasen, V., Chan, T., 1999. A three-dimensional numerical model for thermos-hydro-mechanical deformation with hysteresis in a fractured rock mass. International Journal of Rock Mechanics and Mining Sciences 37 (2000) 89-106.

Guo, G., Fall, M (2018). Modelling of dilatancy-controlled gas flow in bentonite-based materials with double porosity and double effective stress concepts. Engineering Geology 243(4):253-271.

Guo, G., Fall, M (2019). Modelling of preferential gas flow in heterogeneous and saturated bentonite based on phase field method. Computer & Geotechnics 116: 103206.

Guo, G., Fall, M (2021a). Advances in modeling of hydromechanical processes in gas migration within saturated bentonite. Engineering Geology 287: 106123.

Guo, G., Fall, M (2021b). A thermodynamically consistent phase field model for gas migration in saturated bentonite accounting for initial stress state. Transport in Porous Media 137(11):1-38.

Guo and Fall (2021c). Advances in modeling of hydromechanical processes in gas migration within saturated bentonite. Engineering Geology 287: 106123.

Hadley, G.R., 1985. PETORS-A program for calculating transport of heat, water, water vapour and air through a porous material. Sandia National Laboratories Report SAND84-0878, Albuquerque, N.M.

Haijtink, B., Rodwell,W., 1998. Project on the effects of GAS in underground storage facilities for radioactive waste. Project PEGASUS — Report EUR 18167 EN.

Harrington, J.F., Dela Vaissière, R., Noy, D.J., Cuss, R.J. and Talandier, J., 2012. Gas flow in Callovo-Oxfordian claystone (COx): results from laboratory and field-scale measurements. Mineralogical Magazine, 76, 3303–3318.

Harrington, J.F., Graham, C.C., Cuss, R.J. and Norris, S., 2017. Gas network development in a precompacted bentonite experiment: evidence of generation and evolution. Applied Clay Science, 147, 80–89.

Harrington, J.F. and Horseman, S.T., 1999. Gas transport properties of clays and mudrocks. In: APLIN, A.C., FLEET, A.J. & MACQUAKER, J.H. (eds) Muds and Mudstones: Physical and Fluid Flow Properties. Geological Society of London, London, Special Publications, 158, 107–124, https://doi.org/10.1144/GSL. SP.1999.158.01.09.

Hatch, L. P., 1953. Ultimate disposal of radioactive waste. American scientist. 41-3:410-412.

Ho, C.K. and Webb, S.W., 2006. Gas transport in porous Media. Published by Springer, P.O.A Box 17, 3300 AA Dordrecht, The Netherlands.

Hoch, A.R. 2005. Scoping calculations to determine if gas generated in a repository might migrate to the biosphere in solution. Serco Assurance Report, SA/ENV-0786.

Hoch, A.R., Jackson, C.P. and Rodwell. W.R. 2002. Modelling of the transport of radon by gas migrating from a radioactive waste repository. Serco Assurance Report, Serco- ERRA-0446.

Hoch, A.R., Myatt, B.J., Rodwell, W.R., Swanton, S.W. and Swift, B.T. 2003. Visualisation and modelling of gas migration through simple models of intersecting channels in a fracture under liquid saturated conditions. Serco Assurance Report, Serco-ERRA-0449.

Hoch, A.R., Swanton, S.W., Manning, M.C., Rodwell, W.R., Swift, B.T. and Duddridge, G.A., 2001. Gas migration in low-permeability fractured rock: theoretical and experimental studies. AEA Technology Report, AEAT-ERRA-0323.

Horseman, S.T., Harringto, J.F., 1997. Study of gas migration in Mx80 buffer bentonite. BGS internal report WE/97/7 to SKB.

Horseman, S.T., Harrington, J.F., Sellin, P., 1999. Gas migration in clay barriers. Engineering Geology, 54: 139-149.

Horseman, S.T., Harrington, J.F. and Sellin, P., 2003. Water and gas movement in Mx80 bentonite buffer clay. Symposium on the Scientific Basis for Nuclear Waste Management XXVII (Kalmar), Materials and Research Society, 15–19 June 2003, Kalmar, Sweden, 807, 715–720.

Hostettler, B., Reisdorf, A. G., Jaeggi, D., Deplazes, G., Bla¨si, H.-R., Morard, A., Feist-Burkhardt, S., Waltschew, A., Dietze, V., and Menkveld-Gfeller, U., 2017. Litho- and biostratigraphy of the Opalinus Clay and bounding formations in the Mont Terri rocklaboratory (Switzerland). Swiss Journal of Geosciences, 110.

Hudson, J. A., Stephansson, O., and Andersson, J., 2005. Guidance on numerical modeling of thermo-hydro-mechanical coupled processes for performance assessment of radioactive waste repositories. International Journal of Rock Mechanics and Mining Sciences 42, (5-6 SPEC. ISS.): 850-870.

IAEA (International Atomic Energy Agency) safety standards for protecting people and the environment classification of radioactive waste general safety guide, No. GSG-1, 2009.

INTERA. 2011. Descriptive Geosphere Site Model. Intera Engineering Ltd. report for the Nuclear Waste Management Organization NWMO DGR-TR-2011-24 R000. Toronto, Canada.

Itasca, 2009. FLAC3D V4.0, Fast Lagrangian Analysis of Continua in 3 Dimensions, User's Guide. Itasca Consulting Group, Minneapolis, Minnesota 438pp.

Jacques, D, Šimůnek, J., 2005. User manual of the multicomponent variably-saturated flow and transport model HP1: description, verification, and examples. Version 1.0, BLG-998. Waste and Disposal, SCK. CEN.

Jaeggi, D., Laurich, B., Nussbaum, C., Schuster, K., and Connolly, P. 2017. Tectonic structure of the ‘‘Main Fault’’ in the Opalinus Clay, Mont Terri rock laboratory (Switzerland). Swiss Journal of Geosciences, 110.

Jensen, M., Lam, T., Luhowy, D., McLay, J., Semec, B. and Frizzell, R., 2009. Ontario Power Generation’s Proposed L&ILW Deep Geologic Repository: An Overview of Geoscientific Studies, Nuclear Waste Management Organization, Toronto, Ontario, Canada, GeoHalifax 2009.

Jia, Y., Song, X.C., Duveau, G., Shao, J.F., 2007. Elastoplastic damage modeling of argillite in partially saturated condition and application. Physics and Chemistry of the Earth 32 (2007) 656-666.

Jing, L.R., Feng X.T., 2013. Numerical modeling for coupled Thermo-Hydro-Mechanical and Chemical processes (THMC) of geological media—international and Chinese experience. Chinese Journal of Rock Mechanics and Engineering. Oct., 2003. 22(10): 1704-1715.

Jockwer, N., 2000. Experimental studies on gas migration in underground rock laboratories in granitic and argillaceous rocks. Gesellschaft für Anlagen- und Reaktorsicherheit mbH (GRS) Theodor-Heuss-Str.4, D 38122 Braunschweig, Germany.

Jockwer, N., 2003. Experimental studies on gas migration in underground rock laboratories in granitic and argillaceous rocks. Gesellschaft für Anlagen- und Reaktorsicherheit mbH (GRS) Theodor-Heuss-Str.4, D 38122 Braunschweig, Germany.

Jockwer, N., 2006. Experimental studies on gas migration in underground rock laboratories in underground rock laboratories in Granitic and Argillaceous rocks. Gesellschaft für Anlagen- und Reaktorsicherheit mbH (GRS).

Jockwer, N., Miehe, R., Müller-Lyda, I, 2000. Untersuchungen zum Zweiphasenfluss und diffusiven Transport in Tonbarrieren und Tongesteinen. – Abschlussbericht (02 E 9017), GRS-167, ISBN-Nr.: 3-931995-33-x.

Johnson, L., Marschall, P., Wersin, P., Gribi, P., 2005. HMCBG Processes Related to the Steel Components in the KBS-3H Disposal Concept. Posiva Working Report 2005–09. Posiva Oy, Eurajoki, Finland.

Johnson, M.D., D.K. Armstrong, B.V. Sanford, P.G. Telford and M.A. Rutka., 1992 Paleozoic and Mesozoic geology of Ontario. In: The Geology of Ontario, Ontario Geological Survey, Special Volume 4, Part 2, 907-1008.

Justinavicius, D., Poskas, P. and Nrkuniene, A. 2016. Gas migration modelling in geological repository module in clay formation and sensitivity analysis. Engineering Geology 213 (2016) 158-168.

Kachanov, L.M., 1958. Time of the rupture process under creep conditions. Isv. Akad. Nauk. SSR. Otd Tekh. Nauk. 8, 26-31.

Klinkenberg, L.J., 1941. The Permeability of Porous Media to Liquids and Gases, API Drilling and production Practice, pp. 200-213.

Kohl, T., Evans, F.K., Hopkirk R.J., and Rybach, L., 1995. Observation and simulation of non-Darcian flow transients in fractured rock. Water resources research, VOL, 33, NO.3, Pages 407-418.

Kolditz, O., Bauer, S., Bilke, L., et al., 2012. OpenGeoSys: an open-source initiative for numerical simulation of thermo-hydro-mechanical/chemical (THM/C) processes in porous media
Kreis, P. 1991. Hydrogen Evolution from Corrosion of Iron and Steel in Low/Intermediate Level Waste Repositories. Nagra Technical Report NTB 91-21.

Kuhl, D., Bangert, F., Meschke, G., 2004. Coupled chemo-mechanical deterioration of cementitious materials. Part i: Modeling. International Journal of Solids and Structures 41, 15-40.

Lege, T., Shao, H., 1996. The brush model-a new approach to numerical modelling of matrix diffusion in fractured claystone, fluid flow through faults and fractures in argillaceous formations, NEA/EC Workshop, Berne, June.

Lege, T., Shao, H., 1996. The brush model-a new approach to numerical modeling of cementitious materials, part I: modeling Int. J. Solids Struct. 41, 15-40.

Lemaitre, J., 1971. Evaluation of Dissipation and Damage in Metals Submitted to Dynamic Loading, Proceedings I.C.M.I, Kyoto, Japan.

Lemaitre, J., Chaboche, J.-L., 1990. Mechanics of Solid MaterialsCambridge University Press,

London.

Leupin, O.X., Bernier-Latmani, R., Bagnoud, A., Moors, H., Leys, N., Wouters, K., and Stroes-Gascoyne, S., 2017a. Fifteen years of microbiological investigation in Opalinus Clay at the Mont Terri rock laboratory (Switzerland). Swiss Journal of Geosciences, 110.

Leupin, O.X., Van Loon, L.R., Gimmi, T., Wersin, P., and Soler, J.M. 2017b. Exploring diffusion and sorption processes at the Mont Terri rock laboratory (Switzerland): lessons learned from 20 years of field research. Swiss Journal of Geosciences, 110.

Liu, X., Zhang, C., Liu, Q., 2009. Multiple-point statistical prediction on fracture networks as Yucca Mountain, 2008. Environ Geo 57:1361-1370.

Li, Z., Fall, M., 2013. Coupled Thermo-Hydro-Mechanical-Geochemical Model for the Assessment of Groundwater Quality due to Impacts from Geological Sequestration of CO2. GeoMontreal, October 2013, Montreal, Canada.

Maeder, U., Jenni, A., Lerouge, C., Gaboreau, S., Miyoshi, S., Kimura, Y., Cloet, V., Fukaya, M., Claret, F., Otake, T., Shibata, M., and Lothenbach, B., 2017. 5-Year chemico-physical evolution of concrete-claystone interfaces, Mont Terri rock laboratory (Switzerland). Swiss Journal of Geosciences, 110.

Mallants, D. and Jacques, D., 2004. Performance assessment for deep disposal of low and intermediate level short-lived radioactive waste in Boom Clay, SCK•CEN-R-3793.

Mallants, D., Jacques, D., and J. Perko, 2007. Modelling multi-phase flow phenomena in concrete barriers used for geological disposal of radioactive waste. Proceedings of the 11th International Conference on Environmental Remediation and Radioactive Waste Management, ICEM07, September 2-6, 2007, Bruges, Belgium.

Manai, T., 1997. EVEGAS – European validation exercise of GAS migration model through geological media. Project EVEGAS — Final Report EUR 17557 EN.

Marschall, P., Croisé, J., Schlickenrieder, L., Boisson, JY., Vogel, P., Yamamoto, S., 2003. Synthesis of hydrogeological investigations at the Mont Terri site (Phases 1 - 5). Mont Terri Technical Report TR 2001-02, Geotechn. Inst. Ltd., Bern, Switzerland.

Marschall, P., Distinguin, M, Shao, H., Bossart, P., Enachescu, C., Trick, T., 2006. Creation and

Evolution of Damage Zones around a Microtunnel in a Claystone Formation of the Swiss Jura Mountains. International Symposium and Exhibition on Formation Damage Control, Louisiana U.S.A., doi: 10.2118/98537-MS.

Marschall, P., Giger, S., De La Vassie`re, R., Shao, H., Leung, H., Nussbaum, C., Trick, T., Lanyon, B., Senger, R., Lisjak, A., & Alcolea, A., 2017. Hydro-mechanical evolution of the EDZ as transport path for radionuclides and gas: insights from the Mont Terri rock laboratory (Switzerland). Swiss Journal of Geosciences, 110.

Marschall P., Horseman S., Gimmi T., 2005. Characterisation of gas transport properties of the Opalinus Clay, a potential host rock formation for radioactive waste disposal. Oil & Gas Science and Technology-Rev.IFP, Vol. 60. No.1, pp. 121-139.

Mayer, K.U., 2000. MIN3P V1.0 User Guide, University of Waterloo, Department of Earth Sciences, 26.06.00.

Mazurek, M., 2004. Long-term used nuclear fuel waste management - Geoscientific review of the sedimentary sequence in southern Ontario. Technical Report TR 04-01, Institute of Geological Sciences, University of Bern, Switzerland.

Mazurek, M., and de Haller, A., 2017. Pore-water evolution and solute-transport mechanisms in Opalinus Clay at Mont Terri and Mont Russelin (Canton Jura, Switzerland). Swiss Journal of Geosciences, 110.

McCarthy, R.F., Swift, B.T. and Rodwell, W.R. 2001. Development of single fracture gas migration model, AEA Technology Report, EAT/ERRA-0324.

McIntosh, J. C., and Walter, L. M. 2006. Paleowaters in silurian-devonian carbonate aquifers: Geochemical evolution of groundwater in the great lakes region since the late pleistocene. Geochimica et Cosmochimica Acta 70, (10): 2454-2479.

McNutt, R.H., 1987. 87Sr, 86Sr ratios as indicators for water-rock interactions: applications to brines found in PreCambrian age rocks from Canada. in Saline waters and gases in crystalline rocks. GAC Special Paper 33. Ed. by P. Fritz and S. Frape. 81-88.

Miller, W., Alexander, R., Chapman, N., Mckinley, J., and Smellie, J.A.T., 2000. Geological disposal of radioactive wastes and natural analogues, Volume 2, 328p.

Millington, R. J., and Quirk, J. P., 1961. Permeability of porous solids, Trans. Faraday Soc., v. 57, p. 1200-1207.

MODEX-REP Mid-Term Report, 2002. Elaboration of hydromechanical coupled models by interpretation of the disturbances observed during the sinking of the main shaft of an underground laboratory in Eastern France, ANDRA, Chatenay-Malabry.

Mott, R.E. and Rodwell, W.R. 1998. A review of two-phase flow in fractures. Nirex Report NSS/R349, UK Nirex Ltd, Harwell.

Müller, H. R., Garitte, B., Vogt, T., Ko¨hler, S., Sakaki, T., Weber, H., Spillmann, T., Hertrich, M., Becker, J. K., Giroud, N., Cloet, V., Diomidis N., & Vietor, T., 2017. Implementation of the fullscale emplacement (FE) Experiment at the Mont Terri rock laboratory (Switzerland). Swiss Journal of Geosciences, 110.

Nagra, 2002a. Projekt Opalinuston – Synthese der geowissenschaftlichen Untersuchungs ergebnisse. Entsorgungsnachweis für abgebrannte Brennelemente, verglaste hochaktive sowie langlebige mittelaktive Abfälle. Nagra Technical Report NTB 02-03, Nagra, Wettingen, Switzerland.

Nagra, 2004. Effects of Post-disposal Gas Generation in a Repository for Spent Fuel, High-level Waste and Long-lived Intermediate Level Waste Sited in Opalinus Clay. Technical Report

NTB 04-06, 2004.

Nagra, 2008. Konzept für die Anlage und den Betrieb eines geologischen Tiefenlagers. Entsorgungsnachweis für abgebrannte Brennelemente, verglaste hochaktive sowie langlebige mittelaktive Abfälle. Technical Report, 175p.

Nagra, 2016. Production, consumption and transport of gases in deep geological repositories according to the Swiss disposal concept. Nagra Technical Report, NTB 16-03, Nagra, Wettingen, Switzerlan.

Nash, P.J., Goodfield, M., Sullivan, N.A. and Rodwell, W.R. 2000. Conceptual studies of the evolution of gas pathways from a radioactive waste repository in fractured rock. AEA Technology Report, AEAT-R-ENV-175.

Nash, P.J., Swift, B.T., Goodfield, M. and Rodwell, W.R. 1998. Modelling Gas Migration in Compacted Bentonite: A report produced for the GAMBIT Club. POSIVA, Helsinki.

Nash, P.J. and Rodwell, W.R. 2000. Modelling of gas migration pathways. Nirex Report NSS/R377, UK Nirex, Harwell.

Nasir, O., 2013. Coupled thermo-hydro-mechanical-chemical (THMC) responses of Ontario's host sedimentary rocks for nuclear waste repositories to past and future glaciations and deglaciations, thesis, department of civil engineering faculty of engineering, University of Ottawa.

Nasir, O., Fall, M., 2014. A simulator for modeling of porosity and permeability changes in near field sedimentary host rocks for nuclear waste under climate change influences. Tunneling and Underground Space Technology 42 (2014) 122-135.

Nasir, O., Fall, M., Son Nguyrn, T., Evgin, E., 2013. Modeling of the thermo-hydro-mechanical–chemical response of sedimentary rocks to past glaciations. International Journal of Rock Mechanics and Mining Sciences. 64:160–174, December 2013.

Nasir, O., Fall, M., Nguyen, T.S., Evgin, E., 2014. Modeling of the Thermo-Hydro-Mechanical-Chemical Response of Ontario Sedimentary Rocks to Future Glaciations. Canadian Geotechnical Journal, 2015, 52(7): 836-850.

Necib, S., Diomidis, N., Keech, P., & Nakayama, M., 2017. Corrosion of carbon steel in clay environments relevant to radioactive waste geological disposals, Mont Terri rock laboratory (Switzerland). Swiss Journal of Geosciences, 110.

Neretnieks, I. 1984. Impact of alpha-radiolysis on the release of radionuclides from spent fuel in a geologic repository. Proceedings of the Materials Research Society Symposium, Boston, MA, 14 November 1983, 26, 1009–1022. http://dx.doi.org/10.1557/PROC-26-1009

Nguyen, T. S., Description of the computer code FRACON, 1996. Stephansson, O., Jing, L., and Tsang, C.-F., (Editors), Coupled Thermo-Hydro-Mechanical Processes of Fractured Media Developments in Geotechnical Engineering, vol.79.

Nguyen, T.S., Le, A.D., 2015. Simultaneous gas and water flow in a damage-susceptible bedded argillaceous rock. Can.Geotech.J.52:18-32.

Nirex, 1997a. Nirex 97: An assessment of the post-closure performance of a deep waste repository at Sellafield, Volume 4: The gas pathway. Nirex Report S/97/012. UK Nirex, Harwell.

Nirex, 2000. Theoretical modelling of gas injection field experiments. Nirex Report NSS/R367, UK Nirex, Harwell.

Nirex, 2006d. Summary note for CoRWM on gas breakthrough time issues. Nirex technical note, Number: 495194, UK Nirex, Harwell.

Nirex 2006g. Analogue evidence for the migration of gases and non-aqueous phase liquids in the geosphere. Nirex Report. N/131.

Norris, S., 2015. EC FORGE project: updated consideration of gas generation and migration in the safety case. In: Shaw, R.P. (Ed.), Gas Generation and Migration in Deep Geological Radioactive Waste Repositories. Geological Society, London, Special Publications, 415, pp. 241–258.

Noronha, J., 2016. Deep geological repository conceptual design report crystalline / sedimentary rock environment. Nuclear waste management organization, APM-REP-00440-0015 R001.

Nussbaum, C., Kloppenburg, A., Cae¨r, T., and Bossart, P., 2017.Tectonic evolution around the Mont Terri rock laboratory, northwestern Swiss Jura: constraints from kinematic forward modelling. Swiss Journal of Geosciences, 110.

NWMO, 2011 Descriptive Geosphere Site Model. Prepared by: Intera Engineering Ltd, NWMO DGR-TR-2011-24.

NWMO. 2011A. “Geosynthesis” Prepared by: Nuclear Waste Management Organization NWMO DGR-TR-2011-11.

NWMO. 2011B. Preliminary safety report. Prepared by nuclear waste management organization. NWMO 00216-SR-01320-00001.

NWMO, 2011C. Descriptive Geosphere Site Model. Prepared by: Intera Engineering Ltd. NWMO DGR-TR-2011-24.

NWMO. 2011E. Postclosure safety assessment: gas modelling. Prepared by Geofirma Engineering Ltd. and Quintessa Ltd. NWMO DGR-TR-2011-31.

OPG letter, 2012. Albert Sweetnam to JRP Chair, “Updated Information in Support of OPG’s Licence Application for a Deep Geologic Repository for Low and Intermediate Level Waste”. CD# 00216-00531-00101.

Ortiz L., Impey M., Einchomb S., 1996. Characterization of gas flow in boom clay, a low permeability plastic rock, fluid flow through fractures in argillaceous formations, NEA /EC Workshop June 1996.

Ortiz, L., Volckaert, G., De Canniere, P., Put, M., Sen, M.A., Horseman, S.T., Harrington, J.F., Impey, M., Einchcomb, S., 1997. Modelling and Experiments on GAS Migration in Repository Host Rocks. Project MEGAS — Final Report EUR 17453 EN.

Ozanam O., Su K., Hoteit N., 2000. First *in-situ* Experiment in the French Underground Laboratory: Vertical Mine-by-Test in the Main Shaft. WM’00 Conference, Tucson – Arizona.

Parkhurst, D.L., Appelo, C.A.J., 1999. User’s Guide to PHREEQC (Version 2): A computer program for speciation, batch-reaction, one-dimensional transport, and inverse geochemical calculations water-resources investigations report 99-4259, U.S. Geological Survey, Denver, Colorado.

Popp, T., Salzer, K., Minkley, W., 2008. Influence of bedding planes to EDZ-evolution and the coupled HM properties of Opalinus Clay. Phys. Chem. Earth Parts A/B/C 33, 374-387.

Poulet, T., Karrech, K., Regenauer-Lieb, K., Fisher, L., and Schauba, P., 2012. Thermal-hydraulic-mechanical-chemical coupling with damage mechanics using ESCRIPTRT and ABAQUS. Tectonophysics, Volumes 526-529, pp 124-132.

Pruess, K. 1987. TOUGH user’s guide. US Nuclear Regulatory Commission Report NUREG/CR-4645 (also Lawrence Berkeley Laboratory Report 20700), 1987.

Pruess, K. 1991. TOUGH2: A general purpose numerical simulator for multiphase fluid and heat flow. Lawrence Berkeley Laboratory Report 29400.

Pruess, K., Oldenburg, C., Moridis, G., 1999. TOUGH2 User's Guide, Version 2.0, Report LBNL-43134. Lawrence Berkeley National Laboratory, Berkeley, California 198pp.

Pusch, R., Ranhagen, L., Nilden, K., 1985. Gas migration through MX-80 bentonite. NAGRA Technical Report NTB 85-36, Baden, Switzerland.

Quintessa Ltd. and Geofirma Engineering Ltd., 2011. Postclosure Safety Assessment: Data. Prepared by: Quintessa Ltd. and Geofirma Engineering Ltd. NWMO DGR-TR-2011-32

Rodwell, W.R., 2000. Research into gas generation and migration in radioactive waste repository systems. Project PROGRESS — Report EUR 19133 EN.

Rodwell, W.R. and Goodfield, M. 2000. A review of mechanisms that might attenuate the flux at the surface of gas from a deep repository. AEA Technology Report, AEATERRA-0084.

Rodwell, W.R. and Nash, P.J. 1992. Mechanisms and modelling of gas migration from deep radioactive waste repositories, June 1992. Nirex report NSS/R250, UK Nirex, Harwell.

Rodwell, W.R., Norris, S., Mäntynen, M. and Vieno, T. et al., 2003. A thematic network on gas issue in safety assessment of deep repositories for radioactive waste (GASNET). European Commission Report, EUR 20620 ISBN 92-894-6401-1. European Commission, Luxembourg. 48 p.

Rohmer, J., Seyedi, D. M., 2010. Coupled large scale hydro-mechanical modeling for caprock failure risk assessment of CO2 storage in deep saline aquifers. Oil and Gas Science and Technology: Rev IFP, 2010, 65(3): 503-517.

Rutqvist, J., Ijiri, Y., Yamamoto, H., 2011. Implementation of the barcelona basic model into TOUGH–FLAC for simulations of the geomechanical behavior of unsaturated soils. Computers & Geosciences Volume 37 751 –762.

Rutqvist, J., Tsang, C.F., 2003. TOUGH-FLAC: a numerical simulator for analysis of coupled thermal-hydrologic-mechanical processes in fractured and porous geological media under multi-phase flow conditions. In: Proceedings of the TOUGH Symposium 2003, Lawrence Berkeley National Laboratory, Berkeley.

Rutqvist, J., Wu, Y. S., 2002. A modeling approach for analysis of coupled multiphase fluid flow, heat transfer, and deformation in fractured porous rock. International Journal of Rock Mechanics & Mining Sciences Volume 39 429-442.

Rutqvist, J., Wu, Y. S., Tsang, C. F. and Bodvarsson, G., 2002. A modeling approach for analysis of coupled multiphase fluid flow, heat transfer, and deformation in fractured porous rock. International Journal of Rock Mechanics and Mining Sciences, 39: 429-442.

Rutqvist, J., Zheng, L.G., Chen, F., Liu, H.H., Birkholzer J., 2013. Modeling of coupled thermo-hydro-mechanical processes with links to geochemistry associated with bentonite-backfilled repository tunnels in clay formations. This article is published with open access at Springerlink.com. Rock Mech Rock Eng. DOI 10,1007/s00603-013-0375-x.

Salari, M.R., Saeb, S., Willam, K.J., Patchet, S.J., Carrasco, R.C., 2004. A coupled elastoplastic damage model for geomaterials. Comput. Methods Appl. Mech. Engrg. 193; 2625-2643.

Schuster, K., Alheid, H.J., Böddener, D., 2001. Seismic investigation of the excavation damaged zone in Opalinus Clay. Eng. Geol. 61, 189–1997.

Schuster, K., Amann, F., Yong, S., Bossart, P. and Connolly, P., 2017. High-resolution mini-seismic methods applied in the Mont Terri rock laboratory (Switzerland). Swiss Journal of Geosciences, 110.

Sellin, P. (ed.) 2014. Experiments and Modelling on the behaviour of EBS. FORGE Reprot, D3.38. :s.n, s.l.

Shao, H., and Schuster, K., 2009. Permeability measurements of Opalinus Clay (Mont Terri) HG-B: combined permeability tests and borehole seismic measurement. B3.1-10856/2009. BGR, Hanover.

Shao, J. F., Chiarelli, A. S., Hoteit, N., 1998. Modeling of coupled elastoplastic damage in rock materials, Int. J. Rock Mech. Miner. Sci. 35 (4-5) (paper no. 115).

Shaw, R.P. 2015b. The Fate of Repository Gases (FORGE) project. In: Shaw, R.P. (ed.) Gas generation and migration in deep geological radioactive waste repositories. Geological Society, London, Special Publications, 415, 1–7, https://doi.org/10.1144/SP415.17.

Shehata, A., Fall, M., Detellier C. 2020. Impact of groundwater chemistry and temperature on the swelling and microstructural properties of bentonite-sand mixtures for barriers for radioactive wastes repositories. Bulleting of Engineering Geology and the Environment 80(2): 1857-1873.

Smart, N. R., Carlson, L., Hunter, F. M. I., Karnland, O., Pritchard, A. M., Rance, A. P.& Werme, L. O. 2006. Interactions Between Iron Corrosion Products and Bentonite. Serco Assurance Report SA/EIG/ 12156/C001.

ŠolcovÁ O., Schneider P., 2006. Experimental determination of transport parameters, Gas transport in porous media, P245-272.

Singleton, M.J., Sonnenthal, E.L., Conrad, M.E. and DePaolo, D.J., 2003. Multiphase reactive transport modeling of stable isotope fractionation of infiltrating unsaturated zone pore water and vapor using TOUGHREACT. Earth Sciences Division, Lawrence Berkeley National Laboratory, Berkeley, CA, 94720, USA.

Sonnenthal, E., Spycher, N., Apps, J.A., and Simmons, A., 1998. Thermo-hydro-chemical predictive analysis for the drift-scale heater test, Yucca Mountain Project Level 4 Milestone SPY289M4, Lawrence Berkeley National Laboratory, Berkeley, California.

Sonnenthal, E., Spycher, N., 2000. Drift-scale coupled processes model, analysis and model report (AMR) N0120/U0110, Yucca Mountain Nuclear Waste Disposal Project, Lawrence Berkeley National Laboratory, Berkeley, California.

Sonnenthal, E.L., Spycher, N., 2001. Drift-scale coupled processes (DST and THC seepage) models. AMR N0120/U0110 Rev.01, Yucca Mountain Project, Lawrence Berkeley National Laboratory, Berkeley, California.

Spycher, N.F., Sonnenthal, E.L., and Apps, J. A., 2003a. Fluid flow and reactive transport around potential nuclear waste emplacement tunnels at Yucca Mountain, Nevada, J. Contam. Hydrol., v.62-63, P 653-673.

Stenhouse, M.J. and Grogan, H. 1991. Review of reactions of methane and hydrogen in the geosphere and biosphere. Nirex Report NSS/R262.

Su, K., 2007. Development of hydro-mechanical models of the Callovo-Oxfordian Argilites for the geological disposal of radioactive waste. MODEX report. EUR 20844.

Talandier, J., 2007a. Couplex-Gaz Benchmark. Synthesis of results for case 1. http://www. andra.fr/couplex/couplex_andra2.pdf (accessed 2016 05 11).

Talandier, J., 2007b. Couplex-Gaz Benchmark. Case 2. 3D modelling of a disposal area for vitrified waste. http://www.andra.fr/couplex/couplex_andra5.pdf (accessed 2016 05 11).

Tanai, JNC., Gallé, C., 1998. Migration des gaz et pression de rupture dans une argile destinée à la barrière ouvragée d'un stockage profond. Bull. Soc. Geol. France 169 5, pp. 675–680.

Tang, C.A., Tham, L.G., Lee, P.K.K., Yang, T.H., Li, L.C., 2002. Coupled analysis of flow, stress and damage (FSD) in rock failure. Int. J. Rock Mech. Min. Sci. Geomech. Abstr. 39 (4), 477–489

Tao, J., Wu, Y., Elsworth, D., Li, P., Hao, Y., 2019. Coupled thermos-hyrdo-mechanical-chemical modeling of permeability evolution in a CO_2-Circulated geothermal reservoir. Hindawi, geofluids. Volume 2019, Article ID 521730, 15 pages.

Taron, J., Elswotth, D., Min, K.B., 2009. Numerical simulation of thermal-hydrologic-mechanical-chemical processes in deformable, fractured porous media. Int. J. Rock Mech. Min. Sci.46 (5), 842-854.

Thomas, L. K., Katz, D. L. and Tek, M. R. 1968. Threshold pressure phenomena in porous media. SPE J. (June): 174-184.

Tsang, C.-F. (Ed.), 1987. Coupled Processes Associated With Nuclear Waste Repositories, Academic, Orlando, Fla.

Tsang, CF., Barnichon, JD., Birkholzer, J., Li, XL., Liu, HH., Sillen, X., 2012. Coupled thermo-hydro-mechanical processes in the near field of a high-level radioactive waste repository in clay formations. International Journal of Rock Mechanics and Mining Sciences, 49, 31–44. doi:10.1016/j.ijrmms.2011.09.015.

Van Genuchten, MT., 1980. A closed form equation for predicting the hydraulic conductivity of unsaturated soils. Soil Sci Soc Am J: 44:892-8.

Vidstrand, P., Wallroth, T. and Ericsson, L. O., 2008. Coupled HM Effects in a Crystalline Rock Mass due to Glaciation: Indicative Results from Groundwater Flow Regimes and Stresses from an FEM Study. Bulletin of Engineering Geology and the Environment 67 (2): 187-197.

Vinsot, A., Appelo, C.A.J., Lundy, M., Wechner, S., Cailteau-Fischbach, C., de Donato, P., Pironon, J., Lettry, Y., Lerouge, C., & De Cannie`re, P., 2017. Natural gas extraction and artificial

gas injection experiments in Opalinus Clay, Mont Terri rock laboratory (Switzerland). Swiss Journal of Geosciences, 110.

Volckaert, G., Bernier, F., Sillen, X., Van Geet, M., Mayor, J., Göbel, I., Blümling, P., Su, K., 2004. Similarities and differences in the behaviour of plastic and indurated clays. Euradwaste. INIS-FR-3271, volume 36, issue 17.

Volckaert, G., Ortiz, L., De Cannière, P., Put, M., Horseman, S.T., Harrington, J.F., Fioravante, V. and Impey M.D., 1995. MEGAS: Modeling and Experiments on GAS Migration in Repository Host Rocks. Final report phase 1. Eur. Comm., [Rep.] EUR 16235 EN.

Vomvoris, S., Lanyon, B., Marschall, P., Ando, K., Adachi, T., Fujiwara, A., Yamamoto, S., 2002. Sand/Bentonite Barriers and Gas Migration: The GMT Large-Scale *In-Situ* Test in the Grimsel Test Site. MRS Proceedings, 757, II3.27 doi:10.1557/PROC-757-II3.27.

Vugrinovich R. 1989. Subsurface temperatures and surface heat flow in the Michigan Basin and their relationships to regional subsurface fluid movement.‖ Marine and Petroleum Geology, Volume 6, Issue 1, February 1989, Pages 60-70.

Wei X., Fall M., 2019. Development of numerical simulator for coupled modeling gas migration in host rocks for radioactive waste repositories. Proc. 4th International Conference on Civil, Structural and Transportation Engineering (ICCSTE'19), June 11-12, Ottawa, Canada.

Wieczorek, K., Gaus, I., Mayor, J. C., Schuster, K., García-Siñeriz, J-L., and Sakaki, T., 2017. *In-situ* experiments on bentonitebased buffer and sealing materials at the Mont Terri rock laboratory (Switzerland). Swiss Journal of Geosciences, 110.

Wissmerier, L., Barry, D.A., 2011. Simulation tool for variably saturated flow with comprehensive geochemical reaction in two-and three-dimensional domains. Environ. Modell. Softw. 26 (2), 210-218.

Worgan, K.J., 1990. Scoping calculation for gas dissolution, diffusion and water expulsion in a L/ILW repository. Intera Sciences Report linebreak I1904-7, Version 2.

Xu, T., Apps, J. A., and Pruess, K., 2003b. Reactive geochemical transport simulation to study mineral trapping for CO2 disposal in deep arenaceous formations, J. Geophys. Res., v. 108 (B2), 2071, doi:10.1029/2002JB001979.

Xu, T.F., 2004. TOUGHREACT User's Guide: A simulation program for non-isothermal multiphase reactive geochemical transport in variable saturated geologic media. Earth Sciences Division, Lawrence Berkeley National Laboratory University of California, Berkeley, CA94720.

Xu, T.F., Pruess, K., 1998. Coupled modeling of non-isothermal multiphase flow, solute transport and reactive chemistry in porous and fractured media: 1. Model development and validation. Lawrence Berkeley National Laboratory Report LBNL-42050, Berkeley, California, 38 pp.

Xu, T.F., Sonnenthal, E., Spycher, N. and Pruess, K., 2006. TOUGHREACT-A simulation program for non-isothermal multiphase reactive geochemical transport in variably saturated geologic media: applications to geothermal injectivity and CO2 geological sequestration. Comput. Geosci. 32, 145–165.

Xu, T.F., Sonnenthal, E., Bodvarsson G., 2003a. A reaction-transport model for calcite precipitation and evaluation of infiltration-percolation fluxes in unsaturated fractured rock, J. Contam. Hydrol., v. 64(1-2) p. 113 – 127.

Xu, WJ., Investigation of gas migration in saturated argillaceous rock, 2013. The Faculty of Environmental Sciences at the Technical University of Dresden, dissertation.

Xu, W.J., Shao, H., Hesser, J., Wang, W.Q., Kolditz, O., Popp, T., 2011. Simulation of dilatancy-controlled gas migration process in saturated argillaceous rock. Computational geomechanics. COMGEO II-Proceeding of the 2nd International Symposium on, Computational Geomechanics, pp. 693-703.

Xue, Y., Dang, F., Li, F., and et al., 2018. Seepage-stree-damage coupled model of coal under geo-stress influence, cmc-computers materials and continua, vol. 54, no.1, pp. 43-59.

Xue, Y., Dang, F., Shi, F., Li, R. and Cao, Z.Z., 2018. Evaluation of gas migration and rock damage characteristics for underground nuclear waste storage based on a coupled model, Science and Technologh of Nuclear Installations, vol 2018, article ID 2973279, 10 pages.

Xue, Y., Gao, F. and Liang, X., 2017. Permeability and pressure distribution characteristics of the roadway surrounding rock in the damaged zone of an excavation. International journal of Mining Science and Technology, vol. 27, no. 2, pp.211-219.

Yang, D., Billiotte, J., Su, K., 2010. Characterization of the hydromechanical behavior of

argillaceous rocks with effective gas permeability under deviatoric stress. Engineering Geology, 114(3-4), 116–122. doi:10.1016/j.enggeo.2010.04.002.

Yang, J., Fall, M, 2021a. Hydro-mechanical modeling of gas transport in clayey host rocks or nuclear waste repositories. International journal of Rock Mechanics and Mining Sciences 14:104987.

Yang, J., Fall, M, 2021b. A two-scale hydro-mechanical-damage model for simulation of preferential gas flow in saturated clayey rocks. Computer & Geotechnics 138: 104365.

Yang, J., Fall, M, 2021c. A dual porosity poroelastic model for simulation of gas flow in saturated claystone as a potential host rock for deep geological repositories. Tunnelling and Underground Space Technology 115(4):104049.

Yang, J., Fall, M, 2021d. A two-scale time dependent damage model for preferential gas flow in clayey rock materials. Mechanics of Materials 158: 103853.

Yang, J., Fall, M 2021e. Coupled hydro-mechanical modelling of dilatancy controlled gas flow and gas induced fracturing in saturated claystone. International Journal of Rock Mechanics and Mining Sciences 138: 104584.

Yang, J., Fall, M, Guo, G. 2020. A Three-Dimensional Hydro-mechanical Model for Simulation of Dilatancy Controlled Gas Flow in Anisotropic Claystone. Rock Mechanics and Rocks Engineering, 53, 4091–4116.

Yu, C., Matray, J.-M., Gonc¸alve`s, J., Jaeggi, D., Gra¨sle, W., Wieczorek, K., Vogt, T., & Sykes, E. (2017). Comparative study of methods to estimate hydraulic parameters in the hydraulically undisturbed Opalinus Clay (Switzerland). Swiss Journal of Geosciences, 110.

Yu, L., Weetjens, E., 2009. Summary of gas generatiom and migration (SCK.CEN-ER-106.09/L Yu/P-85)..

Yu Z.W., Zhang Y. J., Zhang Q., Xu T. F., Algorithm of TOUGHREACT links to FLAC3D. Journal of Jilin university (Earth Science Edition), 2013 (43): 199-206.

Zhang, C-L., Rothfuchs, T., 2004. Experimental study of the hydro-mechanical behavior of the Callovo/Oxfordian argillite. Applied clay science 26, 325-336.

Zhang, C-L., 2015. Investigation of gas migration in damaged and resealed claystone. Gas generation and migration in deep geological radioactive waste repositories, Geological society, London, special publications, 415, 75-93.

Zheng, C., Wang, P., 1998. MT3DMS Documentation and User's Guide.

Zhenze L., 2017. Modeling thermal-hydraulic-mechanical-chemical processes in rocks and seals for deep geological disposal, final report for Canadian Nuclear Safety Commission.

Ziefle, G., Matray, J-M., Maßmann, J., and Möri, A., 2017. Coupled hydraulic-mechanical simulation of seasonally induced processes in the Mont Terri rock laboratory (Switzerland). Swiss Journal of Geosciences, 110.

Zienkiewicz, O.C., Lyness, J., Owen, D.R. J., 1977. Three Dimensional Magnetic Field Determination Using A Scalar Potential –A Finite Element Solution, IEEE Trans. On Mag., Vol. MAG-13, No.5, Sept.

Appendix A. Laboratory and Field Experiments for Gas Migration

A.1. Laboratory experiments

A few laboratory studies have been conducted during the past decade to understand gas migration. The basic laboratory experiments will be introduced and the significant laboratory tests conducted by the investigators will then be summarized and briefly discussed.

A.1.1. Oedometer type experiments

There are two oedometer type experiments in this chapter, the relative gas permeability test and the gas breakthrough experiments. The goal of these experiments is to measure the change of non-destructively in saturation of a clay core caused by gas flow.

A.1.1.1. Relative gas permeability

Gas permeability is a function of the degree of saturation. To determine it, there are a series of gas flow experiments carried out on artificial clay plugs with different degrees of saturation and dry density of 1.7 g/cm^3. The clay plugs were made by uniaxial compaction of clay powder with a homogeneous water content. (Volckaert et al., 1995)

Clay powders with different water contents can be produced in the following ways:

- 0%: clay powder is dried in an oven at 110℃ for 48h;
- 2.6%: clay powder in equilibrium with the laboratory atmosphere;
- 2.6%<w<9%: put the shelves with thin layers in a climatic cabinet. The relative humidity in the cabinet can be regulated at 1% precisely. Until the required water content is obtained, the powder relative humidity should be regularly checked.
- 9%<w<18%: take out the shelves with humid clay powder (8% to 9%) of the climatic chamber. Spray over the shelves with very fine mist of water.

To avoid the transfer of the compacted sample and a gap between the sample and the wall of the cell, the prepared clay powder should be directly compacted in the permeameter. The theoretical height of the samples could be regulated by the press which has been equipped with a displacement transducer. The precision of the sample is 0.02 mm. The following equation is used to calculate the corresponding plug height:

$$h = G(1-\omega)/(1.7s) \quad \text{(A.1)}$$

where: h: height of the plum (cm)

G: weight of the clay sample (g)

s: surface of the permeameter cell (11.34 cm^2)

ω: water content (weight %)

This equation cannot be applied if the water content of the sample is higher than 9%.

The inlet pressure controlled the pressure gradient, the outlet pressure was the atmospheric pressure. Usually argon gas was used as the experimental gas. By using simple soap bubble flow meters and a chronometer, the gas flow could be measured at the outlet. To make sure that the precision of the flow measurement was less than 1%, the measurement time was at least 100 sec. In addition, each measurement was repeated three times to avoid errors. It took three different gradients (ΔP = 0.0025, 0.05, 0.1 MPa and / or ΔP = 0.1, 0.2, 0.3 MPa) to determine the gas permeability of each clay plug.

The results are summarized in Table A-1. The following equation is used to calculate the degree of saturation in the table with the clay grain density (ρ_{gr}) of 2.7 g/cm^2:

$$S = (\rho \cdot \omega/\rho_{\omega})/1 - (\rho \cdot (1-\omega)/\rho_{gr}) \quad \text{(A.2)}$$

where: S: degree of saturation

ρ: bulk density of the clay plug

ρ_{ω}: density of water

ρ_{gr}: clay grain density (2.7 g/cm^2)

In conclusion, the measurements can cover the saturation range from 0% to 95%. From Table A-1, it can be seen that the filters can influence the measured flow rate with about 10 to 20% when the samples below 40% saturation. The gas flow is very sensitive to the density. Due to the strong elastic reaction of the clay it becomes very hard to reach the required density.

It seems that the relative gas permeability becomes 0 at a saturation of about 90%. There are no continuous gas channels remaining available and the gas breakthrough pressure becomes >0 at this saturation. It is the "residual point". Figure A.1 describes the relationship between relative permeability, capillary pressure and saturation (Thomas, et al. 1968). The relative gas permeability versus saturation is given in Figure A.2. It can be seen from Figure A.1 that the relative permeability remains close to 1 when the saturation is less than 40%. After the 40% saturation, the relative permeability sharp drops to about 5%. (Volckaert et al., 1995)

Table A-1 Gas permeability experiments results (Volckaert et al., 1995)

ρ g/cm^3	S **%**	**Flow Nml / sec** $\Delta P(P)$ **[MPa]**	$\Delta P(P)$ **[MPa]**	$\Delta P(P)$ **[MPa]**	$\Delta P(P)$ **[MPa]**	$\Delta P(P)$ **[MPa]**	**H**
		0.025 (0.125)	0.05 (0.15)	0.1 (0.2)	0.2 (0.3)	0.3 (0.4)	cm
1.702	44.4	0.171	0.395	0.904			1.89
1.703	42.8	0.166	0.389	0.893			1.895
1.702	44.4	0.159	0.328	0.769			1.891
1.701	39.4	0.289	0.630	1.485			1.93
1.701	34.1	0.203	0.460	1.064			1.94
1.702	31.5	0.323	0.750	1.724			1.96
1.702	26.3	0.417	0.857	1.923			1.97
1.703	23.8	0.337	0.773	1.786			1.975
1.700	23.1	0.357	0.781	1.808			2.025

1.700	11.3	0.217	0.500	1.145			2.025
1.700	11.3	0.222	0.510	1.545			2.025
1.700	11.3	0.270	0.586	1.351			2.025
1.700	11.3	0.212	0.475	1.095			2.07
1.704	0	0.280	0.658	1.151			2.07
1.704	0	0.266	0.591	1.364			2.07
1.704	0	0.252	0.581	1.389			1.83
1.641	73.0			0.128	0.313	0.579	1.77
1.668	85.0			0	0	0	1.73
1.694	92.5			0	0	0	1.775
1.631	89.9			0	0	0.003	1.74
1.659	95.4			0.0012	0.0026	0.0044	1.78
1.687	78.4			0.109	0.270	0.472	1.785
1.656	82.8			0.029	0.068	0.122	1.77
1.726	74.0			0.034	0.081	0.139	1.809
1.700	68.6			0.132	0.323	0.575	1.84
1.687	61.3			0.194	0.475	0.833	1.82
1.703	63.5			0.119	0.277	0.495	1.86
1.708	50.7			0.271	0.679	1.186	1.83
1.731	54.8			0.174	0.408	0.714	2.035
1.733	4.7	0.400	0.833	1.92			2.015
1.733	4.9	0.323	0.676	1.56			2.05
1.707	4.7	0.417	0.862	2.00			2.065
1.708	0	0.392	0.806	1.852	4.55		2.065

1.708	0	0.392	0.833	1.923	4.762		2.065
1.708	0	0.370		1.852	4.762		

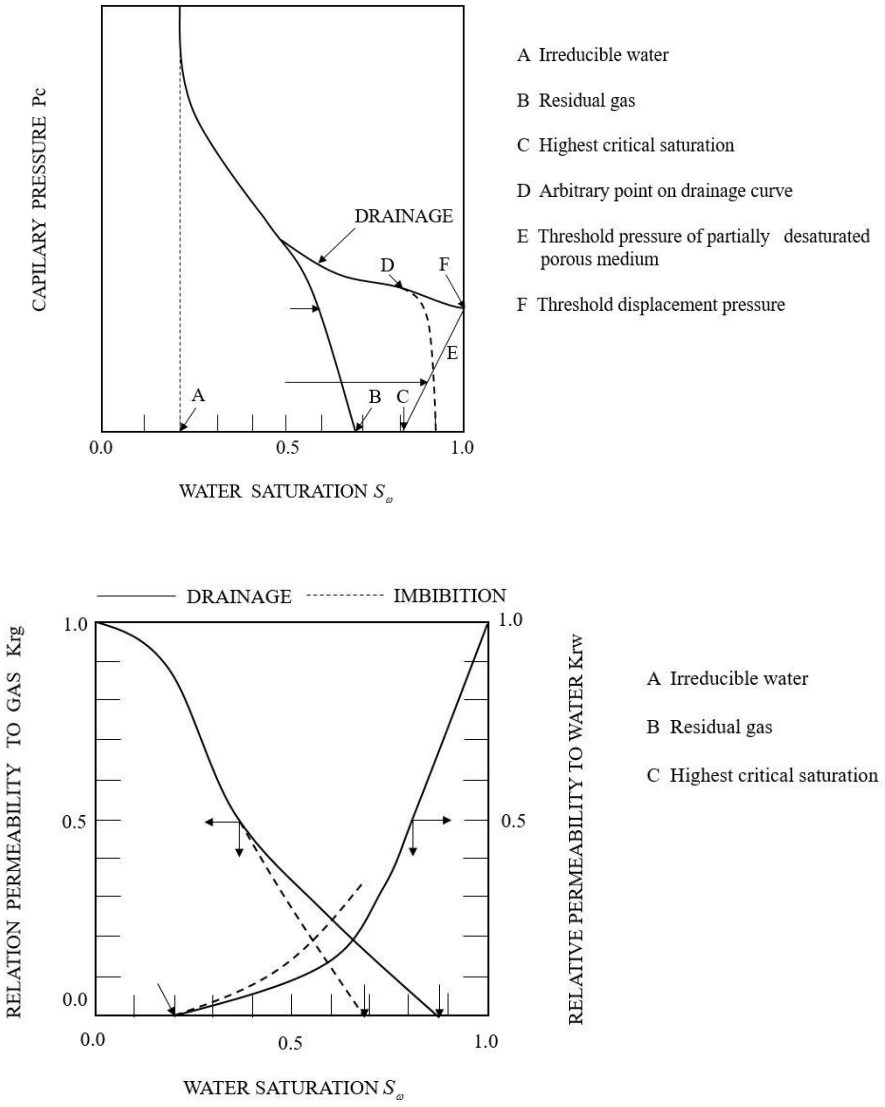

Figure A.1 Relationship between relative permeability, capillary pressure and saturation (Volckaert et al., 1995)

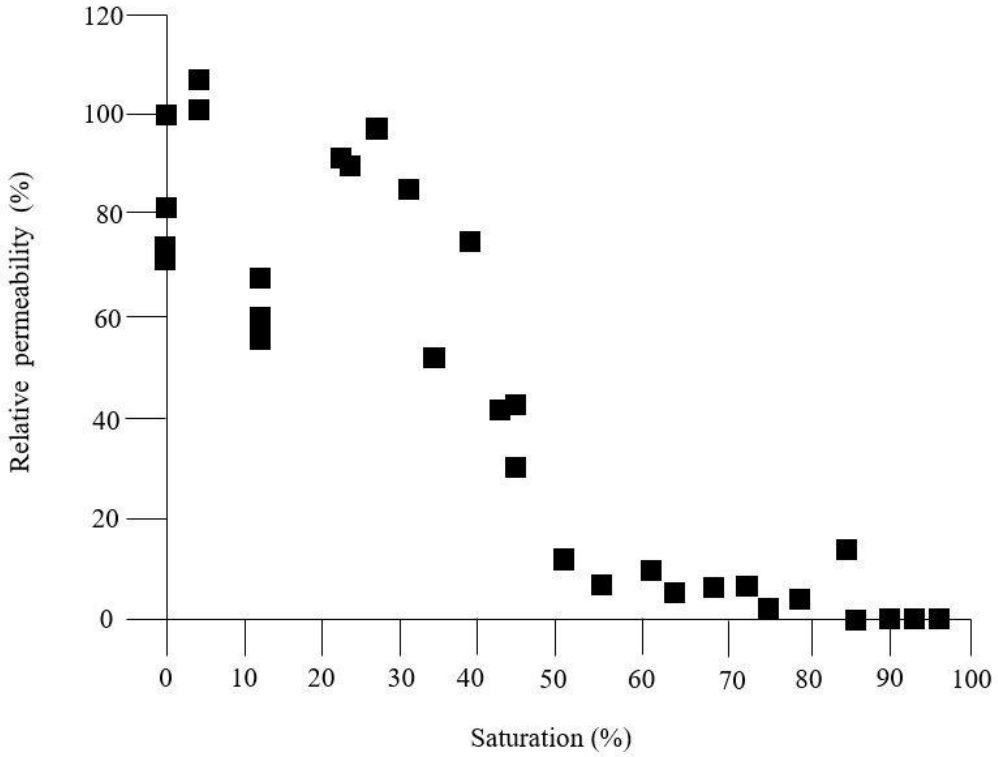

Figure A.2 Relative gas permeability versus saturation (Volckaert et al., 1995)

A.1.1.2. Gas breakthrough experiments

The Figure A.3 shows the experimental set-up of the gas breakthrough experiments conducted by Volckaert et al. (1995). There are three essential parts for the set-up: a permeameter cell and two flow monitoring systems. The system can measure in or out flow of gas or water at constant pressure.

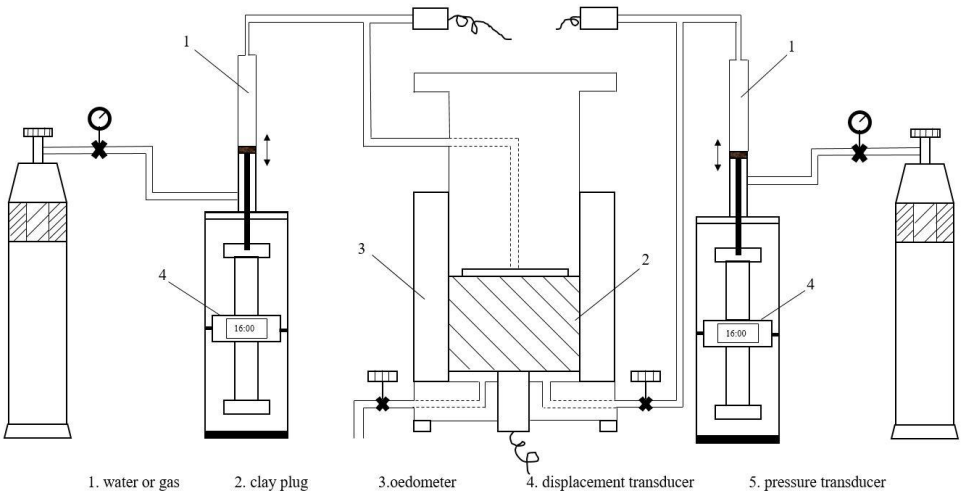

Figure A.3 Breakthrough experiments experimental set-up (Volckaert et al., 1995)

To suit different types of experiments, there are three kinds of basic set-up.

- **Constrained samples**

  For the fully constrained samples. For this kind of experiments, the permeameter cell is placed in an adaptable rigid frame and a screw blocks the cell's piston. There are two series of experiments: Preliminary gas breakthrough experiments and Second series of experiments.

Preliminary gas breakthrough experiments

The pore-radii (r_p) is calculated by the Laplace's equation:

$$P_c = 2\sigma cos\theta / r_p \qquad \text{(A.3)}$$

where: σ: surface tension of water = $7.0\text{e} - 2\ N/m$

θ: contace angle = 45°

P_c: gas breakthrough pressure

r_p: pore-radii

It is very clear to see in Table A-2 that the hydraulic conductivity has a relationship with the breakthrough pressure. The important conclusion is that the breakthrough pressure will be lower

in the direction parallel to the bedding plane than in the one orthogonal to it. From Figure A.4, after breakthrough occurred, the pressure was further raised and the gas flow could be measured. The gas flow very rapidly raised with increasing gradient.

Table A-2 Results of the gas breakthrough experiment (Volckaert et al., 1995)

Plug Height cm	**Bulk Density** g/cm^3	**Orientation**	**Hydraulic conductivity** $m/s \times 10^{-12}$	**Break-through pressure** MPa	**Maximum pore radius** m $\times 10^{-9}$	**Flow** $10^{-4} mlSTP/min$
4.25	2.029	vertical	2.3	2	49	NA
5.255	2.017	horizontal	3.6	1.2	82	35
5.00	2.040	vertical	1.8	1.5	66	3400
4.71	2.024	Na	2.1	0.9	110	460
2.765	2.038	vertical	3.4	2.2	45	7.1
5.00	Na	45°	7.4	1.4	71	28
3.575	Na	horizontal	7.5	<1.5	>66	NA
3.20	Na	Na	3.3	2.4	41	2.2
3.995	20.82	artificial plug	1.5	2.9	34	1.1

Na: not available

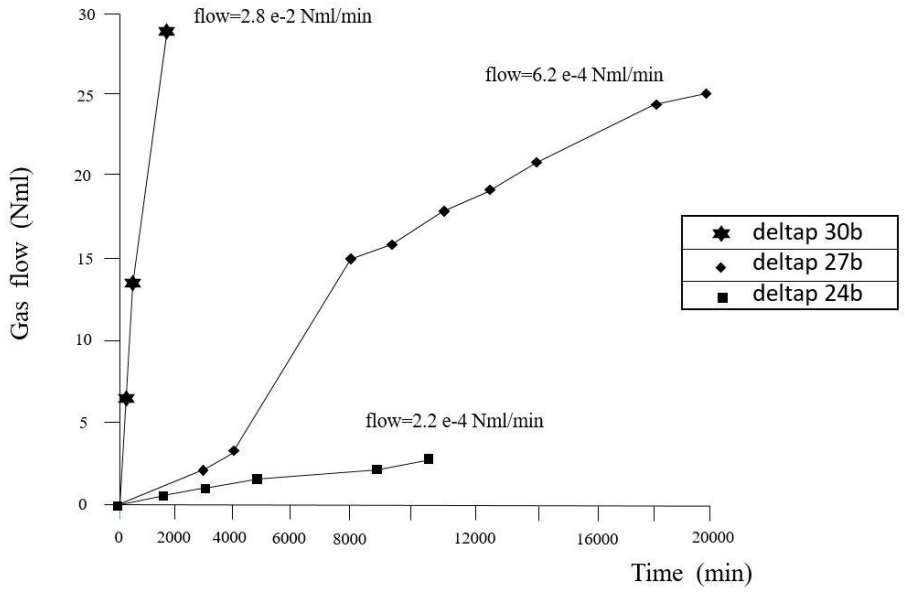

Figure A.4 The function of time and gas overpressure based on gas flow breakthrough (Volckaert et al., 1995)

Second series of experiments

These experiments focused on the precise determination of the hydraulic conductivity, breakthrough pressure, the time elapsed between the last gas pressure increase and gas breakthrough, as well as the development of the gas flow after breakthrough and the saturation profile at the end of the experiment. The saturation is calculated by the following equation:

$$S = \mathrm{w}/\mathrm{n} \tag{A.4}$$

where: *S:* saturation

w: volumetric water content

n: porosity

The porosity is decided by:

$$n = 1 - \rho_d/\rho_g \tag{A.5}$$

where: n: porosity ρ_d: dry density ρ_g: grain density (2.7 g/cm^3)

Gas breakthrough did not happen immediately with the gas pressure increased. It will only occur several hours or days later. Pusch et al (1985) observed the delay in the gas migration research on MX-80 bentonite. Davies (1991) proposed the relationship between the breakthrough pressure and the hydraulic conductivity in this series experiments:

$$P_c = 1.48 \cdot 10^{-4} K^{-0.346} \quad \text{(A.6)}$$

where: P_c: breakthrough pressure in MPA

K: hydraulic conductivity in *m/s*

- **Constant vertical stress**

  For this type, the permeameter cell is placed under a Wyckham Farrance mechanical load frame and the displacement gauge can show the consolidation of the sample with a 2 μm precision. The aims of the constant vertical stress experiments are to simulate better the *in-situ* conditions and to measure the gas entry pressure and the water outflow before breakthrough.

- **X-ray tomography**

In this case, an X-ray transparent permeameter cell is constructed. Based on the relationship between the attenuation of X-rays by a material and the density of the material, the principle of X-ray tomography is developed. It needs to calibrate the X-ray tomography in a function of the volumetric water content for the dry density since the linear attenuation coefficient not only depends on the density but also on the atomic number. Three cross-sections of each clay plug were taken by X-ray tomography. The results are given in Table A-3 and Figure A.5. The aim of these experiments was to measure the change of non-destructively in saturation of a clay core caused by gas flow (Volckaert et al., 1995).

Table A-3 Results of the calibration of the C-ray tomography (Volckaert et al., 1995)

Sample	**Density**		W_v	N_r	$rd_{c,m}$	$rd_{c,std}$	$rd_{p,w}$	$rd_{p,std}$
	dry g/cm^3	**bulk** g/cm^3						
1	1.702	1.702	0	1	1178.3	140	1197	19
				2	1197.5	209		
				3	1216.6	252		
2	1.70	1.786	8.6	1	1262.6	245	1262	20
				2	1258.1	211		
				3	1249.3	140		
				4	1294.3	272		
3	1.70	1.873	17.3	1	1355.1	162	1375	17
				2	1368.6	176		
				3	1389.3	164		
				4	1388.0	107		
4	1.730	1.959	22.9	1	1419.3	83	1414	8
				2	1404.7	83		
				3	1417.5	118		
5	1.70	1.977	27.7	1	1487.3	318	1443	38
				2	1418.7	138		
				3	1423.6	150		
6	1.70	2.024	32.4	1	1533.6	170	1538	9
				2	1528.5	101		
				3	1539.7	142		
				4	1548.9	185		

HU: Hounsfield units

W_v: volumetric water content (%)

N_r: number of the cross section

$rd_{c,m}$: mean radiological density of the cross section (HU)

$rd_{c,std}$: standard deviation of the radiological density of the cross section (HU)

$rd_{p,w}$: mean radiological density of the plug (HU)

$rd_{p,std}$: standard deviation of the radiological density of the plug (HU)

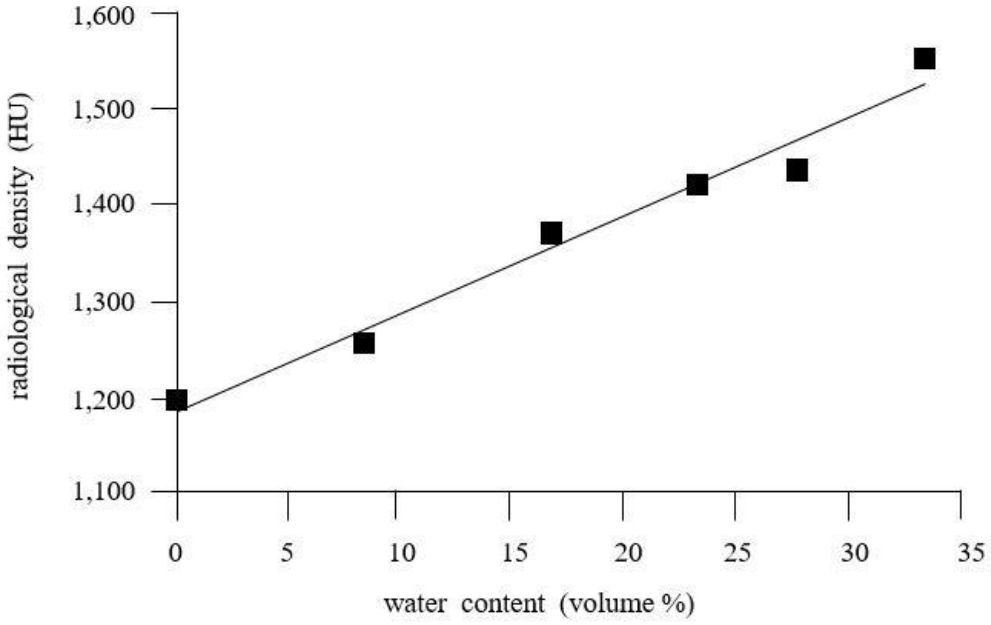

Figure A.5 Calibration of the X-ray tomography for Boom clay with the 1.7 dry density (Volckaert et al., 1995)

From the results of the calibrate experiments, it can be obtained:

$$HU=1188+10.12w_v \quad (A.7)$$

where: W_v: Volumetric water content

Regression coefficient 0.999

Errors on the parameter respectively 3% and 14%

A.1.1.3. Triaxial experiment-axial flow

The experiment equipment by Volckaert et al. (1995) is shown in Figure A.6. There are five main components: a sample assembly, a pressure vessel with the pressure control equipment, a fluid injection system, a back-pressure system, and a microcomputer-based data acquisition system.

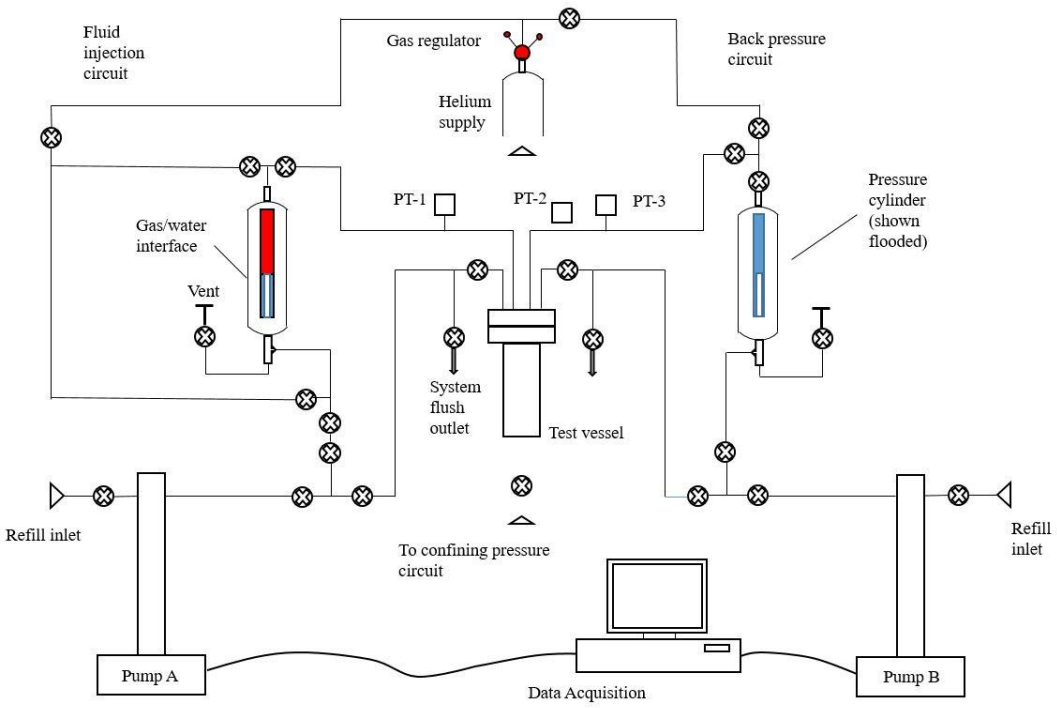

Figure A.6 Testing system schematic (Volckaert et al., 1995)

For the gas injection tests, the testing system governing differential equation assumed isothermal conditions can be expressed as the following form:

$$\frac{dp_{gi}}{dt} = \frac{p_0 \rho_{STP}}{\rho_0 V_{sys}} (Q_p - Q_i) \tag{A.8}$$

where: P_{gi}: instantaneous pressure

V_{sys}: volume of the helium in upstream injection system

ρ_{STP}: density of helium under the standard temperature and pressure (STP)

ρ_0: density at $20℃$.

$P_0 = 1MPa$: unit pressure

Q_p: volumetric rate of the pumping

Q_i: volumetric rate of flow into the specimen

For the injection pump C with a constant rate of volume displacement, it can be written as

$$V_{sys} = V_{sys}(t) = V_{start} - C_t \tag{A.9}$$

where: V_{start}: initial volume of helium

t elapsed time after starting the pump

C: a constant rate of volume displacement

From the equation A-8, when Q_p is precisely equal to Q_i at STP, P_{gj} will become constant. If Q_i is equal to the STP flow-rate from the downstream face Q_0, the gas flow will be happening under steady-state conditions. From equation 3.8 and equation 3.9, except Q_i, the parameters are known or can be quantified in the experiments.

A.1.1.4. Triaxial experiments-radial flow

There are three series of triaxial experiments: the first series tests under room temperature, the second tests under room temperature and the third series tests at high temperature. The apparatus of the second series tests is modified based on the first one and the same with the third one. In this study, just the first series tests are introduced. Volckaert et al. (1995) have provided more details on the second and third series tests.

The first series of experiments under room temperature were conducted by using specially designed apparatus which could control the gas pressure and temperature. The triaxial apparatus is shown in Figure A.7. In the first stage of the experiment, it should achieve a selected tensional state. When the output gas chamber is filled with water and a back pressure is applied for several days, the specimen is consolidated. When the specimen is recorded by a linear vertical transducer, it should increase the vertical load to prevent swelling. And then the consolidation can be monitored. In the second stage, a low pressure (about 10 to 15kPa) will be supplied to the two gas

chambers. The gas migrates from the input chamber to the hollow needle by opening the valve. Then the gas can contact the soil. During this stage, the stability of the system is maintained by a time lag. The second stage will be maintained for many hours. The gas pressure is increased 50 kPa each step when no gas flow is recorded until a gas flow is generated.

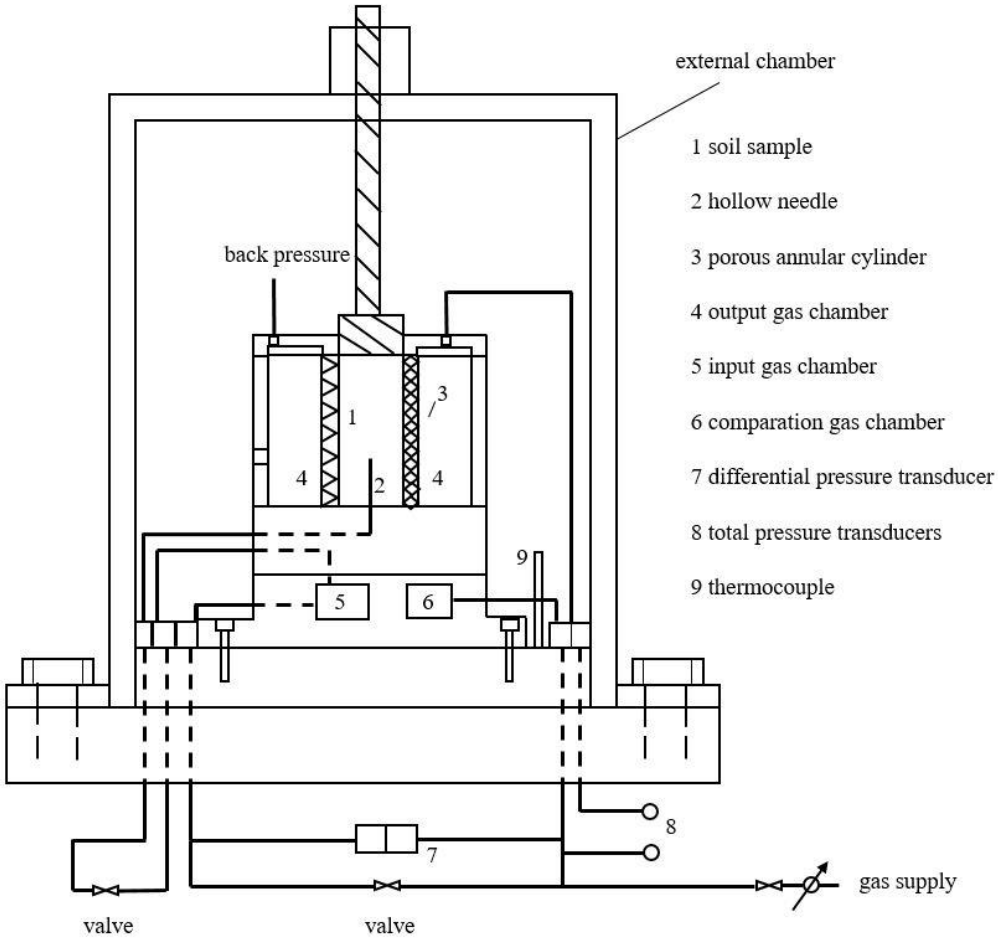

Figure A.7 Triaxial test apparatus (Volckaert et al., 1995)

From the first series of the experiments, the main observation can be summarized as:

- It is a postulation that the breakthrough happened when: P_{gas}(gas pressure) $> \sigma_v'$ (prefixed vertical stress).
- Two small channels were observed at the end of the experiments. They were from the needle tip toward external surface.

- For all experiments, no dispersion of gas through the soil took place.
- The rate of gas pressure decay on the soil specimen is proportional to the applied gas pressure and vertical effective stress. (Volckaert et al., 1995)

A.1.1.5. Other laboratory experiments

There are many other researchers who have conducted laboratory experiments to study gas migration. Key laboratory experiments are briefly discussed below.

- **Gas migration test by Gallé (2000)**

Gallé (2000) proposed a controlled gas migration experiments with $Fo - Ca$ clay as a possible candidate for the disposal clay-engineered barrier in France. The gas migration and permeability were determined by using an oedometer-type vessel that was developed by Tanai and Gallé (1998) as shown in Figure A.8. Gallé (2000) used several different dry densities (1.6, 1.7, 1.8 and $1.9 g/cm^3$) of compacted clay specimens for the degrees of water saturation from 70% to 100%. During the gas injection tests, without any water backpressure and mechanical stress, gas pressure was applied to one end of the clay specimen by incremental steps. During every gas injection step, the gas pressure was maintained until the flow is steady. Then, the gas outflow rates was measured. Gallé (2000) suggested that the gas issue cannot be underestimated for the long-term engineered clay barrier stability. .

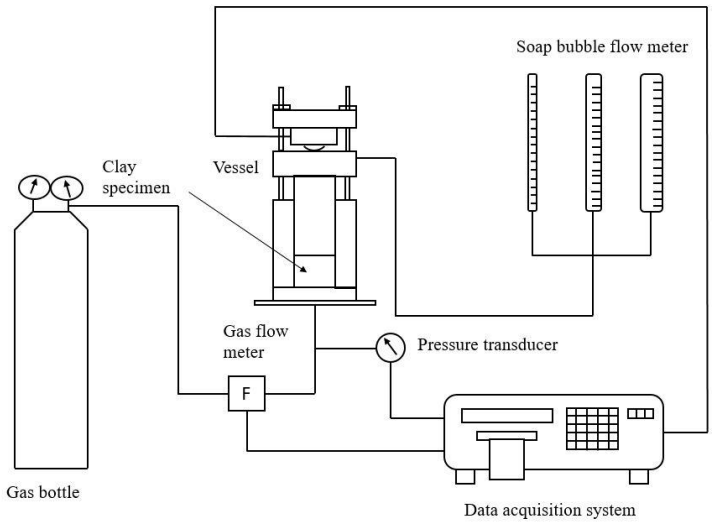

Figure A.8 Schematic of the experimental gas migration testing system (Tanai et al. 1998)

- **Modified Hassler cell by Jockwer (2006)**

Jockwer (2006) introduced the Constant-Pressure-Desaturation method and modified Hassler cell. The Constant-Pressure-Desaturation method is used to determine the two-phase flow parameters. First, the nitrogen gas flow through the dry sample at a defined constant injection pressure was measured. Second, the sample was removed and then saturated with water. Finally, the single-phase flow of water through the sample as a defined constant injection pressure was measured. The injection pressure of the non-wetting phase was increased stepwise to determine the gas flow at lower saturation levels of the wetting phase. The effective permeability is calculated with the Darcy equation for every saturation level. The modified Hassler cell was used to determine the two-phase flow variables at different water saturation. The cylindrical samples with 50mm diameter and 100 mm length were installed in the uniaxial cells. The compaction pressures were up to 100 MPa. The isostatic confining pressure was between 0 and 2.5 MPa. The maximum gas and water injection pressure was below 75% of the confining pressure. The results show that the single-phase water permeabilities of the samples depend on the clay content. Permeabilities are between $5.3 \cdot 10^{-15}$ and $2.9 \cdot 10^{-16} m^2$ with 10% clay, between $1.2 \cdot 10^{-16} m^2$ and $7.7 \cdot 10^{-18} m^2$ with 25% clay (Jockwer, 2006). For the two-phase flow, the gas breakthrough pressure is about 0.03 MPa for the initial water-saturated samples with 10% clay. 20% of the water in the pore volume at this pressure, and the pressure increases up to 0.05 MPa with the 20% saturation. When the pressure increases further, the pore water is just added 5 to 10%. It means that the residual water saturation is of 10 to 20% (Jockwer, 2006). It is shown from the results that the van Genuchten (van Genuchten, 1980) approach is most suitable to describe the relative-permeability-saturation relationship (RPS) and the capillary-pressure-saturation relationship (CPS) of clay-sand mixtures (Jockwer et al. 2000). The relative gas permeability and the capillary pressure can be expressed by the following equations:

$$k_{rg} = (1 - S_e)^r \cdot \left(1 - S_e^{\frac{1}{m}}\right)^{2m} \quad with\ S_e = \frac{S_w - S_{wr}}{1 - S_{wr} - S_{gr}} \tag{A.10}$$

$$P_c = \frac{1}{\alpha} \cdot \left(S_e^{\frac{1}{m}} - 1 \right)^{\frac{1}{n}} \quad with\, m = 1 - \frac{1}{n} \tag{A.11}$$

where: S_w: water saturation

S_{wr}: residual water saturation

S_{gr}: residual gas saturation

S_e: effective water saturation

K_{rg} and P_c: relative gas permeability and capillary pressure respectively

since α is known as constants, the two parameters m (or n) and γ can be then derived from the data.

Arnedo et al. (2008) conducted a series of dipole tests to investigate gas flow through clay barriers in the cylindrical samples shown in Figure A.9. During the tests, the test specimen is confined volumetrically. The preferential paths were formed by using needles. After testing, the samples revealed that discontinuities followed the compaction layers. It could have some influence during the gas flow. Arnedo et al. (2008) observed a large-scale breakthrough pressure when a marked pressure peak was recorded in the upstream vessel.

- **Permeability tests on the argillite by Davy et al. (2007)**

Davy et al. (2007) performed a time-consuming experimental program that lasted six months. This test mainly focused on studying the coupled effects of mechanical and chemo-hydraulic loading on gas and water permeability of cracked argillite located in the EDZ. As a potential host for the radioactive waste repository, many European countries (e.g. Belgium, France, Switzerland, and the UK) are now studying argillite formations. Davy et al. (2007) conducted two tests, steady state gas flow test and transient water flow test, on pre-cracked argillite samples which were drilled from the French Meuse / Haute Marne URL, Bure site with different depths in the argillite layers. Table A-4 shows the permeability tests on the argillite samples and their main characteristics about petro-physical aspect.

Table A-4 Permeability tests on the argillite samples and their main characteristics about petro-physical aspect from ANDRA (Davy et al. 2007)

Plug no.	EST5600	MSE761	MSE748
Borehole no.	EST205	MSE101	MSE101
Extraction date	16/09/2000	-	14/01/1995
Upper extraction depth (m)	467.47	567.72	564.5
Lower extraction depth (m)	467.77	568.02	564.80
Cored sample quantity	2	4	2
Permeability test type	Steady state gas flow	Steady state gas flow (1 test) and transient water flow (3 tests)	Transient water flow
Density	2.43	2.31	2.35
Water content (%)	7.4	8.3	7.3
Sonic celerity V_p (m/s)	3170	3146	3170
CaCO_3(%)	24.0	19.4	25.2

From the experimental observations, Davy et al. (2007) summarized the conclusions as follows:

(1) According to the results of gas flow tests, the upon crack closure (cc) with the values during $10^{-13} - 10^{-16} m^2$ mainly decided permeability *K*.

(2) From the from transient water flow tests, permeability varies with test between $10^{-18} - 10^{-21} m^2$.

(3) Based on the two types of the tests results, permeability is also affected by the confining pressure (P_c) especially during the first three loading-unloading phases.

(4) Swelling causes more closure and additional pressure in the crack area while it will not conduce to unloading in the crack zone.

(5) A very close connection exists between H_2O and the crack closure amplitude and permeability.

(6) The physico-chemical phenomena have extremely rapid kinetics to control the macro-crack self-sealing.

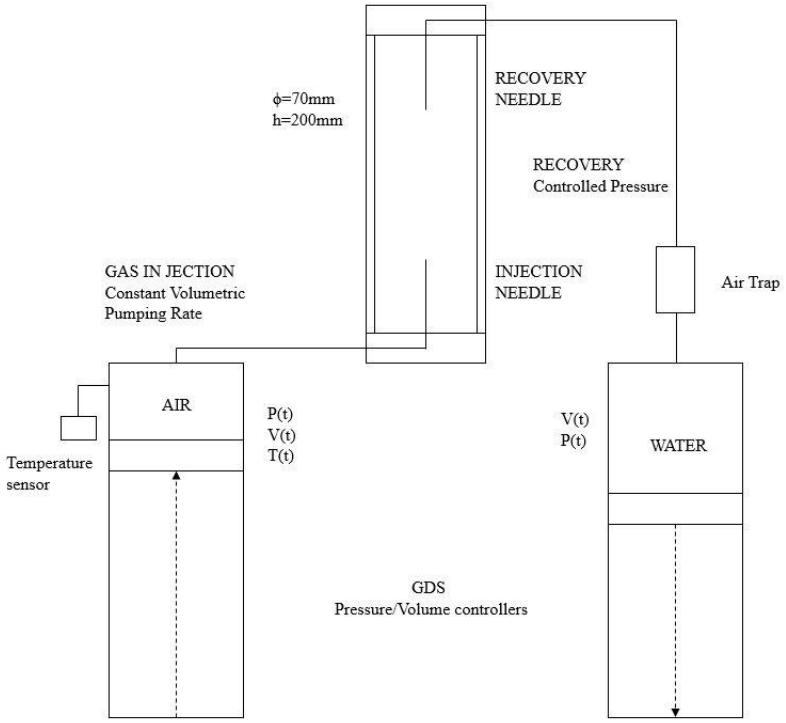

Figure A.9 Gas injection in soil samples using needles Schematic experimental setup (Arnedo et al., 2008)

- **Gas migration tests on cylindrical samples by Horseman and Hrrington (1997, 1999)**

Horseman and Harrington (1997, 1999) performed seven gas migration tests on cylindrical samples of saturated compacted MX-80 bentonite, applying different values of isotropic confining stress and 1 MPa water backpressure. Figure A.10 shows the experimental findings of one sample of test results on specimen MX80-4A (HS). Horseman et al. (1999) got several observations from the experimental research.

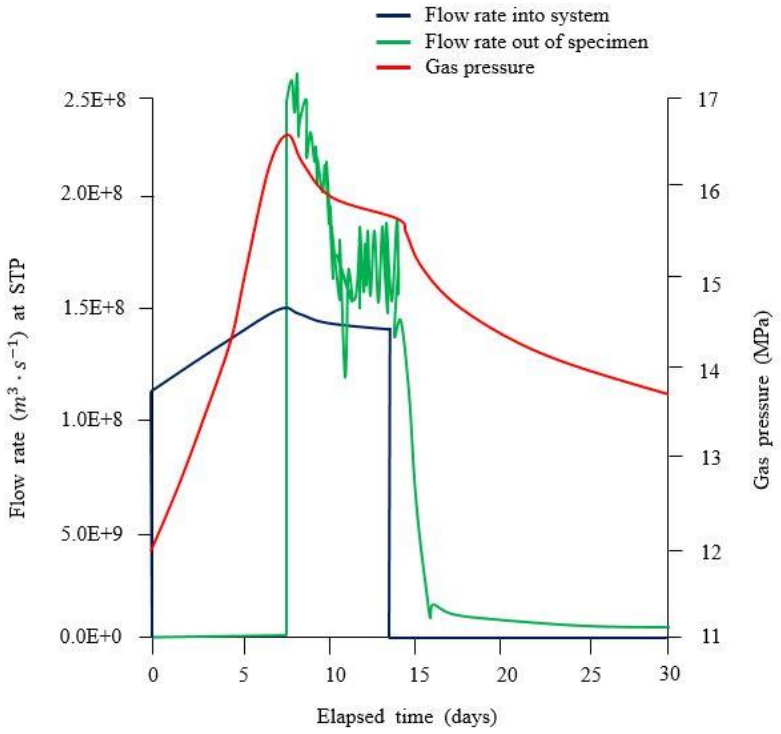

Figure A.10 Test MX80-4A during the first injection and shut-in stage the development of flow rate into system, injection pressure and outgoing flux (Horseman and Harrington, 1999)

- **Two tests of gas flow in Callovo-Oxfordian clatstone**

In order to investigate which kind of mechanism(s) control the advecive gas flow, British Geological Survey (BGS, UK) and LAEGO-ENSG-Université de Lorraine (Nancy, France) carried out two kinds of experiments on Callovo-Oxfordian claystone (CO_X) (Cuss et al., 2014). These two experiments will be introduced as follow

(1) The experiment at BGS

The original aims of the test are to investigate the influences of the changing effective stress; to determine the volumetric deformation at the beginning of the gas flow and to differentiate the different flow mechamisms (Cuss et al., 2012). Figure A.11 shows the apparatus of stress-path permeameter (SPP) used in the experiment. The SPP was bespoke to solve the very small volumetric strains including axial and radial deformation possibly caused by the onset of gas flow. Figure A.12 shows the schematic of the SPP.

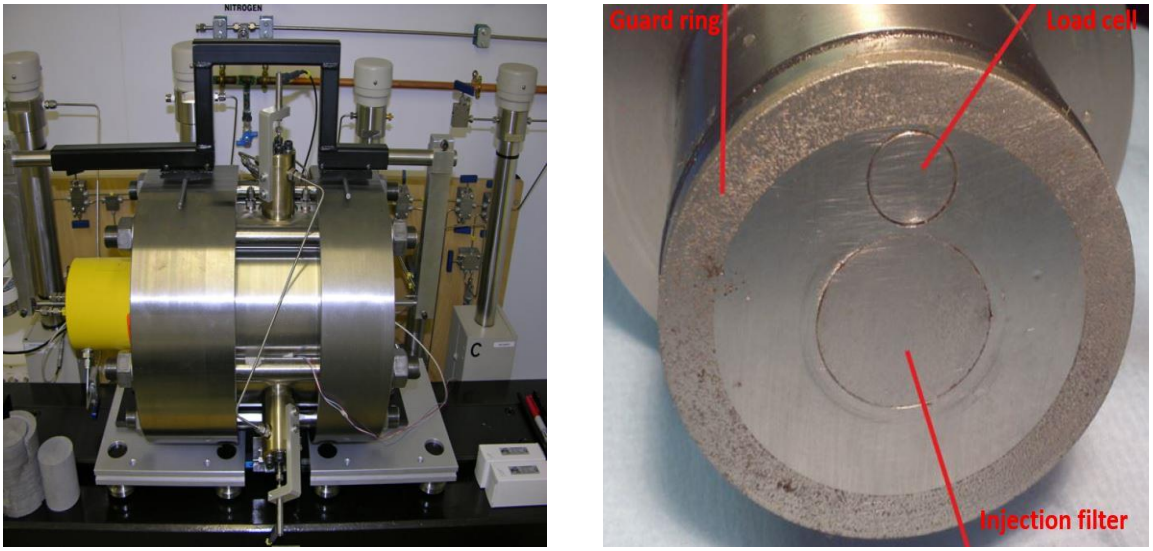

(A) (B)

Figure A.11 (A) traxial SPP apparatus; (B) the injection filter and guard-ring arrangement of the end platen (Cuss et al., 2012)

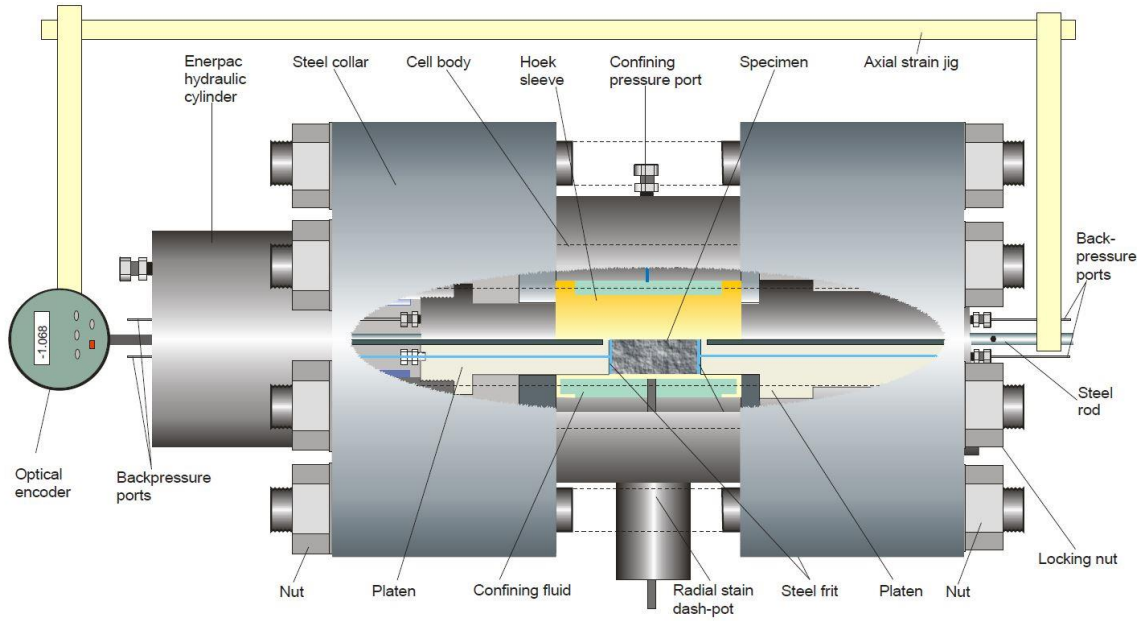

Figure A.12 Schematic of the Stress-path Permeameter (SPP) (Cuss et al., 2012)

There are 6 main components of the SPP (Cuss et al., 2012):

1) An improved flexible Hoek sleeve with a main pressure vessel body was used to fix the specimen (Figure A.13).

2) Three dash pots (Figure A.14) were used to measure the radial strain of the sample directly. They were installed along with the radial mid-plane of the sample. There were also two functions of the pressure balanced dash pots that to buffer the force forced upon the sample and to protect the push-rods from pushing out of the pressure vessel.

3) An Enerpac single acting hydraulic ram which was the main part of the axial load system was pressurised by an ISCO-500 series D syringe pump.

4) A confining pressure system could calculate the radial strain measurements by using the volume change. It was composed by an ISCO-500 series D syringe puma and the glycerol confining medium.

5) A pore-pressure system can produce the monitor back-pressure and pore fluid pressure. It contained two ISCO-100 series D syringe pumps.

6) A most advanced custom data acquisition system. It could realize the remote monitoring and control of all experimental parameters conveniently.

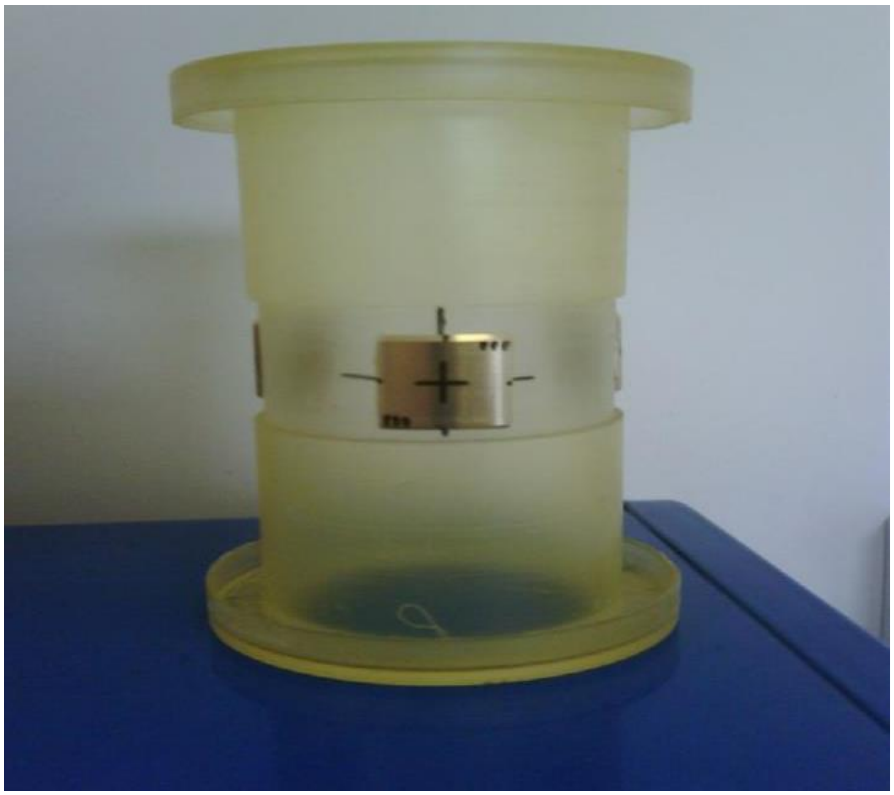

Figure A.13 Modified Hoek sleve with brass additions (Cuss et al., 2012)

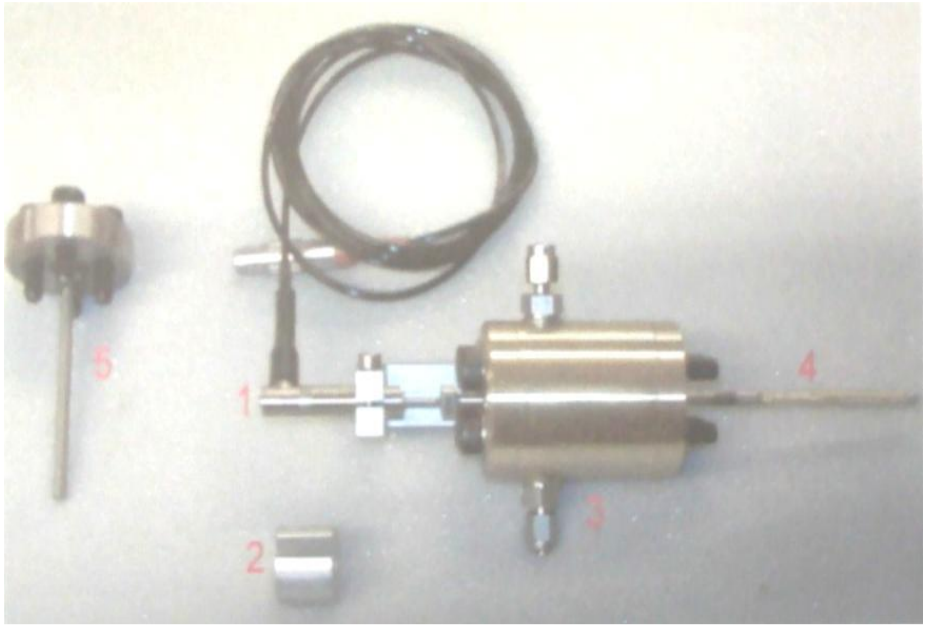

Figure A.14 the pressure balanced dash-pot system (Cuss et al., 2012)

The experiment sample was cylindrical with 56mm diameter and 82mm length. It was fixed axially by the Enerpac hydraulic ram driven by the ISCO syringe pump and loaded 13 Mpa in the axial direction. By using the pore-pressure system, the back-pressure was maintained as constant of 4.5 MPa. A number of pressure sensors, thermocouples and a digital acquisition systems composed the experimental rig which logged data every 2 min (Cuss et al., 2014).

There was one uncertainty during the transport testing. The short-circuiting of the flow system would happen along the jacket of the test sample. Figure A.13 shows the porous stainless-steel annular filter around the outer edge of each platen with a 6 mm wide and 2 mm deep. It could monitor the pore-water pressure and reduce the needless sidewall flow. The whole guard-ring system contained filter, pipework and pressure sensor were saturated with water and flushed. It could eliminate gas from the system. The guard-rings connected to a pressure transducer could assist in hydration with connecting to the injection system and also could provide an independent measure of pore-pressure independently by the control of the control board. The inlet and outlet filters were made up by a porous disc with 20mm in diameter and 2 mm in depth. The guard-rings gave the injection pressure, injection guard-ring pressure, back-pressure, and back guard-ring pressure by monitoring four different points on the sample which could guarantee the data on the hydraulic anisotropy (Cuss et al., 2012).

Helium was used as the test gas during this experiment. The sample was 82.45 mm length and 96% initial saturation. The saturation would become to 100% at the early stages of the test by design. Table A-5 shows the initial geotechnical properties. When the whole test programme finished, the saturation of the sample was nearly 100% (Cuss et al., 2014). The test SPP_Cox-2 (gas flow test) lasted a 566 days totally. In this research, it describes the results from the first 320 days up to the situation achieved at near-steady-state gas flow. Table A-6 show the test boundary conditions at different stage (Cuss et al., 2014).

Table A-5 COx material properties and experimental boundary conditions (Cuss et al., 2014)

		Triaxial geometry BGS	**Triaxial geometry LAEGO**	**Units**
Sample properties	Sample reference	SPP_Cox-2	EST28906-6	
	Location	Bure URL, France	Bure URL, France	
	Borehole/drill core	OHZ1201/EST30341	EST28906	
	Core direction	Parallel to bedding	Normal to bedding	
	Average length	82.45±0.03	76.69	mm
	Average diameter/width	55.85±0.04	37.89	mm
	Volume	2.020×10^{-4}	8.647×10^{-5}	m^3
	Average weight	495.02	203.22	g
	Density	2.451	2.35	g cc^{-1}
	Grain density	2.7	2.71	g cc^{-1}
	Moisture weight	28.7	11.95	g
	Moisture content	6.2	6.3	%
	Dry weight	466	191.27	g
	Dry density	2.31	2.21	g cc^{-1}
	Void ratio	0.174		
	Porosity	14.8	18.5	%
	Degree of satuation	96	85	%
Experimental	Confining pressure	12.5	12	MPa
boundary conditions	Axial load	13	12	MPa
	Pore pressure	4.5-10.5	4/6	MPa
	Back pressure	4.5	3.5	MPa
	Pore fluid chemistry	Chemically balanced pore fluid		

Table A-6 Experimental history of test boundary conditions (Cuss et al., 2014)

Stage number	**Description**	**Axial stress (MPa)**	**Confining stress (MPa)**	**Injection pore pressure (MPa)**	**Test time at start (days)**	**Length of stage (days)**
1	Saturation and swelling	12.5	11.5	4.5	0.1	21.7
2	Equilibration	13.0	12.5	4.5	21.8	26.1
3a	Hydraulic testing	13.0	12.5	8.5	47.9	50.1
3b	Hydraulic testing	13.0	12.5	4.5	98.0	29
4a	Gas injection ramp (constant flow)	13.0	12.5	4.5-9.5	127.0	35.3
4b	Gas injection at constant pressure	13.0	12.5	9.5	162.3	25.5
4c	Gas injection ramp (constant flow)	13.0	12.5	9.5-10	187.8	22.2
4d	Gas injection at constant pressure	13.0	12.5	10	210.0	26.1
4e	Gas injection ramp (constant flow)	13.0	12.5	10-10.5	236.1	18.9
4f	Gas injection at constant pressure	13.0	12.5	10.5	255.0	320.0

At the begining of the test, the loaded stress condition was similar to the *in-situ* conditions at Bure with confining pressure of 12.5 MPa, axial stress of 13 MPa and pore pressure of 4.5 MPa. The test aim of the first stage was to make sure that the sample was in a resaturated situation. The chemically balanced water as the test water to minimize the swelling caused by chemically was injected at the top and bottom of the sample. The following test was the constant head hydraulic test, which would realize all the gas discharged from the sample, and also could get the baseline of the hydraulic propertied like the permeability and specific storage. This two tests took 47 days and 79 days separately (Cuss et al., 2012).

The third part was the gas injection test started on day 131. The Figure A.15(a) shows the test results. It can be seen that in a period of 35 days the gas pressure was from 4.5 increased to 9.5 MPa. There was no flow since the gas pressure kept as constant for 22 days. After that, on day 187 a low flow was initiated by the injection pump until the gas injection pressure raised to 10 MPa. Then with the constant pressure for 26 days, it was no evidence of gas flow. The final period started on day 236 lasted 19 days. The gas injection pressure raised to 10.5 MPa (Cuss et al., 2014).

.

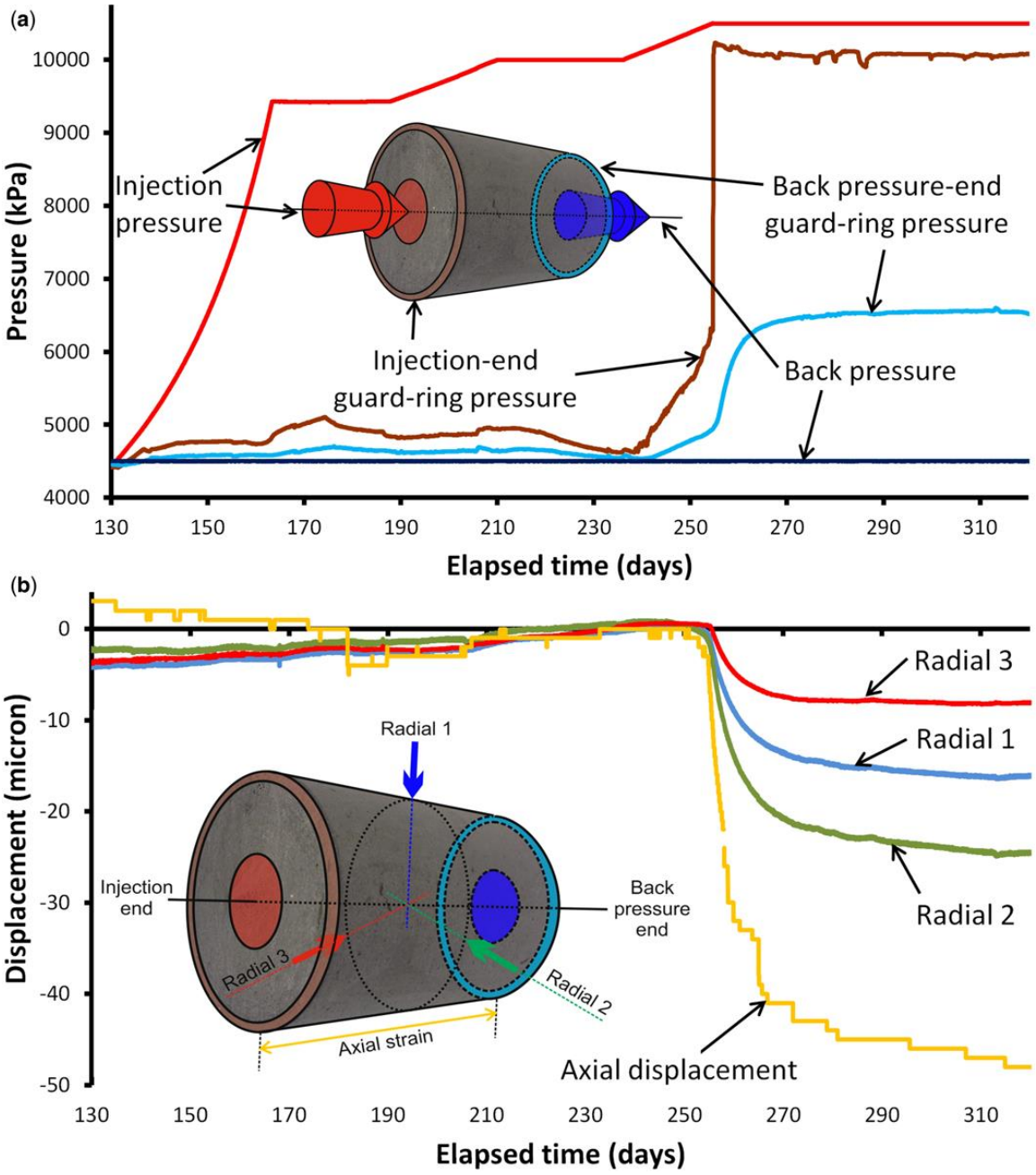

Figure A.15 the BGS test results: (a) the four points within the experimental setup pressure record; (b) four locations on the sample deformation record with obviously dilation. (Cuss et al., 2014).

The first gas entry happened on day 220. There was a significant deflection of the load cell at day 221.875. During this constant-pressure stage, no gas migration occurred. The load cell reading shown a second response at day 237.32. Figure A.15(a) shows the starting of water pressure

increase in the guard ring one day after the first response. Figure A.15(b) shows one day after the increase, the first deformation happened at the mid-plane. And then the water pressure increased in the backpressure guard ring. A hydromechanical response to the start of gas migration and the driven of water from the injection guard ring cause of the geometry of the test apparatus could be explained the main reasons of these phenomena and changes. Around day 255, there was an accelerated dilation at the mid-plane by the gas migration shown in Figure A.15(b) and Figure A.16(b). This phenomenon could not be explained only by the mechanical response of a change in effective stress. Around day 273, gas arrived at the backpressure guard ring. There was a total of 48 μm length and an average radial dilation of c. 16μm occurred after the start of gas flow. It was equal to a total volumetric strain of 0.18%, or a 360μl change in volume of the sample. In the last gas tests, the phenomenon that the gas flow was accompanied by dilation of the COx was identified by the same functional form of radial strain trace and the gas outflow from the sample. (Cuss et al., 2014)

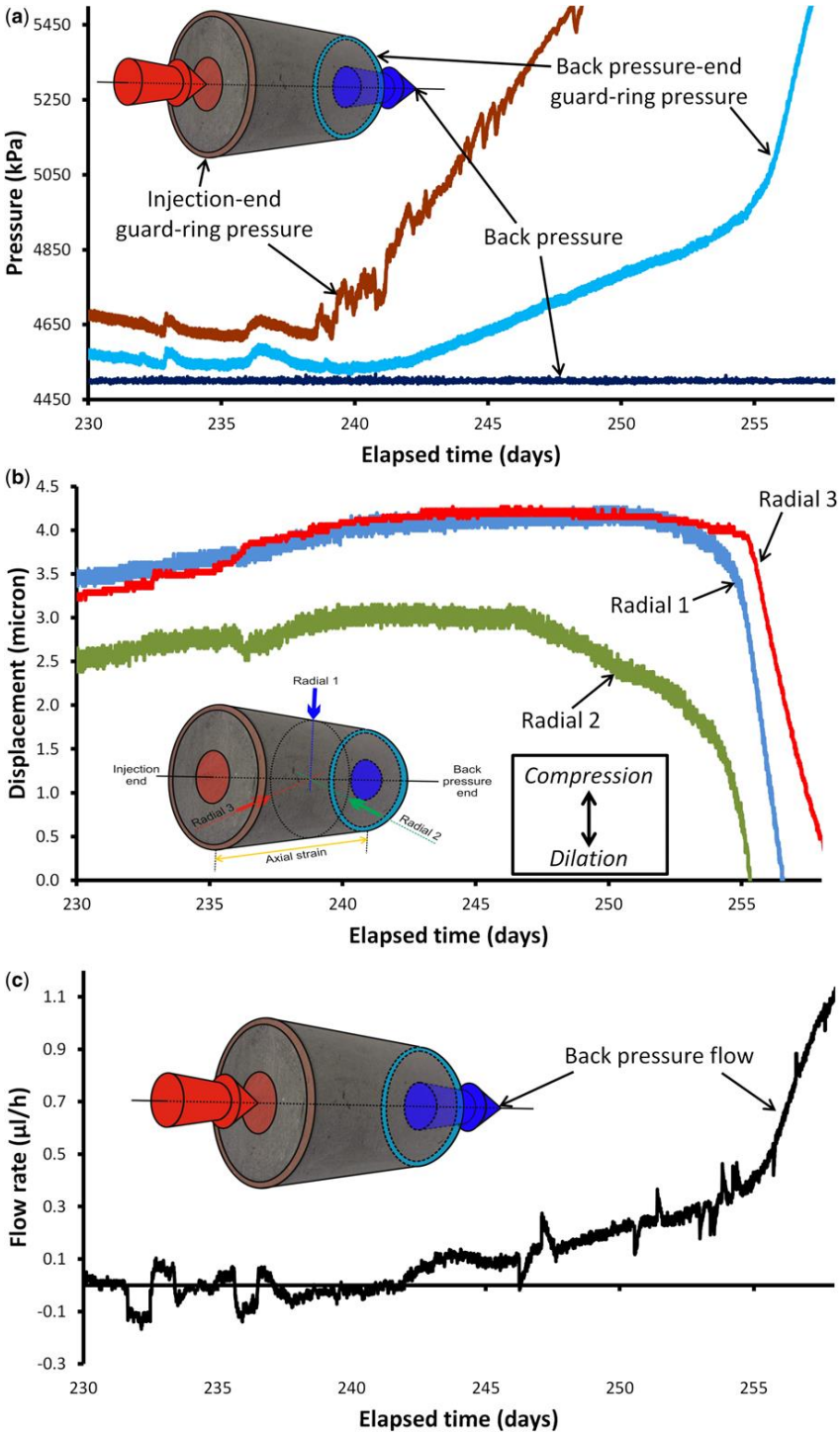

Figure A.16 the data at the beginning of the gas flow: (a) pressure response; (b) deformation; (c) outflow from the sample (Cuss et al., 2014)

(2) The experiment at LAEGO-ENSG-Université de Lorriaine (Nancy)

In order to give rise to dilatancy-controlled gas flow and to gas transport in tensile fractures, a laboratory experiment was carried out at LAEGO-ENSG-Université de Lorriaine (Nancy). The method used at LAEGO is that the strain gauges cemented directly to the sample surface to give axial and lateral strains. Figure A.17 shows the experimental apparatus. The apparatus contains a triaxial load cell, two fluid circuits (one for water and one for gas). The two pressure sensors for measuring the evaluated gas and water pressured installed on both circuits were used throughout the entire test. There were two specific flow meters with different precisions of $10^{-3} gh^{-1}$ and $10^{-4} l\ min^{-1}$ for gas and water. Strain gauges were fixed directly on the sample to measure rge axial and lateral deformations continuously. The confining pressure and the pore (during saturation phase) pressures were produced through ISCO syringe pumps. There still had a third ISCO syringe pump coupled with an oil-to-gas exchange for the gas pressure production located between the pump and the cell. The diameter and height of the sample were 37.89 mm and 76.69 mm separately. The axis was oriented normal to the bedding plane. Table A-5 shows the geotechnical properties (Cuss et al., 2014). The whole procedure of the test contains three steps as following:

1）Sample saturation. This period usually took two to three months. The sample was saturated under the 12 MPa hydrostatic stress with a difference of 0.5 MPa between injected upstream and downstream pressures. During this step, the axial and transversal strains were monitored by the strains gauges.

2）Gas pressure increased. An increased gas injection pressure (4MPa, 6MPa and 8MPa) was applied upstream to the sample. The strains and out gas flow rate were monitored.

3）Rupture induced a deviatoric stress can be applied to induce rupture under the condition that both the metrology and the sample could support.

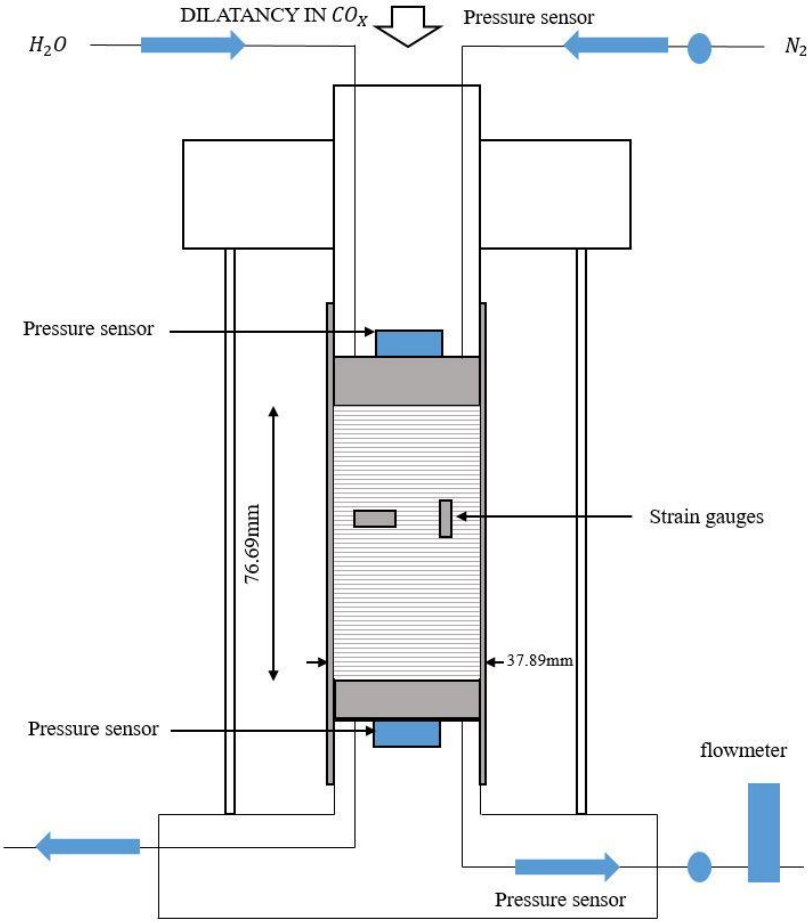

Figure A.17 Schematic of the experimental setup at LAEGO (Cuss et al., 2014)

The experimental observation at LAEGO–ENSG–Université de Lorraine (Nancy):

The whole procedure of the test shows in Figure A.18(a). The sample of CO_x was fully saturated under an isotropic stress of 12 MPa after four months. The initial gas pressure was 4 MPa applied on the sample for 24 days. After ten days, the pressure downstream decreased and then stabilized, with the stabilization of the axial strain four days later (Figure A.18(b)). On day 25, the downstream pressure had a sudden increase to 4.2 MPa since the gas pressure was increased to 6MPa. After that, the downstream pressure decreased steadily. Correspondingly, the axial and lateral strains increased rapidly until day 38. On day 42, the axial strain showed a sharp increase with the sudden decrease of the injection pressure and downstream pressure. It means that the micro-cracks have been generated. The LAEGO experiment clearly shows the gas flow occurred

by dilatant pathway formation.

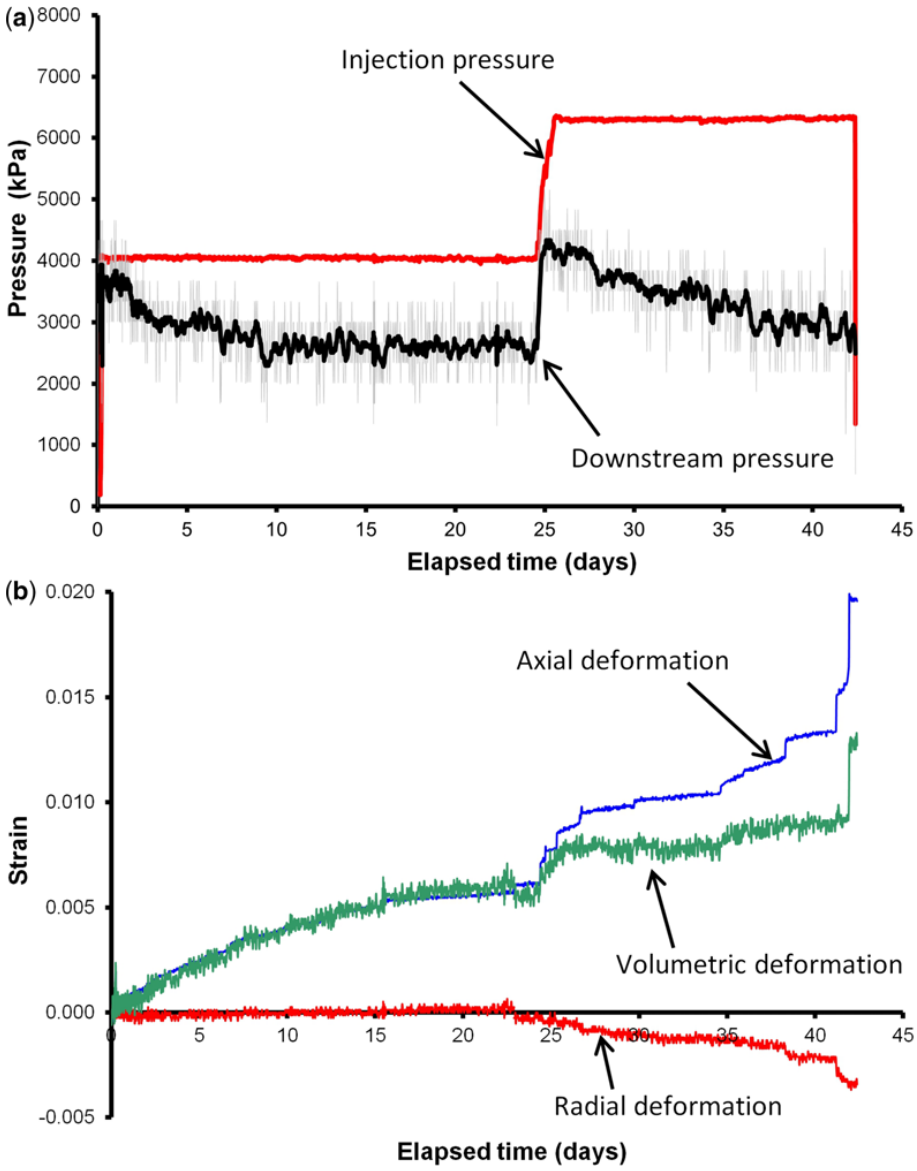

Figure A.18 Test results from the LAEGO test: (a) gas pressure and downstream pressure of the sample; (b) deformation of the sample (Cuss et al., 2014).

- **The gas injection tests conducted by Popp et al. (2007)**

In order to investigate the pressure dependence of the permeability at different pressure clamps with the injection gas pressure, Popp et al. (2007) carried out the injection tests on the Oplinus

clay samples as short-term tests up to several hours under the quasi hydrostatic pressure conditions between 2 and 10 MPa. Table A-7 shows the parameters of the sample.

Table A-7 The Oplinus clay sample parameters for the injection tests (Popp et al., 2007)

Probe	**Height h (mm)**	**Diameter d (mm)**	**Density ρ (g/cm^2)**	**Direction of injection based on the foliation**
307/OPA1	181.58	90.32	2439	0°
307/OPA 2	180.81	90.17	2442	0°
307/OPA 4	160.14	80.08	2450	0°
307/OPA Kon 1	150.45	73.59	2366	90°
307/OPA 11	140.99	80.16	2438	90°

To determine the gas transport properties with increasing gas pressure, the gas pressure is gradually increased in the standard test with constant confining pressure and the permeability is calculated by monitored the gas out flow rate. Figure A.19 shows the results of the multi-phase gas injection test on Oplinus clay. In Figure A.16 (a), the injection pressure started from 1 MPa and the permeability was comparatively high as approximately$10^{-17}m^2$. The gas injection pressure was increased from 1 bar to approximately 9.5 bar. During the gas injection pressure increasing period, the permeability remained almost constant. With a longer holding time with constant injection pressure, there were some fluctuations of the gas flow rate, which indicate the discontinuous gas transport. As the confining pressure increased, the permeability decreased progressively with a significant time-dependent compaction effect (Popp et al., 2007).

In Figure A.19(b), the second gas injection cycle, with a constant confining pressure 3 MPa as shown, the gas penetration behavior differed from the first cycle with a now lower permeability sample since the previously time and load-dependent compaction. Starting from a quasi intrinsic permeability value$< 3 \cdot 10^{-20}m^2$, the permeability initially increased gradually until a plateau with k $\approx 3 \cdot 10^{-19}m^2$ when the gas injection pressure$\geq$ 2.5MPa. It means that the gas injection pressure was lower than the constant confining pressure, the permeability was only slightly dependent on the gas pressure (Popp et al. 2007). There still have other experiments (e.g. gas transport properties of red salt clay; time-dependent permeability development of oplinus clay-

sealing experiments) in Popp et al. (2007) to compare each other with regard to the important hydraulic and petrophysical parameters.

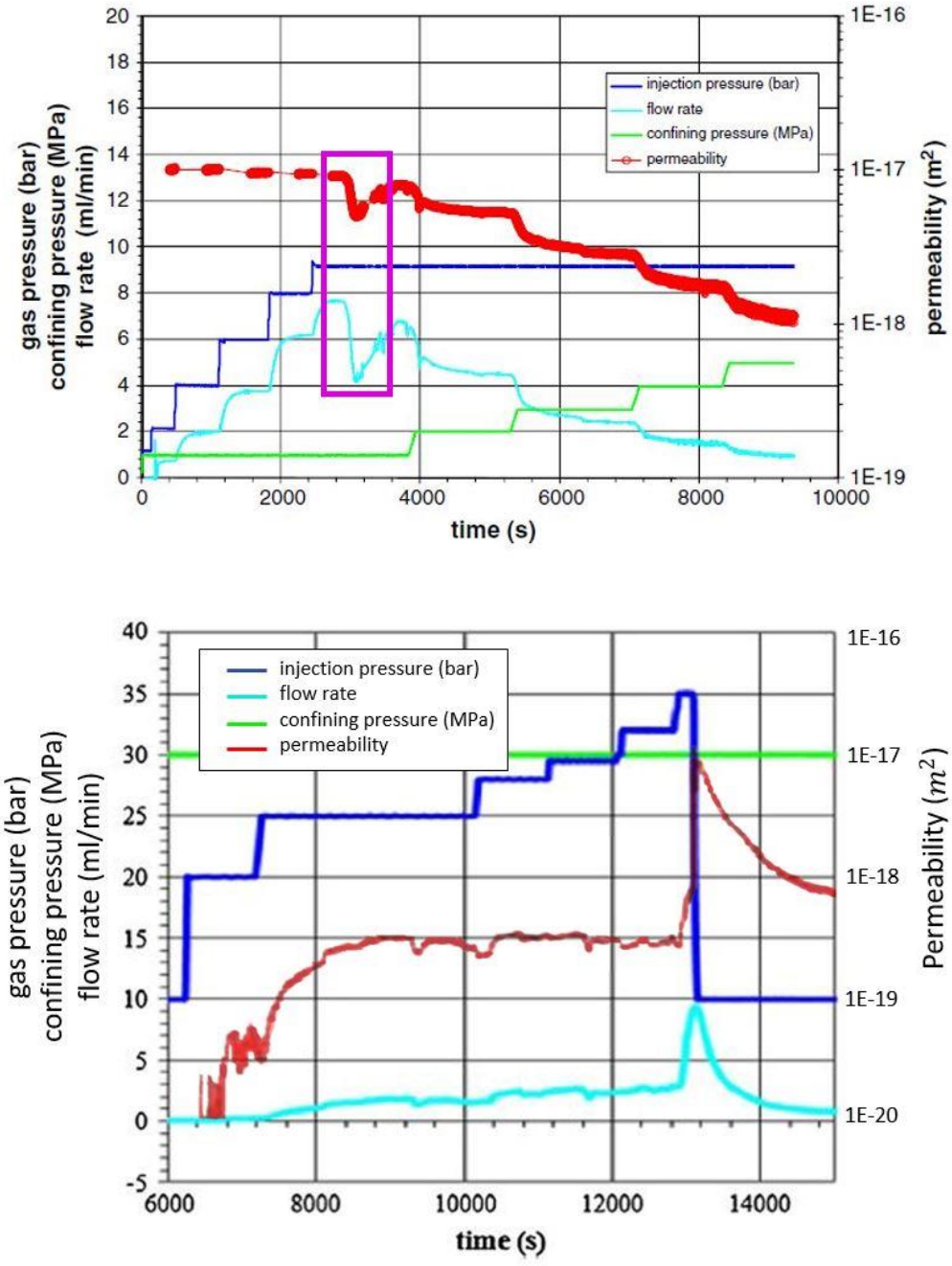

Figure A.19 Gas injection tests to determine the gas transport properties of Oplinus Clay: (a) gas injection pressure changed with time and evaluative confining pressure; (b) gas injection pressure changed with time and constant confining pressure (Popp, 2007).

These laboratory experiments, in underground repository media, indicate that gas migration in mainly controlled by the coupling of hydro-chemical-mechanical processes as also discussed in Fall and Nasir (2012). However, most of the tests were conducted at room temperature, which means that the thermal influences were usually ignored. In deep rock formations of nuclear waste repository, the thermal effect may have significant influence on the gas transport.

A.2. *In-situ* experiments

The investigations of gas migration in host rocks have been conducted in many European countries (e.g. Belgium, France, Italy, Sweden, Switzerland and the UK). In most of these countries, they choose argillaceous rocks as the potential host rock for the disposal radioactive waste repositories: Opalinus Clay in Switzerland, Boom clay in Belgium and Callovo-Oxfordian clay in France (Fall and Nasir, 2012). At Mont Terri Underground Laboratory, the projects "Heater experiment, study of the thermo-hydro-mechanical behavior of the host rock (HE-D)" and "Sealing of boreholes, repository rooms and galleries (SB)" are carried out. The experiments were running in the Opalinus Clay (Jockwer, 2003). There also are some other the *in-situ* tests performed elsewhere, such as the "Full Scale Engineered Barriers Experiment (FEBEX)" conducted in Granite and the "Two phase Flow Experiment in Fractured Rock" (Jockwer, 2003).

Su (2007) summarized the main characteristics of the Boom clay and Callovo-Oxfordian argillites and Opalinus Clay formation as follows:

- **Boom clay**: Boom clay is a kind of marine fine-grained sediment. It formed from about 30 million years ago (Rupelian Age). Because of the grain sizes, organic matters and carbonates, Boom clay has its own way of layering. The distribution of the grain size shows a wide variation. Clay fraction ($<2\ \mu m$) is during 30-70% (average 55%). The majority clay minerals are: illite (50%), smectite and illite-smectite interstratifications (30%), kaolinite (10%) and chlorite (5%), degraded chlorite and illite-chlorite interlayers, and glauconite (3%) (Fall and Nasir, 2012). Usually, Boom clay is considered homogeneous. Table A-8 shows the basic geomechanical characteristics of Boom clay located at the Mol Underground Laboratory.

Table A-8 Boom clay geomechanical characteristics in the Mol Site, Belgium (Su 2007)

Initial total stress	4.5 MPa	Porosity n	0.39
Initial pore pressure	2.25Mpa	Water bulk modulus K_w	0.2-2GPa
Young's modulus E'	300Mpa	Hydraulic conductivity k	$2\times10^{-12} m/s - 4\times10^{-12} m/s$
Poisson's coefficient v^h	0.125	Plastic limit	23-29%
Cohesion c'	300kPa	Liquid limit	55-80%
Friction angle Φ	18°	Plasticity index	32-51%
Uniaxial compressive effective strength Rc	2MPa	Water content	22-27%

- **Callovo-Oxfordian argillites**: as marine sediments, Callovo-Oxfordian was formed from 150 million years ago (Jurassic age). The components of the argillites are:

Clay minerals: 40-45% (lower part illite, regular mixed layer R1 illite smectite, chlorite and kaolinite; upper part: irregular mixed layer R0 illite-smectite)

Carbonate: 20-30%

Quartz slits: 20-30%.

Callovo-Oxfordian argillites are a saturated porous medium with very low permeability from the decrease of the interstitial or the connected pore space which resulted from the coupled effect of sedimentation, compaction and diagenesis. It can be subdivided into three rheological zones from a geomechanical viewpoint: two stiff zones which surround a central and less stiff zone. The basic mechanical characteristics of the Callovo-Oxfordian formation at a depth during 420 to 550m are given in Table A-9.

-**Opalinus Clay**: usually dark grey, silty, calcareous and micaceous clay stones are the main components of Opalinus Clay. It was found to be anisotropic of the mechanical properties and isotropic in transverse. The observation shows that the elastic properties and strength parameters depend on the water content. Table A-10 describes the geomechanical characteristics of Opalinus Clay in Zürcher Weinland (depth of 600m).

Table A-9 Basic mechanical characteristics of the different geological zones in the Callovo-Oxfordian formation (Andra, 2005)

Characteristics	**Rheological zone**			**Overall**
	Upper	**Median**	**Lower**	
Depth (m)	420-455	455-515	515-550	420-550
Initial total stress	12-16 MPa at -500m			
Initial pore pressure	~5 MPa at -500m			
Density (g/cm^3)	2.42	2.42	2.46	2.40-2.45
Water content (% mass)	6.1	7.1	5.9	5.3-8.0
Porosity (%)	14	15.5	13	11.5-17
Young's modulus (GPa)	6.2	5.5	7.2	6.0
Uniaxial compressive strength (MPa)	30	21	21	24
Uniaxial tensile strength (MPa)				2.6
Hydraulic conductivity (m/s)	10^{-13}-10^{-14}			10^{-13}-10^{-14}

Table A-10 Geomechanical characteristics of Oplinus clay (Volckaert et al. 2004)

Site	**Mont Terri**		**Zuricher Weinland**	
	Matrix	**Bedding**	**Matrix**	**Bedding**
Initial vertical stress	6-7 MPa		15.9 Mpa	
Initial max./min. horizontal stress	2-3 MPa/4-5 MPa		22.6-15.1 MPa	
Initial total mean stress	4-5 MPa		18 MPa	
Initial pore pressure	1-2 MPa		6-7 MPa	
Porosity	0.16		0.12	
Young's modulus	6 GPa	3 GPa	10.5 GPa	5 GPa
Poisson's ratio	0.24	0.24	0.27	0.25
Cohesion	3 MPa	1 MPa	6.9-8.6 MPa	1.5-1.7 MPa
Friction angle	25°	23°	21-25°	20-24°
Uniaxial compressive strength	10-16 MPa	No data	30 MPa	6 MPa

Tensile strength	1 MPa	0.5 MPa	2.7 MPa	1.2 MPa
Hydraulic conductivity	$8 \times 10^{-14}\, m/s$	$2 \times 10^{-13}\, m/s$	$2 \times 10^{-14}\, m/s$	$1 \times 10^{-13}\, m/s$

A.2.1. Full-scale engineered barriers experiment (FEBEX)

ENRESA conducted an experiment for the disposal of high level radioactive waste in granite formations in collaboration with NAGRA and European partners at the Grimsel Test Site (Jockwer, 2003). The test was performed in a new gallery with the length of about 70m and the diameter of 2.30m. Two electrical heaters (0.90m diameter, 4.54m length and 100°C surface temperature) and containers were installed concentric with the gallery. Highly compacted bentonite blocks were used to backfill the residual volume in the test field. A concrete plug with a length of 5m sealed the test field with a length of 15m. Figure A.20 shows the schematic diagram of the test field and the equations for the measurement of gas pressure and the collection of gas samples from the pore volume of the buffer.

In 1996, the test field was installed completed and then the heaters started working in February 1997. Heater 1 was switched off in February 2002, while heater 2 is still heating. For the laboratory observation, the concrete plug and heater 1 were removed. In order to determine the long term performance of the buffer, in 2003, some equipment was installed at heater 2 (Jockwer, 2003). The gas generation and migration are investigated by GRS in the test field and in laboratory.

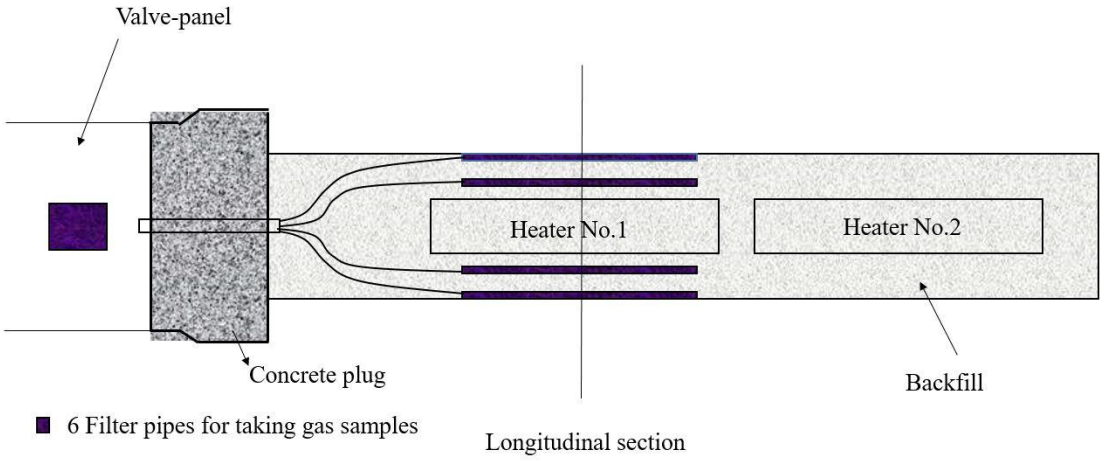

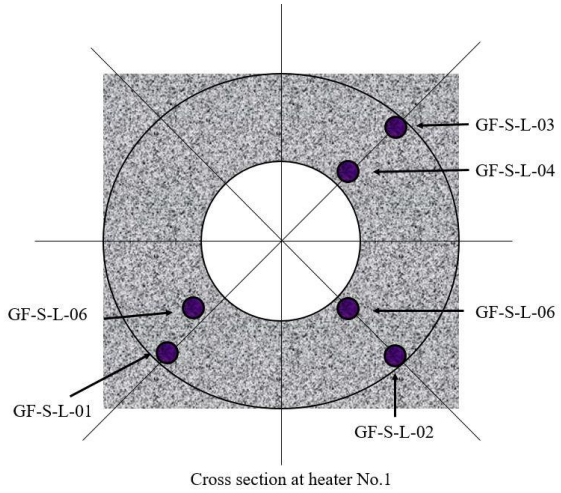

Figure A.20 Schematic diagram of the FEBEX test gallery with the draining pipes for gas sampling (Jockwer, 2003)

The six ceramic draining pipes surrounding the electrical heater in Figure A.20 were used to determine the pore pressure and the gas generation and migration from the buffer material. PFA tubes were operating through the buffer and the concrete plug to a valve panel from both ends of these draining pipes. A data collection system in the PFA tubes could record the gas pressure and take the gas samples for the qualitative and quantitative analyses. Furthermore, the gas injection tests via valve panel and the draining pipes in the non-flooded and in the flooded buffer and the pressure recovery tests in the flooded buffer were conducted for permeability measurements (Jockwer, 2003).

During the whole tests, the observations are as following (Jockwer, 2003):

1) Within the first three years, the formation water of the surrounding host rock made the three draining pipes close to the gallery wall flooded.

2) The water pressure in the host rock was increased up to 0.45 MPa.

3) In the first five years the other three draining pipes did not become flooded.

4) The three draining pipes closed to the heater showed the atmospheric pressure range from 80.4 to 84.2 kPa and a perturbation of 0.5 to 3.0 kPa within one week, which demonstrates that both the concrete plug and the unsaturated bentonite buffer is gastight.

5) In the pipes extracts, the variation of the atmospheric pressure is 0.8 kPa and the gas is exchanged about 1% in the pore volume of the buffer. The gas is rarefied continuously and is replaced at least once a year.

6) For the non-flooded draining pipes, the gas extracted from these pipes shown that the components were carbon monoxide, carbon dioxide, hydrogen, methane, ethane, and propane. It indicated that the gas was released by oxidation, by thermal or microbial decomposition of the organic material within the bentonite buffer and by the corrosion of the metallic components.

The laboratory investigation for the gas generation and migration shows that (Jockwer, 2003):

1) As the result of hydrocarbons oxidation, the concentration of carbon dioxide increased from 0.07 vol% to more than 10 vol%.

2) By the decrease of corrosion and migration through the non-tight concrete plug, the concentration of hydrogen decreased from the beginning of 1 vol% to less than 0.001 vol%

3) By the thermal decompositions of the organic components in the bentonite, the concentration of the hydrocarbons increased from 0.01 vol% to 0.1vol%.

The aforementioned laboratory observations indicate that carbon dioxide is the most important component of the released gas from the bentonite buffer. The amount of carbon dioxide was more than $2m^3$ per 1000 kg of bentonite at the temperature of 100°C. If the closed repository is gastight, an unacceptable high pressure will be generated by this level.

A.2.2. Two phase flow experiment in fractured rock

Äspö Hard Rock Laboratory (Granite) (Sweden) performed a two phase flow test between 1998 and 2000. The experiment was carried in the niche 2715 at the 360m level. In the test, a geological model describing the hydraulic condition for niche 2715 was developed. This model also represented the relevant fracture system and the petrophysical properties of the rock mass. For the single fracture and the surrounding rock mass, the hydraulic pressure, the effective flow parameter values and the gas threshold pressure were determined during the experiment. (Jockwer, 2003)

Äspö diorite and fine-grained granite are the main components of the rock mass. The master fracture is called V2 depending on the scaled used. They performed vast gas threshold pressure tests to measure the gas entry pressure and to choose the best location for the gas dipole test. In V2 fracture, the initial pressure is about 1.8 MPa and the hydraulic conductivity is in the range of $10^{-5} m/sec$ (Jockwer, 2003).

Gas Threshold Pressure (GTHP) is determined by the gas injection test in packed boreholes. The gas injection test can also measure the gas mobility in fractured rock. In fractured crystalline rock, the GTHP is one of the parameters to control gas and water flow. Figure A.21 shows the results of gas threshold pressure measurements. There is no restriction for gas entry into the water bearing V2.

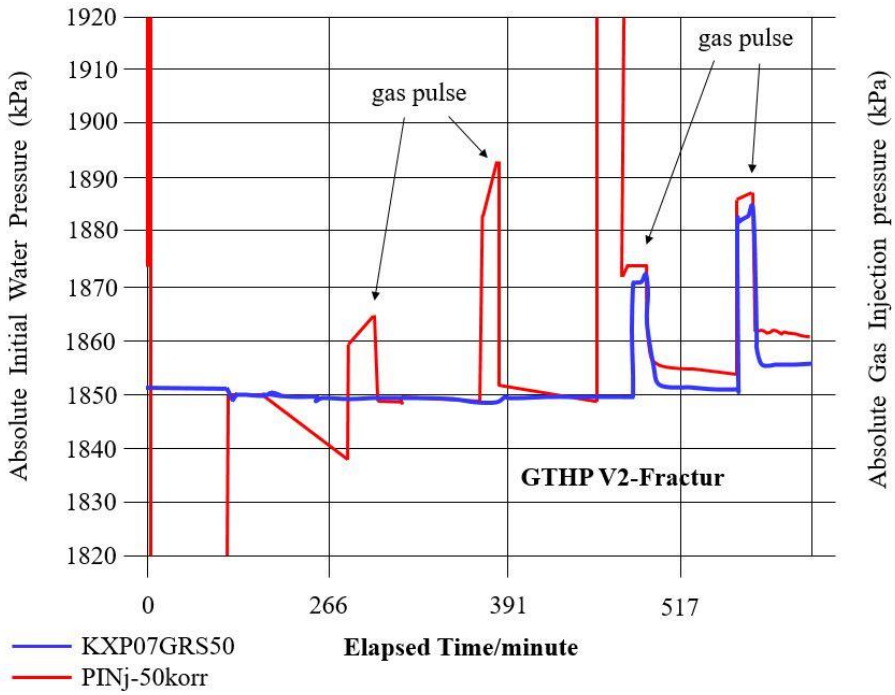

Figure A.21 Gas injection results in the V2 Fracture

A.2.3. The experiments of Mont Terri rock laboratory

Mont Terri rock laboratory is located at the north of the town of St-Ursanne, Switzerland. The international Mont Terri research project investigated and determined the hydrogeological, geochemical and rock mechanical properties of argillaceous formations. The concentrations of the experiments in the Mont Terri rock laboratory were to study:

1) The properties of pristine claystone
2) The perturbation of the Opalinus Clay when an underground opening is constructed
3) The early and late time interplay of the engineered barriers and the natural claystone barrier
4) The ultimate and thorough understanding of the radionuclides migration at near and far-field and timescales

After the experiments, the radionuclide mass generation and migration through the engineered and natural barriers can be estimated more accurately and the predictive numerical tools will be improved of the reliability (Bossart et al., 2017).

The Mont Terri rock laboratory performed a heater experiment (HE-D) from 2003. It investigated the coupled thermo-hydro-mechanical processes in the Opalinus Clay when heating. This experiment lasted for 18 months (six months heating up to 100°C, six months heating to 150°C and another six months for cooling down). During the whole test, GRS (Gesellschaft fu¨r Anlagen- und Reaktorsicherheit gGmbH) was used in the test field to measure the pore water pressure, gas entry pressure, gas permeability and gas diffusivity (Jockwer, 2003).

The field investigations in Opalinus Clay mainly included: hydraulic packer tests as shown in Figure A.22 and the gas injection tests. The packer tests were the main source to get the field data. This data can describe the characteristics of gas transport properties in Opalinus Clay. The gas entry pressure can be determined from the gas injection test. The main results of the gas parameter tests are shown in Table A-11. The determined entry pressure has an obvious dependence on intrinsic permeability.

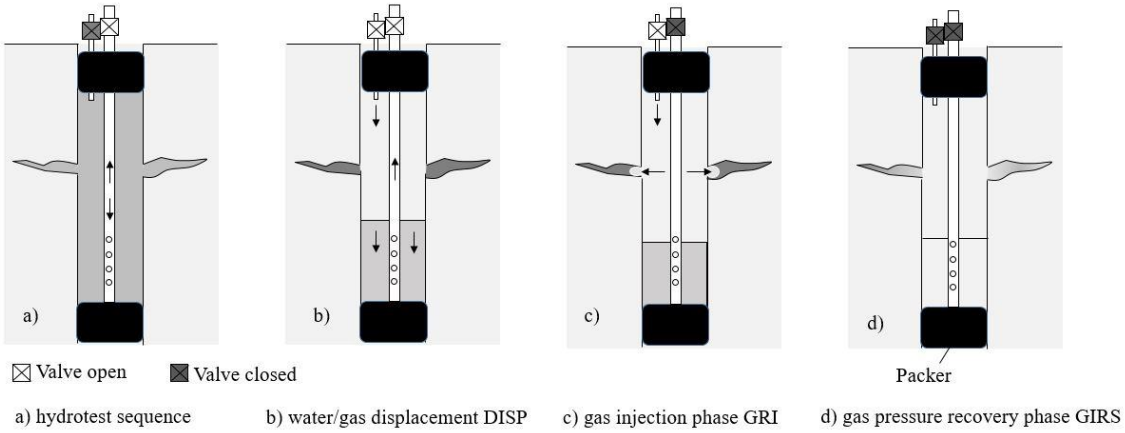

Figure A.22 Gas threshold pressure testing in boreholes (Marschall et al., 2005)

Table A-11 Gas parameters with core specimens from Benken and Mont Terri (Marschall, 2005)

Core sample	Injection period (day)	Direction of flow relative to bedding	Intrinsic permeability k(m^2)	Gas entry pressure p_{ae} MPa
OPA-1	140	90°	$K_p = 3 - 6 \times 10^{-21}$ $K_n = 5 - 7 \times 10^{-2}$	~4
OPA-2	120	0°	3×10^{-21}	7.5-10
BED-B3 06	60	0°	2×10^{-20}	<0.03
BFP 16	110	50°	1.5×10^{-20}	0.5
BWS-E4 06	180	90°	2×10^{-20}	0.2
BED-C5/7	174	35°	2×10^{-20}	0.2
Intrinsic permeability: K_p parallel to bedding, K_n normal to bedding.				

From these field experiments on gas generation and migration, it can be seen that the field results can be used for the developing numerical and simulation tools, since there is good agreement with the results of laboratory investigations. In order to determine the gas permeability in saturated Oplinus Clay and the hydraulic characterization of the tunnel near-field, the borehole tests to investigate the dilatancy-controlled gas migration were conducted under *in-situ* condition. There will be more details about this *in-situ* tests on Chaper 5. For meeting the demands of the performance and safety assessment of the long term nuclear waste repositories, the inthermational DECOVALEX project have been made significant achievement on the numerical methods and

computer codes. Some international conferences (e.g. GeoProc and ComGro) achieved noticeable contributions in the simulation and application of THMC coupling problems in a wider range, such as geothermal reservoir engineering, CO_2 and energy storage, construction of underground repositories (Kolditz et al., 2012). Several simulators were developed to investigate the multiphase flow:

- PORES (Program for Oil Reservoir-Simulation) is a porous medium multiphase flow simulator (Nirex, 1996; 2000). At first, it was used in the oil industry and then developed for the simulation of gas migration in the deep field (Nirex, 2008).

- GWNet is a single structure to simulate the multi-phase flow (Goodfield et al., 2000; Nash et al., 2000)

- FRAC can be used to simulate bubble migration in fractures (Hoch et al., 2001).

- techSIM as an oil industry code, is used for the gas migration simulations (Nirex, 1997a).

- TOUGH2 (Pruess, 1987, 1991) and TOUGHREACT (Xu, 2004) are used for the coupled modelling of the gas migration. Both codes are widely use and have been tested internationally.

- CODE_BRIGHT code was developed on the basis of a new general theory for saline media originally. Then it has been generalized for modelling of coupled thermos-hydro-mechanical (THM) processes in geological media. (DIT-UPC, 2000)

- OpenGeoSys (OGS) is a scientific open-source initiative for thermos-hydro-mechanical-chemical processes in porous media. (Kolditz et al., 2012)

- TOUGH-FLAC simulator to present implantation of the BBM (Barcelona Basic Model) into coupled flow problems involving TOUHGHREACT developed by Xu (2004) and FLAC3D (Itasca, 2009). Yu et al., (2013) used those two pieces of software coupled with each other to realize the multiphase fluid-temperature-rock mechanics coupling analysis.